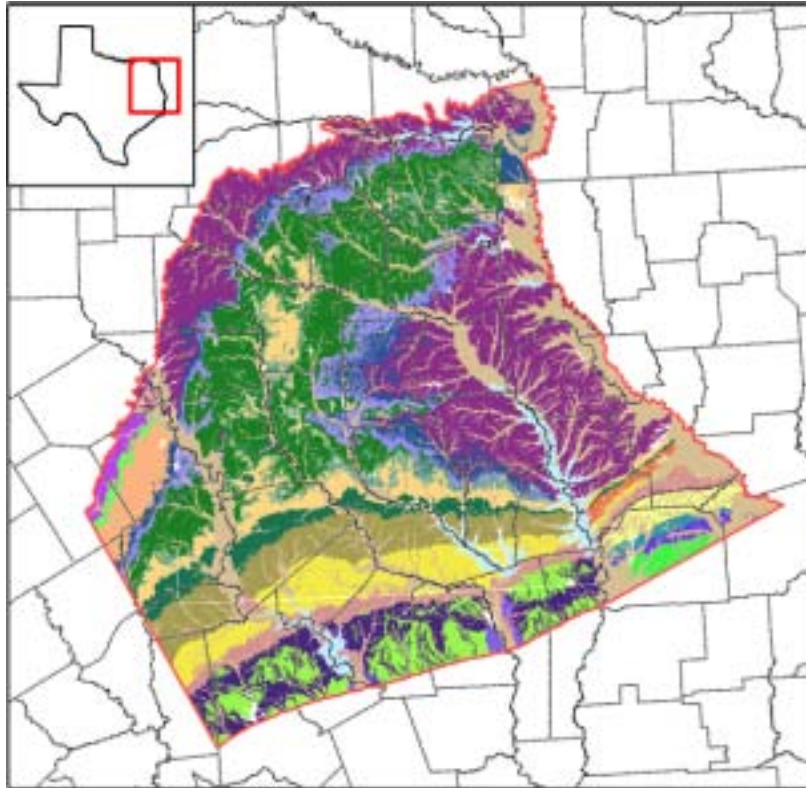


FINAL REPORT

Groundwater Availability Model for the Northern Carrizo-Wilcox Aquifer



Prepared for the:

Texas Water Development Board

Prepared by:

**Dennis Fryar, Rainer Senger,
Neil Deeds, John Pickens
and Toya Jones**



Art J. Whallon, and Kirk E. Dean Parsons

January 31, 2003

TABLE OF CONTENTS

ABSTRACT.....	xiv
1.0 INTRODUCTION.....	1-1
2.0 STUDY AREA.....	2-1
2.1 Physiography and Climate.....	2-10
2.2 Geology.....	2-19
3.0 PREVIOUS INVESTIGATIONS	3-1
4.0 HYDROGEOLOGIC SETTING.....	4-1
4.1 Hydrostratigraphy	4-1
4.2 Structure.....	4-4
4.3 Hydraulic Properties	4-22
4.3.1 Processing of the Hydraulic Property Database.....	4-23
4.3.2 Statistical Analysis of the Hydraulic Property Data	4-23
4.3.3 Spatial Distribution of Hydraulic Property Data.....	4-24
4.3.4 Relationship between Hydraulic Property and Sand Distribution	4-27
4.3.5 Vertical Hydraulic Conductivity	4-28
4.3.6 Storativity.....	4-30
4.4 Water Levels and Regional Groundwater Flow	4-41
4.4.1 Regional Groundwater Flow	4-42
4.4.2 Predevelopment Conditions for the Carrizo Sand and the Wilcox Group....	4-43
4.4.3 Pressure Versus Depth Analysis	4-45
4.4.4 Water-Level Elevations for Model Calibration and Verification.	4-46
4.4.5 Transient Water Levels	4-48
4.5 Recharge	4-86
4.6 Natural Aquifer Discharge.....	4-92
4.7 Aquifer Discharge Through Pumping	4-102
4.8 Water Quality.....	4-112
5.0 CONCEPTUAL MODEL OF GROUNDWATER FLOW IN THE AQUIFER	5-1
6.0 MODEL DESIGN	6-1
6.1 Code and Processor.....	6-1
6.2 Model Layers and Grid.....	6-2
6.3 Boundary Condition Implementation	6-5
6.3.1 Lateral Model Boundaries.....	6-5
6.3.2 Vertical Boundaries.....	6-6
6.3.3 Surface Water Implementation	6-6
6.3.4 Implementation of Recharge.....	6-9
6.3.5 Implementation of Pumping Discharge	6-11
6.4 Model Hydraulic Parameters	6-18
6.4.1 Hydraulic Conductivity.....	6-18
6.4.2 Storativity.....	6-22

TABLE OF CONTENTS (CONTINUED)

7.0	MODELING APPROACH	7-1
7.1	Calibration	7-1
7.2	Calibration Target Uncertainty	7-4
7.3	Sensitivity Analysis	7-6
7.4	Predictions	7-6
8.0	STEADY-STATE MODEL	8-1
8.1	Calibration	8-1
8.1.1	Calibration Targets.....	8-1
8.1.2	Horizontal and Vertical Hydraulic Conductivities.....	8-1
8.1.3	Recharge and Groundwater Evapotranspiration	8-3
8.1.4	General-Head Boundaries and Stream Conductances.....	8-3
8.2	Simulation Results	8-14
8.2.1	Hydraulic Heads.....	8-14
8.2.2	Streams.....	8-16
8.2.3	Water Budget	8-17
8.3	Sensitivity Analysis	8-32
9.0	TRANSIENT MODEL	9-1
9.1	Calibration	9-1
9.2	Simulation Results	9-5
9.2.1	Hydraulic Heads.....	9-5
9.2.2	Stream Leakance	9-9
9.2.3	Water Budget	9-9
9.3	Sensitivity Analysis	9-49
10.0	MODEL PREDICTIVE SIMULATIONS	10-1
10.1	Drought of Record	10-1
10.2	Predictive Simulation Results.....	10-8
10.3	Predictive Simulation Water Budget	10-34
11.0	LIMITATIONS OF THE MODEL	11-1
11.1	Limitations of Supporting Data	11-1
11.2	Limiting Assumptions	11-3
11.3	Limits for Model Applicability.....	11-5
12.0	FUTURE IMPROVEMENTS	12-1
12.1	Supporting Data	12-1
12.2	Future Model Improvements	12-2
13.0	CONCLUSIONS	13-1
14.0	ACKNOWLEDGEMENTS	14-1
15.0	REFERENCES.....	15-1

LIST OF FIGURES

Figure 2.1	Location of the three Carrizo-Wilcox GAMs.....	2-4
Figure 2.2	Location of study area showing county boundaries, cities, lakes, and rivers.	2-5
Figure 2.3	Areal extent of the major aquifers in the study area.....	2-6
Figure 2.4	Location of Regional Water Planning Groups in the study area.	2-7
Figure 2.5	Location of Groundwater Conservation Districts in the study area.	2-8
Figure 2.6	Map showing the major river basins in the study area.	2-9
Figure 2.7	Ecological regions in the study area.	2-12
Figure 2.8	Topographic map of the study area.	2-13
Figure 2.9	Average pan evaporation rate, in inches per year, in the study area.	2-14
Figure 2.10	Location of precipitation gages in the study area (Period of Record is 1900 to 1999).	2-15
Figure 2.11	Average annual precipitation (1961-1990) over the study area in inches per year (Source: Oregon Climate Service, Oregon State University, PRISM data set).	2-16
Figure 2.12a	Annual precipitation time series for gages in Angelina, Cherokee, Ellis, and Franklin counties (Source: National Climatic DataCenter, Texas Natural Resources Information System).	2-17
Figure 2.12b	Annual precipitation time series for gages in Kaufman, Montgomery, Navarro, and Shelby counties (Source: National Climatic DataCenter, Texas Natural Resources Information System).	2-18
Figure 2.13	Surface geology of the study area.	2-22
Figure 2.14	Generalized stratigraphic section for the Carrizo-Wilcox aquifer in Texas (after Ayers and Lewis, 1985; Hamlin, 1988; Kaiser et al., 1978).	2-23
Figure 2.15a	Structural cross sections A-A' and B-B' showing the major hydrostratigraphic units in the East Texas Basin from Fogg and Kreitler (1982), indicating general groundwater flow patterns. Cross-section locations are shown on Figure 2.13.	2-24
Figure 2.15b	Structural cross section C-C' showing the major hydrostratigraphic units in the East Texas Basin from Fogg and Kreitler (1982), indicating general groundwater flow patterns. Cross-section location is shown on Figure 2.13.	2-25
Figure 3.1	Northern Carrizo-Wilcox GAM boundary with previous modeling study boundaries which have included the Carrizo-Wilcox aquifer.....	3-5
Figure 4.1.1	Hydrostratigraphy and model layers.	4-3
Figure 4.2.1	Structural setting of the study area.	4-7
Figure 4.2.2	Structure contour map of the base of the Wilcox Group (CI = 500 ft).....	4-8
Figure 4.2.3	Structure contour map of the top of the lower Wilcox (CI = 500 ft).....	4-9
Figure 4.2.4	Structure contour map of the top of the middle Wilcox (CI = 500 ft).....	4-10
Figure 4.2.5	Structure contour map of the top of the Wilcox Group (CI = 500 ft).	4-11
Figure 4.2.6	Structure contour map of the top of the Carrizo (CI = 500 ft):	4-12

LIST OF FIGURES (CONTINUED)

Figure 4.2.7	Structure contour map of the top of the Reklaw Formation (CI = 500 ft).....	4-13
Figure 4.2.8	Structure contour map of the top of the Queen City (CI = 500 ft).....	4-14
Figure 4.2.9	Thickness map of the lower Wilcox (CI = 100 ft).....	4-15
Figure 4.2.10	Thickness map of the middle Wilcox (CI = 100 ft).....	4-16
Figure 4.2.11	Thickness map of the upper Wilcox (CI = 100 ft).....	4-17
Figure 4.2.12	Thickness map of the Carrizo (CI = 100 ft).....	4-18
Figure 4.2.13	Thickness map of the Reklaw (CI = 100 ft).....	4-19
Figure 4.2.14	Thickness map of the Queen City (CI = 100 ft).....	4-20
Figure 4.2.15	Thickness map of formations above the Queen City (CI = 250 ft).....	4-21
Figure 4.3.1	Screening of hydraulic conductivity data.....	4-31
Figure 4.3.2	Cumulative distribution function (CDF) curves of hydraulic conductivity for the modeled aquifer units.....	4-32
Figure 4.3.3	Variogram for hydraulic conductivity data from the Carrizo Sand.....	4-33
Figure 4.3.4	Variogram and kriged map of hydraulic conductivity for the Carrizo Sand.....	4-34
Figure 4.3.5	Variogram and kriged map of hydraulic conductivity for the upper Wilcox.....	4-35
Figure 4.3.6	Variogram and kriged map of hydraulic conductivity for the middle Wilcox.....	4-36
Figure 4.3.7	Variogram and kriged map of hydraulic conductivity for the lower Wilcox.....	4-37
Figure 4.3.8	Variogram and kriged map of hydraulic conductivity for the Queen City.....	4-38
Figure 4.3.9	Histogram of (a) net-sand thickness for the entire Wilcox Group and (b) maximum sand thickness and hydraulic conductivity (Log K) of the upper Wilcox.....	4-39
Figure 4.3.10	Percent sand for the Wilcox Group, based on sand maps by Kaiser et al. (1978) and Fisher and McGowen (1967) (CI = 10 percent).....	4-40
Figure 4.4.1	Relationship between the Carrizo Sand and the Wilcox Group in the study area.....	4-53
Figure 4.4.2	Water-level measurement locations for the hydrostratigraphic units in the study area.....	4-54
Figure 4.4.3	Groundwater flow lines drawn from the Carrizo-Wilcox potentiometric surface (from Fogg and Kreitler, 1982).....	4-55
Figure 4.4.4	Location and model layer for predevelopment water-level elevation targets.....	4-56
Figure 4.4.5	Water-level measurement locations used for the pressure-depth analysis (for measurements prior to 1950).....	4-57
Figure 4.4.6	Pressure versus depth analysis results (for measurements prior to 1950).....	4-58
Figure 4.4.7	Water-level measurement locations used for the pressure-depth analysis (for all measurements).....	4-59
Figure 4.4.8	Pressure versus depth analysis results (for all measurements).....	4-60
Figure 4.4.9a	Water-level elevation contours for the Queen City Sand at the start of model calibration (January 1980).....	4-61

LIST OF FIGURES (CONTINUED)

Figure 4.4.9b	Water-level elevation contours for the Carrizo Sand at the start of model calibration (January 1980).	4-62
Figure 4.4.9c	Water-level elevation contours for the upper Wilcox at the start of model calibration (January 1980).	4-63
Figure 4.4.9d	Water-level elevation contours for the middle Wilcox at the start of model calibration (January 1980).	4-64
Figure 4.4.9e	Water-level elevation contours for the lower Wilcox at the start of model calibration (January 1980).	4-65
Figure 4.4.10a	Water-level elevation contours for the Carrizo Sand at the end of model calibration (December 1989).	4-66
Figure 4.4.10b	Water-level elevation contours for the upper Wilcox at the end of model calibration (December 1989).	4-67
Figure 4.4.10c	Water-level elevation contours for the middle Wilcox at the end of model calibration (December 1989).	4-68
Figure 4.4.10d	Water-level elevation contours for the lower Wilcox at the end of model calibration (December 1989).	4-69
Figure 4.4.11a	Water-level elevation contours for the Carrizo Sand at the end of model verification (December 1999).	4-70
Figure 4.4.11b	Water-level elevation contours for the upper Wilcox at the end of model verification (December 1999).	4-71
Figure 4.4.11c	Water-level elevation contours for the middle Wilcox at the end of model verification (December 1999).	4-72
Figure 4.4.11d	Water-level elevation contours for the lower Wilcox at the end of model verification (December 1999).	4-73
Figure 4.4.12	Long-term transient water-level elevations for well 37-36-102 completed to the Carrizo-Wilcox in Nacogdoches County.	4-74
Figure 4.4.13	Model layer for locations with transient water-level data.	4-75
Figure 4.4.14	Example hydrographs for wells located in Nacogdoches and Angelina counties.	4-76
Figure 4.4.15	Example hydrographs for wells in the study area.	4-77
Figure 4.4.16a	Water-level decline in the Carrizo Sand from the start of model calibration (January 1980) to the end of model calibration (December 1989).	4-78
Figure 4.4.16b	Water-level decline in the Carrizo Sand from the start of model calibration (January 1980) to the end of model verification (December 1999).	4-79
Figure 4.4.17a	Water-level decline in the upper Wilcox from the start of model calibration (January 1980) to the end of model calibration (December 1989).	4-80
Figure 4.4.17b	Water-level decline in the upper Wilcox from the start of model calibration (January 1980) to the end of model verification (December 1999).	4-81
Figure 4.4.18a	Water-level decline in the middle Wilcox from the start of model calibration (January 1980) to the end of model calibration (December 1989).	4-82

LIST OF FIGURES (CONTINUED)

Figure 4.4.18b	Water-level decline in the middle Wilcox from the start of model calibration (January 1980) to the end of model verification (December 1999).	4-83
Figure 4.4.19a	Water-level decline in the lower Wilcox from the start of model calibration (January 1980) to the end of model calibration (December 1989).	4-84
Figure 4.4.19b	Water-level decline in the lower Wilcox from the start of model calibration (January 1980) to the end of model verification (December 1999).	4-85
Figure 4.5.1	Major reservoirs in the study area.	4-90
Figure 4.5.2	Hydrographs for select reservoirs in the study area.	4-91
Figure 4.6.1	Stream gain/loss studies in the study area (after Slade et al., 2002).	4-100
Figure 4.6.2	Documented spring locations in the study area.	4-101
Figure 4.7.1	Population density for the Northern Carrizo-Wilcox GAM study area.	4-108
Figure 4.7.2	Younger (Layer 1) pumpage (AFY), 1990.	4-109
Figure 4.7.3	Reklaw (Layer 2) pumpage (AFY), 1990.	4-109
Figure 4.7.4	Carrizo (Layer 3) pumpage (AFY), 1990.	4-110
Figure 4.7.5	Upper Wilcox (Layer 4) pumpage (AFY), 1990.	4-110
Figure 4.7.6	Middle Wilcox (Layer 5) pumpage (AFY), 1990.	4-111
Figure 4.7.7	Lower Wilcox (Layer 6) pumpage (AFY), 1990.	4-111
Figure 5.1	Conceptual groundwater flow model for the Northern Carrizo-Wilcox GAM.	5-5
Figure 5.2	Schematic diagram of transient relationships between recharge rates, discharge rates, and withdrawal rates for an unconfined aquifer basin (from Freeze, 1971).	5-6
Figure 6.2.1	Model grid of the Northern Carrizo-Wilcox GAM.	6-4
Figure 6.3.1	Layer 1 (Queen City) boundary conditions and active/inactive cells.	6-12
Figure 6.3.2	Layer 2 (Reklaw) boundary conditions and active/inactive cells.	6-13
Figure 6.3.3	Layer 3 (Carrizo) boundary conditions and active/inactive cells.	6-14
Figure 6.3.4	Layer 4 (upper Wilcox) boundary conditions and active/inactive cells.	6-15
Figure 6.3.5	Layer 5 (middle Wilcox) boundary conditions and active/inactive cells.	6-16
Figure 6.3.6	Layer 6 (lower Wilcox) boundary conditions and active/inactive cells.	6-17
Figure 8.1.1	Calibrated horizontal hydraulic conductivity field for Layer 3 (Carrizo).	8-6
Figure 8.1.2	Calibrated horizontal hydraulic conductivity field for Layer 4 (upper Wilcox).	8-7
Figure 8.1.3	Calibrated horizontal hydraulic conductivity field for Layer 5 (middle Wilcox).	8-8
Figure 8.1.4	Calibrated horizontal hydraulic conductivity field for Layer 6 (lower Wilcox).	8-9
Figure 8.1.5	Calibrated vertical anisotropy (K_h/K_v) field for Layer 2 (Reklaw).	8-10
Figure 8.1.6	Calibrated recharge distribution for the steady-state model.	8-11

LIST OF FIGURES (CONTINUED)

Figure 8.1.7	ET extinction depth distribution for the steady-state model.	8-12
Figure 8.1.8	Calibrated maximum groundwater ET rate distribution for the steady-state model.....	8-13
Figure 8.2.1a	Simulated steady-state hydraulic heads and residuals for Layer 1 (Queen City).	8-21
Figure 8.2.1b	Scatterplot of simulated and measured hydraulic heads for Layer 1 (Queen City).	8-22
Figure 8.2.2a	Simulated steady-state hydraulic heads and posted residuals for Layer 3 (Carrizo).	8-23
Figure 8.2.2b	Scatterplot of simulated and measured hydraulic heads for Layer 3 (Carrizo).....	8-24
Figure 8.2.3a	Simulated steady-state hydraulic heads and residuals for Layer 4 (upper Wilcox).....	8-25
Figure 8.2.3b	Scatterplot of simulated and measured hydraulic heads for Layer 4 (upper Wilcox).....	8-26
Figure 8.2.4a	Simulated steady-state hydraulic heads and residuals for Layer 5 (middle Wilcox).....	8-27
Figure 8.2.4b	Scatterplot of simulated and measured hydraulic heads for Layer 5 (middle Wilcox).....	8-28
Figure 8.2.5	Simulated steady-state hydraulic heads for Layer 6 (lower Wilcox).	8-29
Figure 8.2.6	Steady-state model stream gain/loss (negative values denote gaining streams).....	8-30
Figure 8.2.7	Simulated stream gain/loss compared to measurements compiled by Slade et al. (2002) for selected stream segments.	8-31
Figure 8.3.1	Steady-state sensitivity results for Layer 3 (Carrizo) using target locations.	8-35
Figure 8.3.2	Steady-state sensitivity results for Layer 3 (Carrizo) using all active gridblocks.....	8-35
Figure 8.3.3	Steady-state sensitivity results for Layer 1 (Queen City) using all active gridblocks.	8-36
Figure 8.3.4	Steady-state sensitivity results for Layer 2 (Reklaw) using all active gridblocks.....	8-36
Figure 8.3.5	Steady-state sensitivity results for Layer 4 (upper Wilcox) using all active gridblocks.	8-37
Figure 8.3.6	Steady-state sensitivity results for Layer 5 (middle Wilcox) using all active gridblocks.	8-37
Figure 8.3.7	Steady-state sensitivity results for Layer 6 (lower Wilcox) using all active gridblocks.	8-38
Figure 8.3.8	Steady-state sensitivity results where the vertical hydraulic conductivity of Layer 2 (Reklaw) is varied.	8-38
Figure 8.3.9	Steady-state sensitivity results where streambed conductivity is varied.	8-39
Figure 8.3.10	Steady-state sensitivity results where recharge is varied.	8-39
Figure 9.1.1	Target well locations for the different layers used in the transient calibration.	9-4

LIST OF FIGURES (CONTINUED)

Figure 9.2.1	Simulated hydraulic head distribution for Layer 1 (Queen City) at the end of the transient model calibration (December 1989).....	9-15
Figure 9.2.2	Simulated and measured hydraulic head distribution for Layer 3 (Carrizo) at the end of the transient model calibration (December 1989).	9-16
Figure 9.2.3	Simulated and measured hydraulic head distribution for Layer 4 (upper Wilcox) at the end of the transient model calibration (December 1989).	9-17
Figure 9.2.4	Simulated and measured hydraulic head distribution for Layer 5 (middle Wilcox) at the end of the transient model calibration (December 1989).	9-18
Figure 9.2.5	Simulated and measured hydraulic head distribution for Layer 6 (lower Wilcox) at the end of the transient model calibration (December 1989).	9-19
Figure 9.2.6	Residuals at target wells for Layer 3 (Carrizo) at the end of the transient model calibration (December 1989).	9-20
Figure 9.2.7	Residuals at target wells for Layer 4 (upper Wilcox) at the end of the transient model calibration (December 1989).	9-21
Figure 9.2.8	Residuals at target wells for Layer 5 (middle Wilcox) at the end of the transient model calibration (December 1989).....	9-22
Figure 9.2.9	Residuals at target wells for Layer 6 (lower Wilcox) at the end of the transient model calibration (December 1989).	9-23
Figure 9.2.10	Scatterplots of simulated and measured hydraulic heads for the different layers at the end of the transient model calibration (December 1989).	9-24
Figure 9.2.11	Scatterplots of simulated and measured hydraulic heads for the different layers at the end of the transient model verification (December 1999).	9-25
Figure 9.2.12	Simulated and measured hydraulic head distribution for Layer 3 (Carrizo) at the end of the transient model verification (December 1999).	9-26
Figure 9.2.13	Simulated and measured hydraulic head distribution for Layer 4 (upper Wilcox) at the end of the transient model verification (December 1999).	9-27
Figure 9.2.14	Simulated and measured hydraulic head distribution for Layer 5 (middle Wilcox) at the end of the transient model verification (December 1999).	9-28
Figure 9.2.15	Simulated and measured hydraulic head distribution for Layer 6 (lower Wilcox) at the end of the transient model verification (December 1999).	9-29
Figure 9.2.16a	Selected hydrographs of simulated (lines) and measured (points) hydraulic heads in the northern part for Layer 3 (Carrizo).....	9-30
Figure 9.2.16b	Selected hydrographs of simulated (lines) and measured (points) hydraulic heads in the central part for Layer 3 (Carrizo).	9-31
Figure 9.2.16c	Selected hydrographs of simulated (lines) and measured (points) hydraulic heads in the southern part for Layer 3 (Carrizo).....	9-32

LIST OF FIGURES (CONTINUED)

Figure 9.2.17a	Selected hydrographs of simulated (lines) and measured (points) hydraulic heads in the northern part for Layer 4 (upper Wilcox).....	9-33
Figure 9.2.17b	Selected hydrographs of simulated (lines) and measured (points) hydraulic heads in the central part for Layer 4 (upper Wilcox).....	9-34
Figure 9.2.17c	Selected hydrographs of simulated (lines) and measured (points) hydraulic heads in the southern part for Layer 4 (upper Wilcox).....	9-35
Figure 9.2.17d	Selected hydrographs of simulated (lines) and measured (points) hydraulic heads in the western part for Layer 4 (upper Wilcox).....	9-36
Figure 9.2.18a	Selected hydrographs of simulated (lines) and measured (points) hydraulic heads in the northern part for Layer 5 (middle Wilcox).....	9-37
Figure 9.2.18b	Selected hydrographs of simulated (lines) and measured (points) hydraulic heads in the central part for Layer 5 (middle Wilcox).....	9-38
Figure 9.2.18c	Selected hydrographs of simulated (lines) and measured (points) hydraulic heads in the western part for Layer 5 (middle Wilcox).....	9-39
Figure 9.2.19	Selected hydrographs of simulated (lines) and measured (points) hydraulic heads in Layer 6 (lower Wilcox).	9-40
Figure 9.2.20	Average recharge for the transient simulation period (1980-1999).	9-41
Figure 9.2.21	Simulated stream gain/loss for May 1989.	9-42
Figure 9.2.22	Simulated stream gain/loss for November 1989.	9-43
Figure 9.2.23a	Simulated and measured stream flow at gauging station 8032000 on the Neches River.....	9-44
Figure 9.2.23b	Simulated and measured stream flow at gauging station 8065000 on the Trinity River.....	9-45
Figure 9.2.23c	Simulated and measured stream flow at gauging station 8022040 on the Sabine River.....	9-46
Figure 9.2.24	Simulated stream gain/loss compared to measurements compiled by Slade et al. (2002) for selected stream segments.....	9-47
Figure 9.2.25	Time history of water budgets for (a) streams and reservoirs, (b) recharge and ET, and (c) pumpage.	9-48
Figure 9.3.1	Transient sensitivity results for Layer 3 (Carrizo) using target locations.....	9-52
Figure 9.3.2	Transient sensitivity results for Layer 3 (Carrizo) using all active gridblocks.....	9-52
Figure 9.3.3	Transient sensitivity results for Layer 1 (Queen City) using all active gridblocks.....	9-53
Figure 9.3.4	Transient sensitivity results for Layer 2 (Reklaw) using all active gridblocks.....	9-53
Figure 9.3.5	Transient sensitivity results for Layer 4 (upper Wilcox) using all active gridblocks.....	9-54
Figure 9.3.6	Transient sensitivity results for Layer 5 (middle Wilcox) using all active gridblocks.....	9-54
Figure 9.3.7	Transient sensitivity results for Layer 6 (lower Wilcox) using all active gridblocks.....	9-55
Figure 9.3.8	Transient sensitivity results where the vertical hydraulic conductivity of Layer 2 (Reklaw) is varied.	9-55
Figure 9.3.9	Transient sensitivity results where recharge is varied.....	9-56

LIST OF FIGURES (CONTINUED)

Figure 9.3.10	Transient sensitivity results where the horizontal hydraulic conductivity of the Wilcox is varied.....	9-56
Figure 10.1.1	Standard precipitation index (SPI) curves for the Lufkin rain gage (#415424-Angelina Co.) for 1 month, 1 year, 2 year, 3 year time periods.....	10-5
Figure 10.1.2	Standardized precipitation indices for precipitation gages in the region.	10-6
Figure 10.1.3	Standardized precipitation index averaged for all gages in the region from 1950-1960.	10-7
Figure 10.2.1	Simulated 2000 (a) and 2050 (b) heads surfaces for Layer 1 (Queen City).	10-11
Figure 10.2.2	Difference between 2000 and 2050 simulated head surfaces for Layer 1 (Queen City).	10-12
Figure 10.2.3	Simulated 2000 (a) and 2050 (b) heads surfaces for Layer 3 (Carrizo).....	10-13
Figure 10.2.4	Difference between 2000 and 2050 simulated head surfaces for Layer 3 (Carrizo).	10-14
Figure 10.2.5	Simulated 2000 (a) and 2050 (b) heads surfaces for Layer 4 (upper Wilcox).	10-15
Figure 10.2.6	Difference between 2000 and 2050 simulated head surfaces for Layer 4 (upper Wilcox).....	10-16
Figure 10.2.7	Simulated 2000 (a) and 2050 (b) heads surfaces for Layer 5 (middle Wilcox).	10-17
Figure 10.2.8	Difference between 2000 and 2050 simulated head surfaces for Layer 5 (middle Wilcox).....	10-18
Figure 10.2.9	Simulated 2000 (a) and 2050 (b) heads surfaces for Layer 6 (lower Wilcox).	10-19
Figure 10.2.10	Difference between 2000 and 2050 simulated head surfaces for Layer 6 (lower Wilcox).....	10-20
Figure 10.2.11	Simulated 2010 head surface (a) and drawdown from 2000 (b), Layer 3 (Carrizo).	10-21
Figure 10.2.12	Simulated 2010 head surface (a) and drawdown from 2000 (b), Layer 4 (upper Wilcox).....	10-22
Figure 10.2.13	Simulated 2020 head surface (a) and drawdown from 2000 (b), Layer 3 (Carrizo).	10-23
Figure 10.2.14	Simulated 2020 head surface (a) and drawdown from 2000 (b), Layer 4 (upper Wilcox).....	10-24
Figure 10.2.15	Simulated 2030 head surface (a) and drawdown from 2000 (b), Layer 3 (Carrizo).	10-25
Figure 10.2.16	Simulated 2030 head surface (a) and drawdown from 2000 (b), Layer 4 (upper Wilcox).....	10-26
Figure 10.2.17	Simulated 2040 head surface (a) and drawdown from 2000 (b), Layer 3 (Carrizo).	10-27
Figure 10.2.18	Simulated 2040 head surface (a) and drawdown from 2000 (b), Layer 4 (upper Wilcox).....	10-28

LIST OF FIGURES (CONTINUED)

Figure 10.2.19	Selected hydrographs from predictive simulation to 2050, Layer 3 (Carrizo).....	10-29
Figure 10.2.20	Selected hydrographs from predictive simulation to 2050, Layer 4 (upper Wilcox).....	10-30
Figure 10.2.21	Selected hydrographs from predictive simulation to 2050, Layer 5 (middle Wilcox).....	10-31
Figure 10.2.22	Selected hydrographs from predictive simulation to 2050, Layer 6 (lower Wilcox).....	10-32
Figure 10.2.23	Simulated difference in head surfaces between the average condition 2050 simulation and the DOR 2050 simulation.....	10-33

LIST OF TABLES

Table 2.1	River basins in the Northern Carrizo-Wilcox GAM study area (BEG, 1996).....	2-3
Table 3.1	Previous groundwater models of the Carrizo-Wilcox aquifer in the study area.	3-1
Table 4.2.1	Data sources for layer elevations for the Northern Carrizo-Wilcox GAM.	4-4
Table 4.3.1	Summary statistics for horizontal hydraulic conductivity.	4-24
Table 4.3.2	Summary of literature estimates of Carrizo-Wilcox specific yield.	4-30
Table 4.4.1	Target values for calibration of the steady-state model to predevelopment conditions.	4-50
Table 4.5.1	Review of recharge rates for the Carrizo-Wilcox aquifers in Texas (after Scanlon et al., 2002).	4-88
Table 4.5.2	Characteristics of reservoirs in study area.	4-89
Table 4.6.1	Stream flow gain/loss in the study area (after Slade et al., 2002, Table 1).	4-95
Table 4.6.2	Documented springs in the study area.	4-96
Table 4.7.1	Rate of groundwater withdrawal (AFY) from all model layers of the Carrizo-Wilcox aquifer for counties within the study area.	4-107
Table 8.1.1	Calibrated hydraulic conductivity ranges for the steady-state model.	8-5
Table 8.2.1	Calibration statistics for the steady-state model.	8-19
Table 8.2.2a	Water budget for the steady-state model. All rates reported in acre-ft/yr.	8-20
Table 8.2.2b	Water budget for the steady-state model with values expressed as a percentage of inflow or outflow.	8-20
Table 9.2.1	Calibration statistics for the transient model.	9-11
Table 9.2.2	Calibration statistics for the hydrographs shown in Figures 9.2.16a – 9.2.19.	9-12
Table 9.2.3	Water budget for transient model. All rates reported in acre-ft/yr.	9-14
Table 10.3.1	Water budget for predictive simulations. All rates reported in acre-ft/yr.	10-35

APPENDICES

- Appendix A Brief Summary of the Development of the Carrizo-Wilcox Aquifer in Each County and List of Reviewed Reports
- Appendix B Standard Operating Procedures (SOPs) for Processing Historical Pumpage Data TWDB Groundwater Availability Modeling (GAM) Projects
- Appendix C Standard Operating Procedures (SOPs) for Processing Predictive Pumpage Data TWDB Groundwater Availability Modeling (GAM) Projects
- Appendix D1 Tabulated Groundwater Withdrawal Estimates for the Carrizo-Wilcox for 1980, 1990, 2000, 2010, 2020, 2030, 2040, and 2050
- Appendix D2 Post Plots of Groundwater Withdrawal Estimates for the Carrizo-Wilcox for 1980, 1990, 2000, 2010, 2020, 2030, 2040, and 2050
- Appendix D3 Carrizo-Wilcox Groundwater Withdrawal Distributions by County
- Appendix E Using SWAT with MODFLOW in a Decoupled Environment
- Appendix F Water Quality
- Appendix G Draft Report Comments and Responses

ABSTRACT

This report documents a three-dimensional groundwater model developed for the northern Carrizo-Wilcox aquifer in northeastern Texas. The model was developed using MODFLOW and consists of six layers which include four layers for the Carrizo-Wilcox aquifer, and additional layers for the overlying Reklaw and Queen City formations. The model incorporates the available information on structure, hydrostratigraphy, hydraulic properties, stream flow, and recharge estimates. The purpose of this model is to provide a tool for making predictions of groundwater availability through 2050 based on current projections of groundwater demands during drought-of-record conditions. The model has been calibrated to predevelopment conditions (prior to significant groundwater withdrawal), which are considered to be at steady state. The steady-state model reproduces the predevelopment aquifer heads well within the estimated head uncertainty. The model was also calibrated to transient aquifer conditions from January 1980 through December 1989, incorporating monthly variations in recharge, streamflow, and pumping. The transient model reproduces aquifer heads within the calibration measures and available estimates of aquifer-stream interaction. The transient-calibrated model was verified by simulating aquifer conditions for the verification period between January 1990 and December 1999, reproducing observed aquifer heads within the calibration measures and available estimates of aquifer-stream interaction. The initial estimates of hydraulic conductivity in the model required some adjustment to better reproduce the observed water-level declines in the confined section of the Carrizo-Wilcox aquifer during the transient period.

The verified model was used to make predictions of aquifer conditions for the next 50 years based upon projected pumping demands as developed by the Regional Water Planning Groups. The predictive modeling indicated noticeable rebound of hydraulic heads in some areas of the confined section even though total pumping showed a gradual increase. This was due to changes in pumping for individual layers in certain areas during the transition from the historical period to the predictive period.

This model provides an integrated tool for the assessment of water management strategies to directly benefit state planners, Regional Water Planning Groups (RWPGs), and Groundwater Conservation Districts (GCDs). The applicability of the model is limited to regional-scale

assessments of groundwater availability (e.g., tens of miles) due to the relatively large grid blocks (1 mile²) over which pumping and hydraulic property data are averaged in the model. In addition to uncertainty in pumping and hydraulic property data, the model is limited to a first-order approach of coupling surface water and groundwater, and does not provide a rigorous solution to surface water flow in the region.

1.0 INTRODUCTION

The Carrizo-Wilcox Aquifer is classified as a major aquifer in Texas (Ashworth and Hopkins, 1995) ranking third in the state for water use (430,000 acre-feet per year [AFY]) in 1997 behind the Gulf Coast aquifer and the Ogallala aquifer (TWDB, 2002). The aquifer extends from the Rio Grande in South Texas to East Texas and continues into Louisiana and Arkansas. The Carrizo-Wilcox aquifer provides water to all or parts of 60 Texas counties with the greatest historical use being in and around the Tyler, Lufkin-Nacogdoches, and Bryan-College Station metropolitan centers and in the Wintergarden region of South Texas (Ashworth and Hopkins, 1995).

The Texas Water Code codified the requirement for the development of a State Water Plan that allows for the development, management, and conservation of water resources and the preparation and response to drought, while maintaining sufficient water available for the citizens of Texas (TWDB, 2002). Senate Bill 1 (SB1) and subsequent legislation directed the TWDB to coordinate the regional water planning process through a process based upon public participation. Also, as a result of SB1, the approach to water planning in the state of Texas has shifted from a water-demand based allocation approach to an availability-based approach.

Groundwater models provide a tool to estimate groundwater availability for various water use strategies and to determine the cumulative effects of increased water use and drought. A groundwater model is a numerical representation of the aquifer system capable of simulating historical and predicting future aquifer conditions. Inherent to the groundwater model, are a set of equations which are developed and applied to describe the physical processes considered to be controlling groundwater flow in the aquifer system. It can be argued that groundwater models are essential to performing complex analyses and in making informed predictions and related decisions (Anderson and Woessner, 1992). As a result, development of Groundwater Availability Models (GAMs) for the major Texas aquifers is integral to the state water planning process as defined in SB1. The purpose of the GAM program is to provide a tool that can be used to develop reliable and timely information on groundwater availability for the citizens of Texas to ensure adequate supplies or recognize inadequate supplies over a 50-year planning period.

The Northern Carrizo-Wilcox GAM has been developed using a modeling protocol which is standard to the groundwater model industry. This protocol includes: (1) the development of a conceptual model for groundwater flow in the aquifer, (2) model design, (3) model calibration, (4) model verification, (5) sensitivity analysis, (6) model prediction, and (7) reporting. The conceptual model is a conceptual description of the physical processes which govern groundwater flow in the aquifer system. We reviewed the available data and reports for the model area in the conceptual model development stage. Model design is the process used to translate the conceptual model into a physical model, in this case a numerical model of groundwater flow. This involved organizing and distributing model parameters, developing a model grid and model boundary conditions, and determining the model integration time scale. Model calibration is the process of modifying model parameters so that observed field measurements (e.g., groundwater levels in wells) can be reproduced. The northern Carrizo-Wilcox model was calibrated to predevelopment conditions (prior to significant resource use) which are considered to be at steady-state and to transient aquifer conditions from 1980 through 1990. Model verification is the process of using the calibrated model to reproduce observed field measurements not used in the calibration to test the model's predictive ability. The model was verified against measured aquifer conditions from 1990 through 1999. Model sensitivity analyses were performed by varying model input parameters for both the steady-state and transient models to offer insight on the uniqueness of the model and on the uncertainty in model parameter estimates. Model predictions were performed to estimate aquifer conditions for the next 50 years based upon projected pumping demands developed by the Regional Water Planning Groups. This report documents the modeling process and results from conceptual model development through predictions (2000 to 2050) according to standard requirements specified by the TWDB in their Request for Qualifications. The model and associated data files are publicly available. These files, along with this report, are available at the TWDB GAM website at <http://www.twdb.state.tx.us/GAM>.

Consistent with state water planning policy, the Northern Carrizo-Wilcox GAM was developed with the support of stakeholders through quarterly stakeholder forums. The purpose of this GAM is to provide a tool for Regional Water Planning Groups, Groundwater Conservation Districts, River Authorities, and state planners for the evaluation of groundwater availability and to support the development of water management strategies and drought

planning. The East Texas Regional Water Planning Group (Region I) plans to meet 59% of their projected water needs by the year 2050 through the use of existing groundwater supplies. The North East Texas Regional Water Planning Group (Region D) plans to meet 25% of their 2050 projected water needs through existing groundwater supplies and an additional 2% through new groundwater resources. The GAM provides a tool for use in assessing the future availability of these supplies.

2.0 STUDY AREA

The Carrizo-Wilcox aquifer is comprised of hydraulically connected sands from the Wilcox Group and the Carrizo Formation of the Claiborne Group (Ashworth and Hopkins, 1995). The Carrizo-Wilcox aquifer extends across Texas from the Rio Grande in the southwest to the Sabine River in the northeast and beyond into Louisiana and Arkansas. The Carrizo-Wilcox aquifer is classified as a major aquifer in Texas providing groundwater resources to all or part of 60 Texas counties (Ashworth and Hopkins, 1995).

Because of its large size, the Carrizo-Wilcox aquifer was divided by the TWDB for modeling purposes into three areas, with each being modeled separately. The three Carrizo-Wilcox GAMs are the Northern Carrizo-Wilcox GAM, the Central Carrizo-Wilcox GAM, and the Southern Carrizo-Wilcox GAM (Figure 2.1). These GAMs have significant overlap areas as shown in Figure 2.1. This study documents the Northern Carrizo-Wilcox GAM. The model area, shown in Figure 2.2, includes all or parts of the following Texas counties: Anderson, Angelina, Bowie, Camp, Cass, Cherokee, Franklin, Freestone, Greg, Grimes, Harrison, Henderson, Hopkins, Houston, Jasper, Leon, Limestone, Madison, Marion, Montgomery, Morris, Nacogdoches, Navarro, Newton, Panola, Polk, Rains, Red River, Robertson, Rusk, Sabine, San Augustine, San Jacinto, Shelby, Smith, Titus, Trinity, Tyler, Upshur, Van Zandt, Walker, and Wood. The model also covers all or part of several parishes in Louisiana, including Caddo, De Soto, Natchitoches, Rapides, Red River, Sabine, and Vernon, and a portion of Miller County in Arkansas.

Groundwater model boundaries typically are defined on the basis of surface or groundwater hydrologic boundaries. Figure 2.3 shows the surface outcrop and downdip subcrop of the major aquifers in the study area. The Northern Carrizo-Wilcox GAM is bounded laterally on the northeast by the Red River in Louisiana and Arkansas, and by the surface water basin divide between the Trinity and Brazos rivers in the southwest. The Trinity-Brazos basin divide serves as the model boundary in the outcrop (presumed groundwater flow divide) and was extended into the subsurface to the down-dip boundary of the model. The upper boundary of the model was defined by the ground surface in the outcrop of the Carrizo-Wilcox aquifer extending south to the extent of the Queen City outcrop. The lower boundary is the base of the Wilcox Group representing the top of the Midway Formation. The down-dip boundary of the Carrizo-

Wilcox aquifer extends past the limits of fresh water to the updip limit of the Wilcox growth fault zone (Bebout et al., 1982).

The study area encompasses parts of five regional water-planning areas (Figure 2.4). These include: (1) the North East Texas Region (Region D), (2) Region C, (3) the East Texas Region (Region I), (4) Region H, and (5) the Brazos Region (Region G). The study area includes all or parts of the following Groundwater Conservation Districts (Figure 2.5): (1) the Anderson County Underground Water Conservation District, (2) the Brazos Valley Groundwater Conservation District (3) the Neches and Trinity Valleys Groundwater Conservation District, (4) the Piney Woods Groundwater Conservation District, (5) the Bluebonnet Groundwater Conservation District, (6) the Lone Star Groundwater Conservation District, (7) the Mid-East Texas Groundwater Conservation District, and (8) the Lake Country Groundwater Conservation District.

The model area intersects five major river basins from west to east: (1) the Brazos, (2) the Trinity, (3) the Neches, (4) the Sabine, and (5) the Red River basins (Figure 2.6). In the model area, the Red River Basin has been further subdivided into the Sulphur River Basin, the Cyprus Creek Basin, and the Red River Basin. The model domain also intersects the San Jacinto River Basin, but only in the downdip portion of the model where there is no direct interaction between streams and the model. Eight river authorities (Angelina-Neches River Authority, Brazos River Authority, the Lower Neches Valley Authority, the Red River Authority, the Sabine River Authority, the San Jacinto River Authority, the Sulphur River Basin Authority, and the Trinity River Authority) are present in the study area.

Rivers and streams in the Northern Carrizo-Wilcox GAM study area are perennial and tend to gain flow from the underlying geology. Table 2.1 provides a listing of the river basins in the study area along with the river length in Texas, the river basin area in Texas, and the number of major reservoirs within the river basin in Texas (BEG, 1976).

Table 2.1 River basins in the Northern Carrizo-Wilcox GAM study area (BEG, 1996)

River Basin	Texas River Length (mi)	Texas River Basin Drainage Area (square miles)	Number of Major Reservoirs
Brazos	840	42,800	19
Trinity	550	17,696	14
Neches	416	10,011	4
Sabine	360	7,426	2
Red	680	30,823	7
San Jacinto	70	5,600	2

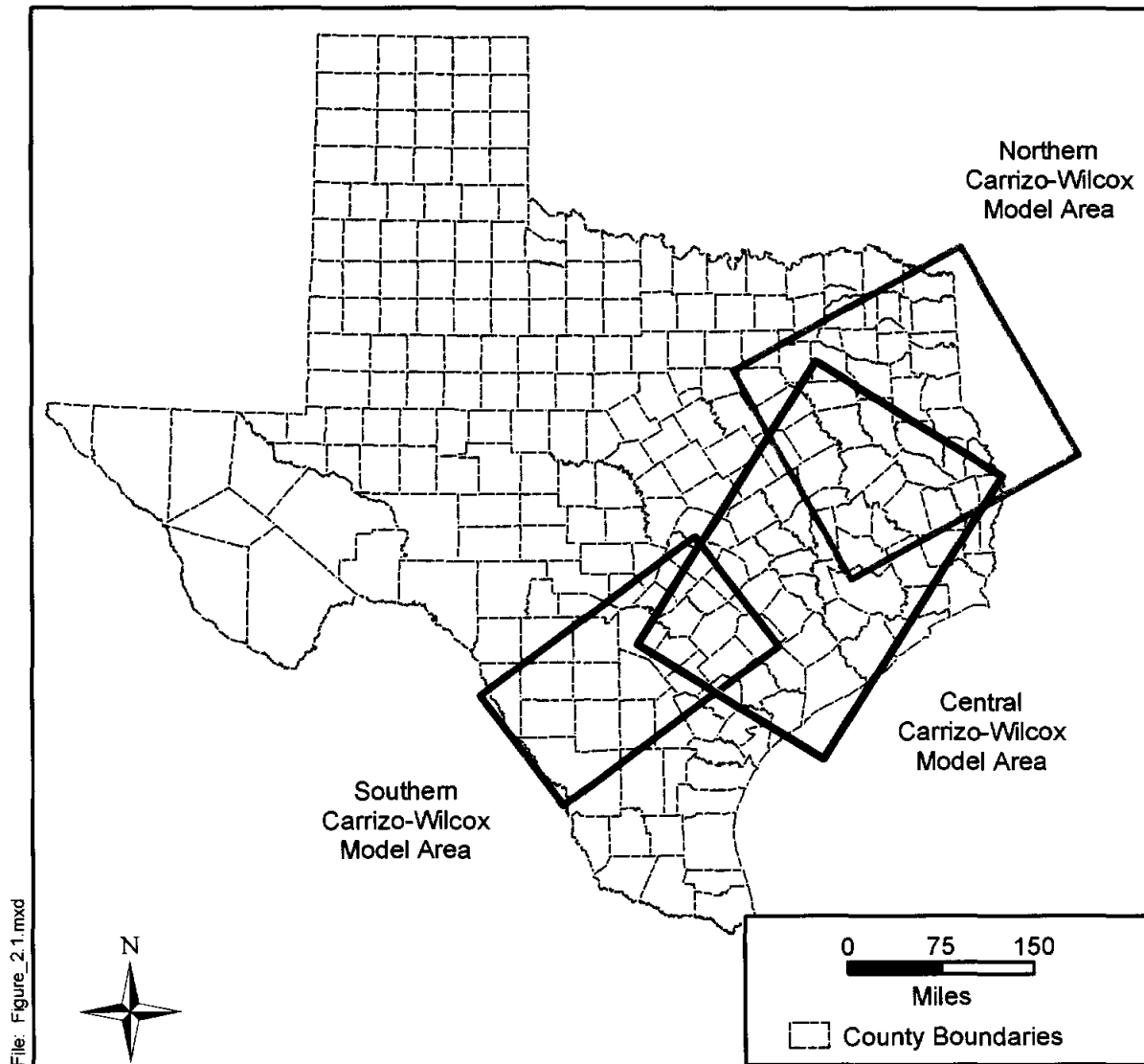


Figure 2.1 Location of the three Carrizo-Wilcox GAMs.

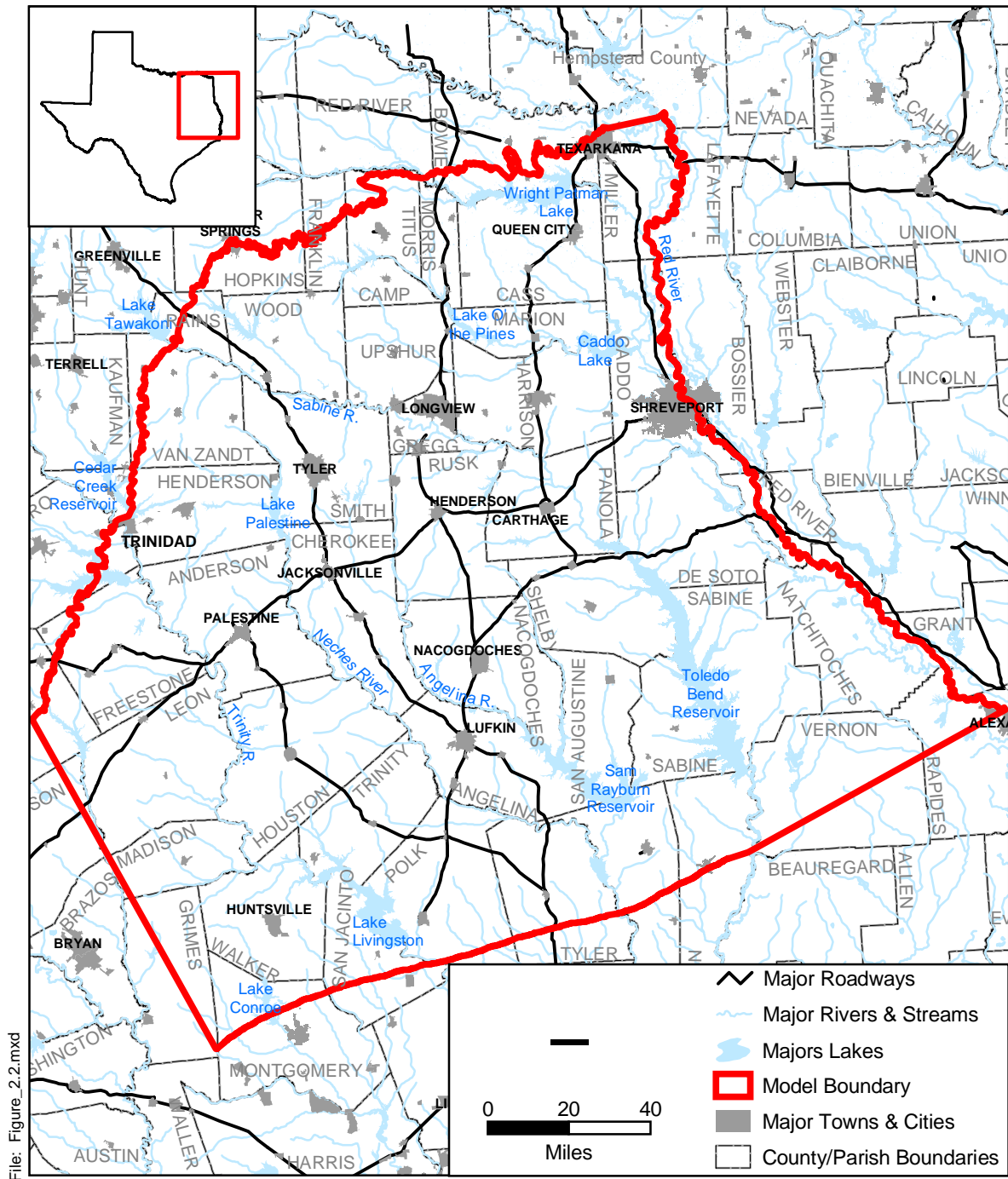
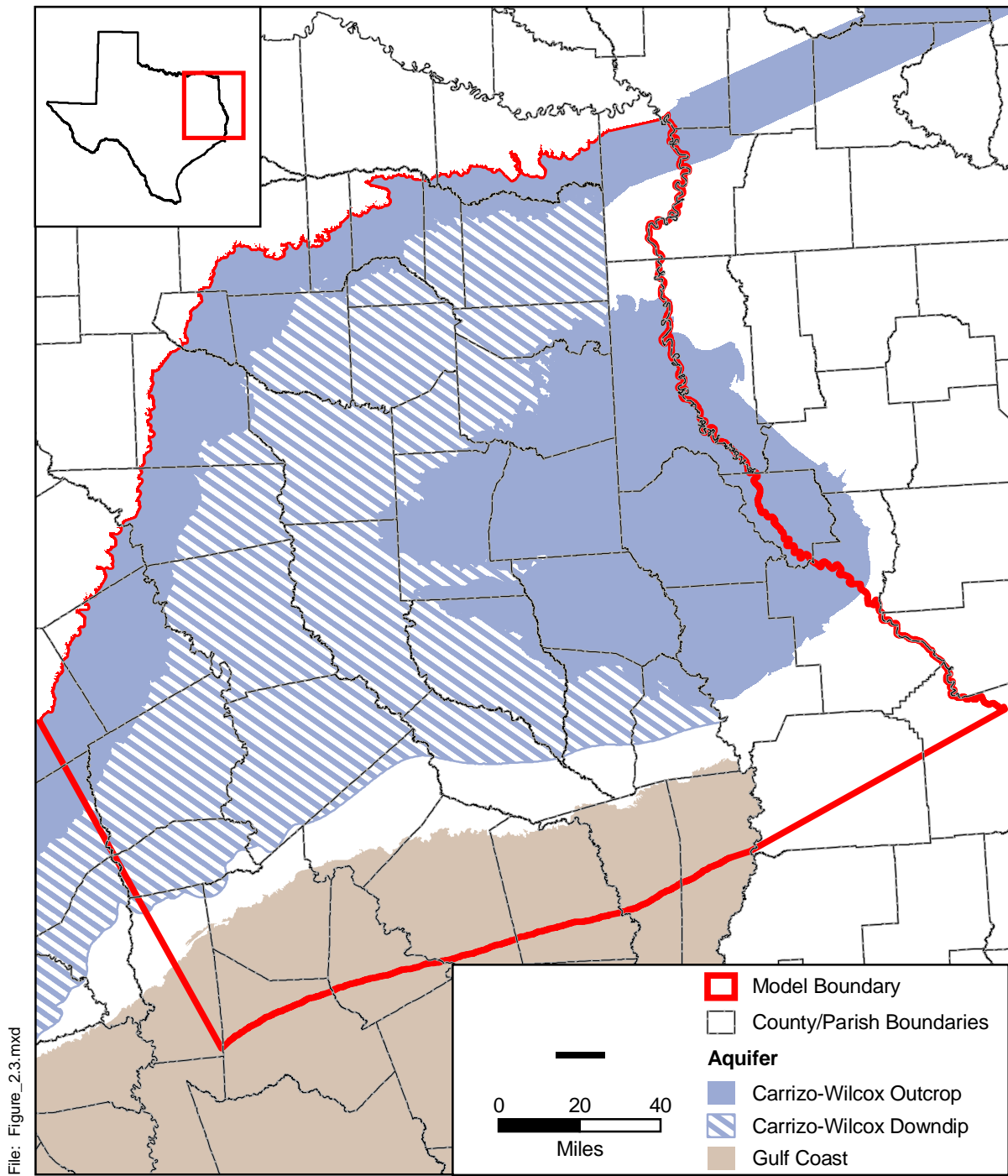
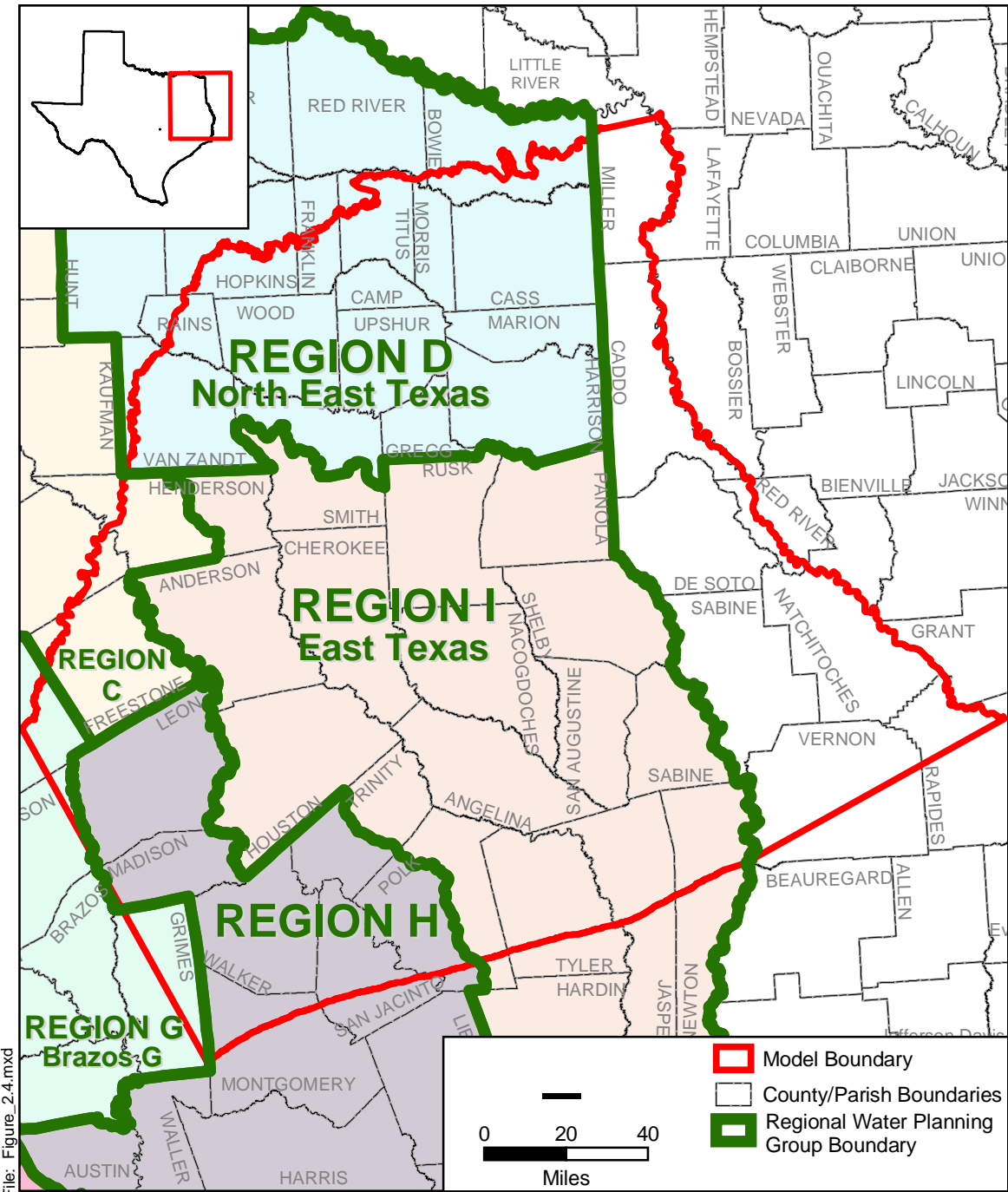


Figure 2.2 Location of study area showing county boundaries, cities, lakes, and rivers.



Source: Online: Texas Water Development Board, September 2002, Bureau of Economic Geology

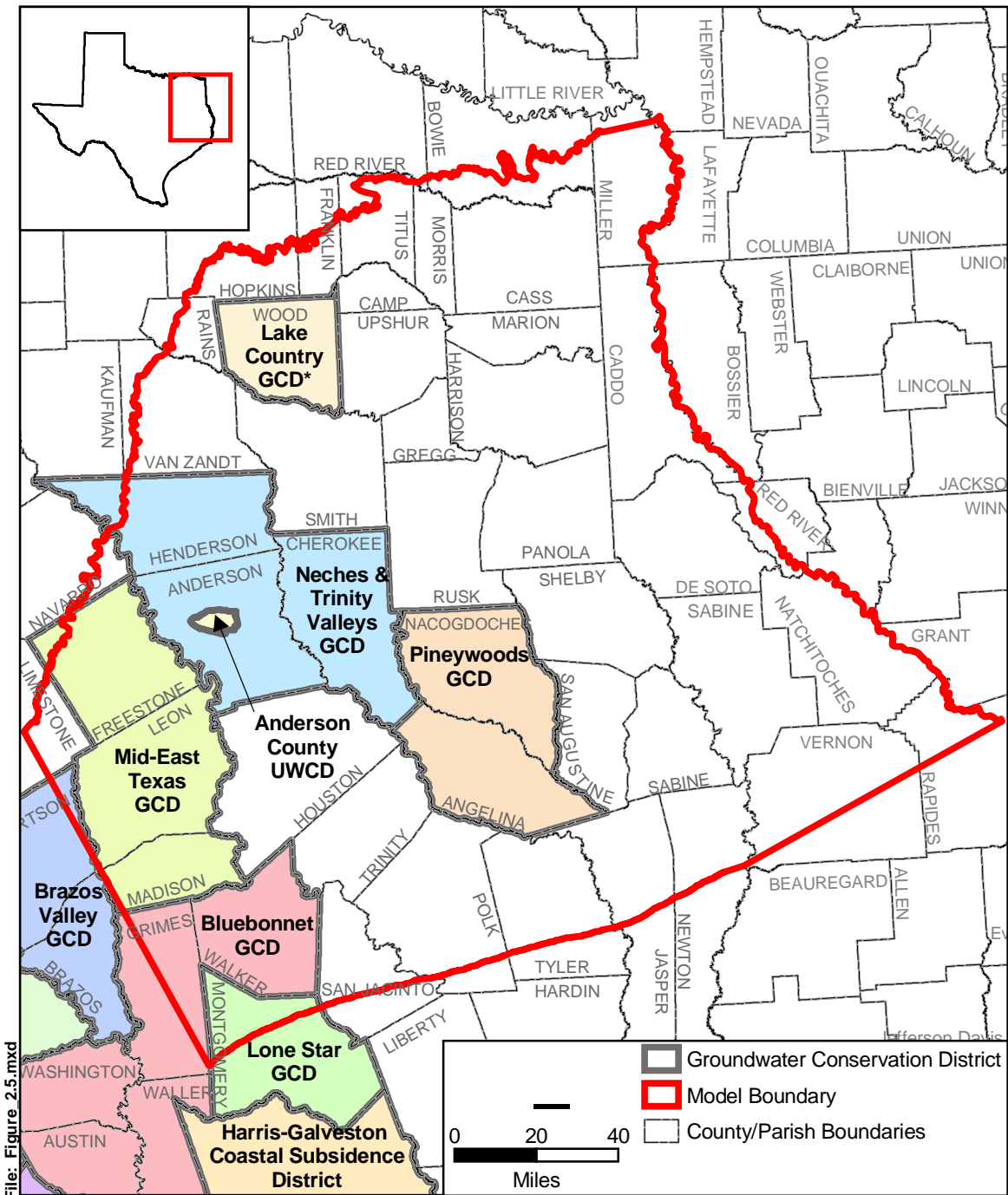
Figure 2.3 Areal extent of the major aquifers in the study area.



File: Figure_2.4.mxd

Source: Online: Texas Water Development Board, September 2002

Figure 2.4 Location of Regional Water Planning Groups in the study area.



File: Figure 2.5.mxd

*=Pending Confirmation
 UWCD=Underground Water Conservation District
 GCD=Groundwater Conservation District
 Source: Online: Texas Water Development Board, December 2002

Figure 2.5 Location of Groundwater Conservation Districts in the study area.

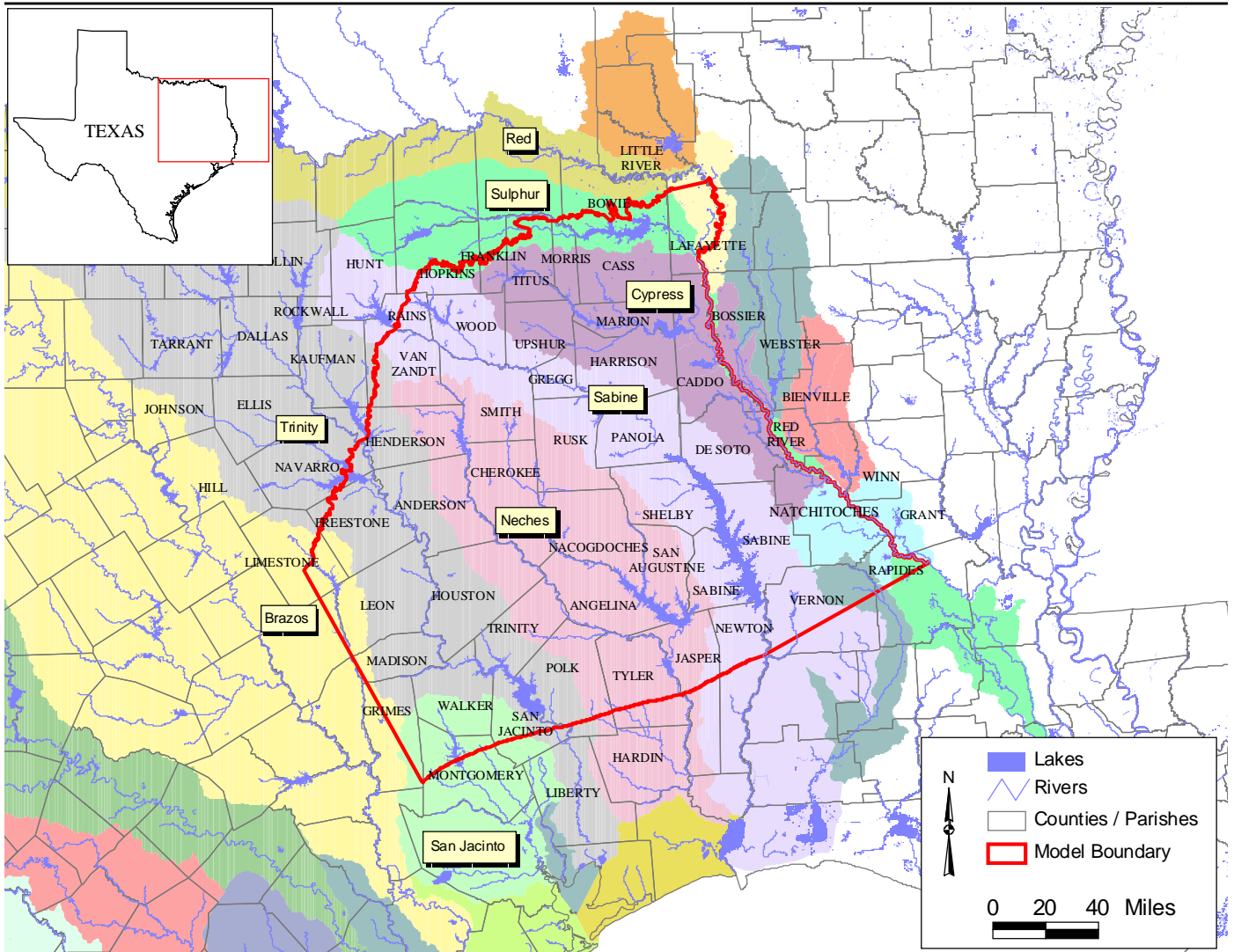


Figure 2.6 Map showing the major river basins in the study area.

2.1 Physiography and Climate

The study area is located in north-central and northeast Texas and extends into far western Louisiana and Miller County, Arkansas. The study area falls within the Gulf Coastal Plains physiographic region. The Gulf Coastal Plains region has been subdivided into several area designations based upon vegetation and topography. In the study area, these include the Piney Woods, the Oak Woods and Prairies, the Blackland Prairie, and the South-Central Plains in Arkansas and Louisiana (Figure 2.7). The Piney Woods, predominant in East Texas, are characterized as hilly with predominantly pine forests, with hardwoods occurring with pine in river valleys. The South-Central Plains region in Arkansas and Louisiana is analogous to the Piney Woods region in East Texas. In the Oak Woods and Prairies region in the western part of the study area, the terrain flattens slightly and the timber changes from pine to predominantly oak. Only small areas of Blackland Prairie extend eastward into the model area.

Figure 2.8 provides a topographic map of the study area. Ground surface elevation varies from greater than 600 feet above sea level on isolated basin divides (ridges) to less than 100 feet above sea level in river valleys and in the southeastern part of the study area. In general, ground surface elevation decreases from the northwestern portion of the study area to the east and south. Superimposed on top of this trend is significant elevation change associated with dissected stream valleys.

The climate in the northern half of the study area is generally mild with an annual average temperature of 65°F (TWDB, 2002, Region D Plan). The mean high temperature for July is 94°F and the mean low temperature for January is 32°F (TWDB, 2002, Region D Plan). In the southern half of the study area, the average maximum temperature in July is approximately 93°F and the average minimum temperature for January is 36°F (TWDB, 2002, Region I Plan). Average annual pan evaporation rates range from 58 inches per year in the western portion of the study area to as low as 38 inches per year in the northeastern portion of the study area (Figure 2.9).

For the study area, historically there have been precipitation data available at approximately 250 stations (Figure 2.10) from 1930 through 2000. The spatial distribution is relatively dense in the model domain across the period of record (Figure 2.10). However, the

number of available gages in any given year is quite variable with a general chronological increase in the number of gages available. Available precipitation gages increase from 25 in 1931 to 50 in 1942 to a high of 92 gages in the late 1960s and early 1970s. Most gages began measuring precipitation in the 1930s or 1940s. The earliest monthly precipitation records in the area extend as far back as 1930. The average period of record in the study area is 41 years and the longest is 69 years through 1999. For the period of record, the average number of gages recording precipitation in a given year is 69.

Based upon the available precipitation records, the average annual precipitation in the study area is 45.6 inches. Historical average annual precipitation varies from a low of 34.4 inches in Frost (Navarro County) to a high of 59.9 in Jasper County. The PRISM (Parameter-elevation Regressions on Independent Slopes Model) precipitation data set developed and presented online by the Oregon Climate Service at Oregon State University¹ provides a good distribution of average annual precipitation across the model area based upon the period of record from 1961 to 1990. Figure 2.11 provides a raster data post plot of average annual precipitation across the model study area. Generally, the average annual precipitation increases from west to east from a low of 36 inches per year in the western part of the study area to a high of 59 inches per year in the far southeast portion of the study area. Figure 2.12 shows annual precipitation recorded at eight representative precipitation gages representative of the model area and located in Angelina, Cherokee, Ellis, Franklin, Kaufman, Montgomery, Navarro, and Shelby counties.

¹ www.ocs.orst.edu/prism/

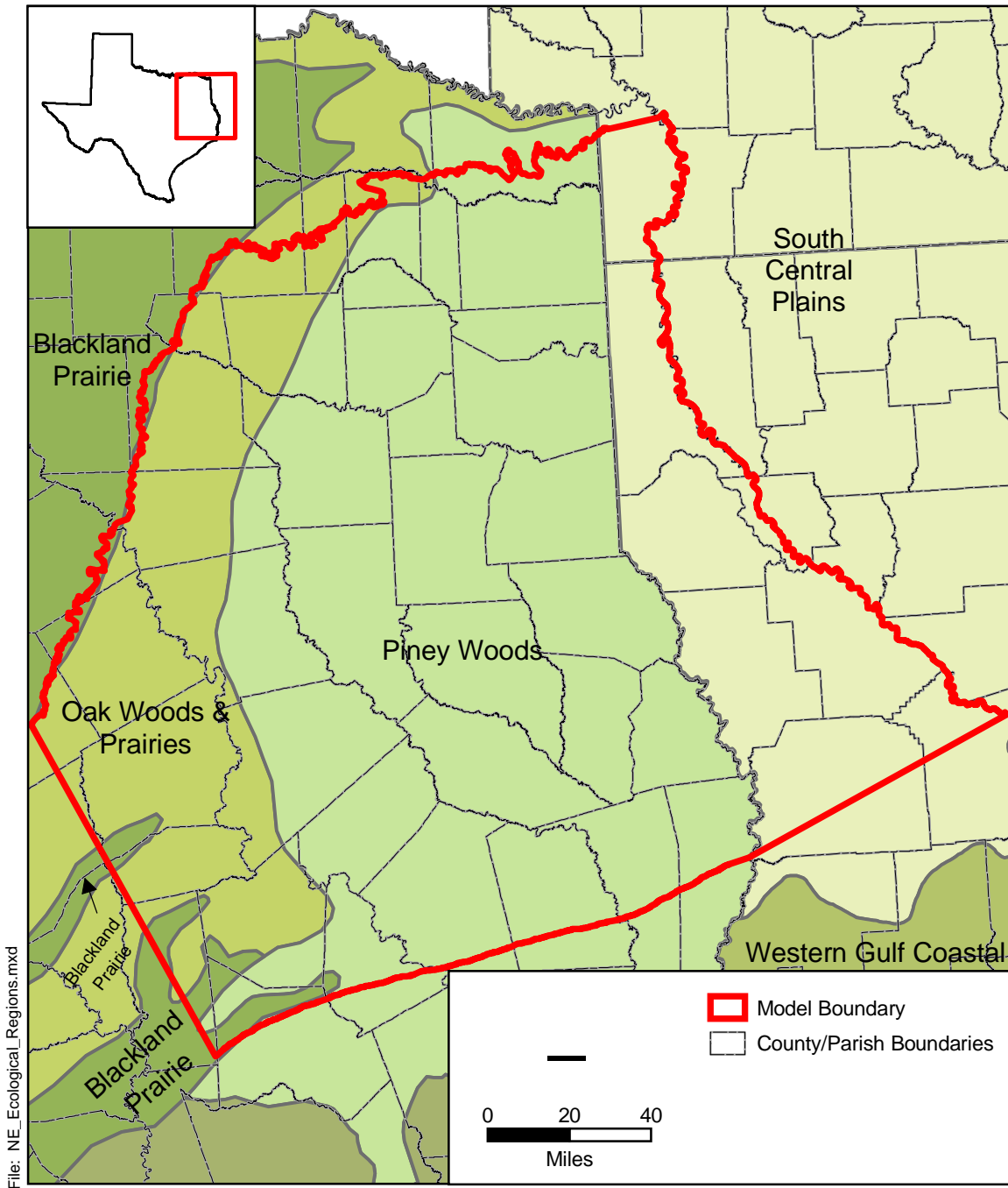


Figure 2.7 Ecological regions in the study area.

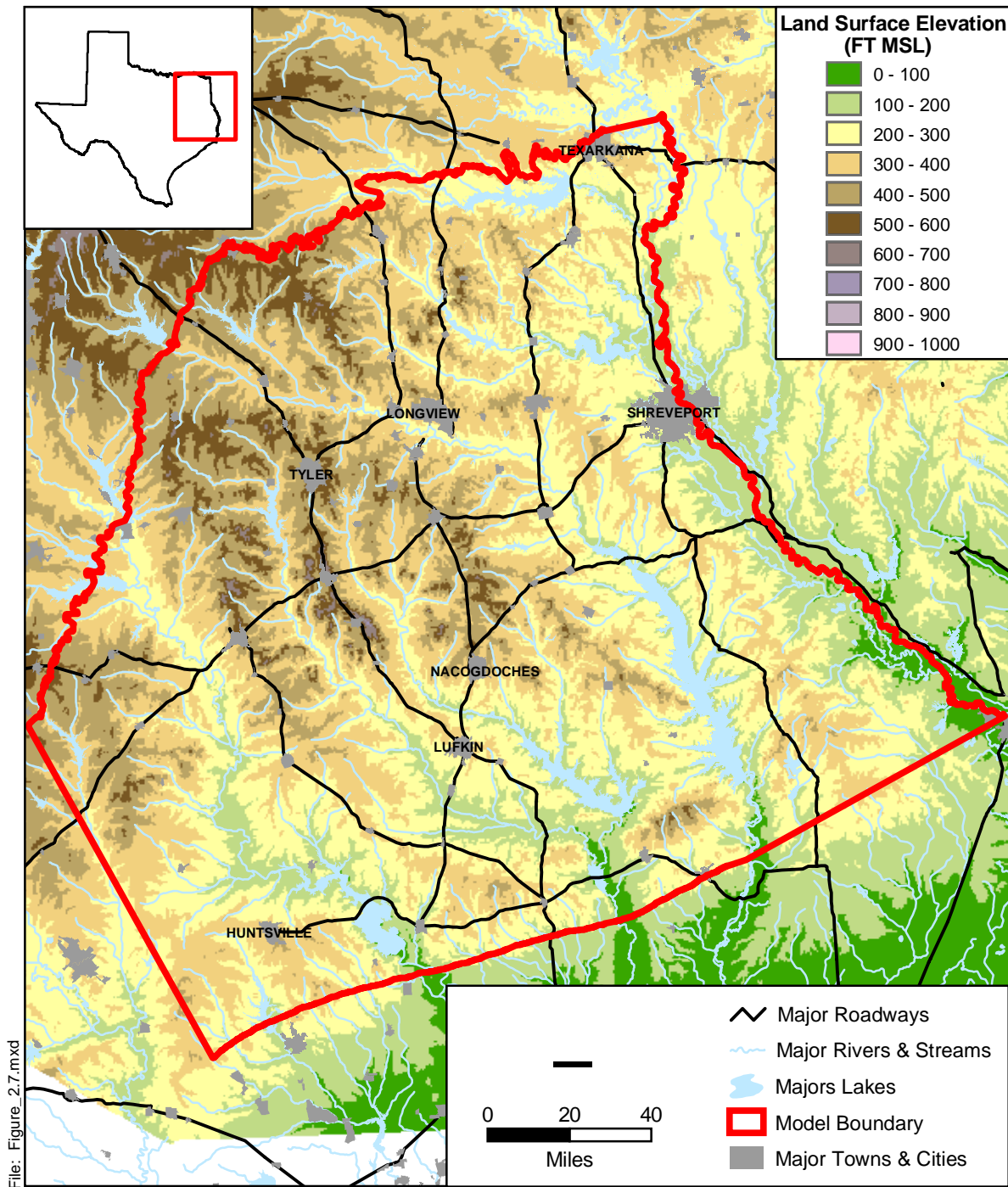
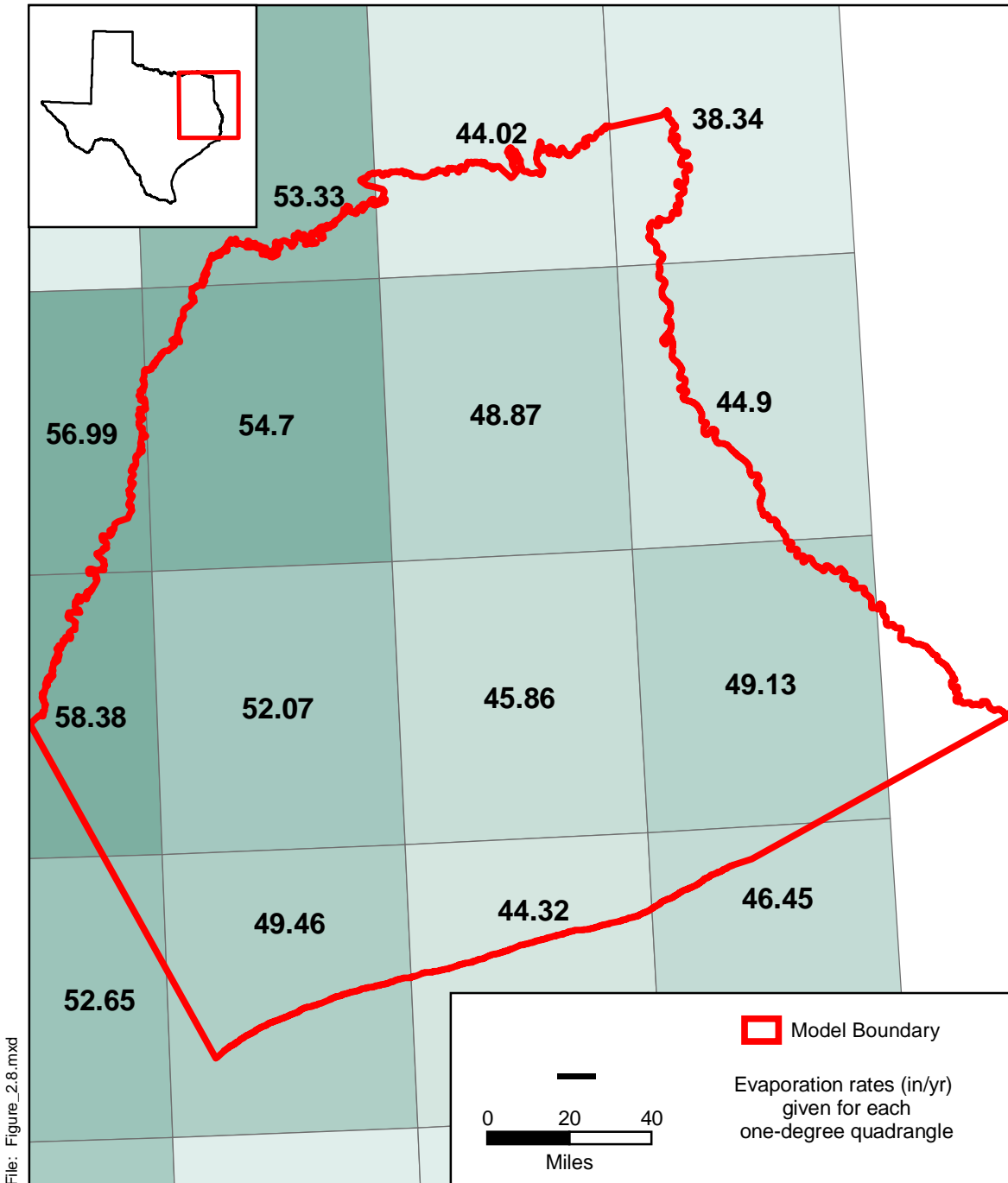
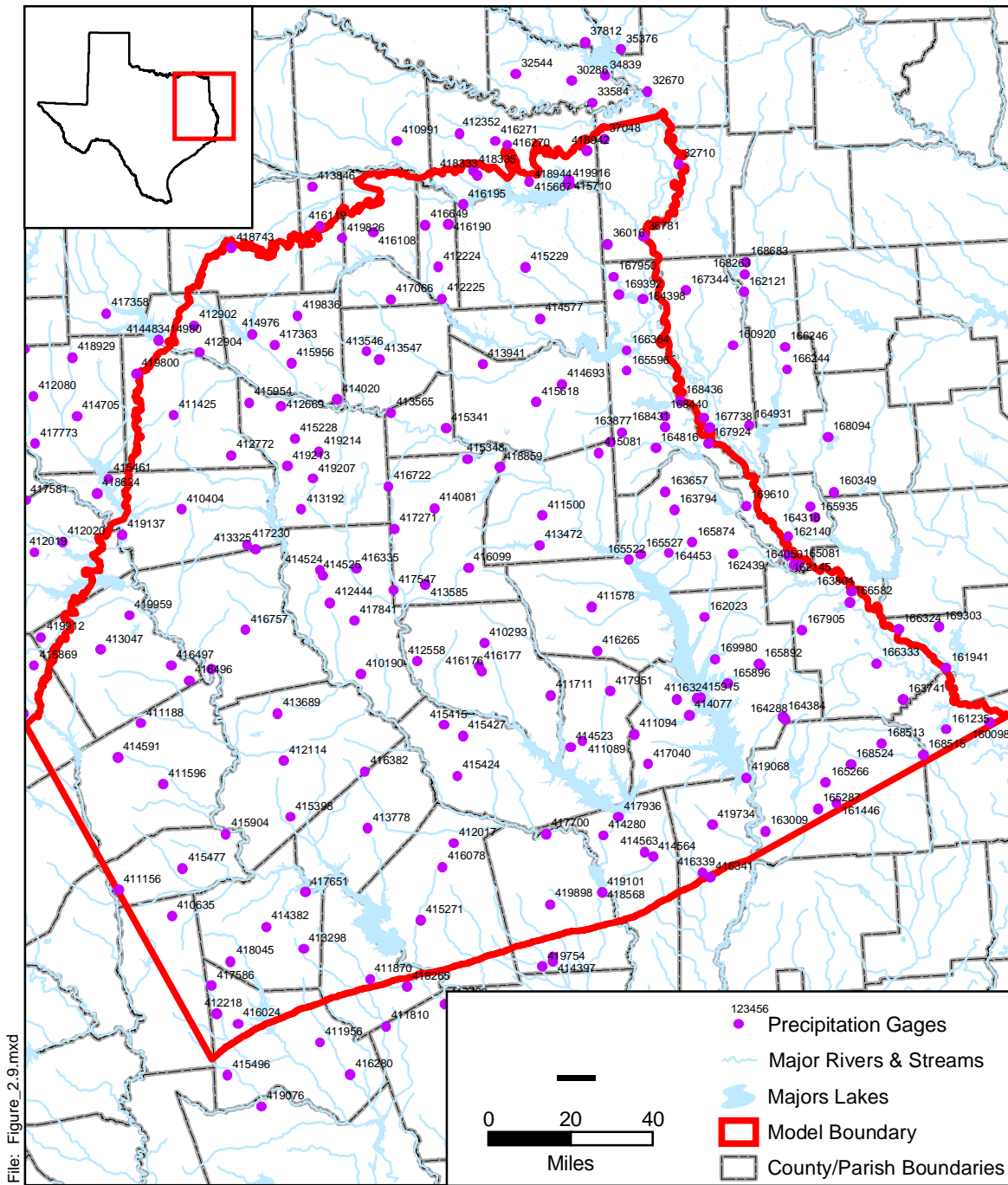


Figure 2.8 Topographic map of the study area.



Source: Online: Texas Water Development Board, September 2002

Figure 2.9 Average pan evaporation rate, in inches per year, in the study area.



Source: Online: National Climatic Data Center

Figure 2.10 Location of precipitation gages in the study area (Period of Record is 1900 to 1999).

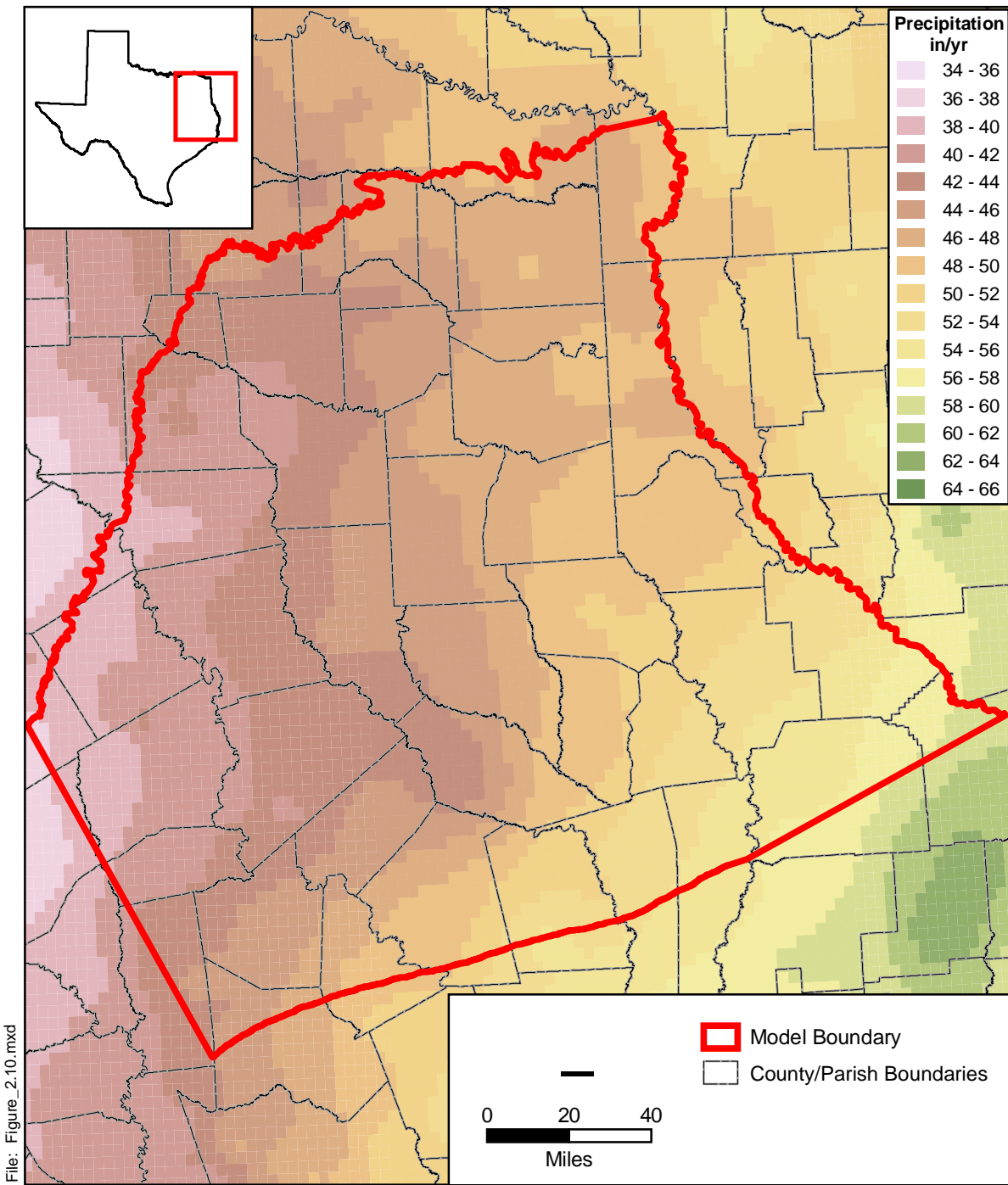


Figure 2.11 Average annual precipitation (1961-1990) over the study area in inches per year (Source: Oregon Climate Service, Oregon State University, PRISM data set).

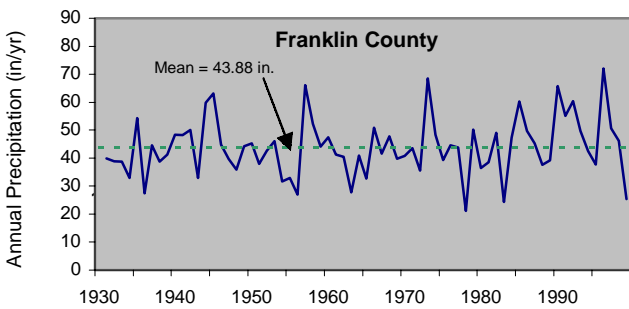
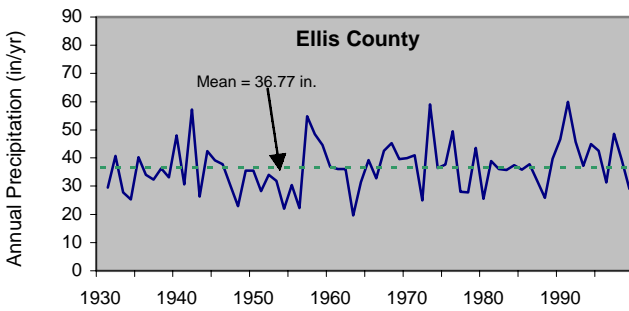
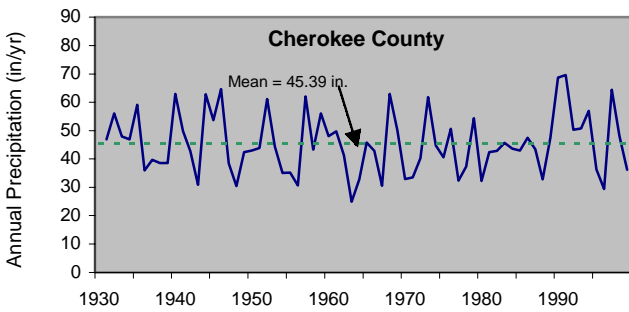
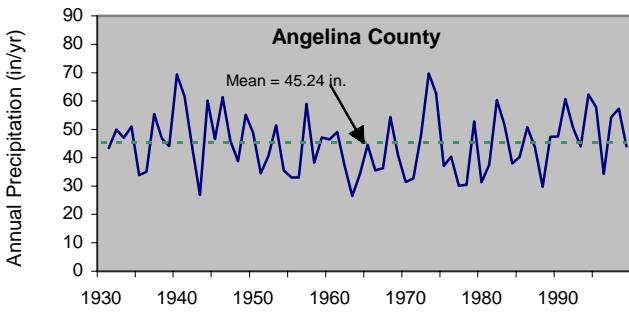


Figure 2.12a Annual precipitation time series for gages in Angelina, Cherokee, Ellis, and Franklin counties (Source: National Climatic DataCenter, Texas Natural Resources Information System).

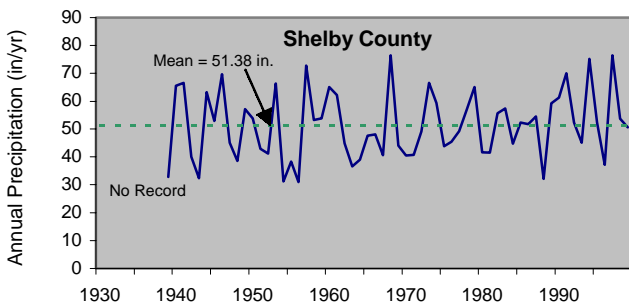
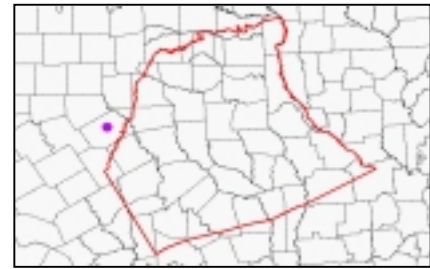
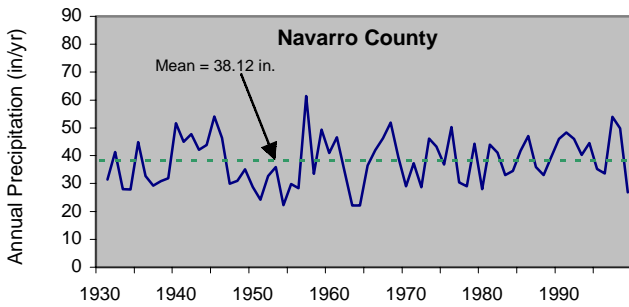
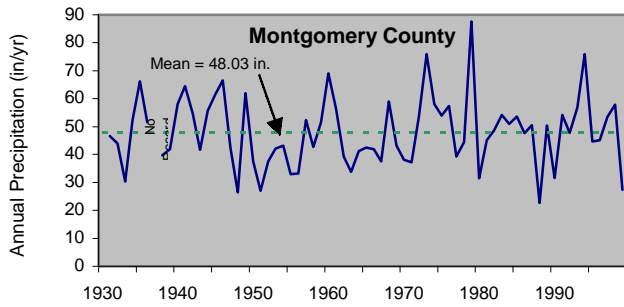
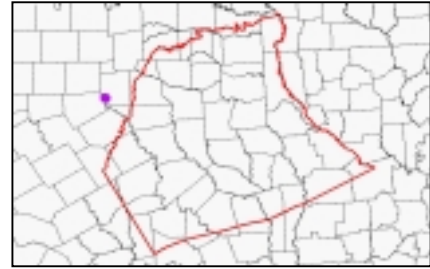
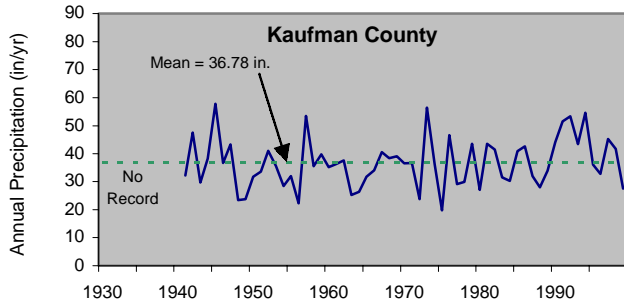


Figure 2.12b Annual precipitation time series for gages in Kaufman, Montgomery, Navarro, and Shelby counties (Source: National Climatic DataCenter, Texas Natural Resources Information System).

2.2 Geology

The sediments that form the aquifers in the study area are part of a gulf-ward thickening wedge of Cenozoic sediments deposited in the East Texas Basin and the Houston Embayment of the Gulf Coast Basin. Deposition has been influenced by regional crust subsidence, episodes of sediment inflow from areas outside of the Gulf Coastal Plain, and eustatic sea-level change (Grubb, 1997). Galloway et al. (1994) characterized Cenozoic sequences in the Gulf Coast with the following three characteristics. Deposition of Cenozoic sequences is characterized as an offlapping progression of successive, basinward thickening wedges. These depositional wedges aggraded the continental platform and prograded the shelf margin and continental slope from the Cretaceous shelf edge to the current Southwest Texas coastline. Deposition occurred along sand-rich, continental margin deltaic depocenters within embayments (Rio Grande, Houston, and Mississippi Embayments) and was modified by growth faults and salt dome development.

The primary Paleogene depositional sequences in ascending stratigraphic order are the lower Wilcox, the upper Wilcox, the Carrizo, the Queen City, the Sparta, the Yegua-Cockfield, the Jackson, and the Vicksburg-Frio (Galloway et al., 1994). Each of these depositional sequences is bounded by marine shales and finer grained sediments representing transgressions (i.e., Reklaw and Weches formations).

Figure 2.13 shows a geologic map of the area showing the Tertiary sediments comprising the aquifers of interest in this study as well as the Quaternary undivided sediments. The Carrizo and Wilcox sediments outcrop along a belt extending along the northern extent of the study area. The Wilcox, and to a lesser degree the Carrizo, also outcrop on the Sabine Uplift in the eastern portion of the model in East Texas and extending eastward into Louisiana. The Queen City and Sparta Sand formations are at ground surface across the majority of the East Texas Basin. South of the Sabine Uplift, the surface geology and outcrop pattern are oriented southwest-northeast coincident with depositional strike, the paleo-shelf, and perpendicular to basin subsidence.

Figure 2.14 shows a representative stratigraphic section for the Carrizo-Wilcox aquifer in Texas. The Carrizo-Wilcox aquifer extends from south Texas northeastward through East Texas into Arkansas and Louisiana. The aquifer consists of fluvial-deltaic sediments of the upper Paleocene and lower Eocene Wilcox Group and Carrizo Sand. The aquifer is underlain by

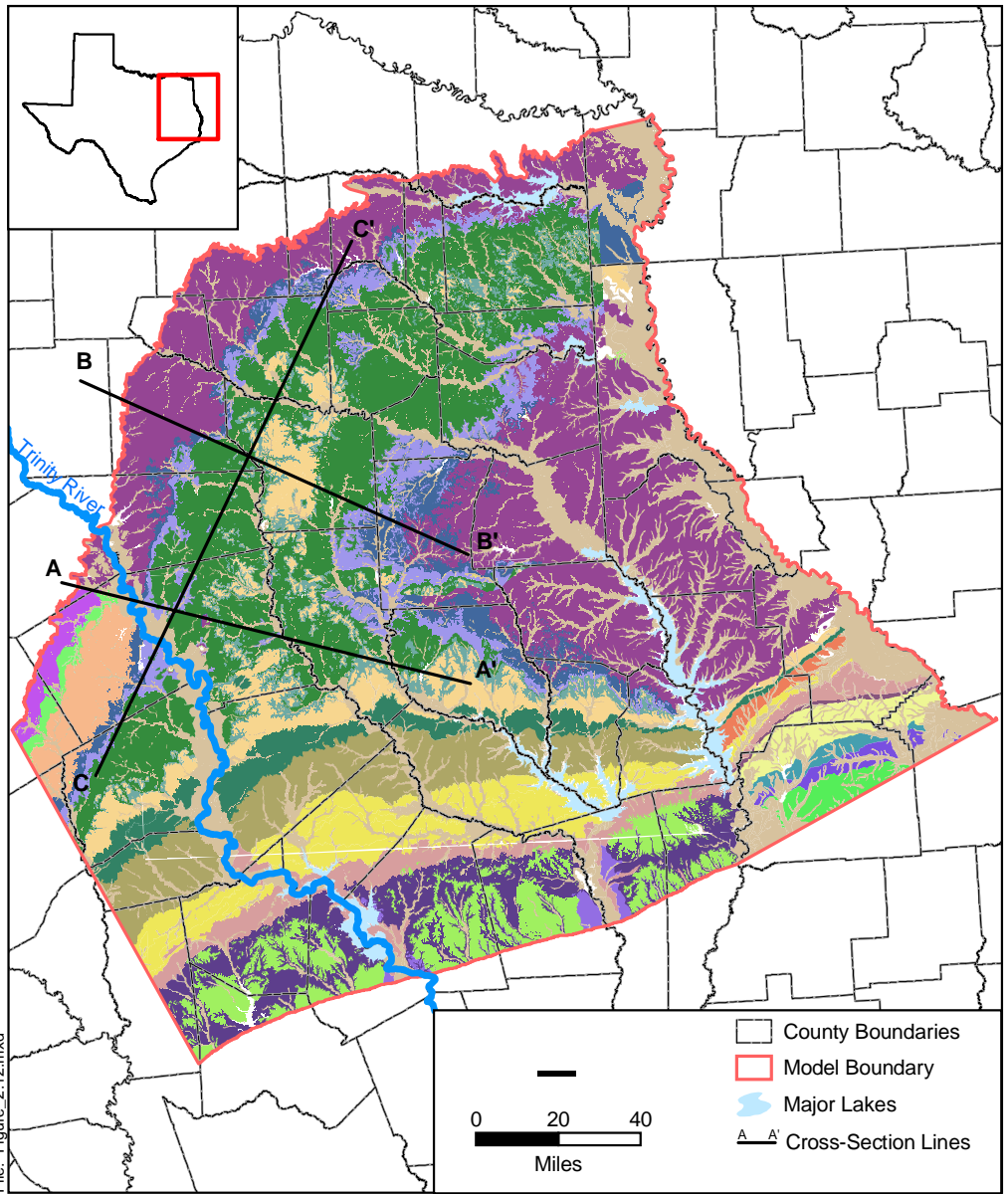
marine deposits of the Midway Group and overlain by the Reklaw Formation, representing a semi-confining unit between the Carrizo Sand and the shallow aquifer of the Queen City Formation.

The complexity of the hydrostratigraphy in the East-Texas Basin is shown in a set of cross-sections by Fogg and Kreitler (1982) together with the inferred groundwater flow patterns (Figure 2.15). The traces of the different sections are indicated in Figure 2.13.

In the western portion of the study area, the Wilcox Group is subdivided into the Hooper, the Simsboro, and the Calvert Bluff formations, corresponding to deltaic, fluvial, and fluvial-deltaic facies, respectively, which occur throughout east-central Texas (Kaiser, 1974). In the Sabine Uplift area, east of the Trinity River, the Simsboro is no longer identifiable and the Wilcox is divided informally into a lower and an upper unit (Kaiser, 1990). The lower Wilcox represents the facies equivalent of the Hooper Formation and the upper Wilcox includes both of the Simsboro and the Calvert Bluff equivalent fluvial and fluvial-deltaic facies, respectively (Kaiser, 1990). The Carrizo Sand unconformably overlies the Wilcox Group and is separated from the Wilcox by a thin regional marine-transgressive unit, which is included as an informal member in the upper Wilcox (Kaiser, 1990). The Carrizo Sand is composed primarily of relatively homogenous fluvial sands and only locally and in the northernmost area contains a significant portion of interbedded muds. The Reklaw Formation consists of variable amounts of mud and sand and is considered the upper confining stratum of the Carrizo-Wilcox aquifer. In the northeastern part the study areas, the Reklaw clays become discontinuous providing a more permeable connection between the Carrizo sand and the overlying Queen City Formation. In Marion and Harrison counties, the combined Wilcox, Carrizo, Reklaw, and Queen City are collectively referred to as the Cypress aquifer (Fogg and Kreitler, 1982). Above, the finer grained Weches Formation separates the Queen City Sand from the overlying Sparta Sand that occurs only locally in the study area.

The Carrizo is a fairly homogeneous sand unit overlying the thicker, more heterogeneous Wilcox Group. The Wilcox Group is a multi-aquifer system composed of fluvial channel sand distributed within the lower permeability interchannel sands and clays. In the study area, the Wilcox Group consists of up to 3,000 ft of interbedded lenticular sands, mud, and lignite. Sand layers constitute about 50 percent of the total Wilcox with thickness ranging from a few feet to

about 200 ft, consisting of fine grained to coarse grained quartz sand with various amounts of silt and clay. Fisher and McGowen (1967) mapped the net-sand distributions of the Wilcox Group in northeast Texas, identifying a dendritic pattern of north-south trending high net-sand channels feeding the principal delta systems of the ancestral Gulf of Mexico. Kaiser et al. (1978) refined the spatial pattern of major sand channels of the fluvial system in the combined Wilcox Group north of Houston, Angelina, and Nacogdoches counties. More recently, Kaiser (1990) mapped maximum sands (single thickest sand) and major sand (any sand of at least 40 ft thickness) to better identify the major continuous channel sands and exclude thinner and less continuous splay and overbank sands. Kaiser's 1990 study area was limited to the area surrounding the Sabine uplift and could not be combined with the earlier net-sand maps of Kaiser et al. (1978). However, the major and maximum sand maps showed similar dendritic patterns as the earlier net-sand maps. For this study, the net-sand map by Kaiser et al. (1978) was combined with the original net-sand map of Fisher and McGowen (1967) covering the southern part of the study area to produce a net-sand map for the entire model area, which is described in detail in Section 4.



West of Trinity River	East of Trinity River	Louisiana
	Quaternary Deposits	Cockfield Formation
	Lisie Formation	Blounts & Castor Creek Member
	Beaumont/Catahoula Formation	Williamson Creek Member
	Fleming Formation	Dough Hills Member
	Jackson Group	Carnahan Bayou Member
	Yegua Formation	Lena Member
	Cook Mtn. & Stone City Form.	
	Sparta Formation	
	Weches Formation	
	Queen City Sand	
	Reklaw Formation	
	Carrizo Sand	
	Wilcox Group	
	Midway Group	
Calvert Bluff Formation		
Simsboro Formation		
Hooper Formation		

Figure 2.13 Surface geology of the study area.

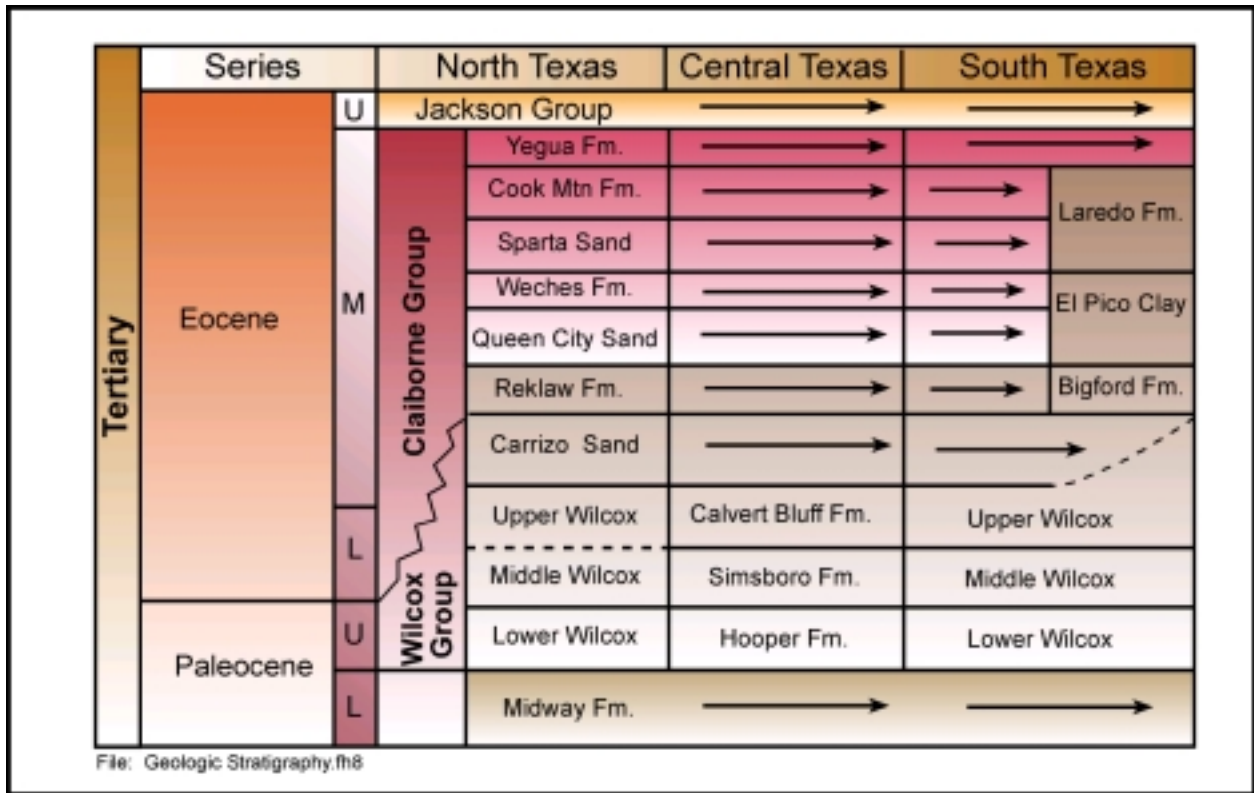


Figure 2.14 Generalized stratigraphic section for the Carrizo-Wilcox aquifer in Texas (after Ayers and Lewis, 1985; Hamlin, 1988; Kaiser et al., 1978).

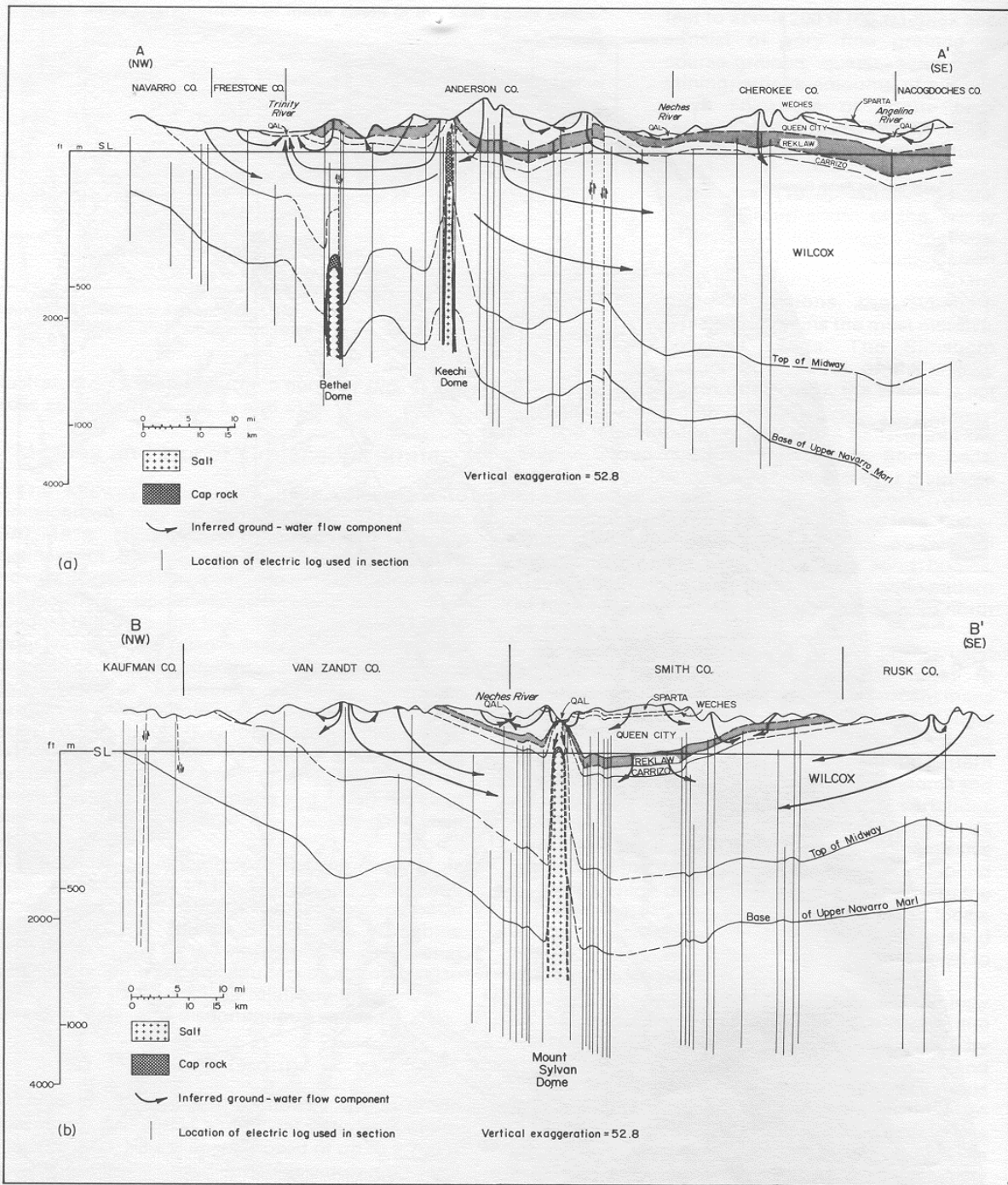


Figure 2.15a Structural cross sections A-A' and B-B' showing the major hydrostratigraphic units in the East Texas Basin from Fogg and Kreitler (1982), indicating general groundwater flow patterns. Cross-section locations are shown on Figure 2.13.

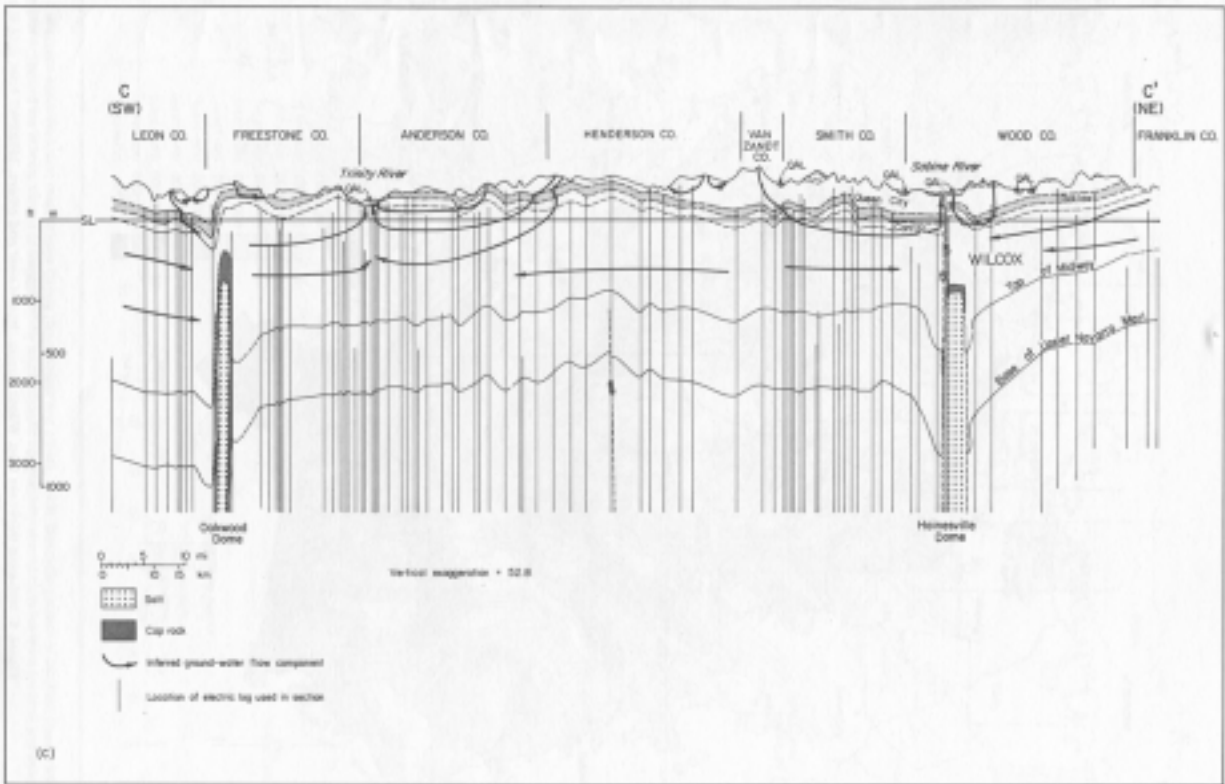


Figure 2.15b Structural cross section C-C' showing the major hydrostratigraphic units in the East Texas Basin from Fogg and Kreitler (1982), indicating general groundwater flow patterns. Cross-section location is shown on Figure 2.13.

3.0 PREVIOUS INVESTIGATIONS

The northern Carrizo-Wilcox aquifer has been studied by many investigators (see Table 3.1) and numerous groundwater bulletins have been prepared by the Texas Water Development Board for the counties in the study area. The East Texas Basin in particular has been the focus of extensive study by the Bureau of Economic Geology when the East Texas salt domes were being considered for their suitability in isolating high-level radioactive waste. Of these, the studies which are most relied on in this report are Kaiser (1974), Kaiser et al. (1978), Fogg and Kreitler (1982), Fogg et al. (1983), and Kaiser (1990).

Table 3.1 Previous groundwater models of the Carrizo-Wilcox aquifer in the study area.

Model	Code	No. of Carrizo-Wilcox Layers	Calibration	Predictive Simulations
Garza (1975)	Unknown	Unknown	Unknown	Unknown
Fogg et al. (1983)	TERZAGI	3	Steady-state	No
Ryder (1988)	Research	2	Steady-state	No
Williamson et al. (1990)	Research	2	Steady-state (1980)	No
Ryder & Ardis (1991)	Research	2	Steady-state (1910) Transient (1910-1982)	Yes
Thorkildsen and Price (1991)	Unknown	Unknown	Unknown	Unknown
TWDB East-Texas Model (unpublished)	MODFLOW	4	Steady-state (1985) Transient	2050
Harden and Assoc. (2000)	MODFLOW	5	Steady-state (1950) Transient (1950 -1998)	50 year

Kaiser (Kaiser, 1974; Kaiser et al., 1978; and Kaiser, 1990) studied the sand geometry and lignite occurrence in the Paleocene-Eocene of East Texas. He investigated the stratigraphy and structure of the Wilcox Group which included the mapping of sand thickness, maximum sand thickness, and sand percent across a large portion of the model study area. Fogg and Kreitler (1982) studied the hydraulics and geochemical facies of the Eocene aquifers of East Texas. They extensively investigated the hydrogeologic setting, aquifer hydraulics, and groundwater chemistry. From a synthesis of this data, they made conclusions regarding aquifer flow and inter-aquifer flow dynamics.

Fogg et al. (1983) developed a detailed three-dimensional groundwater flow model in the area surrounding Oakwood Dome, located in southeast Freestone County and north-central Leon County. This modeling study is briefly discussed below with other groundwater flow models

which have been developed for the Carrizo-Wilcox aquifer in the Northern Carrizo-Wilcox GAM study area. Figure 3.1 shows the model boundaries for the Northern Carrizo-Wilcox GAM as it relates to previous modeling study boundaries. Table 3.1 lists these previous investigations along with some basic model characteristics to provide a basis for the following discussion.

Garza (1975) developed the earliest Carrizo-Wilcox model in the study area evaluating the effects of a proposed reservoir on groundwater conditions in the Carrizo-Wilcox aquifer and Trinity River Alluvium. Fogg et al. (1983) developed a three-dimensional model of the Carrizo-Wilcox aquifer in Leon and Freestone counties in the Trinity River Basin. The model used was an integrated finite difference code called TERZAGI. The major contribution of this study was the investigation of methods for developing effective grid block hydraulic conductivities for the heterogeneous stacked channel sequences which typify the Wilcox Group in East Texas. This model also performed a detailed sensitivity analysis to better understand the plausible ranges of vertical and horizontal hydraulic conductivities, vertical to horizontal anisotropy ratios, and the hydraulic conductivity of the Reklaw Formation.

The United States Geological Survey (USGS) has developed super-regional models which incorporate the entire Carrizo-Wilcox aquifer in Texas (Ryder, 1988; Ryder and Ardis, 1991) and in the entire Gulf Coast Region (Williamson et al., 1990) as part of the RASA (Regional Aquifer-System Analysis) studies. Their analyses modeled from the Midway Formation through the Gulf Coast aquifer systems. The Carrizo-Wilcox aquifer was modeled as two layers, generally a lower and middle Wilcox aquifer and a upper Wilcox and Carrizo aquifer. Ryder (1988) reported that the model objectives were to define the hydrogeologic framework and hydraulic characteristics of the Texas coastal plain aquifer systems, delineate the extent of freshwater and density of saline water in the various hydrogeologic units, and describe the regional groundwater flow system. A steady-state calibration to predevelopment conditions was performed using a research code developed by Kuiper (1985).

The entire U.S. Gulf Coast aquifer system above the Midway Formation was modeled by Williamson et al. (1990) using the research code developed by Kuiper (1985). The model consisted of a steady-state calibration to predevelopment conditions, a steady-state calibration to 1980 water-level data, and transient simulations from 1935 to 1980. The model objectives were “to help in the development of quantitative appraisals of the major groundwater systems of the

United States, and to analyze and develop an understanding of the groundwater flow system on a regional scale, and to develop predictive capabilities that will contribute to effective management of the system”.

Ryder and Ardis (1991) extended the work performed by Ryder (1988) and developed another model of the coastal plain aquifers in Texas. The model, developed using the research code developed by Kuiper (1985), was calibrated to both steady-state predevelopment conditions and transient conditions from 1910 to 1982. In addition, transient predictive simulations were performed using the calibrated model. The objectives for the modeling study consisted of (1) defining the hydrogeologic framework and hydraulic characteristics of the aquifer systems, (2) delineating the extent of fresh to slightly saline water in various hydrogeologic units, (3) describing and quantifying the groundwater flow system, (4) analyzing the hydrologic effects of man’s development on the flow system, and (5) assessing the potential of the aquifer systems for further development.

Thorkildsen and Price (1991) modeled the Carrizo-Wilcox aquifer in the northern Carrizo-Wilcox aquifer study area but only model results were documented. R.W. Harden and Associates (2000) developed a Carrizo-Wilcox aquifer model in support of the Brazos Regional Water Plan (Region G). This model was developed using MODFLOW and divided the Carrizo-Wilcox into five layers including the Newby Formation. The purpose of the model was to provide a first-order analysis to confirm Carrizo-Wilcox groundwater availability as it was defined in the Regional Water Planning Group Region G plan. The model was calibrated to steady-state conditions in 1950 and transient conditions from 1950 to 1998 and was used to perform predictive simulations through 2050. The TWDB developed an unpublished model called the East Texas Model in 2000. This model was developed to improve understanding of groundwater availability in East Texas.

Each of these models provides information which is both relevant and useful to the study of groundwater availability in the northern Carrizo-Wilcox aquifer study area. However, many traits of the previous investigations have made development of the current GAM necessary to meet the GAM specifications defined by the TWDB. Specifically, GAM models are expected to (1) be well documented and publicly available, (2) utilize standard modeling tools which are

non-proprietary (MODFLOW), and (3) be calibrated both in steady-state and transiently and capable of adequately simulating a verification period following a calibration period.

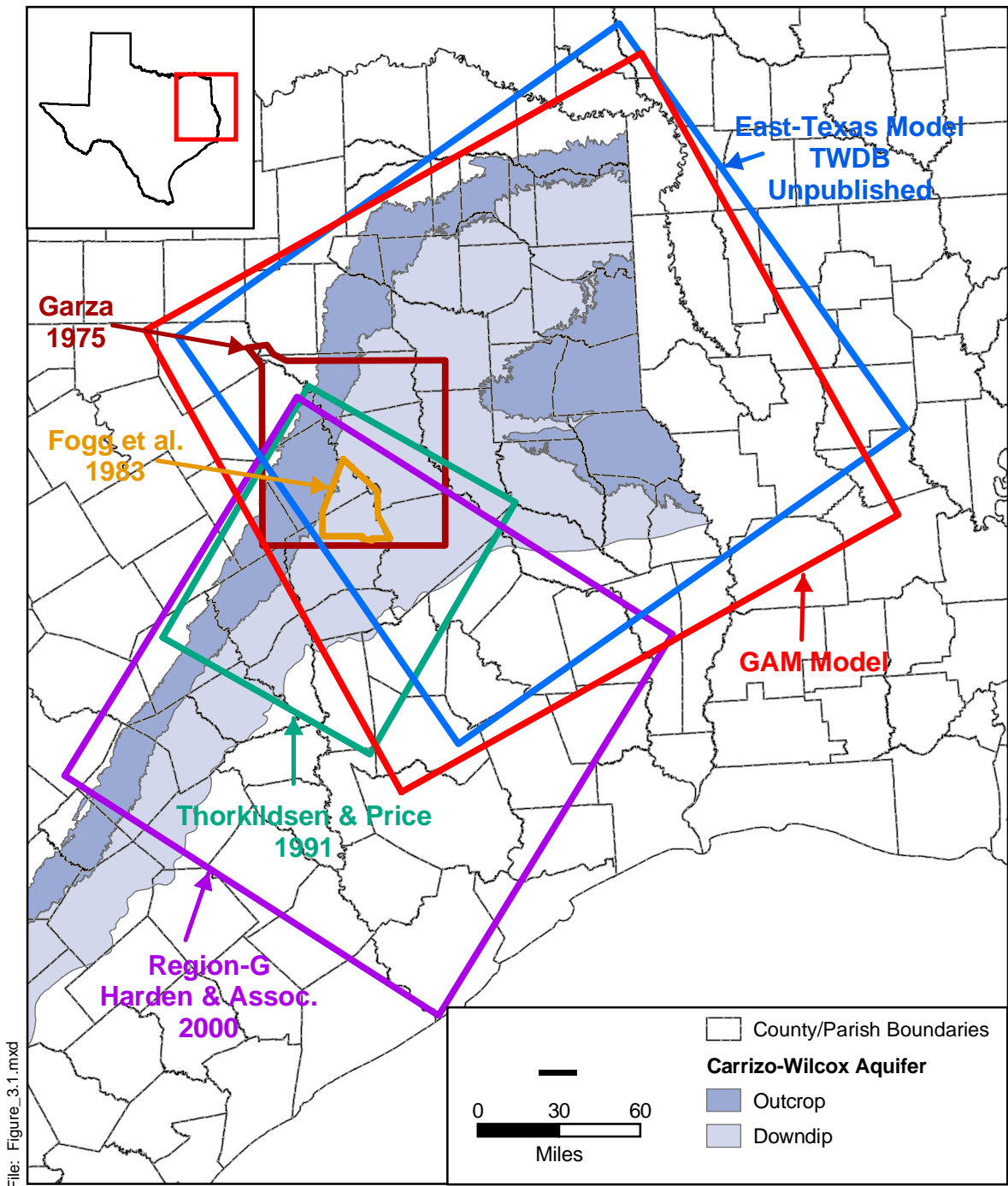


Figure 3.1 Northern Carrizo-Wilcox GAM boundary with previous modeling study boundaries which have included the Carrizo-Wilcox aquifer.

4.0 HYDROGEOLOGIC SETTING

The hydrogeologic setting of the Carrizo-Wilcox aquifer is defined by the hydrostratigraphy, hydraulic properties, structure, regional groundwater flow, surface and groundwater interaction, and recharge and discharge. The characterization of the hydrogeologic setting is based on previous geologic and hydrologic studies in the area and detailed compilation and analyses of structure maps, hydraulic properties, water-level data, spring and stream flow data, and climatic information.

4.1 Hydrostratigraphy

The Carrizo-Wilcox aquifer extends from south Texas northeastward through east Texas into Arkansas and Louisiana. The aquifer consists of fluvial-deltaic sediments of the upper Paleocene and lower Eocene Wilcox Group and Carrizo Sand. The aquifer is bounded below by marine deposits of the Midway Group and above by the Reklaw Formation, representing a semi-confining unit between the Carrizo Sand and the shallow aquifer of the Queen City Formation.

The northern model area extends from the groundwater divide between the Brazos and Trinity rivers to the Red River. In the western portion of the study area, the Wilcox Group is subdivided into the Hooper, Simsboro, and Calvert Bluff formations, corresponding to deltaic, fluvial, and fluvial-deltaic facies, respectively, which occur throughout east-central Texas (Kaiser, 1974). In the Sabine Uplift area, east of the Trinity River, the Simsboro is no longer identifiable and the Wilcox is divided into informal lower and upper units. The lower Wilcox represents the facies equivalent of the Hooper Formation and the upper Wilcox includes both the Simsboro and the Calvert Bluff equivalent fluvial and fluvial-deltaic facies, respectively (Kaiser, 1990). Even though the structure and various sand maps in the Sabine uplift area distinguish only the upper and lower Wilcox (Kaiser, 1990), a predominantly fluvial facies at the bottom and a fluvial-deltaic facies at the top can be identified within the upper Wilcox corresponding to the subdivision of the Wilcox Group in Central Texas as mapped by Ayers and Lewis (1985).

The Carrizo Sand unconformably overlies the Wilcox Group and is separated from it by a thin regional marine-transgressive unit, which is included as an informal member in the upper Wilcox (Kaiser, 1990). The Carrizo Sand is composed primarily of relatively homogenous

fluvial sands and only locally and in the northernmost area contains a significant portion of interbedded muds. The Reklaw Formation consists of variable amounts of mud and sand and is considered the confining strata of the Carrizo-Wilcox aquifer. However, in the northeastern part the clay strata become more discontinuous making the Reklaw probably more pervious to vertical flow between the Carrizo and the overlying Queen City. In Marion and Harrison counties, the combined Wilcox, Carrizo, Reklaw, and Queen City units are referred to as the Cypress aquifer (Fogg and Kreitler, 1982). Above, the Weches Formation separates the Queen City Sand from the overlying Sparta Sand that occurs only locally in the area.

The proposed hydrostratigraphic layers of the Carrizo-Wilcox aquifer for the northern model (Figure 4.1.1) include the main depositional facies of the Wilcox Group and the Carrizo Sand. The Reklaw confining unit is represented by a separate layer, accounting for variations in aquitard thickness and facies change from predominantly clay to mixed clay and sand in the northeastern part of the study area. The Queen City aquifer is represented as the top layer of the model to better define the hydraulic gradient across the confining Reklaw Formation. This allows for evaluating potential leakage between the Carrizo and the shallow Queen City aquifer. Potential recharge through leakage from the Queen City aquifer may be important in case of extensive pumpage in the shallow confined Carrizo aquifer. The top layer has assigned recharge boundary conditions reflecting the shallow water table that follows the topography. Younger formations that lie above the Sparta Sand in the southern part of the model are represented in the model by general head boundary conditions accounting for the hydraulic connection between the Queen City and Sparta aquifers to the shallow water table.

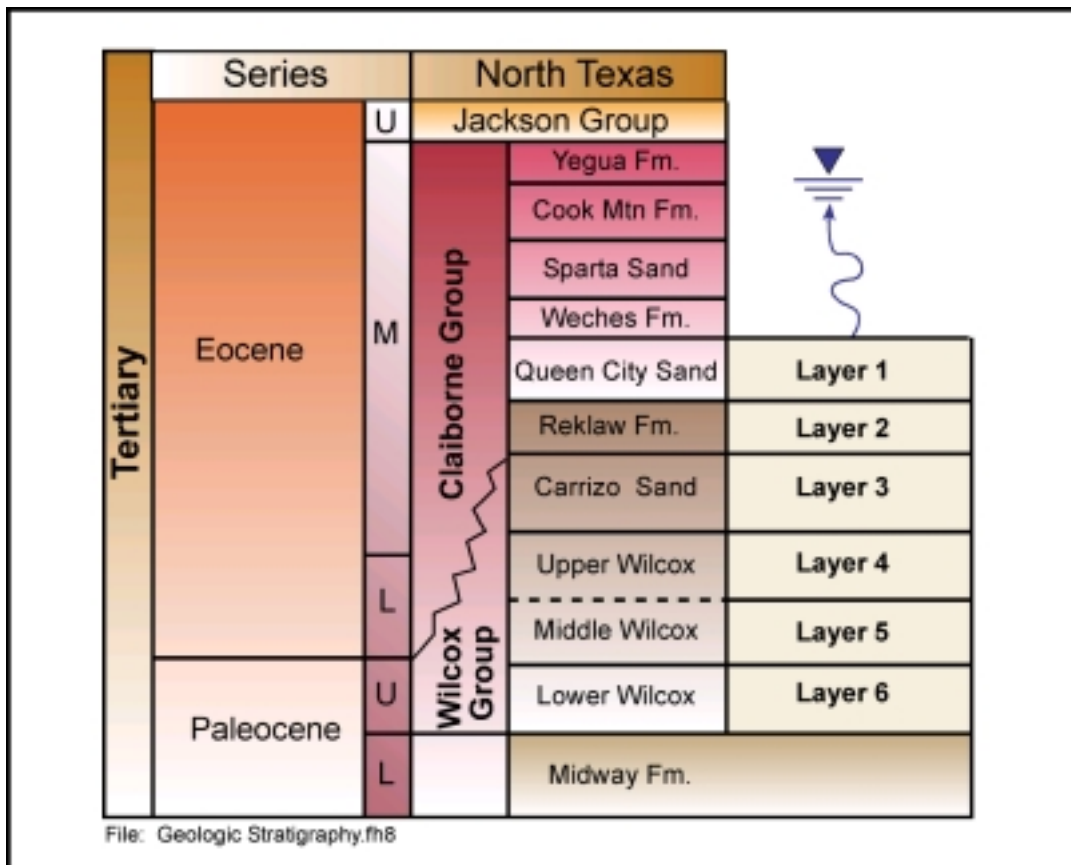


Figure 4.1.1 Hydrostratigraphy and model layers.

4.2 Structure

The geologic structure of the northern Carrizo-Wilcox model is dominated by the East Texas Basin in the north and central model area, the Sabine Uplift in the eastern model area, and the Houston Embayment in the southern portion of the model area (Figure 4.2.1). The structure surfaces of the different hydrostratigraphic units used for the GAM were compiled from different sources, which are summarized in Table 4.2.1.

Table 4.2.1 Data sources for layer elevations for the Northern Carrizo-Wilcox GAM.

Model Layer Boundary	East Texas Model (TWDB, unpublished)	Wilson and Hosman (1988) (USGS RASA)	Kaiser (1990)	Central Carrizo-Wilcox GAM	Surface Elevations (USGS)
Top of Queen City	X				X
Top of Reklaw	X	X		X	X
Top of Carrizo	X	X		X	X
Top of Wilcox	X	X		X	X
Top of Middle Wilcox	X			X	X
Top of Lower Wilcox	X		X	X	X
Base of Wilcox	X	X		X	X

Data Format for the Various Sources:

Data Source	Report Number	Format
East Texas Model TWDB (unpublished)		Text files containing x, y, and elevation.
Wilson and Hosman (1988)	USGS Open-File Report 87-677	Printed tables.
Kaiser (1990)	BEG	Printed tables.
Central Carrizo-Wilcox GAM		Text files containing x, y, and elevation.
USGS DEM (Outcrop Surface Elevations)		DEM files.

The processing of the structure data required several steps. The data from the different sources were digitized and converted to GAM coordinates and merged for the individual structure surfaces. The data were initially kriged to identify problems. Problems were solved through a combination of eliminating data sources, removing data points, and/or defining guide points to constrain the kriging algorithm. The data were kriged again and delimited to the corresponding subcrop areas. The kriged and delimited data were then merged with the outcrop

elevation grid, which was developed from U.S. Geological Survey digital elevation model (DEM) data. The final kriged structure surfaces were then used to calculate layer thicknesses, which were checked (and modified, as appropriate) to insure that layer thicknesses were not less than 20 ft throughout the model.

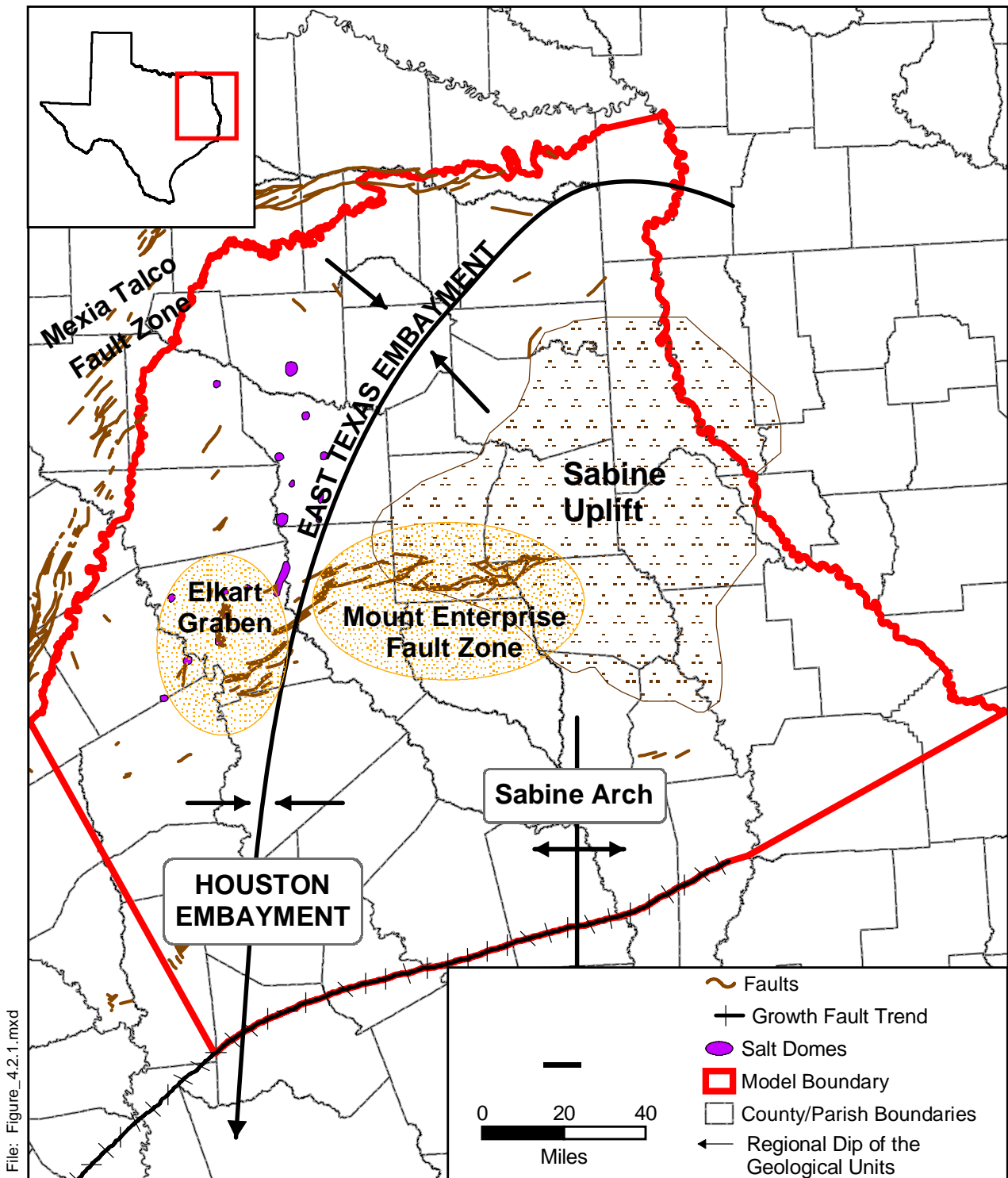
Figures 4.2.2 through 4.2.8 show the structure contour maps of the different hydrostratigraphic units. The structure maps show the data locations and identify the source of the data. The base of the Wilcox dips east and west toward the East Texas Embayment north of the Elkhart - Mount Enterprise Fault Zones. To the south, the strike of the base of the Wilcox is more east-west trending and the surface dips more steeply toward the Houston Embayment (Figure 4.2.2). The top of the lower Wilcox, shown in Figure 4.2.3, shows a similar structure as the base of the Wilcox. Also shown in Figures 4.2.2 and 4.2.3 is a line delineating the northern extent of the lower Wilcox, which extends from south of the Sabine Uplift west-northwest toward the western outcrop of the Wilcox Group. That is, north of the subcrop line the structure surface of the base of the Wilcox and top of the lower Wilcox are the same. As indicated by the different data points, the top of the Hooper Formation identified in east-central Texas correlates with the top of the lower Wilcox northeast of the Trinity River.

The structure at the top of the middle Wilcox extends the top of the Simsboro Formation mapped in central Texas into an arbitrary horizon in the upper Wilcox, which is based on the TWDB's East Texas Model (Figure 4.2.4). The constructed structure of the top of the Wilcox Group (Figure 4.2.5) utilized additional data sources from the USGS RASA study to define the top of the Wilcox in easternmost Texas. The upper Wilcox in the Sabine Uplift area is eroded and its surface corresponds to the land-surface elevation. The top of the Carrizo-Wilcox aquifer is represented by the structure surface, shown in Figure 4.2.6, which combines data from the TWDB's East Texas Model, RASA, and from Ayers and Lewis (1985). The top of the Reklaw Formation, representing the major confining layer of the Carrizo-Wilcox aquifer is shown in Figure 4.2.7. The top layer, represented by the Queen City Formation is shown in Figure 4.2.8, which is based entirely on data from TWDB's East Texas Model.

The thickness maps of the various hydrostratigraphic units are shown in Figures 4.2.9 through 4.2.15, which were constructed based on the elevation difference in the structure contour maps (Figures 4.2.2 through 4.2.8). The thickness of the lower Wilcox decreases to the north,

where it was eroded north of an east-west trending line representing the subcrop extent of the lower Wilcox (Figure 4.2.9). The lower Wilcox thickens rapidly southward into the Houston Embayment. The thickness map of the middle Wilcox extends to the northern outcrop of the Wilcox Group (Figure 4.2.10). In the southwestern part of the area, the middle Wilcox corresponds to the Simsboro Formation of the Central Carrizo-Wilcox GAM area. East of the Trinity River, the top of the middle Wilcox was picked as used in TWDB's East Texas Model. As a result, the thickness map of the middle Wilcox shows a relatively large increase east of the Trinity River. The thickness map of the upper Wilcox (Figure 4.2.11) shows a similar pattern east of the Trinity River. Overall, the upper Wilcox is somewhat thinner than the middle Wilcox. The thickness of the Carrizo is typically 100 to 200 ft or less in the study area (Figure 4.2.12); only to the southwest in the downdip section does the thickness increase significantly. The thickness of the Reklaw Formation in the East-Texas Embayment ranges between less than 40 ft to about 200 ft (Figure 4.2.13) and increases to over 600 ft in the downdip section toward the Houston Embayment. The thickness of the Queen City shows relatively large variations in the East Texas Embayment where the formation crops out (Figure 4.2.14). The Queen City generally decreases in thickness downdip and pinches out toward the southeastern part of the model area. Younger sediments form a wedge above the Queen City, which increases in thickness to more than 6000 ft toward the southern boundary of the study area (Figure 4.2.15).

A number of salt domes and salt pillows affect the structural surfaces of the Wilcox Group in the East-Texas Embayment (Figure 4.2.1). The constructed structure maps did not include salt domes penetrating the Wilcox strata, because of the localized nature of these features. In some cases, the domes caused little uplift and faulting of the surrounding sediments, whereas in other cases they resulted in significant uplift and faulting of strata (Fogg and Kreitler, 1982). The latter caused faulting of aquitards and even exposure of underlying aquifers at the surface (e.g., Keechi Dome in Anderson County as indicated in Figure 2.15a) providing potential points of local recharge to the confined Carrizo-Wilcox aquifer.



File: Figure_4.2.1.mxd

Source: W.R. Kaiser (1990)

Figure 4.2.1 Structural setting of the study area.

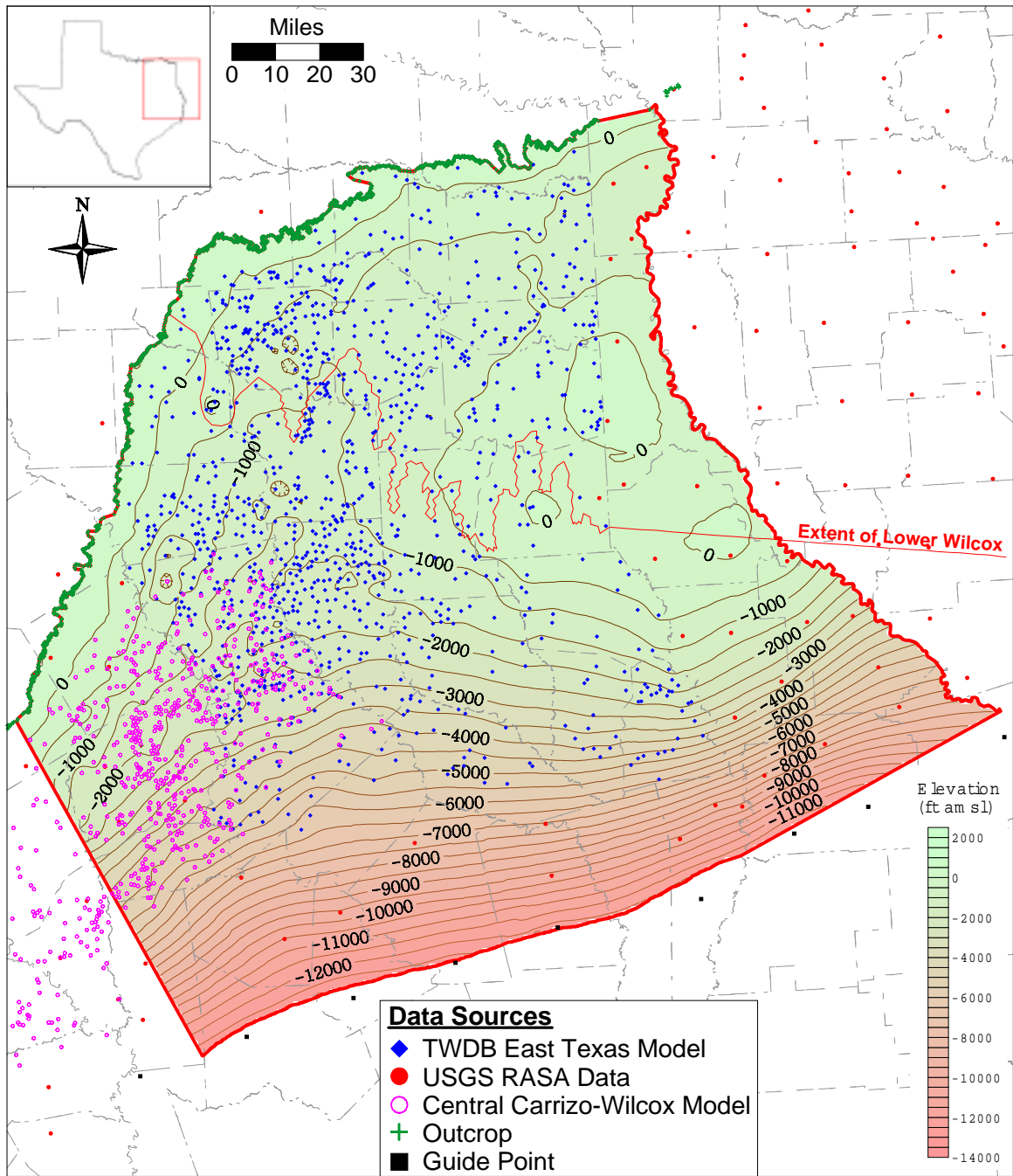


Figure 4.2.2 Structure contour map of the base of the Wilcox Group (CI = 500 ft).

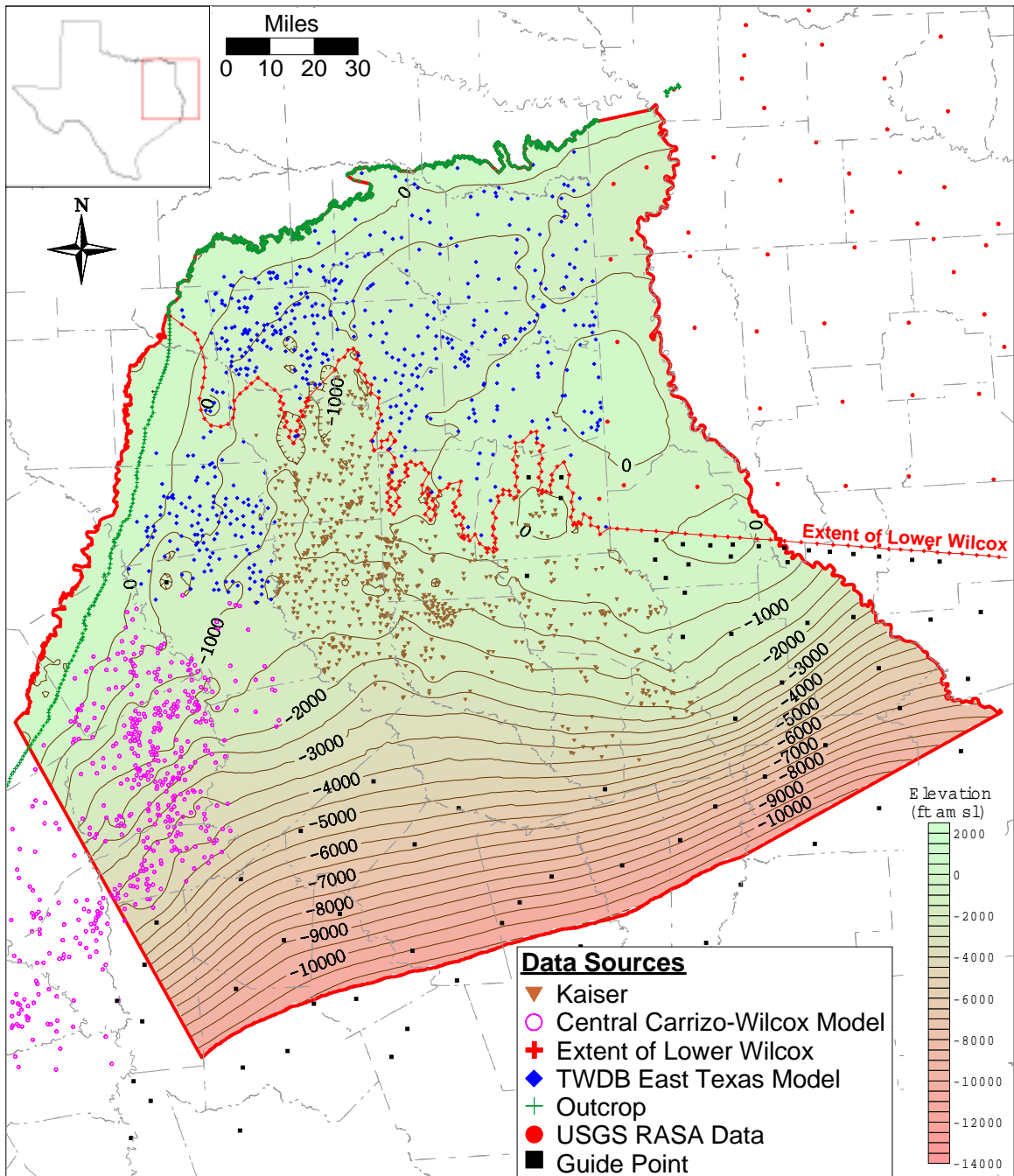


Figure 4.2.3 Structure contour map of the top of the lower Wilcox (CI = 500 ft).

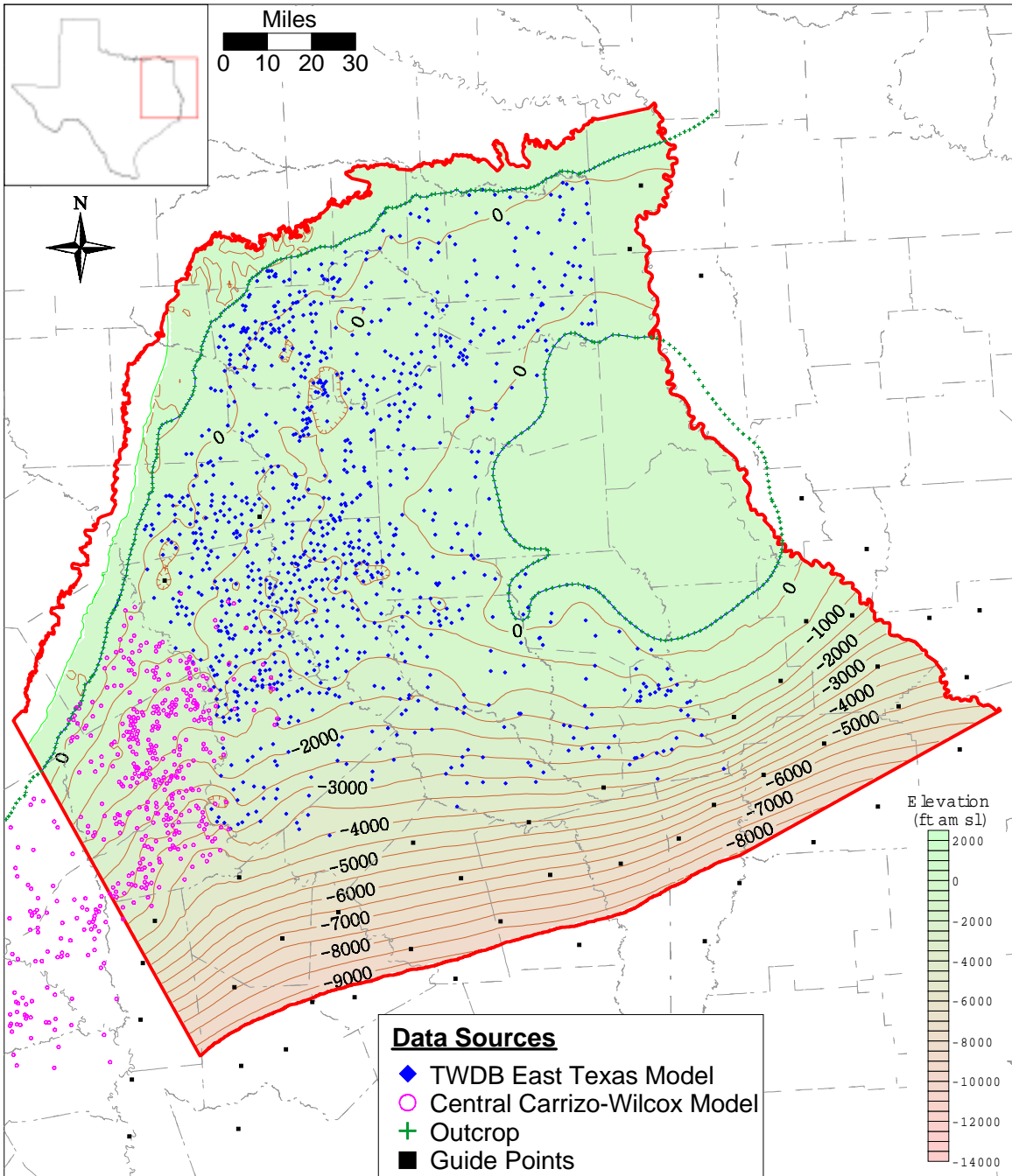


Figure 4.2.4 Structure contour map of the top of the middle Wilcox (CI = 500 ft).

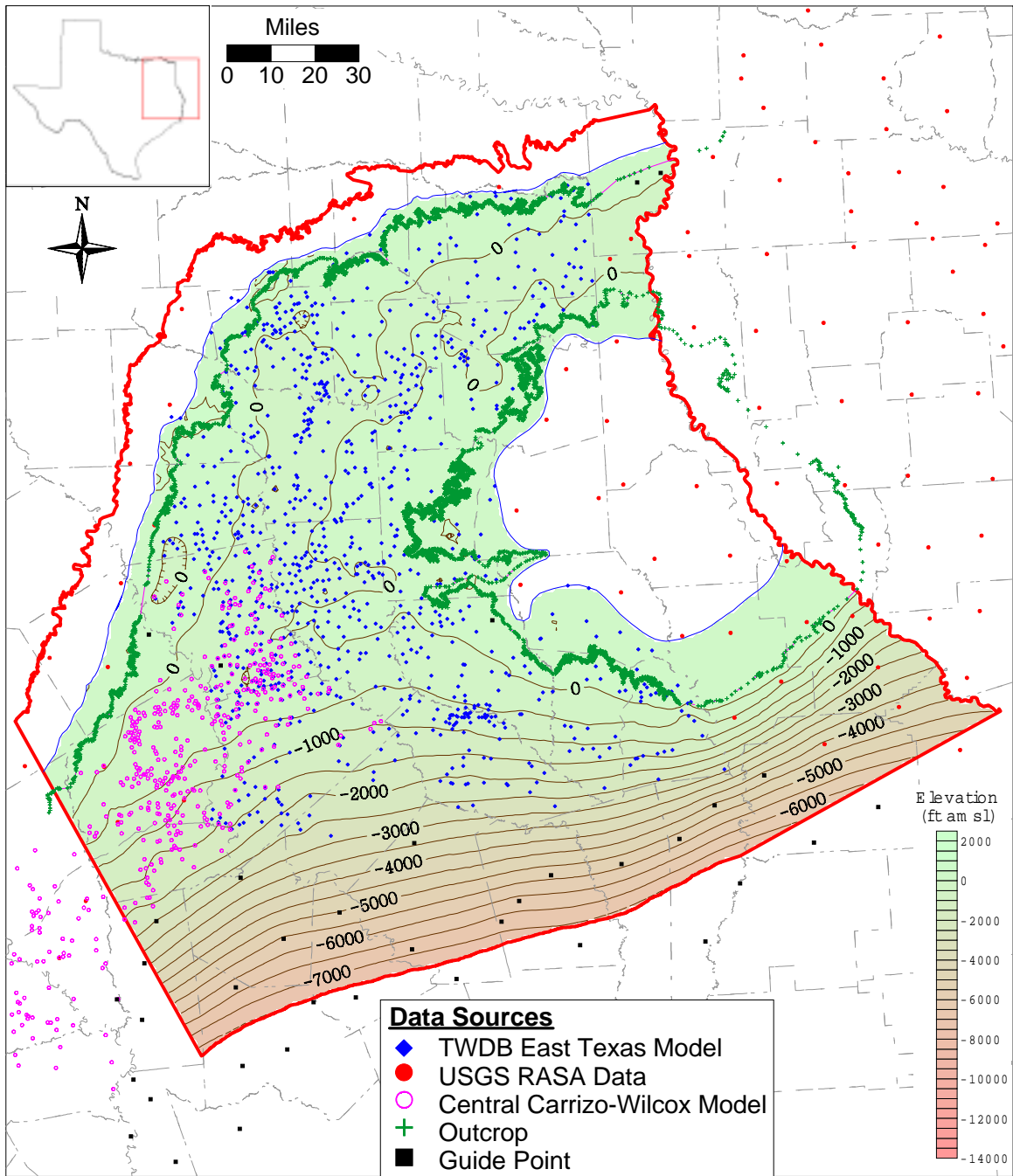


Figure 4.2.5 Structure contour map of the top of the Wilcox Group (CI = 500 ft).

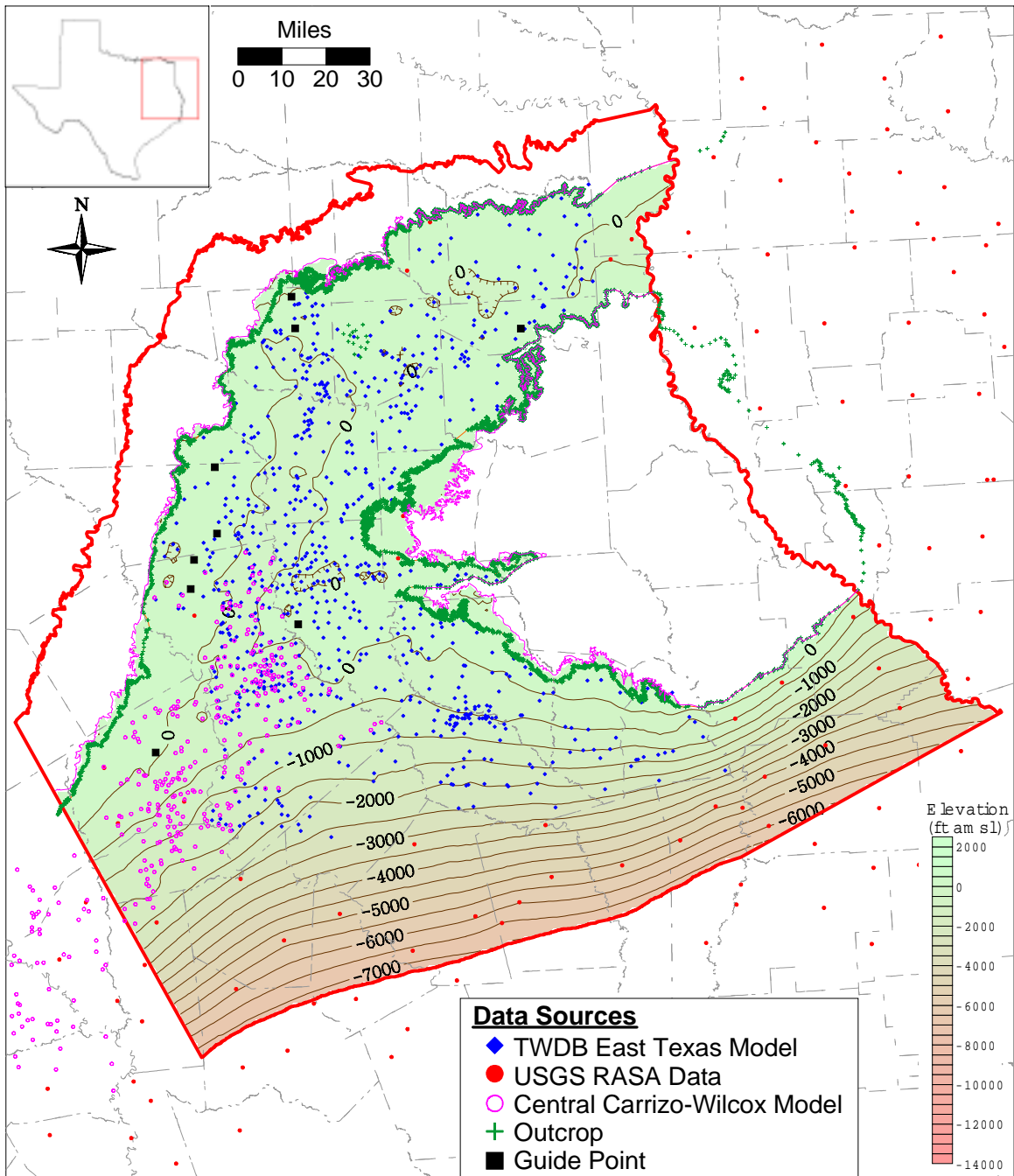


Figure 4.2.6 Structure contour map of the top of the Carrizo (CI = 500 ft).

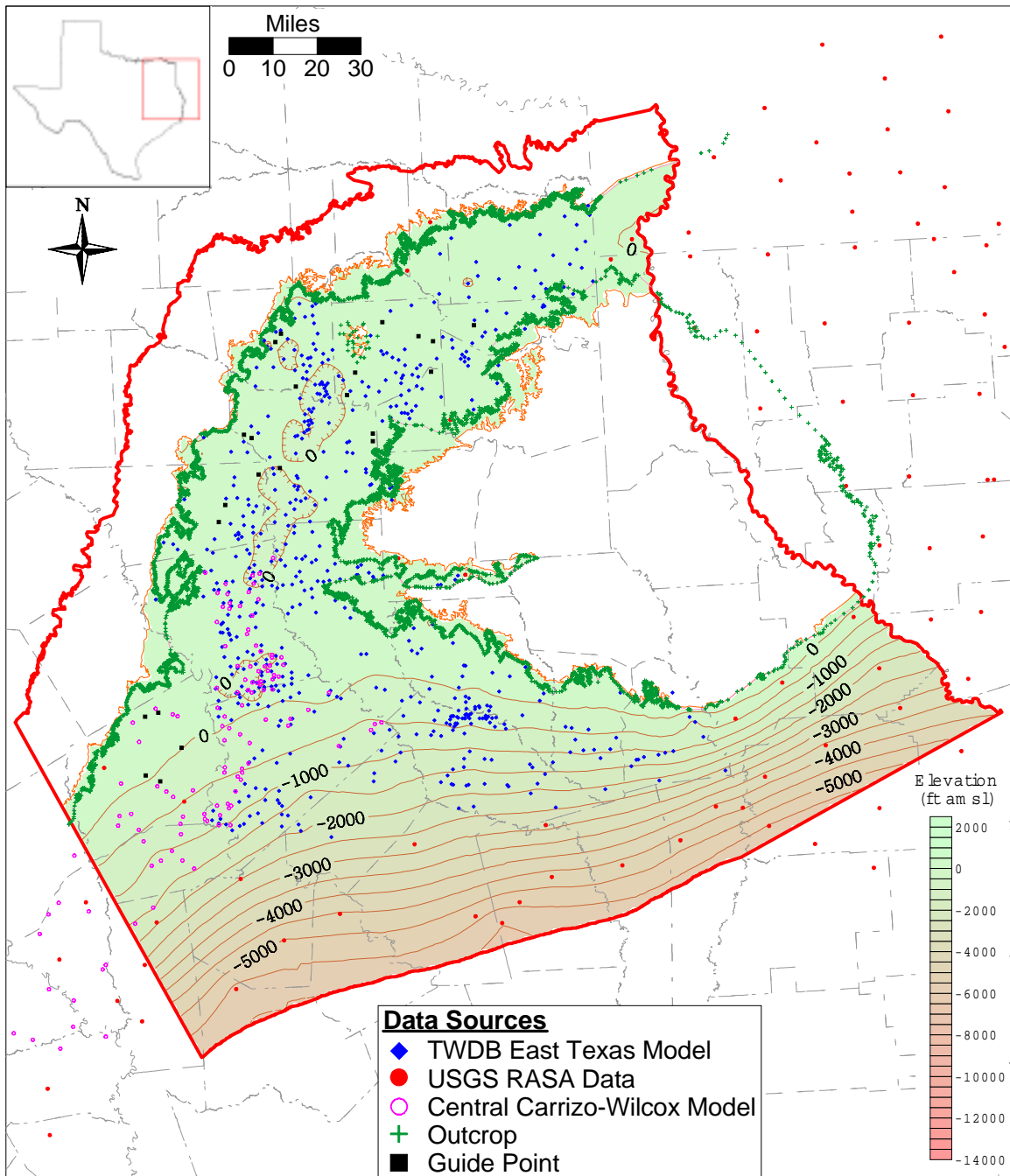


Figure 4.2.7 Structure contour map of the top of the Reklaw Formation (CI = 500 ft).

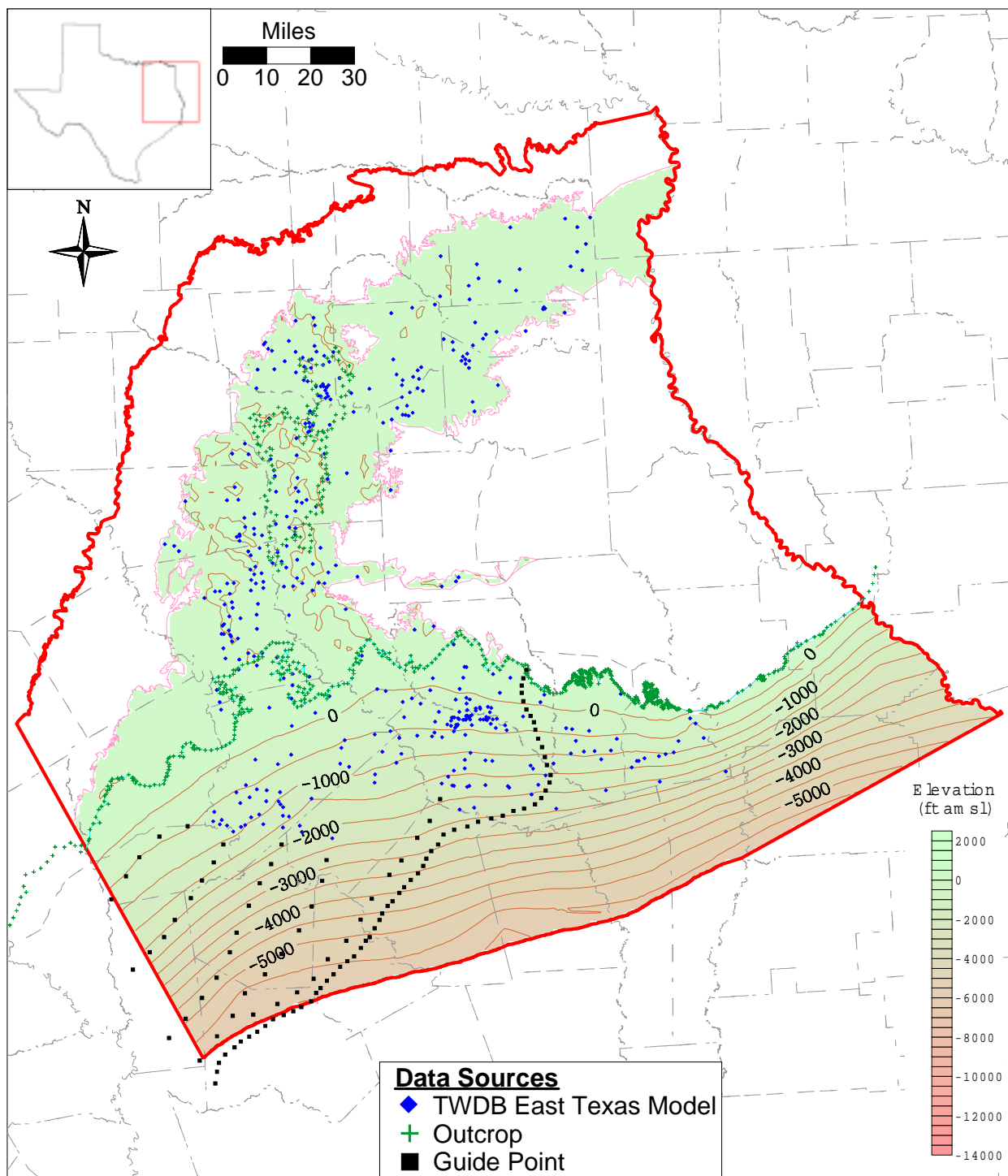


Figure 4.2.8 Structure contour map of the top of the Queen City (CI = 500 ft).

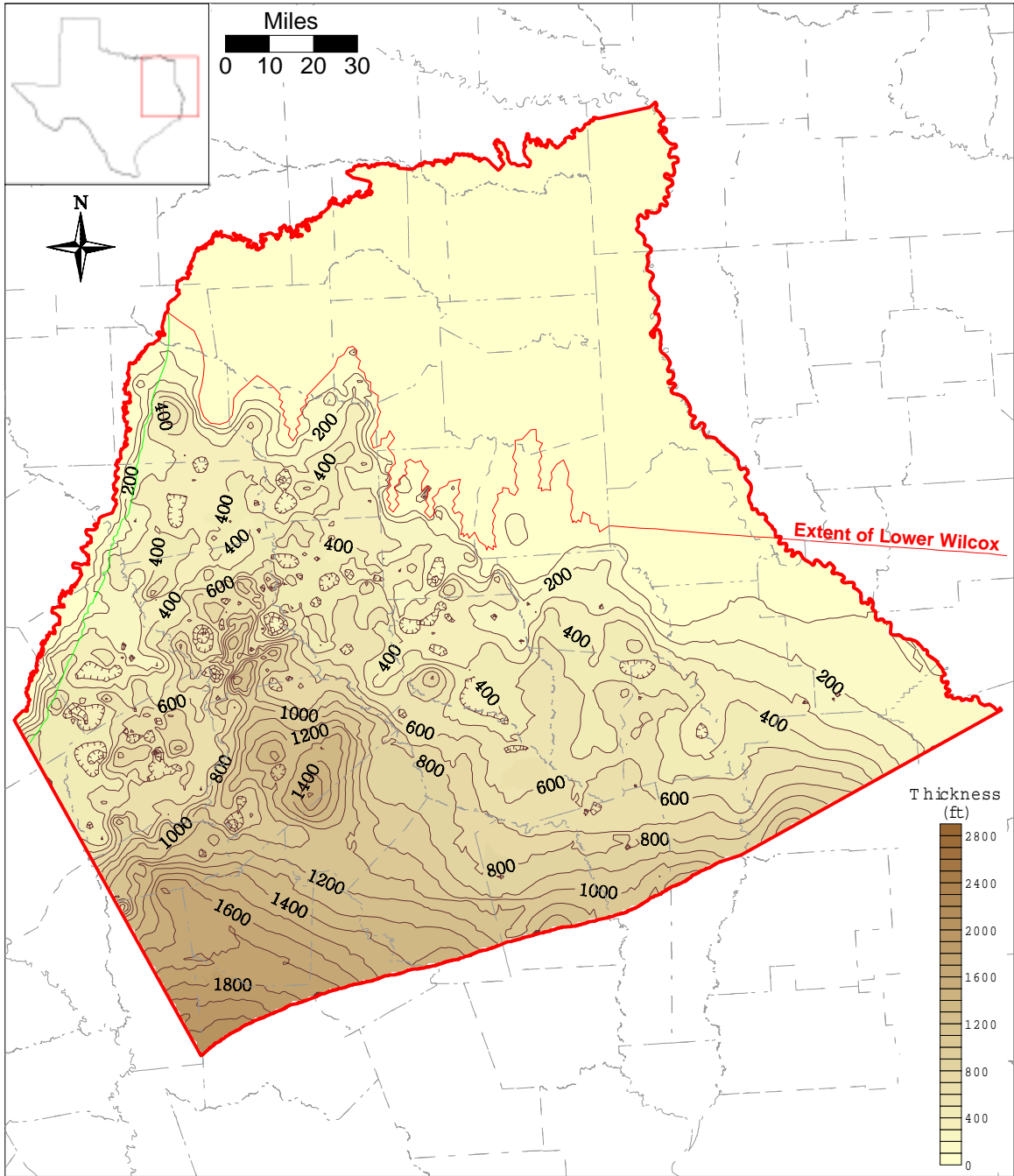


Figure 4.2.9 Thickness map of the lower Wilcox (CI = 100 ft).

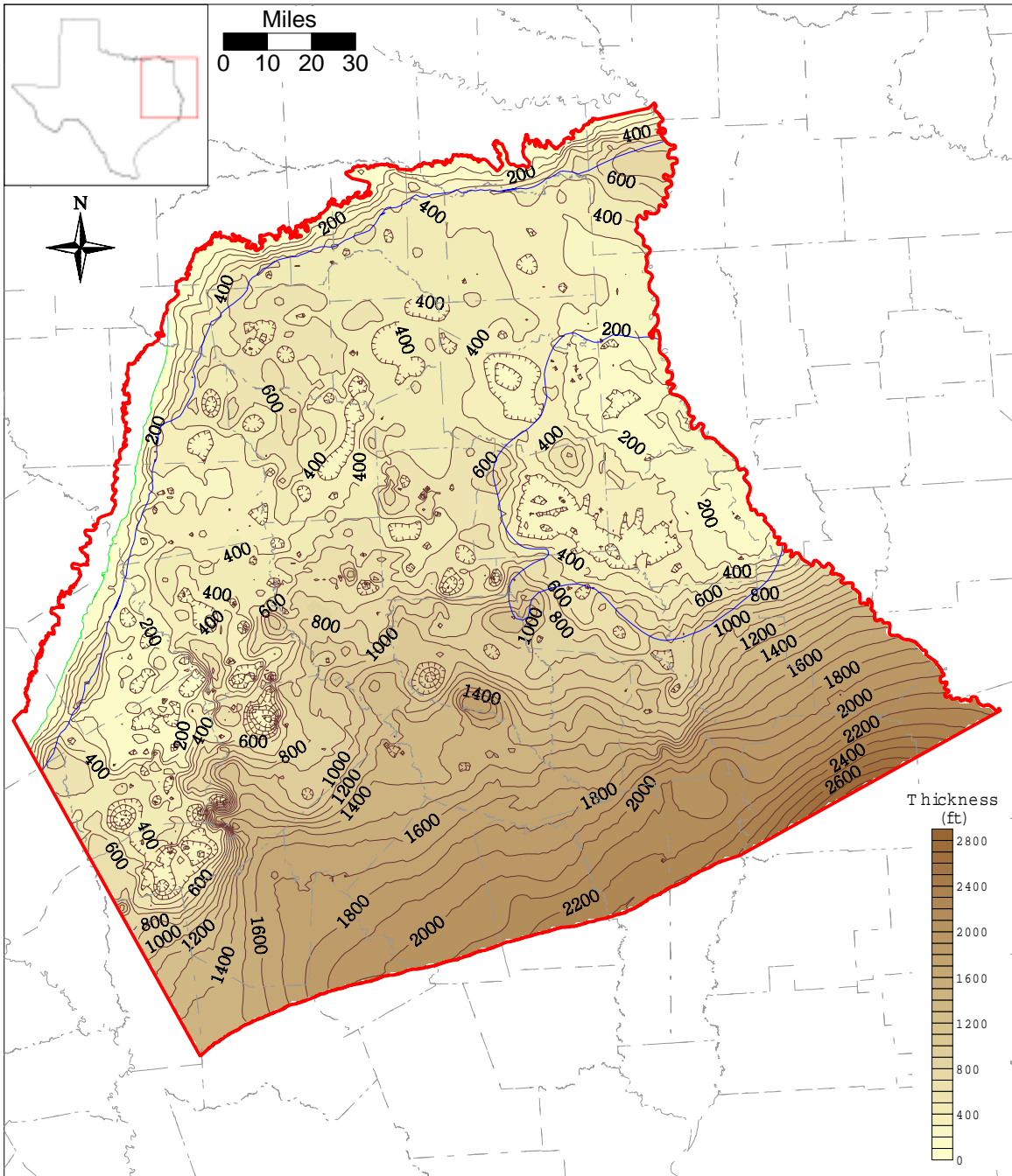


Figure 4.2.10 Thickness map of the middle Wilcox (CI = 100 ft).

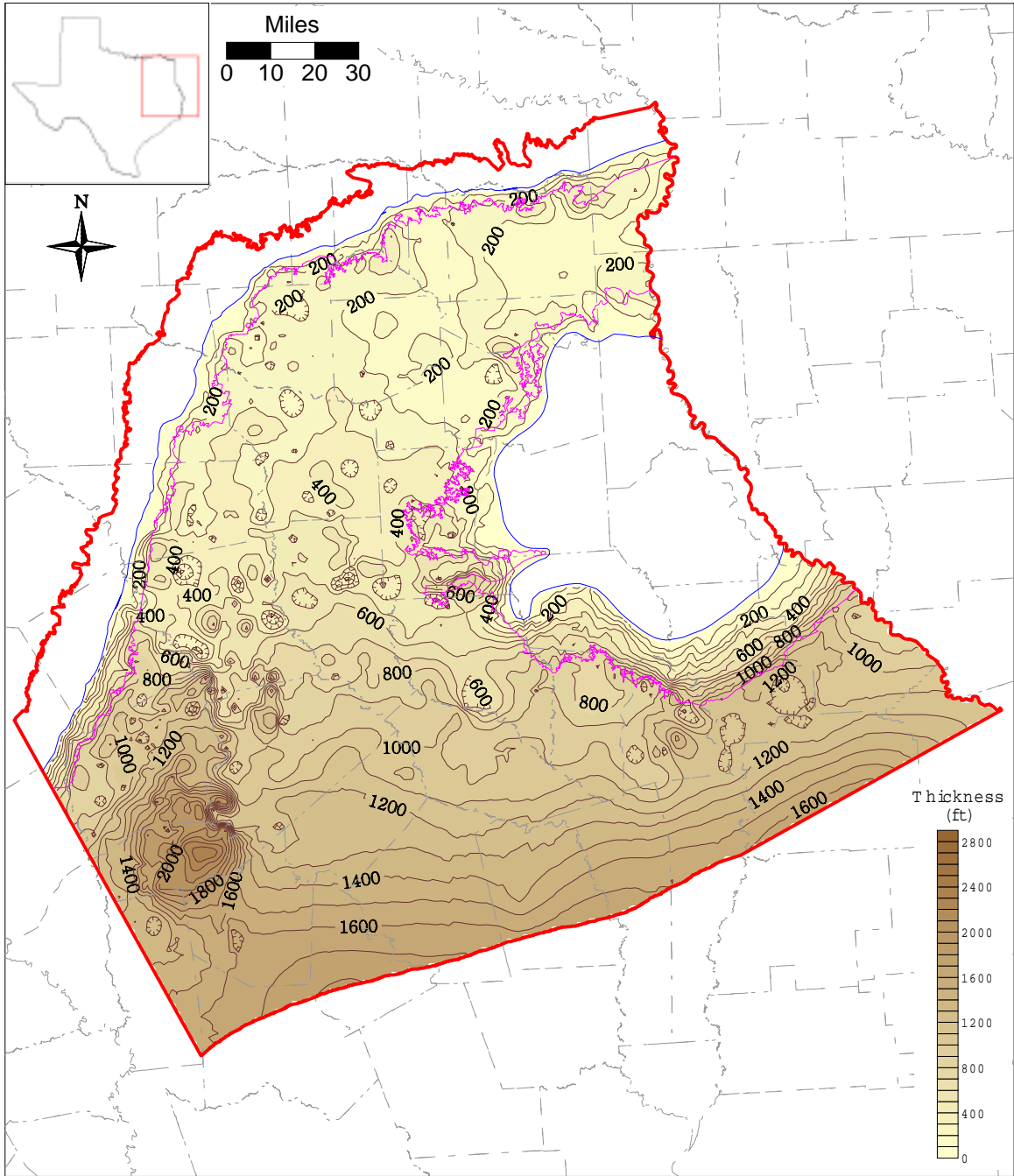


Figure 4.2.11 Thickness map of the upper Wilcox (CI = 100 ft).

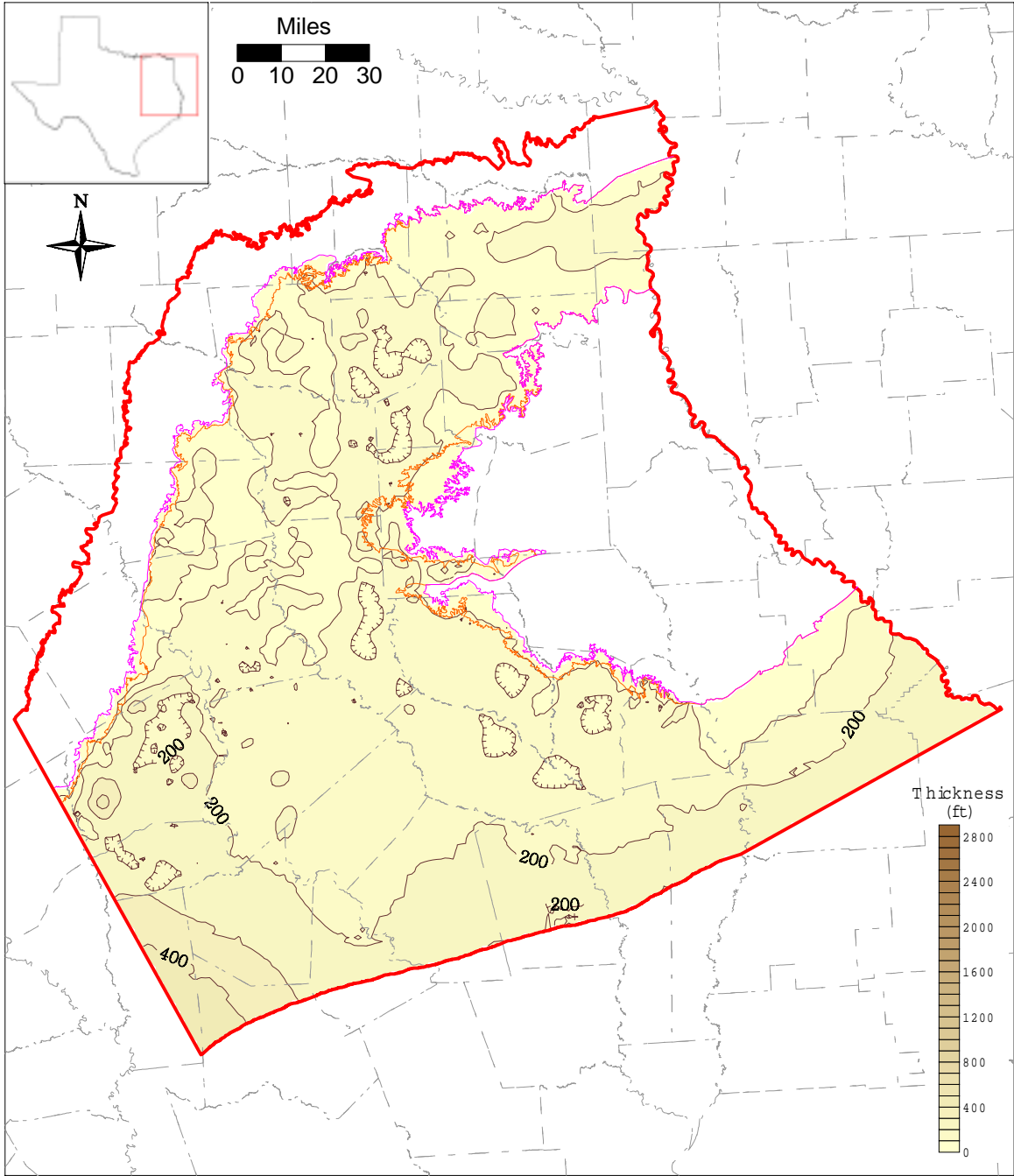


Figure 4.2.12 Thickness map of the Carrizo (CI = 100 ft).

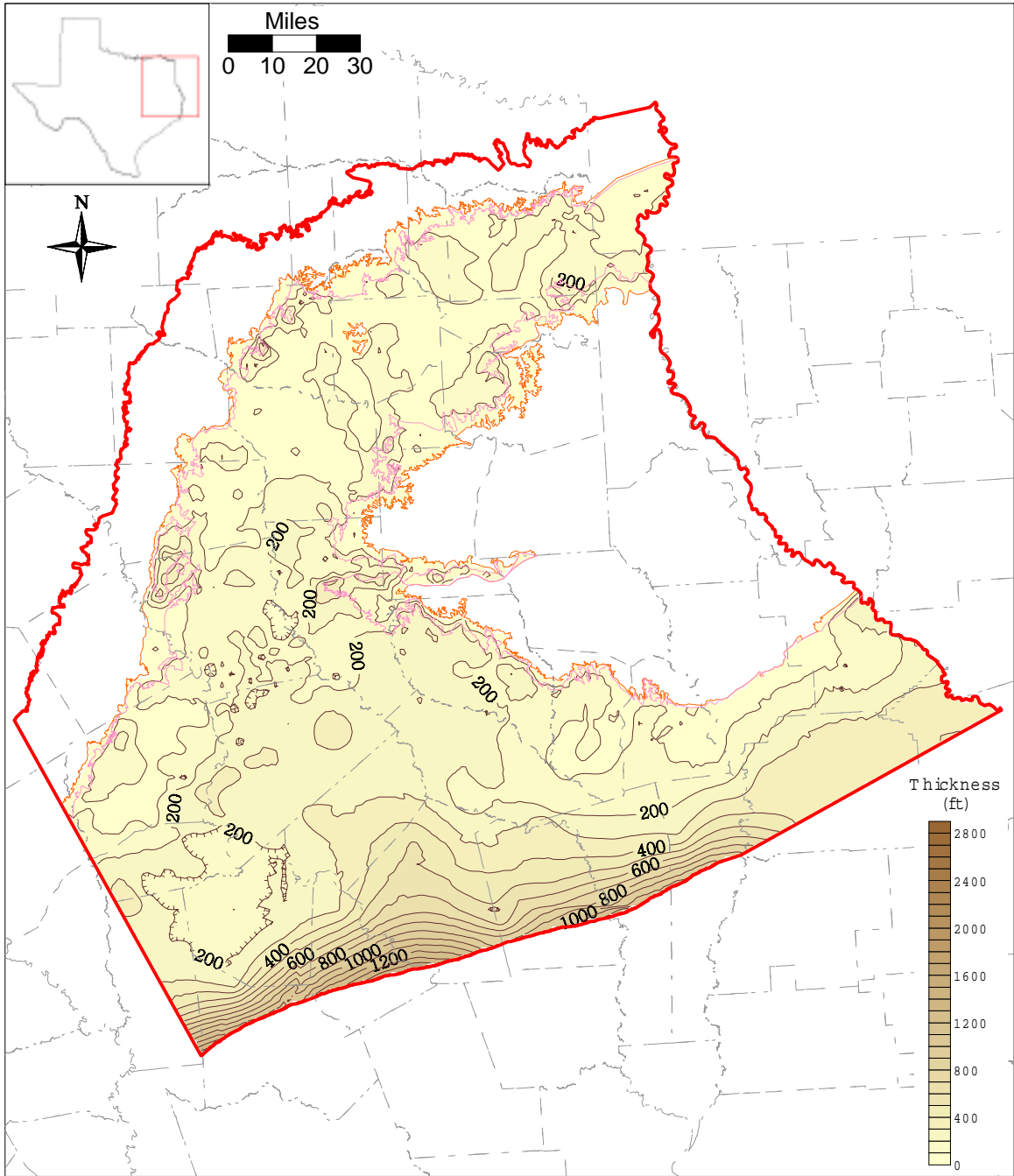


Figure 4.2.13 Thickness map of the Reklaw (CI = 100 ft).

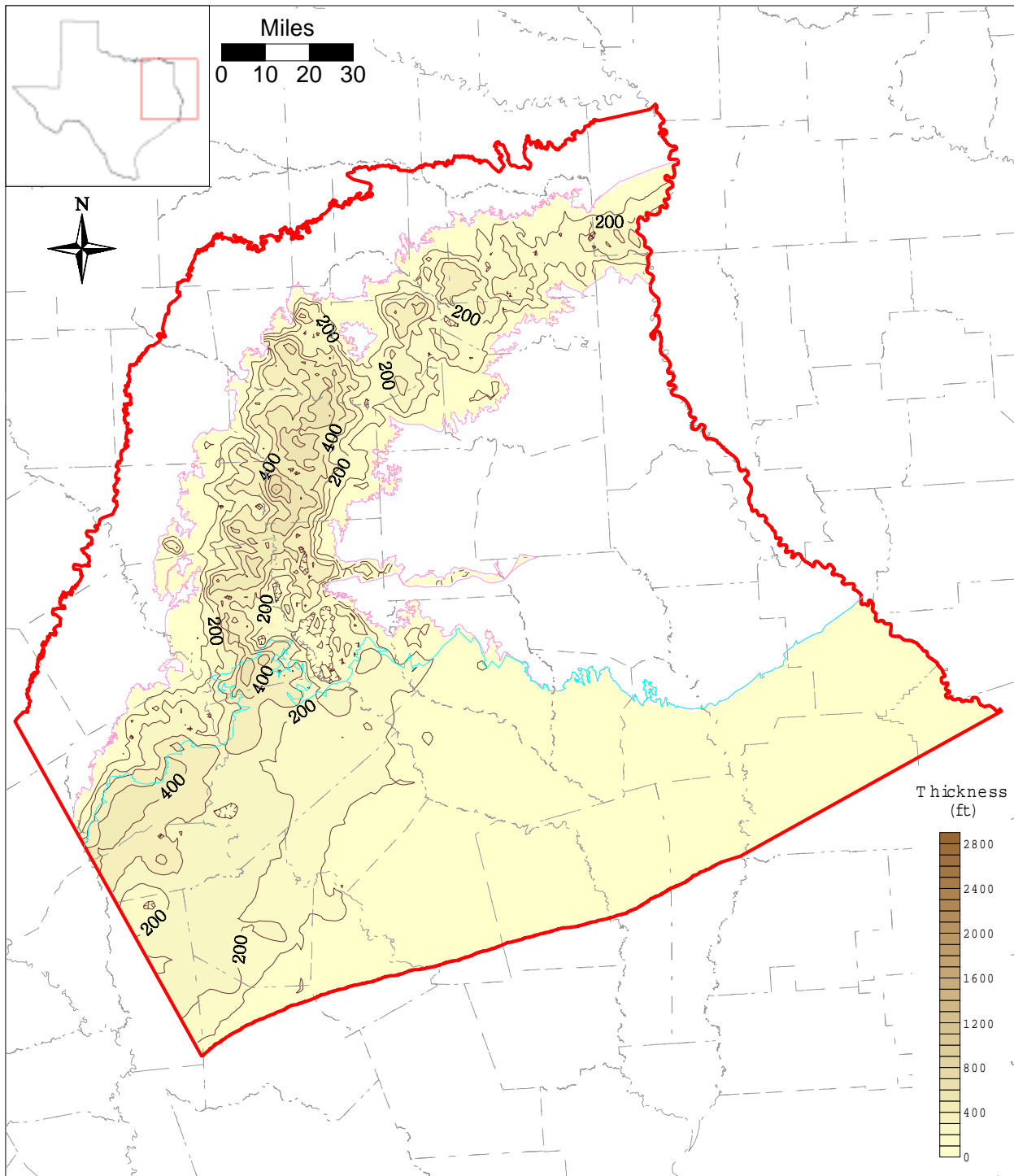


Figure 4.2.14 Thickness map of the Queen City (CI = 100 ft).

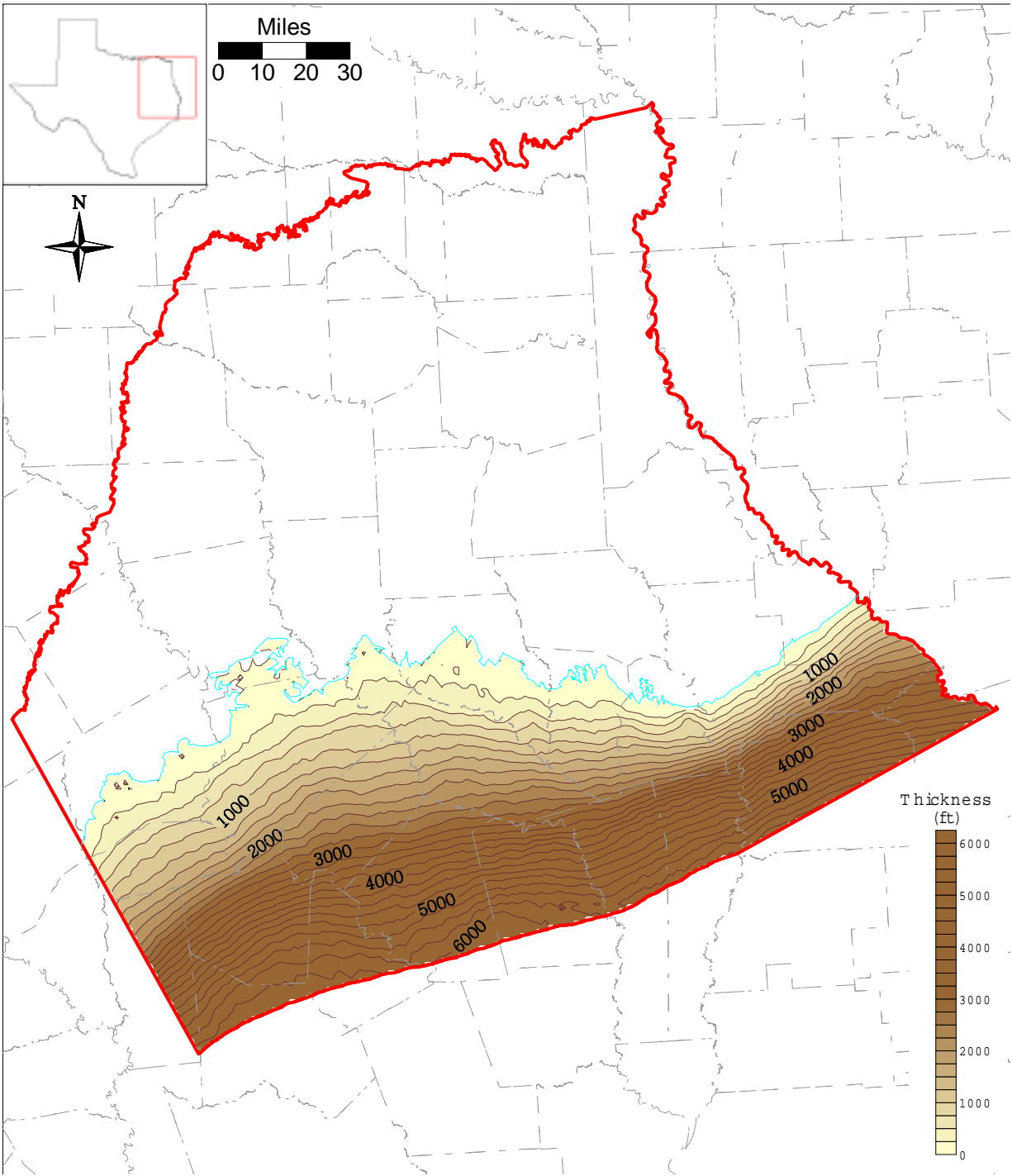


Figure 4.2.15 Thickness map of formations above the Queen City (CI = 250 ft).

4.3 Hydraulic Properties

Information on hydraulic properties of the Carrizo-Wilcox aquifer is based largely on data and sources provided by Mace et al. (2000a). They compiled and statistically analyzed transmissivity, hydraulic conductivity, and storativity data from numerous sources for the entire Carrizo-Wilcox aquifer in Texas. They also analyzed spatial distributions in hydraulic properties in the Carrizo Sands and in the Wilcox Group, suggesting regional trends in kriged transmissivities and hydraulic conductivities. The uneven data coverage and relatively large local-scale variability, expressed in a high nugget in the semivariograms (Mace et al., 2000a), indicate significant uncertainty in the effective hydraulic properties of the aquifer systems. A relationship between hydraulic properties and sand thickness (using sand maps from Bebout et al., 1982) could not be established, even though more detailed local studies did indicate some correlations between different sand facies and hydraulic conductivities (e.g., Payne, 1975; Henry et al., 1980; Fogg, 1986; Thorkildsen and Price, 1991).

The Carrizo aquifer generally consists of fairly homogeneous fluvial sands overlying the multi-aquifer system of the Wilcox Group that is composed of fluvial and deltaic sands distributed among lower permeability interchannel sands and muds. To properly simulate groundwater flow in such a complex depositional environment requires accurate description of both the subsurface arrangement of the various lithofacies (i.e., sand body distributions) and associated hydraulic properties. As pointed out by Fogg (1986), sensitivity of hydraulic head to heterogeneity or interconnectedness of sands in such a complex 3-D aquifer system is relatively low. This results in potential non-unique solutions in model calibrations and concomitant inaccurate representation of simulated groundwater flow patterns. Moreover, hydraulic properties have to be representative for the hydrostratigraphic unit that is implemented as a model layer in the numerical model. That is, both the horizontal and vertical distribution of property measurements is important, which requires information on well locations and screen depths and/or well depths.

The evaluation of the hydraulic property data was done in several steps. Initially, the database from Mace et al. (2000a) was processed in terms of data location relative to the GAM region and to the hydrostratigraphic units. Next, a statistical analysis of the data was performed

evaluating potential variations of different data sources and for different aquifer designations. A geostatistical analysis was then performed characterizing spatial variations of the hydraulic properties. Finally, potential trends in hydraulic properties compared to the depositional trends or sand-body distributions were examined.

4.3.1 Processing of the Hydraulic Property Database

For the Northern Carrizo-Wilcox GAM, the original database from Mace et al. (2000a) was imported into an MS Access Database (file: cw_97_xp.mdb). A new data table that contains a link between the BEG well number and the well location in GAM coordinates was added to the data base (the coordinate conversion from decimal degrees to GAM coordinates was completed in ArcView). A new table (Models) that identified the wells within the northern GAM region was added. This table was created in ArcView by intersecting the GAM outline with the point coverages of the wells. As recommended by Mace et al. (2000a), data from the Texas Railroad Commission (TRRC) and data from slug or bailing tests were excluded in this study, because of a bias toward lower values. Hydraulic conductivity values estimated from well logs were also excluded, as recommended by Mace et al. (2000a), because of a bias toward higher values.

Figure 4.3.1 shows a flow diagram for the screening of hydraulic conductivity data. After discarding the TRRC, well log, slug, and bailing test data, the remaining data were screened for the availability of a horizontal hydraulic conductivity measurement. Some data had a transmissivity measurement, but no estimate of effective thickness (e.g. screen length), and were discarded. If the top and bottom elevation of the well screen was recorded, these were compared to the model layer elevations. The hydraulic conductivity measurement was assigned to the layer that contained the largest fraction of the well screen. If the screen spanned more than three layers, the measurement was discarded. Those data without screen elevation information were checked for the presence of a layer-specific TWBD aquifer code. If this code was available, then the hydraulic conductivity measurement was assigned to that layer. Data marked only with general aquifer codes indicating multiple model layers (e.g. Wilcox Combined or Carrizo-Wilcox) were discarded.

4.3.2 Statistical Analysis of the Hydraulic Property Data

A summary of the statistical analysis of the hydraulic properties for the different hydrostratigraphic units is given in Table 4.3.1. The table summarizes the number of data measurements and the mean and median hydraulic conductivities. The hydraulic conductivities are summarized by layer with cumulative distribution function (CDF) curves in Figure 4.3.2. These distributions appear to be log-normal. The hydraulic conductivities for the different layers range between 0.1 ft/day to about 800 ft/day.

Table 4.3.1 Summary statistics for horizontal hydraulic conductivity.

Layer	Unit	Count	Median Hydraulic Conductivity (ft/d)	Mean Hydraulic Conductivity (ft/d)
1	Queen City	98	4.1	8.1
2	Reklaw	140	3.9	17.6
3	Carrizo	324	4.8	13.4
4	Upper Wilcox	796	5.1	12.8
5	Middle Wilcox	1126	3.3	8.7
6	Lower Wilcox	332	3.5	7.5

Figure 4.3.2 and Table 4.3.1 indicate that the Reklaw Formation, which is considered the upper confining unit for the Carrizo-Wilcox aquifer, has relatively high horizontal hydraulic conductivity. The Reklaw Formation may contain extensive sand layers within the mud units and pumping is reported from the Reklaw. However, some of the wells that are designated as Reklaw wells by aquifer code or by the structure data are probably completed in the underlying Carrizo Formation or overlying Queen City Formation. Because the Reklaw Formation is relatively thin, small errors in the structure surfaces can result in misplacement of screened intervals. Therefore, the hydraulic conductivities for the Reklaw shown in Table 4.3.1 are not considered representative on a regional basis. For the Reklaw confining unit, the more important hydraulic property is the vertical hydraulic conductivity, which is largely controlled by the hydraulic conductivity of the more continuous muds and shales within the Reklaw.

4.3.3 Spatial Distribution of Hydraulic Property Data

The spatial distribution of hydraulic properties is characterized by variogram analysis to quantify spatial correlation and variability (for detailed background information on geostatistics refer to Isaaks and Srivastavs (1989)). The variogram describes the degree of spatial variability

between observation points as a function of distance. Typical hydrogeologic properties show some spatial correlation indicated by low variance for nearby data points that increases with increasing distance to a point where the variance becomes constant which corresponds to the ensemble variance of the entire data set. The variogram quantifies the spatial variability in terms of the correlation length and variance, and provides information on potential trends in the data. The variogram can also be used as a tool to characterize horizontal anisotropy in the hydraulic conductivity distribution since hydraulic conductivity is a function of direction in an aquifer with horizontal anisotropy. A directional-variogram analysis failed to detect any horizontal anisotropy in the hydraulic conductivity fields for the study area.

Figure 4.3.3 shows a variogram of hydraulic conductivities for the Carrizo Sand in the study area. The variogram indicates a steep increase in variance which levels off for distances greater than about 75,000 ft. A function was fitted to the variogram data (experimental variogram), which shows an intercept of 0.12 at zero distance. The corresponding variance of the intercept is referred to as the “nugget”, indicating the local-scale variability of hydraulic conductivity. The nugget amounts to about half of the total variance of 0.3 of the ensemble data, represented by the “sill”, suggesting potentially large variability of hydraulic conductivity in nearby well locations.

The spatial distribution of the property data is then produced by kriging, which uses the variogram information to estimate property values over the area of interest based on the limited number of data points available. Kriging results in some smoothing of the data by taking a weighted average of nearby measurement points.

The kriged hydraulic conductivity distribution for the Carrizo Sand and corresponding variogram are shown in Figure 4.3.4. The variogram indicates relatively large local-scale variability, even though the Carrizo is considered a relatively homogeneous sand. As indicated on the kriged map of hydraulic conductivity, most of the data are in the northern half of the model areas and have a relatively even distribution. In the deeper section south of the East-Texas Embayment, there is little or no data. Also, south of the Sabine Uplift there are very few data points. The hydraulic conductivities range from less than 1 ft/day to about 30 ft/day with distinct local areas of high conductivities in Anderson, Angelina, Nacogdoches, Rusk, Van Zandt and Henderson counties.

The variogram for hydraulic conductivities of the upper Wilcox shows a correlation length of about 100,000 ft and a significantly higher nugget of about 0.19 compared to a sill of about 0.36 (Figure 4.3.5). Even though the correlation length is greater than that of the Carrizo, the variance is greater suggesting greater heterogeneity. As mentioned in Section 2, the Wilcox consists of fluvial and fluvial-deltaic sands embedded in muds with an average of 50% sand. The kriged hydraulic conductivities show a relatively even data distribution in the outcrop and updip confined section of the East-Texas Embayment (Figure 4.3.5). Hydraulic conductivities are more uniform ranging between less than 1 ft/day and 10 ft/day.

The middle Wilcox indicates a variogram with a significantly greater correlation length of about 300,000 ft than those in the upper Wilcox and Carrizo (Figure 4.3.6). However, the nugget is relatively high (0.18) compared to the sill (0.3) indicating large local-scale variability. The higher correlation length for the middle Wilcox compared to the upper Wilcox may be associated with predominantly fluvial deposits corresponding to the Simsboro sands in east-central Texas, which are characterized by blocky sands in subsurface geophysical logs (Kaiser, 1990). The kriged map shows a more uneven data distribution focused to the outcrop and shallow confined section within the East-Texas Embayment (Figure 4.3.6). Again, there were no data available for the deeper confined section in the southern part of the area.

The lower Wilcox variogram indicates no spatial correlation with large variability of the variance as a function of distance Figure (4.3.7). The kriged map shows data coverage only in the western part along the outcrop and shallow confined section and few data point in the Sabine Uplift.

Spatial distribution of hydraulic conductivity for the Reklaw confining unit was not explicitly analyzed, because of limited data and uncertainty in the appropriate assignment of the data points to the Reklaw or adjacent aquifer units. A preliminary evaluation of the hydraulic property data for the Queen City aquifer was performed, indicating relatively small correlation length, lower nugget (0.05), and lower sill (0.2) compared to the Carrizo-Wilcox (Figure 4.3.8). The kriged map shows limited data distribution in the northern half of the area and very few data along the southwestern part of the area. For this particular map, the contours were limited to within a certain radius from the nearest observation point. Again, data from the southern part were not available.

In general, the kriged maps of hydraulic conductivities indicate significant variations in hydraulic conductivities. These values represent horizontal permeabilities of sands within the different hydrostratigraphic units, because most wells tend to be completed and tested in sand intervals. In the Carrizo aquifer, which consists typically of 80 to 100% sand the spatial pattern reflects variability within the sand. The kriged map was extended to the southern model boundary by including false data points to produce a decrease in hydraulic conductivity with depth toward the southern boundary. Such a decrease in hydraulic conductivity with depth is typical in large regional groundwater systems. For the Wilcox, kriging was allowed to extrapolate the contours from data points updip to toward the southern model boundary, indicating a relatively large part of the area that is not constrained by data. Incorporating the hydraulic property information into the numerical model requires an approach that assigns properties where no data are available and produces property values that are representative over the entire layer thickness. This is of particular importance, where the aquifer units consist of significant amounts of muds. In the following section, geologic information is examined for complementing the limited data on hydraulic properties.

4.3.4 Relationship between Hydraulic Property and Sand Distribution

The distribution of sand and muds not only affects the transmissivity of the aquifer but also the groundwater flow. Groundwater tends to flow into more transmissive zones, that consist of well connected sands of relatively high hydraulic conductivity. The hydraulic conductivity data presented in Section 4.3.3 were based on hydraulic tests performed at specific depth intervals which generally do not cover the entire thickness of the aquifer layer. The data are also representative of the sand encountered in the interval rather than an average value over the entire screened section. The kriged hydraulic conductivity maps assume that the sands tested in adjacent wells at different depth intervals are laterally and vertically connected. This is most likely valid for the Carrizo, which is dominantly sand. For the Wilcox Group, which consist of only 50% sand on the average, sand bodies are embedded in a fine grained matrix and may not always be connected. The Wilcox Group is up to 3000 ft thick, allowing for complex vertical stacking of sands within each of the layers. Depositional information has been used to quantify sand-body distribution, indicating that in fluvial systems, sand bodies can be considered connected over a large scale, if sand percent is more than 50 % or even lower (Fogg, 1989).

Sand thicknesses and sand-body distribution are not only important to define the overall transmissivity of the aquifer but can indicate zones of higher permeability. Intuitively, one would expect that sands in the major fluvial channels have generally higher hydraulic conductivities than thinner, more isolated sands. Spatial information on sand distributions could then be used to extrapolate the kriged permeability maps to areas where no hydraulic conductivity data are available. Mace et al. (2000a) examined generalized net sand maps for upper and lower Wilcox by Bebout et al. (1982) and the corresponding transmissivity values covering the Wilcox Group throughout Texas, but did not find a correlation between sand thickness and transmissivity. However, more local studies did show a relationship between sand thickness or specific channel sands and hydraulic conductivities (Payne, 1975; Fogg, 1986).

For the study area, we examined both the net sand thickness of the entire Wilcox (Kaiser et al., 1978) and maximum sands of the upper Wilcox (Kaiser, 1990) for comparison with hydraulic conductivity values. Maximum sand maps are considered more indicative of the major channel sand, ignoring thinner and less continuous splay and overbank sands. However, the maximum sand maps show only a limited thickness range. Histograms of hydraulic conductivities (log-K) by maximum sand thickness and net-sand thickness (Figure 4.3.9), indicated no clear relationship. The net-sand histograms indicate generally higher median log-K values for thicker sands, but the relationship is not systematic over the different sand thickness intervals. The maximum sand histograms do not indicate a clear trend; in this case, there were only three contour levels. There are certain limitations in the analysis. The sand thickness maps are manually contoured taking into account the depositional model. Furthermore, the hydraulic conductivity data points were assigned to the nearest sand thickness contour.

For this study, the net-sand map was primarily used to estimate the transmissivity of the model layer. The sand maps were not used to extrapolate hydraulic conductivity data into areas where specific data points were not available. However, the sand maps were considered valuable information during model calibration in terms of justifying local modification in hydraulic conductivity values.

As mentioned in section 2.2, the net-sand map from Kaiser et al. (1978) did not cover the entire model area, but agreed reasonably well with the earlier map construction by Fisher and McGowen (1967) for the entire Wilcox Group in Texas. The more detailed map from Kaiser et

al. (1978) was combined with the more regional-scale map to construct a net-sand map covering the entire model area. The resulting sand-percent map is shown in Figure 4.3.10.

4.3.5 Vertical Hydraulic Conductivity

Specific data on vertical hydraulic conductivity within the Carrizo-Wilcox aquifer and for the Reklaw confining layer are not available at the scale of this study. Previous modeling studies of the Carrizo-Wilcox aquifer derived estimates of vertical permeability from model calibration. Stochastic modeling studies of a generic aquifer system consisting of two contrasting hydraulic conductivity facies (channel sands and finer grained interchannel sediments) having various degrees of vertical interconnection indicate effective vertical conductivities ranging between the geometric and harmonic mean conductivities (Fogg, 1989).

A lower bound estimate of vertical conductivity can be calculated as the lowest vertical conductivity value measured in a hydrostratigraphic section, assuming complete lateral continuity of the low-permeability zone. Measurements of hydraulic conductivity typically focus on high-permeability zones with a few core data available for low-permeability muds within the Wilcox Group (Bob Harden, personal communication). In the Region G model developed by Harden and Associates (2000), core estimates of clay hydraulic conductivity were used to represent clay strata within the Carrizo-Wilcox aquifer ($K = 5.35 \times 10^{-6}$ ft/day). The effective vertical conductivity for the different aquifer layers were estimated based on a harmonic mean of the individual proportions of sand, silt, and clay (Harden and Associates, 2000).

Fogg et al. (1983) inferred a maximum reasonable horizontal to vertical permeability ratio K_h/K_v (anisotropy ratio) on the order of 10,000 to 1,000 to reproduce the vertical head gradients within the Carrizo-Wilcox aquifer in a groundwater flow model near the Oakwood salt dome in Freestone and Leon counties. A vertical to horizontal anisotropy ratio of 1,000,000 was considered too low to reproduce the general pressure-depth gradients across the model.

Vertical permeability of the Reklaw confining layer can be considered to be less than that of the Wilcox aquifer, because of more continuous mud units. However, toward the northeast the Reklaw contains more sand layers within the muds, which could increase the effective vertical permeability. Fogg et al. (1983) used a vertical hydraulic conductivity of 2.6×10^{-4} ft/day for the Reklaw in their model, which they considered a maximum value corresponding to that

used for the Wilcox. The USGS RASA model for the Texas Gulf Coast aquifer systems reported a vertical hydraulic conductivity of the lower Claiborne confining unit (equivalent to the Reklaw Formation) of 2×10^{-5} ft/day from their calibrated transient model (Ryder and Ardis, 1991), which is lower than the value 1×10^{-4} ft/day calibrated from the steady-state model (Ryder, 1988).

The Carrizo Formation is generally considered to have much lower anisotropy ratios than the Wilcox, because of typically much higher sand content. However, the measured hydraulic conductivities for the Carrizo in this area range over three orders of magnitude (Figure 4.3.2), indicating the potential range in anisotropy. Previous modeling studies indicated anisotropy ratios (K_h/K_v) of 400 based on steady-state calibration (Ryder, 1988) and 11,500 based on transient model calibration (Ryder and Ardis, 1991).

4.3.6 Storativity

The specific storage of a confined saturated aquifer can be defined as the volume of water that a unit volume of aquifer releases from storage under a unit decline in hydraulic head (Freeze and Cherry, 1979). The storativity is equal to the product of specific storage and aquifer thickness and is dimensionless. For unconfined conditions, the storativity is referred to as the specific yield and is defined as the volume of water an unconfined aquifer releases from storage per unit surface area of aquifer per unit decline in water table (Freeze and Cherry, 1979).

Mace et al. (2000a) compiled 107 estimates of storativity and calculated 64 estimates of specific storage from tests of the Carrizo-Wilcox aquifer where the screen length was known. Storativity ranged in magnitude from 1.0×10^{-6} to 0.1 with a geometric mean equal to 3×10^{-4} . Specific storage ranged from about 1×10^{-7} to 1×10^{-4} 1/m with a geometric mean of 4.6×10^{-6} 1/m. The medians were essentially equal to the geometric mean for both distributions demonstrating the lognormal form of both distributions.

Specific yield estimates provided in Table 4.3.2 originate from aquifer tests and from model calibrated values. The range of specific yield is 0.05 to 0.32. Perhaps the most direct estimate of specific yield is from Duffin and Elder (1979). They performed 20 seismic refraction profiles in the Carrizo Sand outcrop in areas west of Gonzales County (located south of the study area).

Table 4.3.2 Summary of literature estimates of Carrizo-Wilcox specific yield.

Source	Specific Yield	Reference
TWDB Report 210	0.25 (average)	Klemt et al. (1976)
TDWR Report 229	0.16 to 0.32	Duffin and Elder (1979)
TWDB/LCRA model	0.05 to 0.3	Thorkildsen et al. (1989)
TWDB Report 332	0.1 to 0.3	Thorkildsen & Price (1991)
USGS OFR 91-64	0.15	Ryder & Ardis (1991)
BEG RI 256	0.29 (Simsboro)	Dutton (1999)
Region G Model	0.15	Harden & Assoc. (2000)

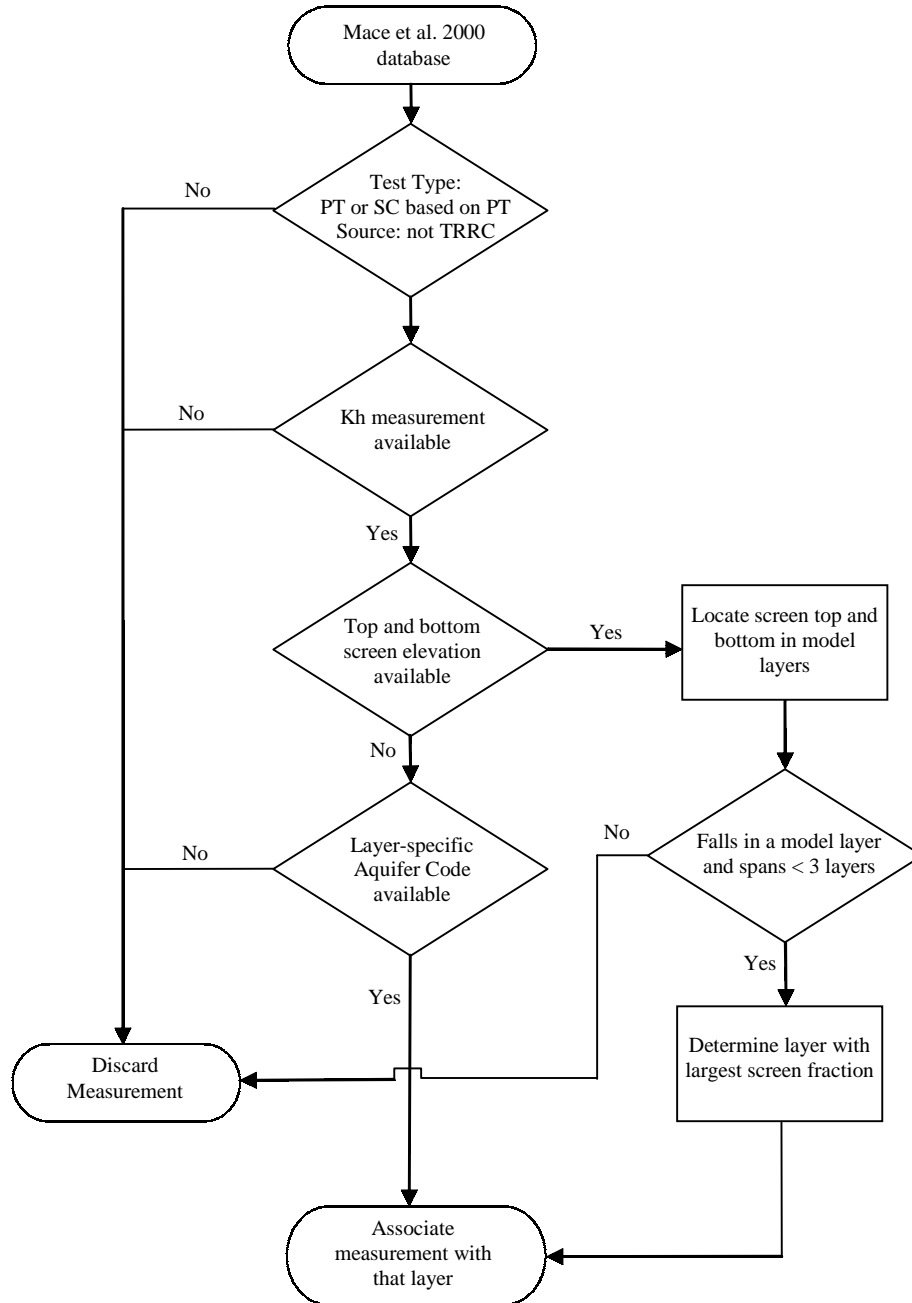


Figure 4.3.1 Screening of hydraulic conductivity data.

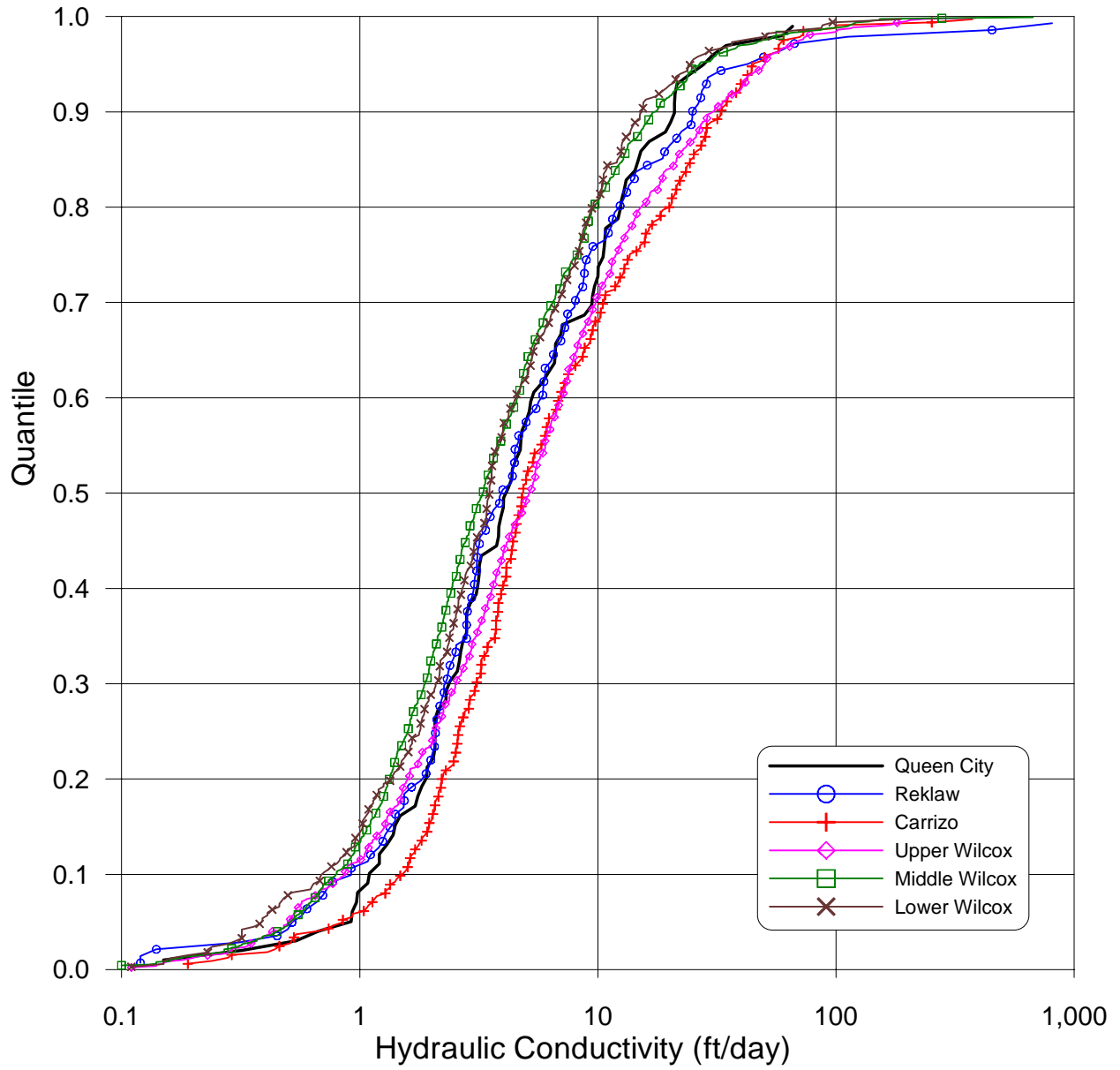


Figure 4.3.2 Cumulative distribution function (CDF) curves of hydraulic conductivity for the modeled aquifer units.

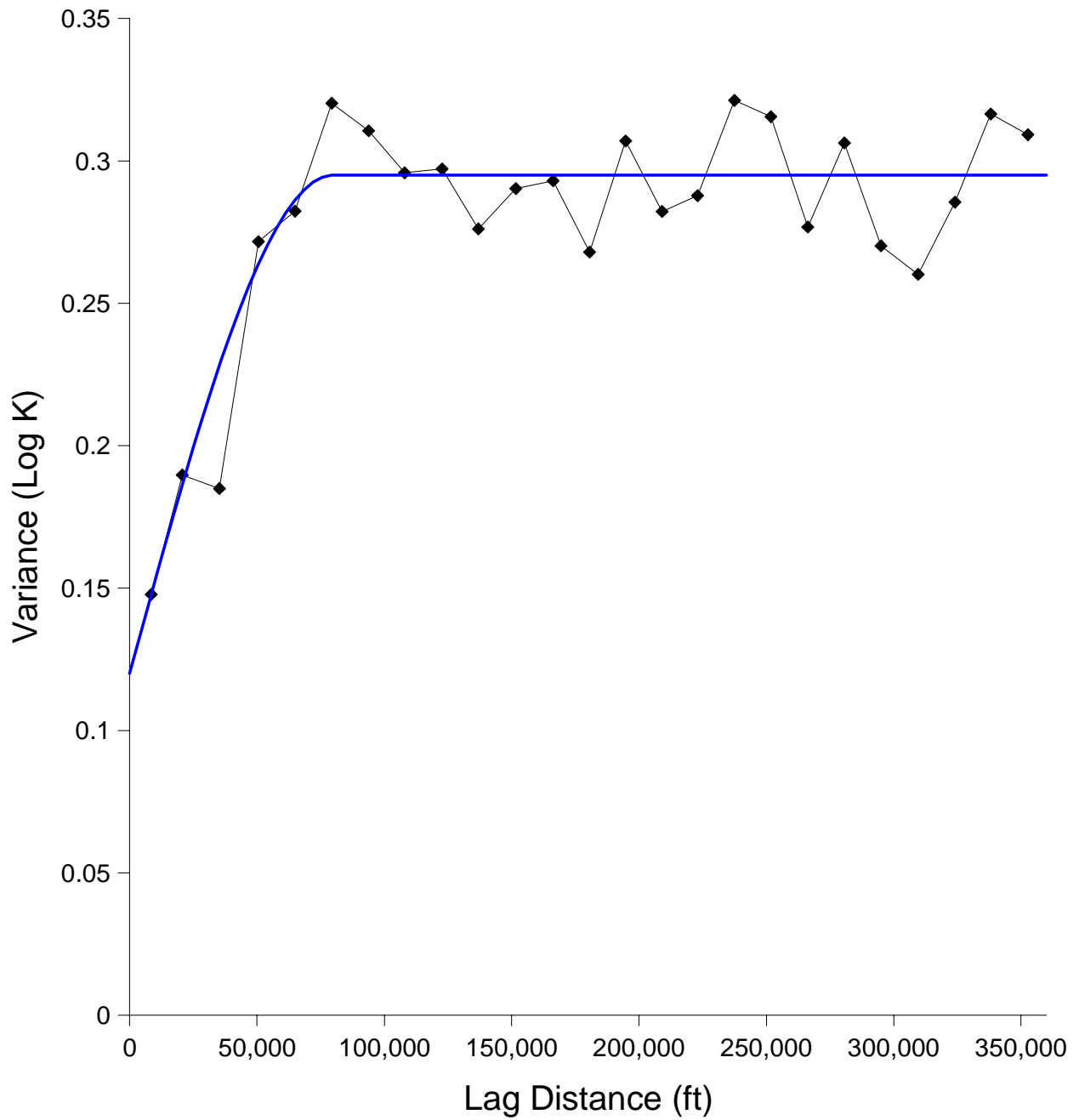


Figure 4.3.3 Variogram for hydraulic conductivity data from the Carrizo Sand.

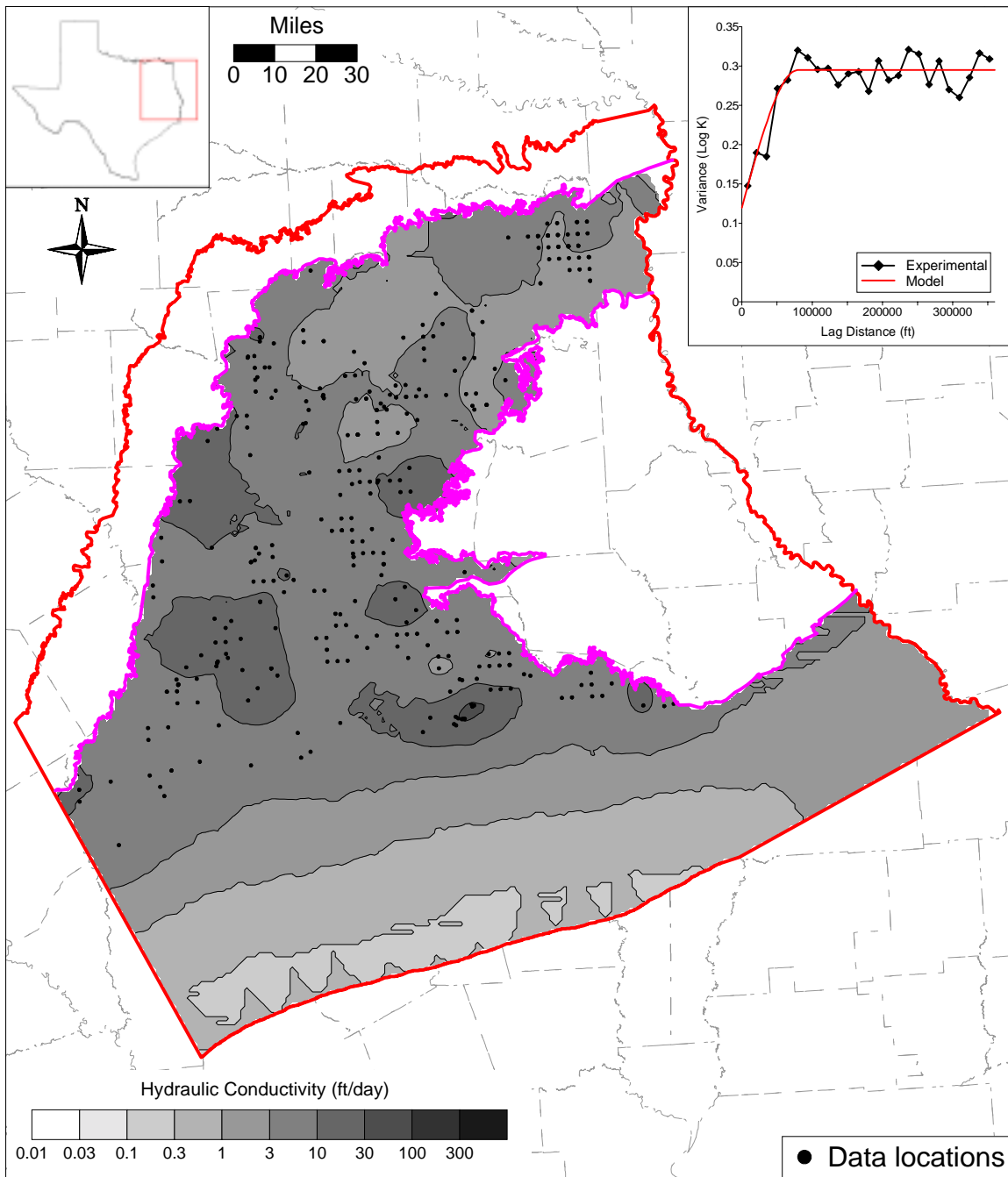


Figure 4.3.4 Variogram and kriged map of hydraulic conductivity for the Carrizo Sand.

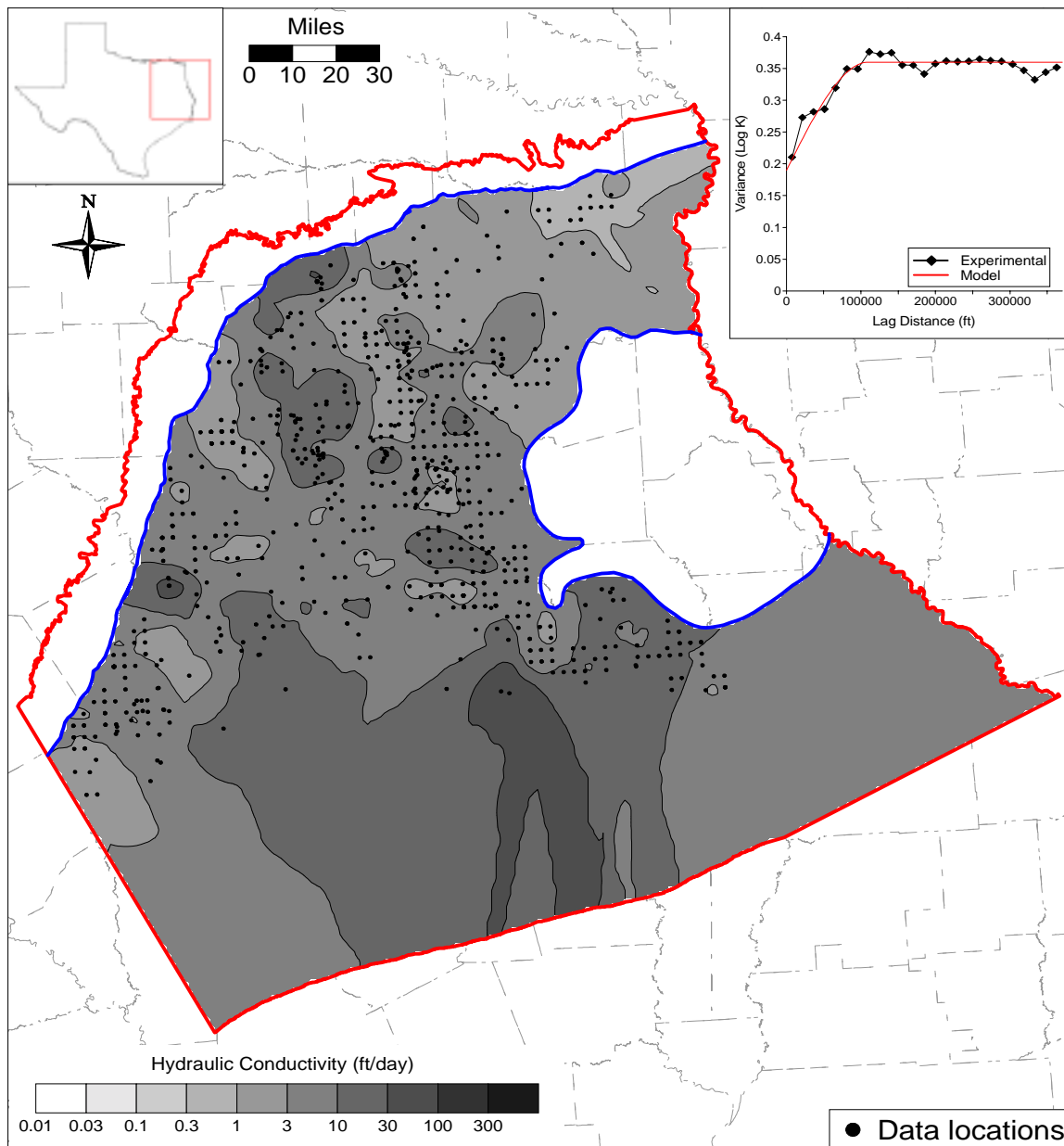


Figure 4.3.5 Variogram and kriged map of hydraulic conductivity for the upper Wilcox.

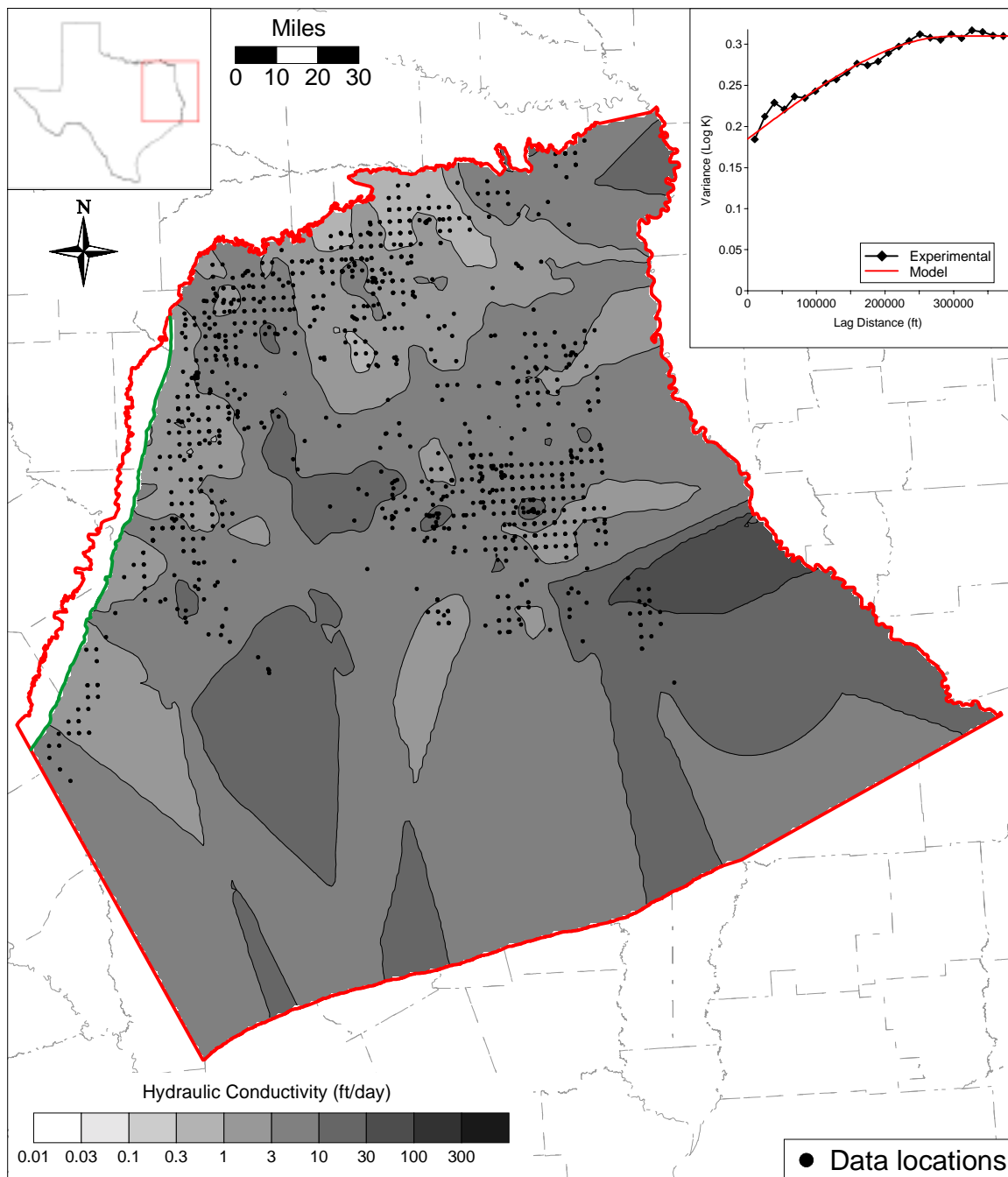


Figure 4.3.6 Variogram and kriged map of hydraulic conductivity for the middle Wilcox.

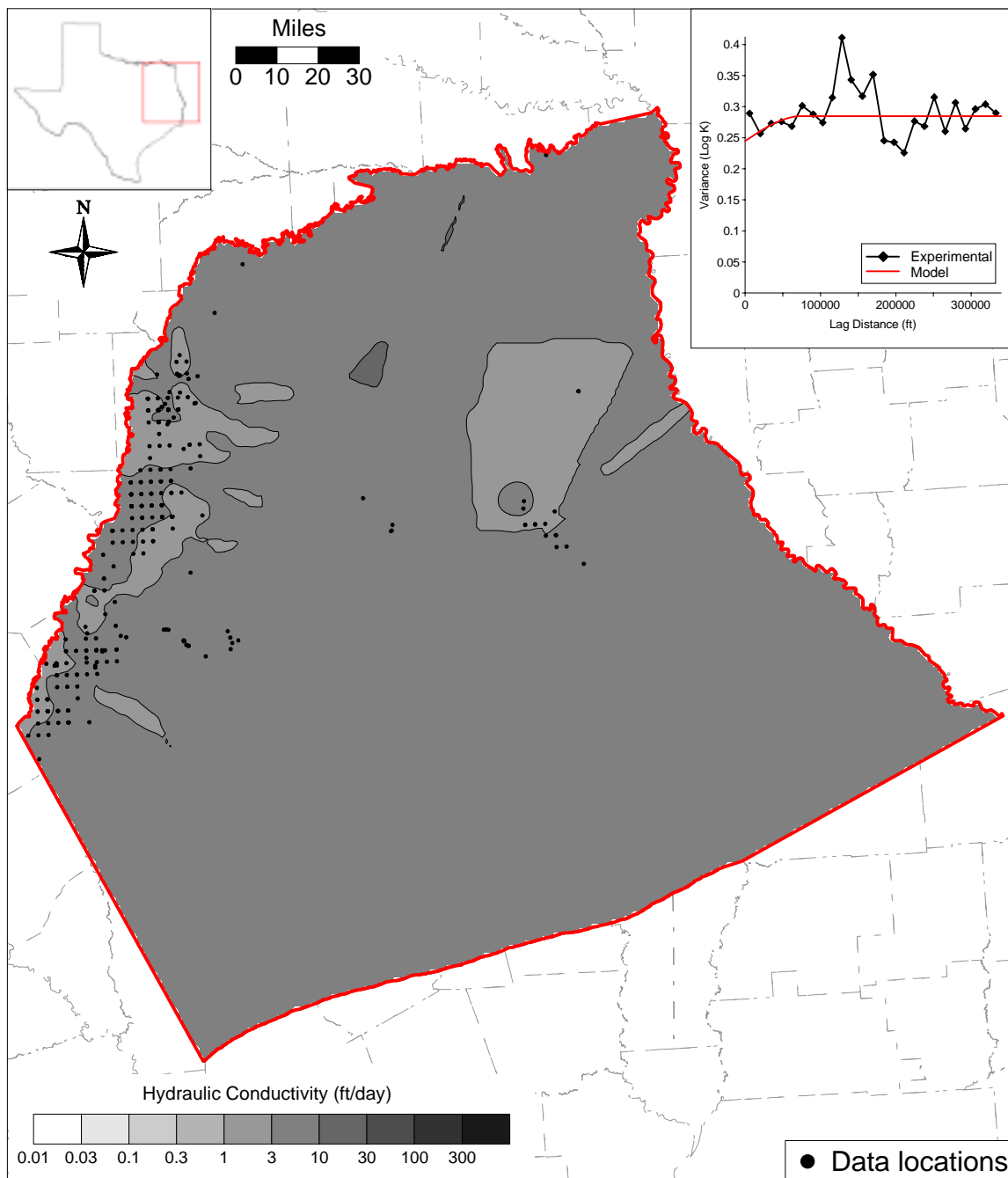


Figure 4.3.7 Variogram and kriged map of hydraulic conductivity for the lower Wilcox.

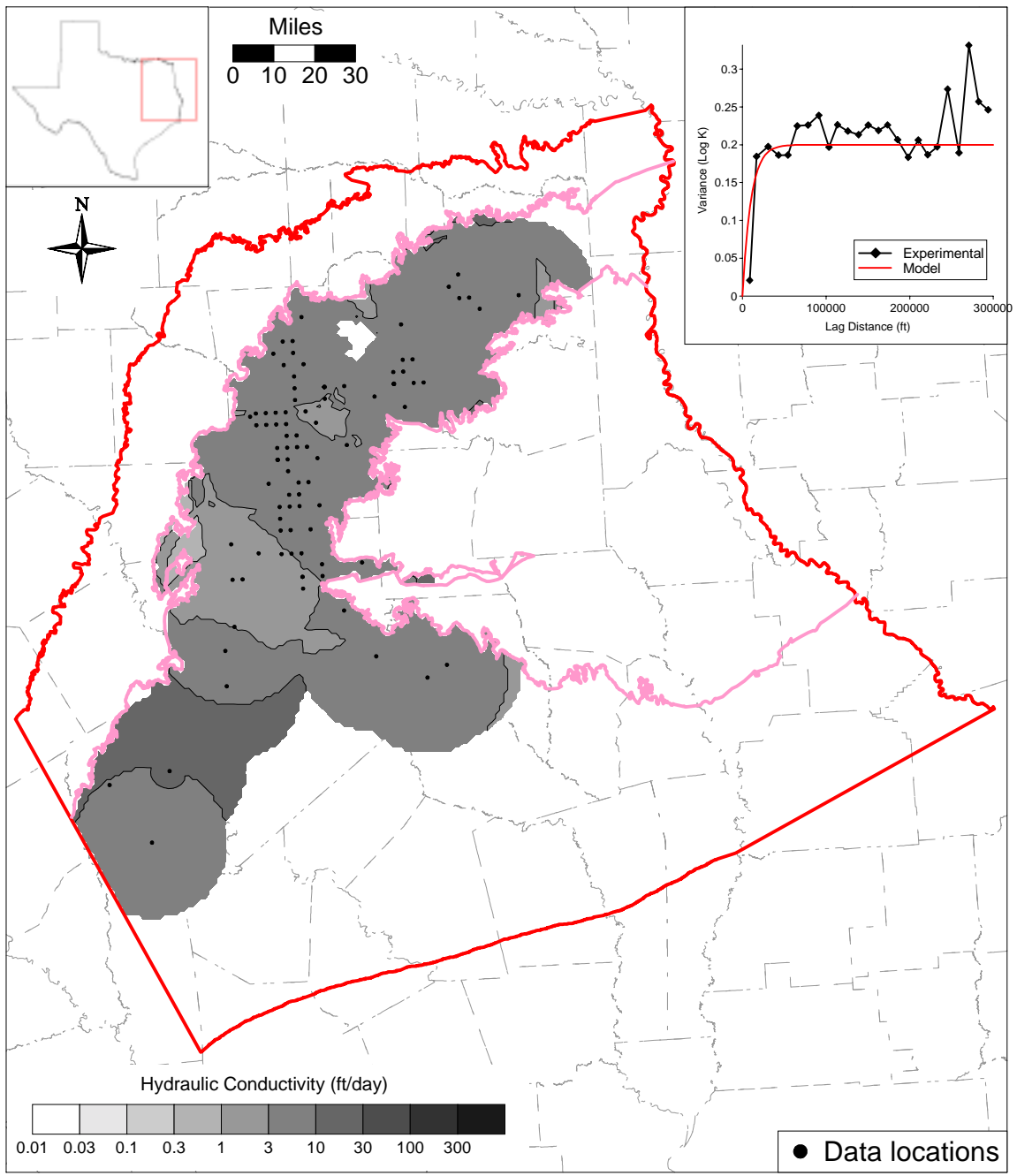
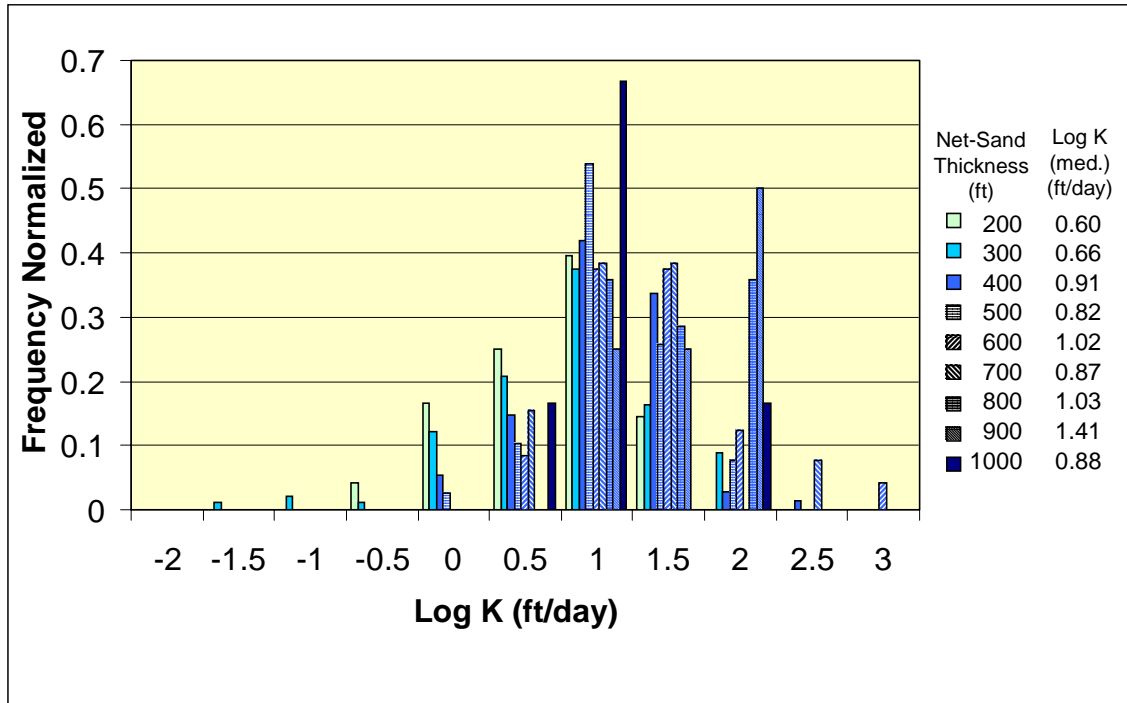
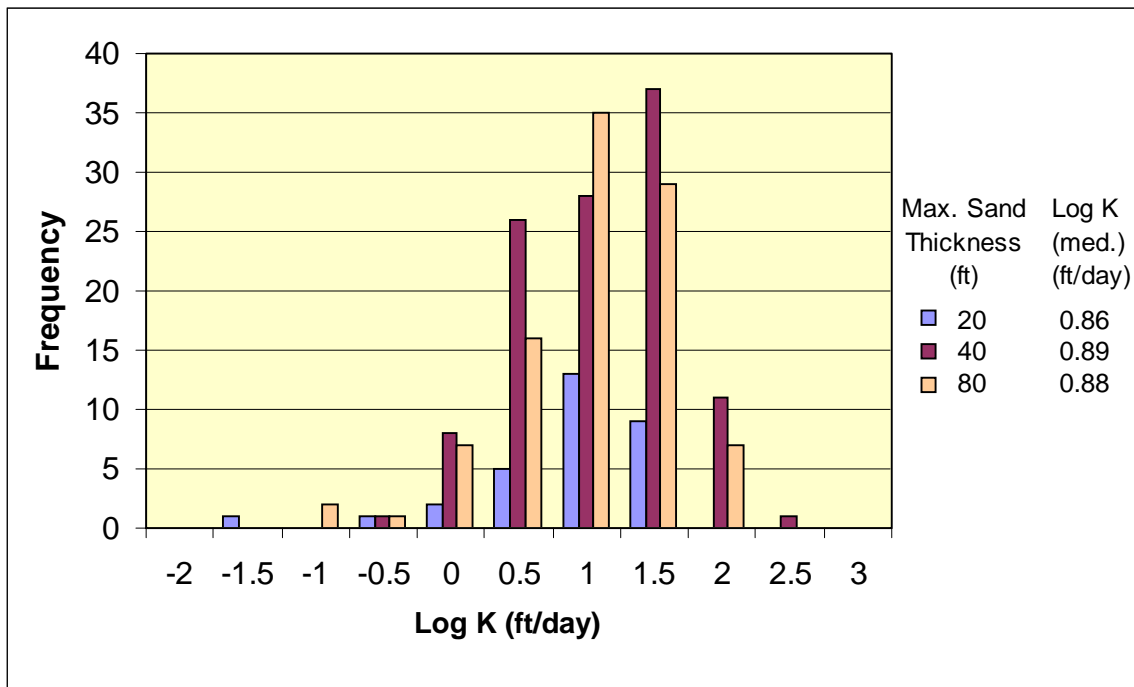


Figure 4.3.8 Variogram and kriged map of hydraulic conductivity for the Queen City.



a.



b.

Figure 4.3.9 Histogram of (a) net-sand thickness for the entire Wilcox Group and (b) maximum sand thickness and hydraulic conductivity (Log K) of the upper Wilcox.

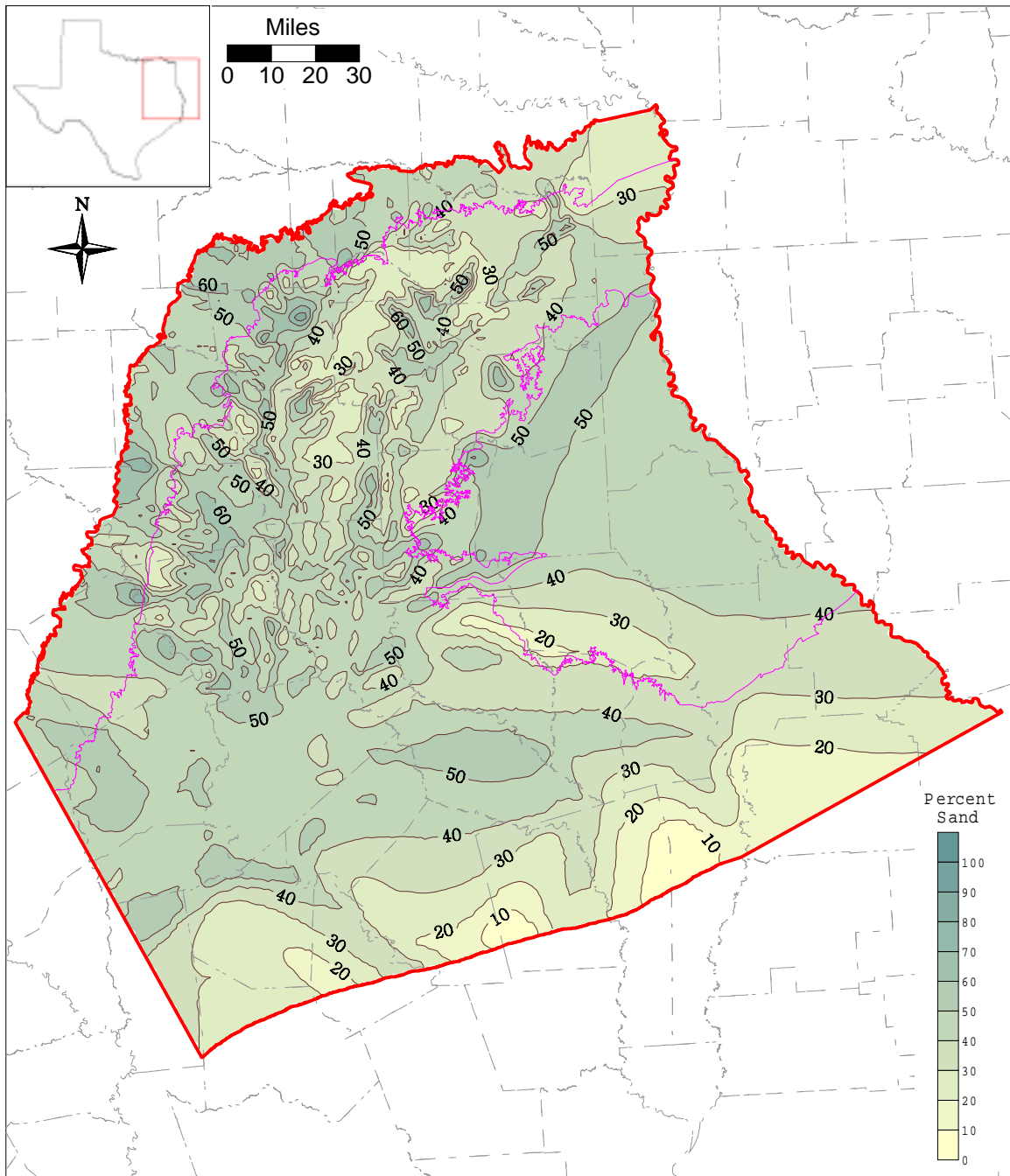


Figure 4.3.10 Percent sand for the Wilcox Group, based on sand maps by Kaiser et al. (1978) and Fisher and McGowen (1967) (CI = 10 percent).

4.4 Water Levels and Regional Groundwater Flow

An extensive literature search was conducted to understand (1) regional groundwater flow in the Carrizo Sand and Wilcox Group prior to extensive development of groundwater resources in the area and (2) the history of groundwater usage from the Carrizo Sand and the Wilcox Group. The literature search included a review of the available county reports, historical USGS reports (predominately water-supply papers), and reports by the various Texas state agencies responsible for water resources (i.e., the Texas Board of Water Engineers, the Texas Water Commission, and the Texas Water Development Board). A summary of all reports reviewed can be found in Appendix A. In addition, water-level data provided by the Texas Water Development Board (TWDB) on their website was used to (1) perform a pressure versus depth analysis, (2) develop water-level elevation contours corresponding to the start time for the transient model (January 1980), the end of the model calibration period (December 1989), and the end of the model verification period (December 1999), and (3) investigate transient water level conditions.

The relationship between the Carrizo Sand and the sands of the Wilcox Group varies across the study area. This variation is graphically presented in Figure 4.4.1. In general, the sands of the Wilcox Group, the Carrizo Sand, the sands of the Reklaw Formation, and the Queen City Sand are hydraulically connected and act as a single aquifer, referred to as the Cypress aquifer, in Cass and Marion counties (Broom, 1971), Camp, Franklin, Morris, and Titus counties (Broom et al., 1965), and Harrison County (Broom and Myers, 1966). The Carrizo Sand and the sands of the Wilcox Group are considered to function as a single aquifer due to their similar properties and hydraulic connection in Wood County (Broom, 1968), Smith County (Dillard, 1963), and Leon County (Peckham, 1965). The sands of the Wilcox Group and the Carrizo Sand are considered a single aquifer in Rains and Van Zandt counties (White, 1973), and San Augustine and Sabine counties (Anders, 1967), with the sands of the Wilcox being the principal source of water. In Upshur and Gregg counties (Broom, 1969), the Carrizo Sand and the sands of the Wilcox Group also act as a single aquifer with the Carrizo Sand being the principal source of water. The Carrizo Sand is missing in Limestone County (Rettman, 1984), and Bowie, Panola, and Shelby counties. The Carrizo Sand and the sands of the Wilcox Group act as separate aquifers in the remaining portions of the study area. The principal aquifer in

Henderson, Freestone, Anderson, and Cherokee counties (William F. Guyton & Associates, 1972), Rusk County (Sandeen, 1987), Caddo Parish, Louisiana (Page and May, 1964), Sabine Parish, Louisiana (Page et al., 1963), and Desoto Parish, Louisiana is the Wilcox aquifer. The principal aquifer in Nacogdoches and Angelina counties (William F. Guyton & Associates, 1970), Houston County (Tarver, 1966), Natchitoches Parish, Louisiana (Newcome et al., 1963), and Miller County, Arkansas (Ludwig, 1972) is the Carrizo Aquifer. Based on data from the TWDB website, the sands of the Wilcox Group are not used as a source of groundwater in Madison County. Neither the Carrizo Sand nor the sands of the Wilcox Group supply groundwater in Trinity County. Only saline water is found in the Carrizo Sand and sands of the Wilcox Group in Grimes County (Baker and Follett, 1974), Walker County (Winslow, 1950), San Jacinto County (Sandeen, 1968), Polk County (Tarver, 1968a), Tyler County (Tarver, 1968b), Montgomery County (Popkin, 1971), and Jasper and Newton counties (Wesselman, 1967). As can be seen from this discussion and Figure 4.4.1, the Carrizo Sand and the sands of the Wilcox Group have a complicated and variable relationship across the study area.

Water-level data for the study area can be found on the TWDB website¹. Water-level data for the Carrizo Sand and Wilcox Group are sparse from about 1929 to the 1950s. Thereafter, the amount of available water-level data increases significantly. Figure 4.4.2 shows well locations at which water-level measurements are available and the hydrologic unit in which each well is completed. These are the data used to investigate water-level elevations for this study.

4.4.1 Regional Groundwater Flow

The discussion on regional groundwater flow in the Carrizo Sand and Wilcox Group provided in this section is taken from Fogg and Kreitler (1982). They studied the hydrochemical facies and groundwater hydraulics of the Eocene aquifers in the East Texas Basin in great detail as part of a research program designed to evaluate the suitability of East Texas salt domes as repositories for high-level nuclear waste.

Water within the Carrizo Sand and the sands of the Wilcox Group is under water-table conditions in the outcrop areas and under artesian conditions down dip of the outcrop. In many areas, artesian pressures within the aquifer were originally sufficient to drive water above ground

surface. Water still flows to the surface in the valleys of the Trinity and Sabine rivers and some of their tributaries in the artesian portion of the aquifers indicating upward flow in these areas. Flowing wells are not observed along the Neches and Angelina rivers, indicating an absence of an upward component of flow along these rivers.

Groundwater movement within the Carrizo Sand and Wilcox Group is significantly influenced by the topography and by the structure of the units. Topographic highs are present in both outcrop areas, with the eastern outcrop belt at higher elevations than the western outcrop. A structural high, which trends from the northwest to the southeast, is present in Upshur, Gregg, and Smith counties (see Section 2). Topographic lows are found in the stream beds both in the outcrops and in the artesian section of the aquifers. In general, groundwater flows from the topographically and structurally high areas to the topographically and structurally low areas (Figure 4.4.3). Several rivers within the outcrops act as major discharge areas. From north to south, these are the Red River, the Sulphur River, Big Cypress Creek, the Sabine River, Neches River, and the Trinity River (Figure 2.2).

Northeast of the structural divide located in Upshur, Gregg, and Smith counties, groundwater in the artesian portion of the aquifers generally flows northeastward toward the Texas-Louisiana border (see Figure 4.4.3). South of the structural divide, the flow of groundwater is generally to the south. The Sabine River between the structural high to the north and a watershed divide to the south interrupts this latter trend. In this area, groundwater flows to the Sabine River. In addition, groundwater west of the Trinity River flows eastward into the Trinity. The Angelina River appears to have little impact on the flow of groundwater in the Carrizo and Wilcox aquifers. Some groundwater converges towards the Neches River. Strata of the Carrizo Sand and Wilcox Group are displaced by faults in the Elkhart Graben-Mount Enterprise fault system. These faults appear to be a partial barrier to horizontal groundwater flow.

4.4.2 Predevelopment Conditions for the Carrizo Sand and the Wilcox Group

Use of waters from the Carrizo Sand and Wilcox Group began in the late 1800s. Early development predominantly consisted of domestic and stock wells. Precipitation is relatively high over most of this region resulting in little need for irrigation. Consequently, large capacity

¹ rio.twdb.state.tx.us/publications/reports/GroundWaterReports/GWDatabaseReports/GWdatabaserpt.htm

irrigation wells are not found in the study area. The most significant use was for municipal and industrial purposes. The cities of Lufkin in Angelina County and Nacogdoches in Nacogdoches County began pumping groundwater from the Carrizo Sand in the 1930s. Heavy industrial pumping by a paper mill (originally the Southland Paper Mills) also occurred in this area. William F. Guyton & Associates (1970) estimated that drawdowns of up to 500 ft have occurred at pumping centers as a result of this municipal and industrial pumpage.

Extensive pumping also began in Upshur, Gregg, Smith, and Rusk counties after discovery of the East Texas Oil Field in 1930-1931. Numerous processes related to the oil industry and the increased population in the area of the oil field created an immediate demand for water. Wells completed to the Carrizo-Wilcox aquifer(s) met these water needs. By the early 1950s, most of the water required by the municipalities in the area near the oil field switched to surface-water sources.

Louisiana began using groundwater from the Carrizo Sand and Wilcox Group as early as 1900. The cities of Shreveport and Bossier City used water from the Wilcox Group for their public supply until they switched to surface water in 1926-1928. Over 60 wells were pumping from the Wilcox Group prior to the first recorded water-level measurements in Louisiana². The Wilcox Group is not used to supply groundwater and very little groundwater is pumped from the Carrizo Sand in Miller County, Arkansas.

Although pumping of the Carrizo Sand and Wilcox Group began early in the 1900s, few water-level data are available prior to 1950 in Texas (TWDB, website) and prior to 1940 in Louisiana (LaDOT, website). A brief description of historical development in each county/parish in the model area can be found in Appendix A. The dates at which wells were first completed to the Carrizo Sand and/or Wilcox Group are also given in the appendix as well as the dates for the first water-level measurements. Based on this information, few of the early water-level measurements available for the Carrizo Sand and Wilcox Group in the study area are considered to be representative of predevelopment conditions. The few data that are considered to represent predevelopment conditions are shown in Figure 4.4.4 and tabulated in Table 4.4.1. Although, these data are insufficient to develop water-level elevation contours corresponding to

² www2.dotd.state.la.us/wells/wells.html

predevelopment, they were used as point targets in calibration of the steady-state model (see Section 8.1).

4.4.3 Pressure Versus Depth Analysis

A study of pressure head versus screen-midpoint depth was conducted using wells having both water-level and screen-depth data on the TWDB website. Water-level measurements taken prior to 1950 in Texas counties constituted the data used for the analysis. The goal of the analysis was to evaluate vertical gradients between the hydrostratigraphic units. The locations of the wells used and the unit in which they are completed are given in Figure 4.4.5. This figure shows that little water-level data and screen data are available for times earlier than 1950. All of the wells completed to the Carrizo Sand are located in Nacogdoches, Angelina, or Anderson counties. Wells completed to the Wilcox Group and the Carrizo-Wilcox are scattered throughout the study area.

Figure 4.4.6 shows the pressure-depth analysis results. The screen midpoints for wells completed in the Carrizo Sand range from a depth of about 200 ft to depths greater than 1200 ft. The range in screen midpoints is about 100 to 1700 ft for wells completed in the Wilcox Group. Some data for the combined Carrizo-Wilcox was available for wells with screen depths ranging from about 225 to 1100 ft. A fit through the data for the 28 wells completed in the Carrizo Sand gives a slope of 1.05, indicating a pressure gradient slightly higher than hydrostatic conditions. A fit through the data for the 36 wells completed in the Wilcox Group gives a slope of 0.94, indicating a pressure gradient slightly less than hydrostatic. The difference in slope between the data for the Carrizo Sand and Wilcox Group suggests a lack of communication between these two hydrologic units. For the ten wells completed to the Carrizo and Wilcox, a linear fit through the data yields a slope of 0.96, indicating a pressure gradient slightly less than hydrostatic.

The pressure-depth data show a relatively large scatter between and within the different aquifer units and, considering the large area and uneven distribution (Figure 4.4.5), can mask different flow regimes. Evaluating pressure-depth trends on a county-by-county area indicates significantly different trends for different counties (Figure 4.4.6). Anderson, Angelina, and Rusk counties have slopes less than one, indicating downward flow, whereas Nacogdoches County has a slope greater than one, indicating upward flow. Data from Angelina and Nacogdoches counties are mostly from the Carrizo. The upward flow indicated for Nacogdoches County may be

associated with upward flow to the Angelina River. All data points from Angelina County are in the vicinity of the Angelina River (Figure 4.4.5) but the pressure-depth trend indicates significant decline due to pumpage. A similar trend is apparent in Rusk County, which is probably due to pumpage. Pressure-depth data covers a wide depth range and may reflect different flow regimes within the Wilcox and Carrizo.

Since few data are available prior to 1950, the pressure-depth analysis was repeated using all wells, regardless of time, for which both water-level and screen data could be found on the TWDB website. In all cases, the analysis used the maximum water level measured in each well. The locations of these data points are shown in Figure 4.4.7. Use of more data resulted in greater coverage of the study area. Figure 4.4.8 shows the results of the analysis. For wells completed in the Carrizo Sand, the Carrizo and Wilcox, and the Wilcox Group, use of all available data results in a significant decrease in the slope and correlation, indicating significant depressurization in the aquifers between 1950 and 2000.

4.4.4 Water-Level Elevations for Model Calibration and Verification.

Model calibration considered the time period from January 1, 1980 to December 31, 1989 and model verification considered the time period from January 1, 1990 to December 31, 1999 (see Section 9.1). Water-level data found on the TWDB website were used to develop water-level elevation contours for the start of calibration, the end of calibration, and the end of verification. Initialization of water levels in the transient model utilized the contours for the time corresponding to the start of calibration (January 1980). The contours for the end of calibration and the end of verification aided in assessing the transient model's ability to represent observed conditions.

Water-level data on the TWDB website are not available at regular time intervals in every well. Therefore, the coverage of water-level data for a particular month or even a year is very sparse. For example, water levels were measured in a total of three wells in January, 1980, and in a total of 118 wells during all of 1980. Because this amount of data is not sufficient to develop contours across the entire model area for every geologic unit at the start of model calibration, measured water levels near the date of interest were also used if they met any of the following criteria:

- The water level for a well with a single measurement was used if the date of the measurement fell within ± 3 years of the date of interest;
- For wells with water-level data at times only before or after the date of interest, the closest measurement to the date of interest was used if the measurement date fell within ± 2.5 years of the date of interest;
- For wells with water-level data at dates both before and after the date of interest, the water level at the date of interest was interpolated if (1) both measurement dates were within ± 2.5 years of the date of interest, (2) one measurement was within ± 2.5 years of the date of interest and the total head difference between the two measurements was less than 100 ft; or (3) the total head difference between the two measurements was less than or equal to 20 ft regardless of measurement dates.

Using this method, a total of 1128 water-level measurements were available for constructing water-level elevation maps for the start of calibration (January 1, 1980).

Figures 4.4.9a-e show the water-level elevation contours for the Queen City Sand (layer 1), the Carrizo Sand (layer 3), the upper Wilcox (layer 4), the middle Wilcox (layer 5), and the lower Wilcox (layer 6) at the start of calibration (January 1, 1980). The water-level elevations shown on these contour maps were used as the initial conditions for the transient model. Contours for the Reklaw Formation could not be generated due to a lack of data. To initialize the model, the average of the water-level elevations for the overlying Queen City Sand and underlying Carrizo Sand were used for the Reklaw Formation.

Note that artificial points were used to construct the contours for the Carrizo Sand, upper Wilcox, and middle Wilcox. These points helped define the cone of drawdown (both laterally and vertically) created by municipal pumpage for the cities of Nacogdoches (Nacogdoches County) and Lufkin (Angelina County) because observed data are not available south of this drawdown center. An artificial point located in southeastern Wood County was used to vertically extend to the middle Wilcox a drawdown observed in the upper Wilcox. These artificial points were needed due to a lack of data in the vicinity of locations known to experience drawdown.

Figures 4.4.10a-d show the water-level elevation contours for the Carrizo Sand, upper Wilcox, middle Wilcox, and lower Wilcox at the end of model calibration (December 31, 1989). An estimated water level in the middle Wilcox was used to vertically extend the drawdown observed in the Carrizo Sand and upper Wilcox caused by municipal pumpage by the cities of Nacogdoches and Lufkin. This estimated point was needed because of a lack of data in an area known to be experiencing drawdown. Figures 4.4.11a-d show the water-level elevation contours for the same units at the end of model verification (December 31, 1999). An estimated water level in the upper and middle Wilcox was used to vertically extend the drawdown observed in the Carrizo Sand caused by municipal pumpage for the cities of Nacogdoches and Lufkin. These estimated points were needed due to a lack of data in areas known to be experiencing drawdown.

4.4.5 Transient Water Levels

Historically, the greatest water-level declines in the Carrizo Sand and Wilcox Group have occurred as a result of municipal pumpage by the cities of Nacogdoches (Nacogdoches County) and Lufkin (Angelina County) and industrial pumpage at a paper mill (formerly the Southland Paper Mill) located on the Nacogdoches-Angelina County border. This municipal and industrial pumping began in the 1930s and continues to the present. Figure 4.4.12 shows the transient water-level record for a well located near the paper mill and completed in the Carrizo Sand and upper Wilcox. The water level in this well decreased 300 ft between May 1947 and November 1985. From 1985 to 1992, the water level increased about 60 ft. In addition to causing large water-level declines in individual wells, this pumping appears to have also affected a large lateral area based on the limited data available south of the pumping center.

Figure 4.4.13 shows the locations for which transient water-level data (hydrographs) are available for the last 20 (1980-1999) years based on data on the TWDB website. Also shown on this figure is either the model layer in which the midpoint of the well screen is located or, where screen data are not available, the model layer in which the bottom of the well is located. Few transient data were available for wells located in the vicinity of the pumpage in Nacogdoches and Angelina counties between January 1980 and December 1999. Wells north of the center in Nacogdoches County for which transient data are available show either no change or an increase in water-level elevations over this period. The water level in several wells increased significantly, such as the 100-ft rise observed in well 37-27-201 (Figure 4.4.14). Most wells

south of this area in Angelina County, on the other hand, show declines in water-level elevations over this 20-year period. The water level in well 37-35-703 declined over 150 ft (see Figure 4.4.14).

In general, water levels in the artesian portions of the Carrizo Sand and Wilcox Group in the study area have remained constant or declined over the last 20 years (1980-1999). The amount of decline has varied from county to county and from well location to well location within a county. The largest declines have been observed in Anderson and Smith counties. In the last 20 years, the water level in well 34-61-501, completed to the Carrizo Sand in Anderson County, has declined over 90 ft, and the water level in well 34-38-805, completed to the Carrizo Sand in Smith County, has declined over 175 ft (Figure 4.4.15). In addition to northern Nacogdoches County, significant water-level increases have also been observed in wells located in Cass and Titus counties. The water level in well 35-07-902, completed in the Carrizo Sand in Cass County, and well 16-49-703, completed in the Wilcox Group in Titus County, have risen over 60 ft in the past 20 years (Figure 4.4.15).

In general, water levels in wells located in the Sabine Uplift on the eastern side of the study area have remained relatively constant (less than ± 15 -ft change) over the last 20 years based on the transient data available on the TWDB website. In contrast, many wells located in the outcrop on the western edge of the study area have recorded decreasing water levels since 1980. For example, the water level in well 39-15-802, completed to the Wilcox Group in Freestone County, has declined over 50 ft in the last 20 years (see Figure 4.4.15).

The changes in water levels between the start of the transient model calibration (January 1980) and the end of model calibration (December 1989) and between the start of model calibration (January 1980) and the end of model verification (December 1999) are illustrated in Figure 4.4.16a-b for the Carrizo Sand, Figure 4.4.17a-b for the upper Wilcox, Figure 4.4.18a-b for the middle Wilcox, and Figure 4.4.19a-b for the lower Wilcox. These figures show a large decline in water levels in the southern portion of the active model area. Water levels in this region, however, are not well known due to a lack of data. A region of large and continual decline is also observed in the Carrizo Sand, and the upper and middle Wilcox in Smith, Upshur, Wood, Van Zandt, and Henderson counties. Based on Figure 4.4.17a-b, water levels in the upper Wilcox have risen in Cass County. This increase is consistent with the transient water-level data

available for wells in this county. Declines in water level observed over one time period but not the other, most likely are the result of variability in available data.

Table 4.4.1 Target values for calibration of the steady-state model to predevelopment conditions.

Well Number	County/Parish	Observed Water-Level Elevation (ft)	Target Water Level Elevation ^(a) (ft)	Model Layer	Source of Observed Water Level
3457801	Anderson	350	274	4	TWDB (website)
3801202	Anderson	427	362	3	TWDB (website)
3735705	Angelina	269	269	3	TWDB (website)
CD- 150	Caddo	344	323	5	LaDOT (website)
CD- 160	Caddo	340	325	5	LaDOT (website)
CD- 271	Caddo	252	156	5	LaDOT (website)
CD- 409	Caddo	335	275	5	LaDOT (website)
CD- 413	Caddo	297	277	5	LaDOT (website)
CD- 418	Caddo	354	325	5	LaDOT (website)
CD- 684	Caddo	337	339	5	LaDOT (website)
1653103	Cass	355	308	4	TWDB (website)
3464305	Cherokee	402	386	3	TWDB (website)
DS- 101	DeSoto	344	235	5	LaDOT (website)
DS- 199	DeSoto	340	310	5	LaDOT (website)
DS- 216	DeSoto	252	316	5	LaDOT (website)
DS- 218	DeSoto	335	197	5	LaDOT (website)
DS- 227	DeSoto	297	339	5	LaDOT (website)
DS- 234	DeSoto	354	299	5	LaDOT (website)
DS- 246	DeSoto	337	238	5	LaDOT (website)
DS- 247	DeSoto	344	298	5	LaDOT (website)
DS- 261	DeSoto	303	313	5	LaDOT (website)
DS- 267	DeSoto	301	291	5	LaDOT (website)
DS- 289	DeSoto	340	248	5	LaDOT (website)
DS- 303	DeSoto	252	300	5	LaDOT (website)
DS- 305	DeSoto	335	251	5	LaDOT (website)
DS- 307	DeSoto	297	247	5	LaDOT (website)
DS- 308	DeSoto	354	287	5	LaDOT (website)
DS- 309	DeSoto	337	285	5	LaDOT (website)
DS- 85	DeSoto	341	304	5	LaDOT (website)
DS-181	DeSoto	303	272	5	LaDOT (website)
1755407	Franklin	493	492	5	TWDB (website)
3406309	Franklin	539	503	3	TWDB (website)
3923703	Freestone	516	477	5	TWDB (website)
3923704	Freestone	522	482	5	TWDB (website)
3924603	Freestone	474	465	3	TWDB (website)
3931410	Freestone	497	490	5	TWDB (website)

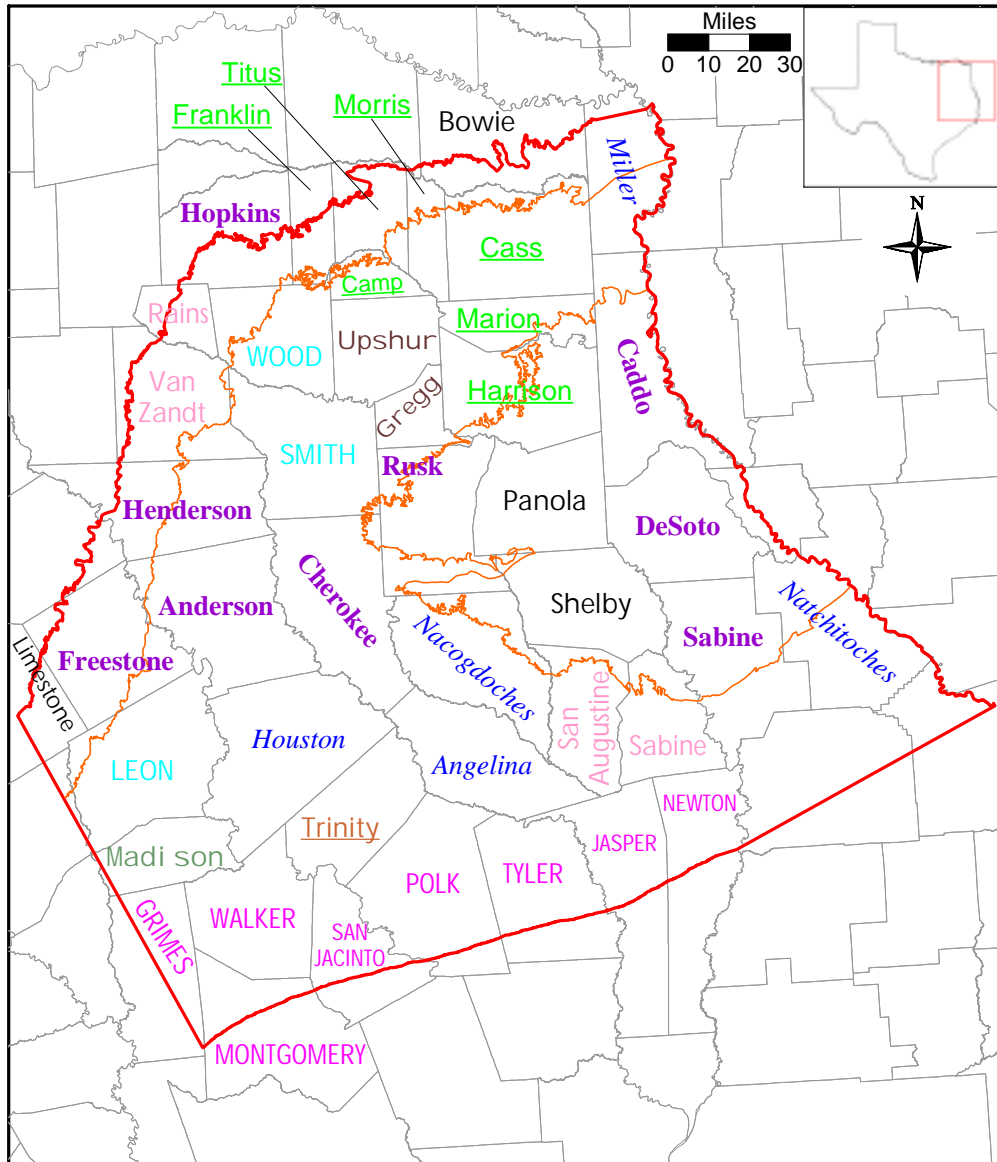
Table 4.4.1 (continued)

Well Number	County/Parish	Observed Water-Level Elevation (ft)	Target Water Level Elevation^(a) (ft)	Model Layer	Source of Observed Water Level
3932208	Freestone	453	438	3	TWDB (website)
3533911	Gregg	300	300	5	TWDB (website)
3534403	Gregg	291	291	5	TWDB (website)
3529301	Harrison	362	328	3	TWDB (website)
3530501	Harrison	367	385	4	TWDB (website)
3531708	Harrison	366	375	5	TWDB (website)
3537301	Harrison	390	334	4	TWDB (website)
3539201	Harrison	361	345	5	TWDB (website)
3539604	Harrison	376	352	5	TWDB (website)
604	Henderson	437	437	5	Duessen (1914)
3441203	Henderson	478	497	5	TWDB (website)
3441903	Henderson	468	444	4	TWDB (website)
1759603	Hopkins	522	498	5	TWDB (website)
1761301	Hopkins	521	518	5	TWDB (website)
3837102	Houston	332	332	3	TWDB (website)
727	Leon	304	304	5	Duessen (1914)
3843101	Leon	262	262	3	TWDB (website)
3939703	Leon	454	435	4	TWDB (website)
3946301	Leon	428	400	4	TWDB (website)
3857701	Madison	286	286	3	TWDB (website)
3711504	Nacogdoches	470	433	3	TWDB (website)
3712301	Nacogdoches	481	437	4	TWDB (website)
3712501	Nacogdoches	474	425	3	TWDB (website)
3712906	Nacogdoches	477	394	3	TWDB (website)
NA- 114	Natchitoches	375	258	5	LaDOT (website)
852	Panola	320	308	5	Duessen (1914)
3547501	Panola	347	354	5	TWDB (website)
3552301	Panola	316	336	5	TWDB (website)
3555301	Panola	305	300	5	TWDB (website)
3563701	Panola	296	295	5	TWDB (website)
3564101	Panola	280	232	5	TWDB (website)
3564201	Panola	280	269	5	TWDB (website)
3704301	Panola	380	347	4	TWDB (website)
3403703	Rains	513	487	5	TWDB (website)
3541202	Rusk	384	384	4	TWDB (website)
3541509	Rusk	370	370	4	TWDB (website)
3543903	Rusk	430	369	4	TWDB (website)
3544503	Rusk	348	296	4	TWDB (website)

Table 4.4.1 (continued)

Well Number	County/Parish	Observed Water-Level Elevation (ft)	Target Water Level Elevation ^(a) (ft)	Model Layer	Source of Observed Water Level
3544701	Rusk	364	350	4	TWDB (website)
3550601	Rusk	447	454	4	TWDB (website)
3550701	Rusk	435	431	4	TWDB (website)
3550911	Rusk	443	458	4	TWDB (website)
3551903	Rusk	405	353	4	TWDB (website)
3558401	Rusk	436	408	4	TWDB (website)
3559603	Rusk	420	437	4	TWDB (website)
3559701	Rusk	421	416	4	TWDB (website)
3560102	Rusk	382	361	4	TWDB (website)
3702801	Rusk	422	422	5	TWDB (website)
3703301	Rusk	446	446	4	TWDB (website)
3703901	Rusk	482	451	4	TWDB (website)
3704201	Rusk	458	420	4	TWDB (website)
3711201	Rusk	548	414	4	TWDB (website)
SA- 148	Sabine	357	312	5	LaDOT (website)
SA- 164	Sabine	331	285	5	LaDOT (website)
SA- 178	Sabine	264	243	5	LaDOT (website)
SA- 203	Sabine	359	330	4	LaDOT (website)
SA- 231	Sabine	278	287	4	LaDOT (website)
3732111	San Augustine	464	360	3	TWDB (website)
3617802	Shelby	293	265	4	TWDB (website)
3705101	Shelby	424	377	4	TWDB (website)
3714501	Shelby	401	389	4	TWDB (website)
3723601	Shelby	422	326	4	TWDB (website)
953	Smith	436	436	3	Duessen (1914)
957	Smith	399	399	5	Duessen (1914)
3428807	Smith	482	457	3	TWDB (website)
3445803	Smith	377	377	3	TWDB (website)
3549405	Smith	438	438	5	TWDB (website)
1649212	Titus	466	399	5	TWDB (website)
3416703	Upshur	450	450	4	TWDB (website)
3426901	Van Zandt	580	522	4	TWDB (website)
3433902	Van Zandt	572	564	5	TWDB (website)
3434101	Van Zandt	588	574	5	TWDB (website)
3435101	Van Zandt	599	570	3	TWDB (website)

^(a) Target values were determined using the reported depth to water and the ground-surface elevation for the 1 mi x 1 mi model grid block containing the well. Often, the average ground-surface elevation assigned to the model grid block differed significantly from the ground-surface elevation at the well.



Cypress Aquifer

CARRIZO-WILCOX AQUIFER
 Carrizo-Wilcox Aquifer; Carrizo principal source
 Carrizo-Wilcox Aquifer; Wilcox principal source
**Separate Carrizo Aquifer and Wilcox Aquifer;
 Wilcox Aquifer is most important**
*Separate Carrizo Aquifer and Wilcox Aquifer;
 Carrizo Aquifer is most productive*
 Wilcox Aquifer only
Carrizo Sand and Wilcox Group not used to supply groundwater
SALINE WATER ONLY IN THE CARRIZO SAND AND WILCOX GROUP
 Carrizo Aquifer only

Figure 4.4.1 Relationship between the Carrizo Sand and the Wilcox Group in the study area.

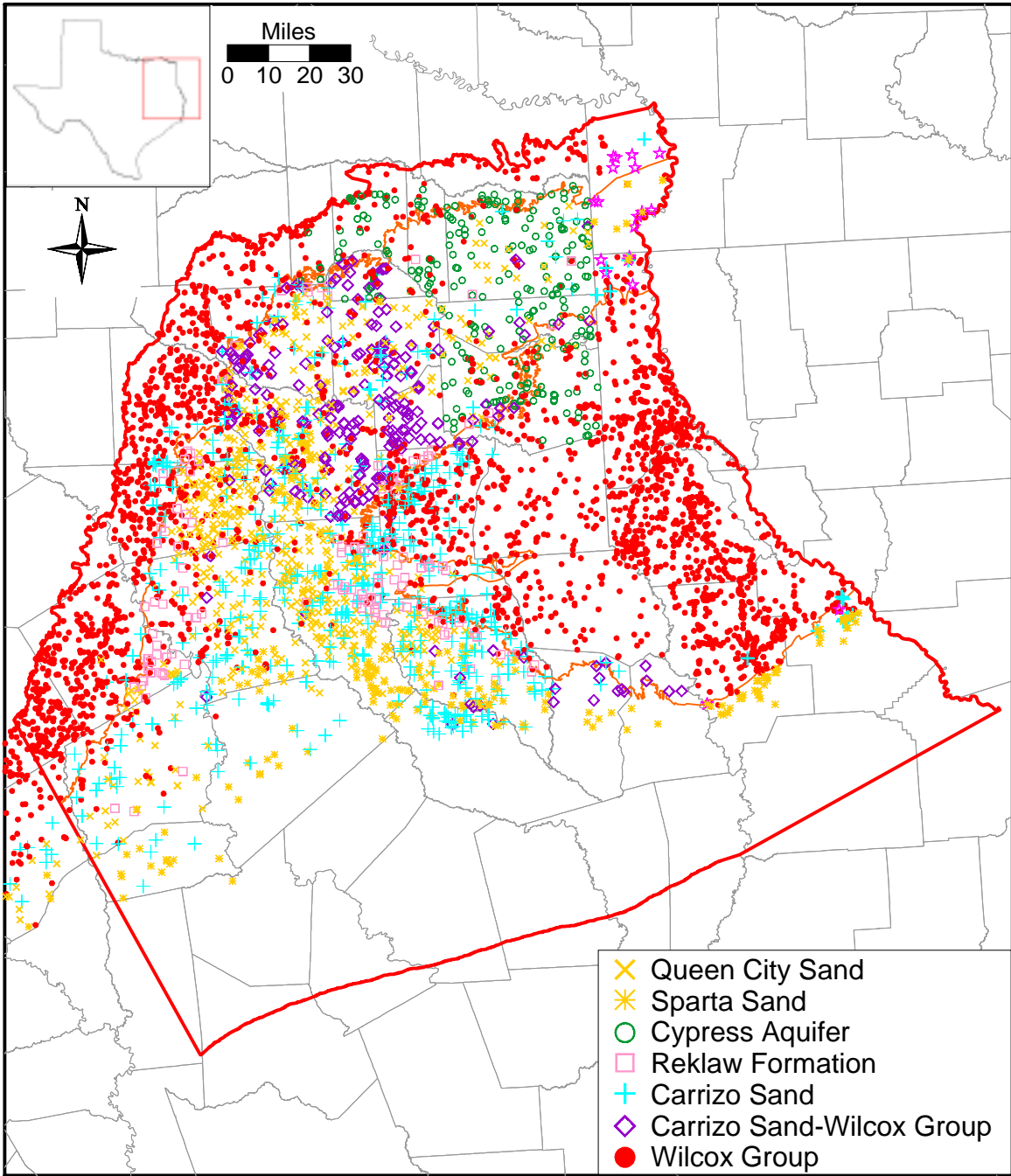


Figure 4.4.2 Water-level measurement locations for the hydrostratigraphic units in the study area.

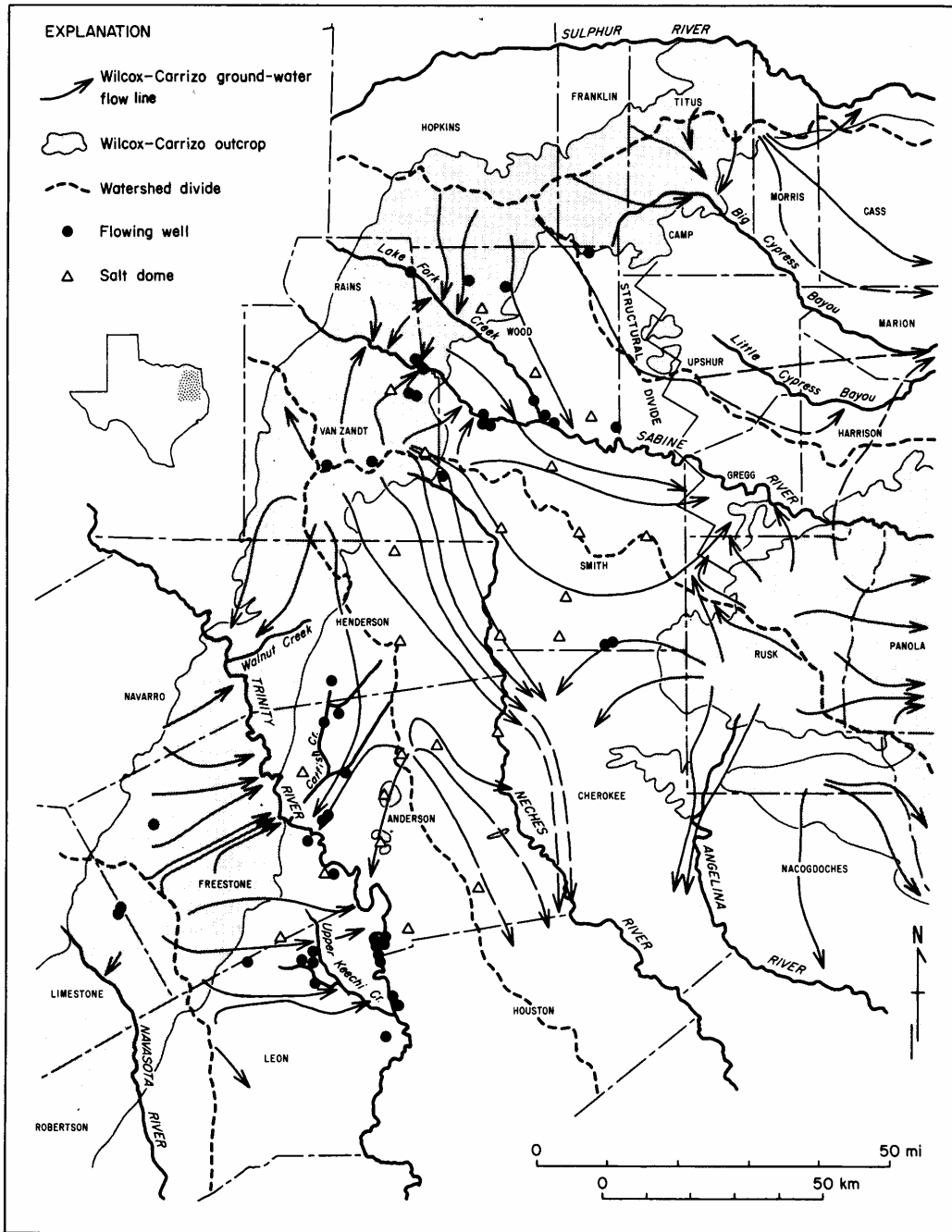


Figure 4.4.3 Groundwater flow lines drawn from the Carrizo-Wilcox potentiometric surface (from Fogg and Kreitler, 1982).

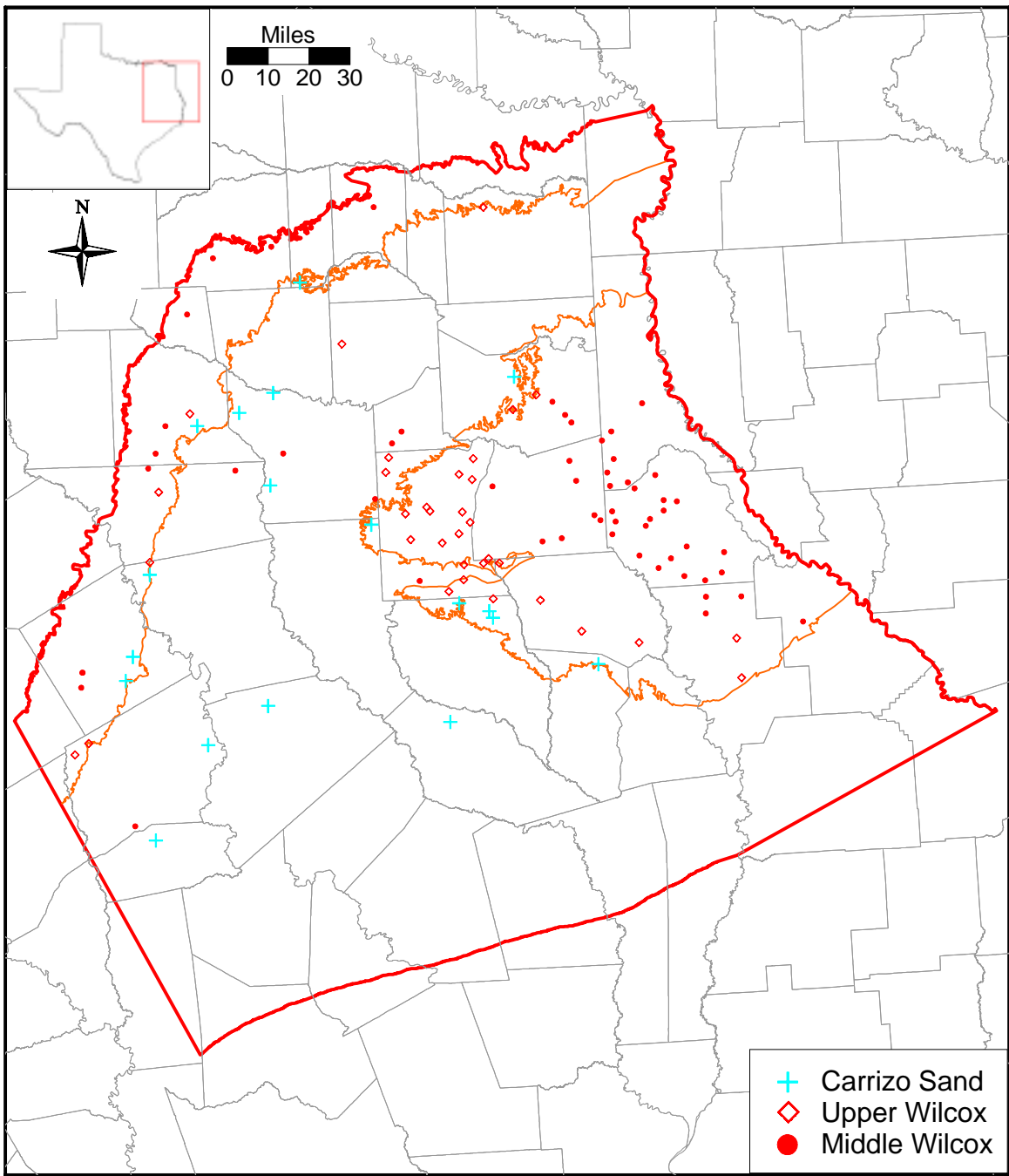


Figure 4.4.4 Location and model layer for predevelopment water-level elevation targets.

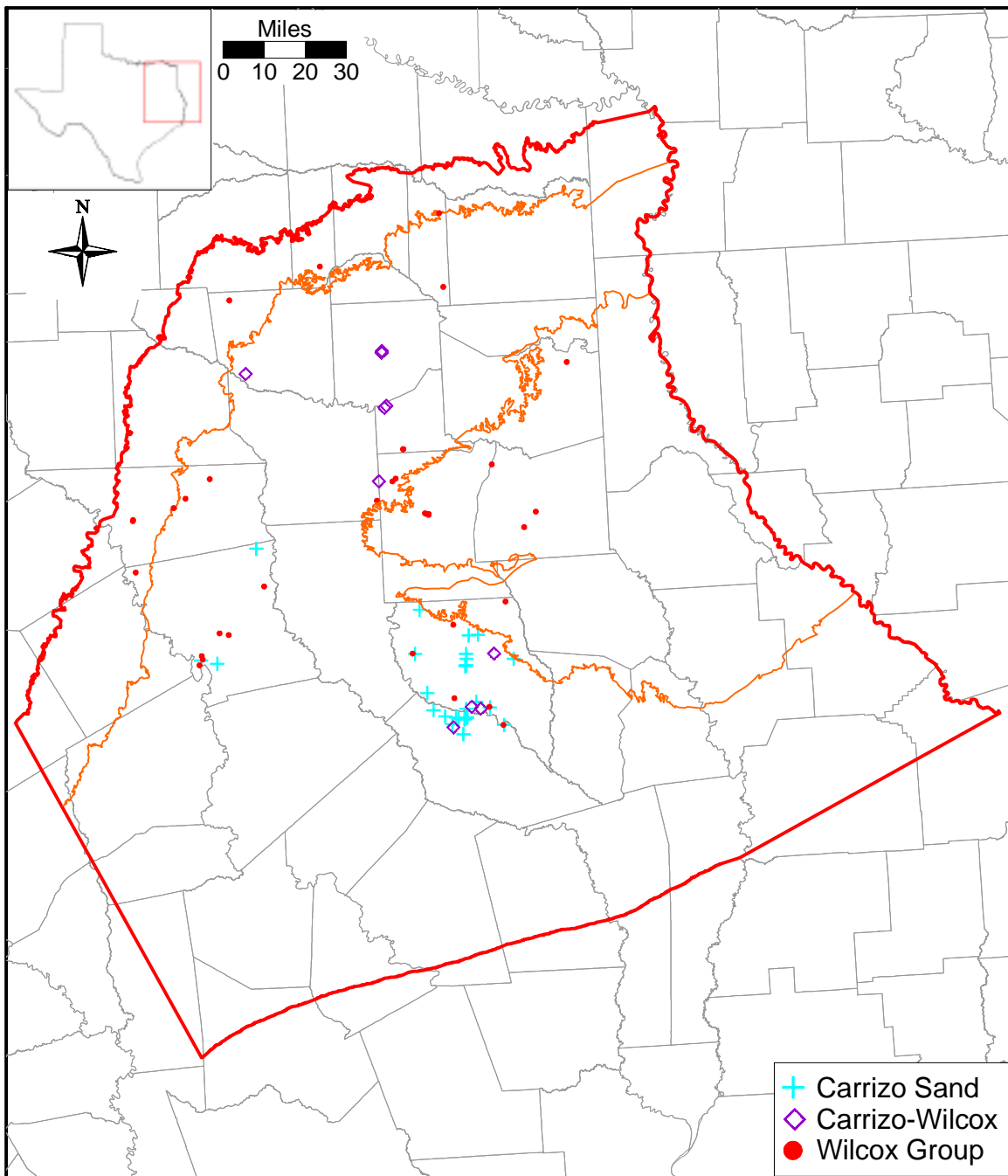


Figure 4.4.5 Water-level measurement locations used for the pressure-depth analysis (for measurements prior to 1950).

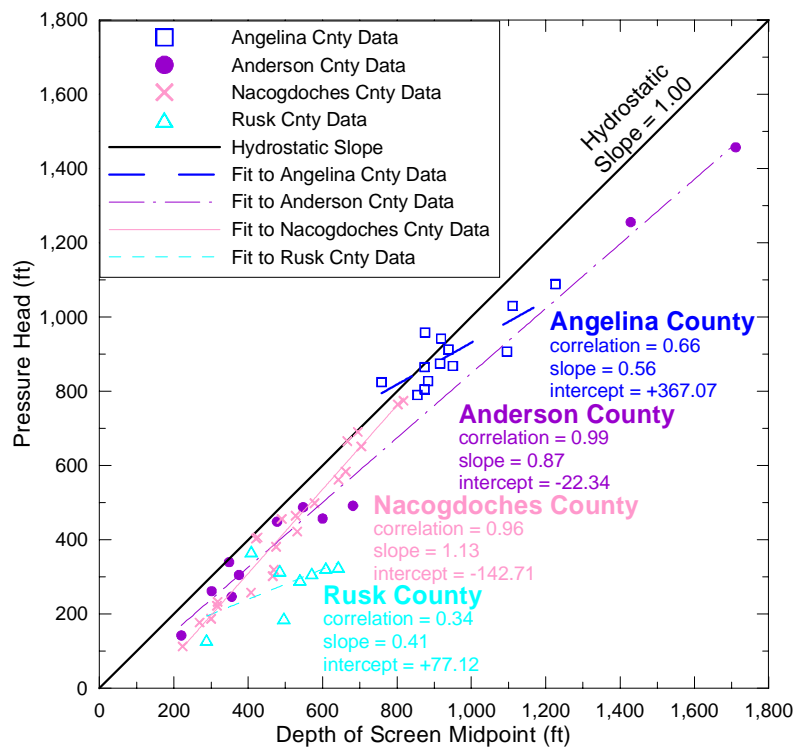
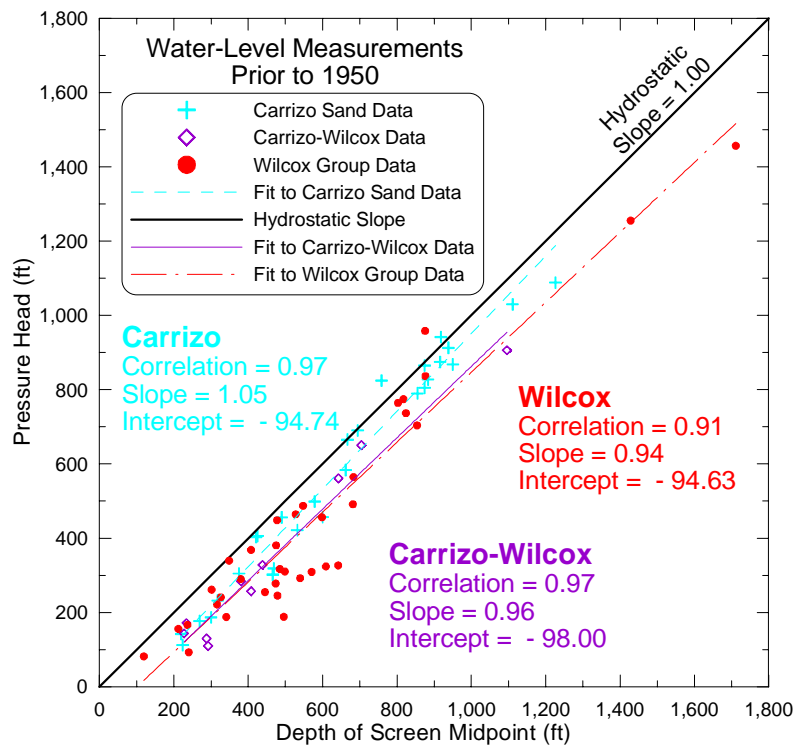


Figure 4.4.6 Pressure versus depth analysis results (for measurements prior to 1950).

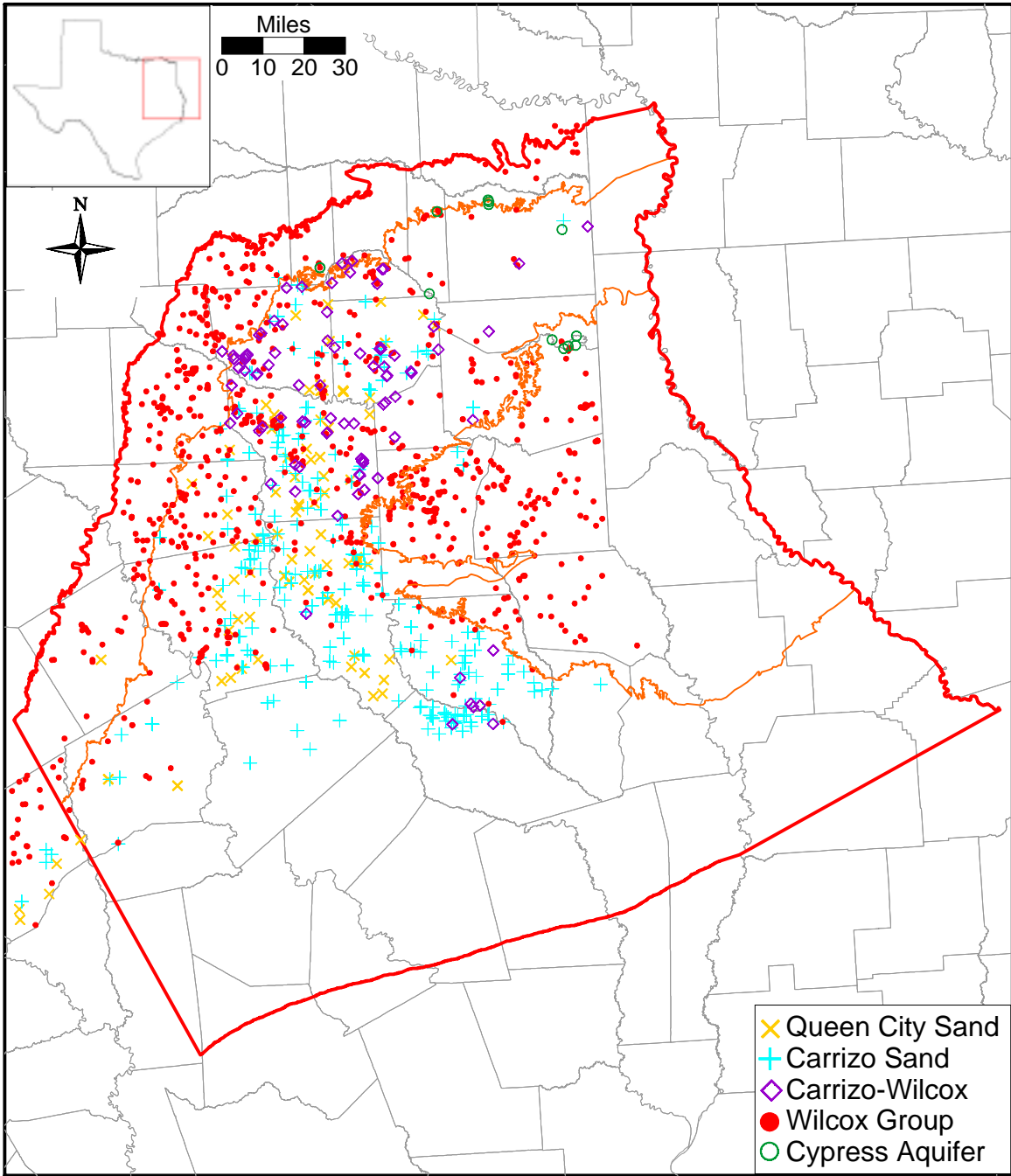


Figure 4.4.7 Water-level measurement locations used for the pressure-depth analysis (for all measurements).

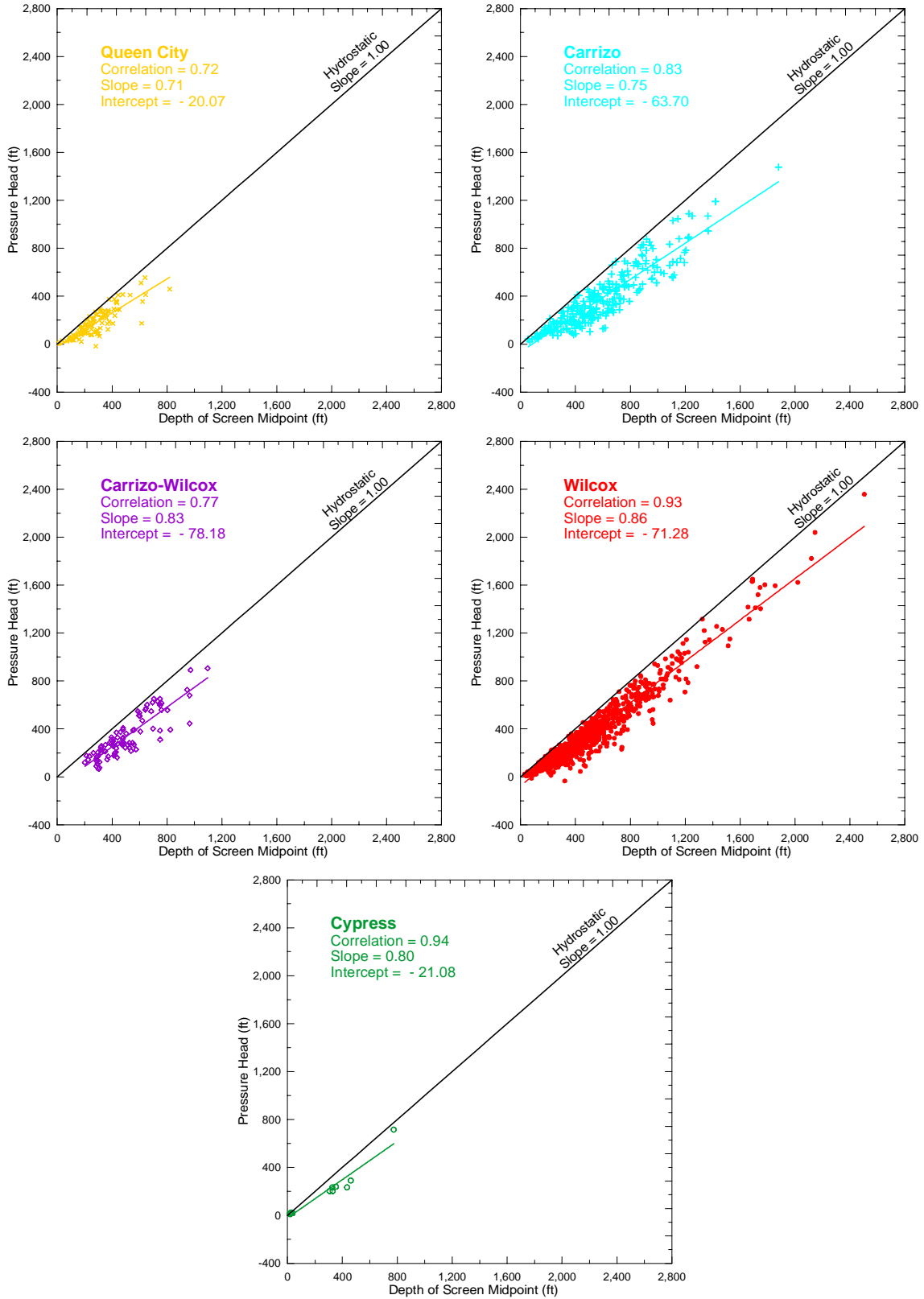


Figure 4.4.8 Pressure versus depth analysis results (for all measurements).

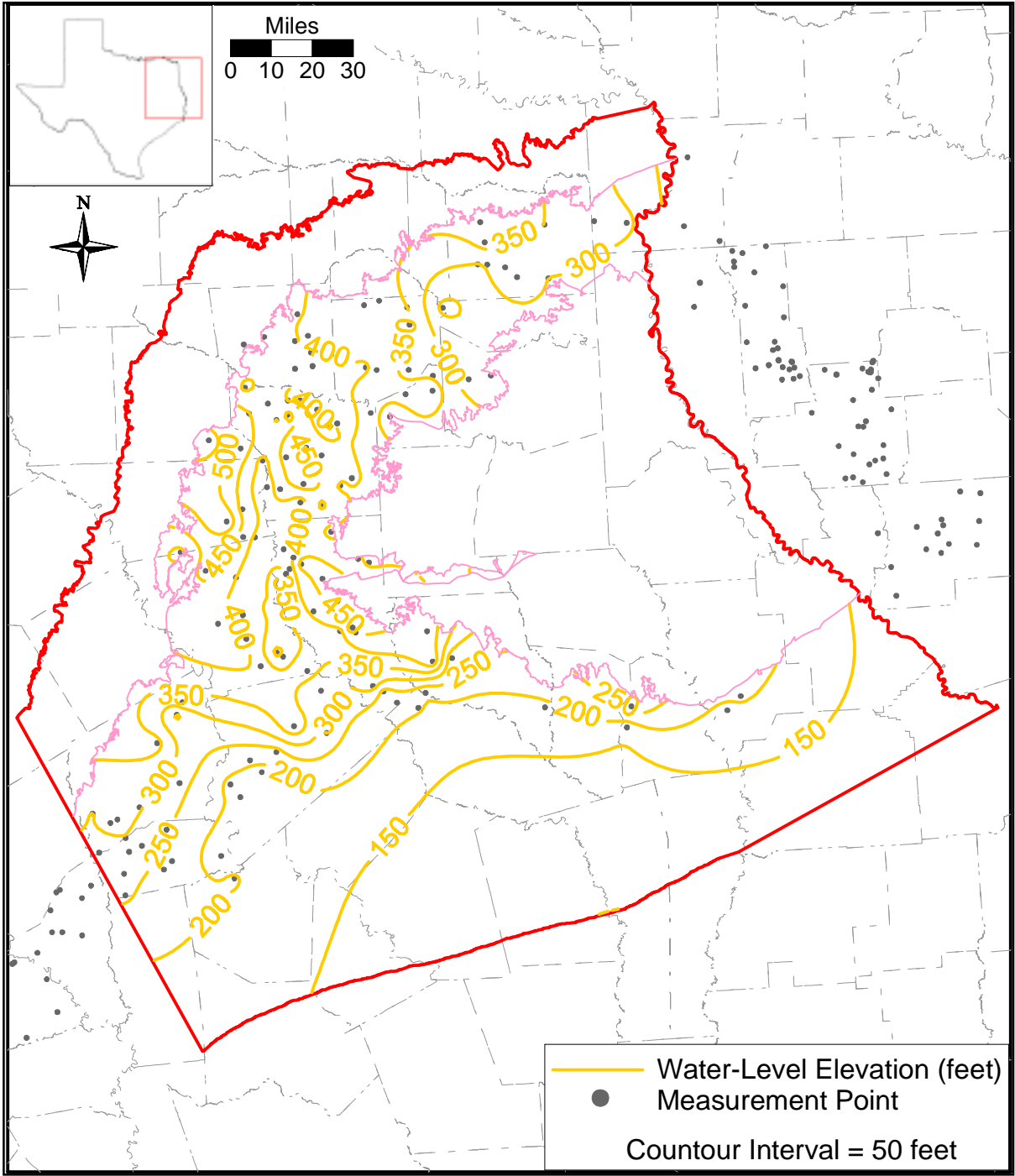


Figure 4.4.9a Water-level elevation contours for the Queen City Sand at the start of model calibration (January 1980).

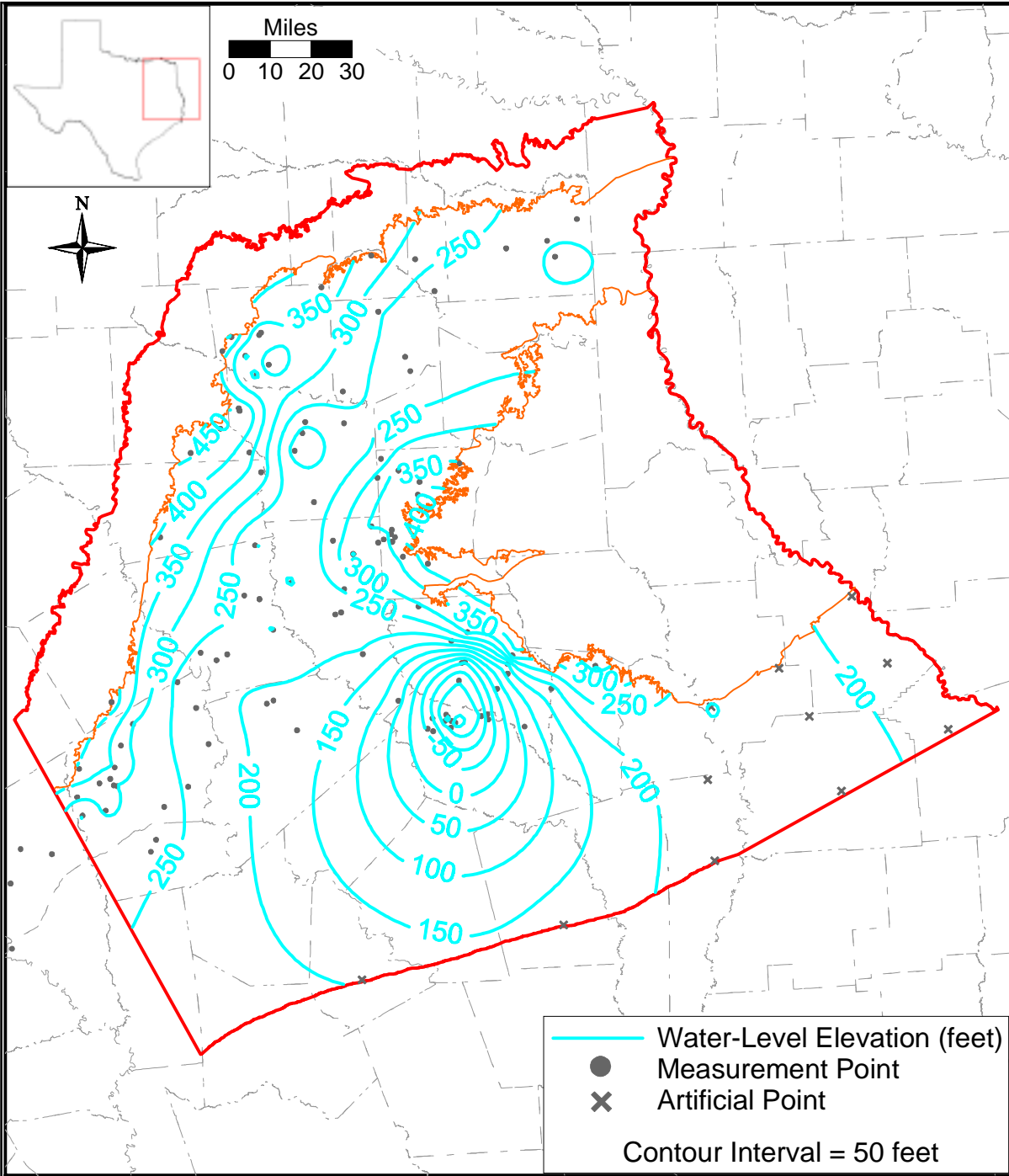


Figure 4.4.9b Water-level elevation contours for the Carrizo Sand at the start of model calibration (January 1980).

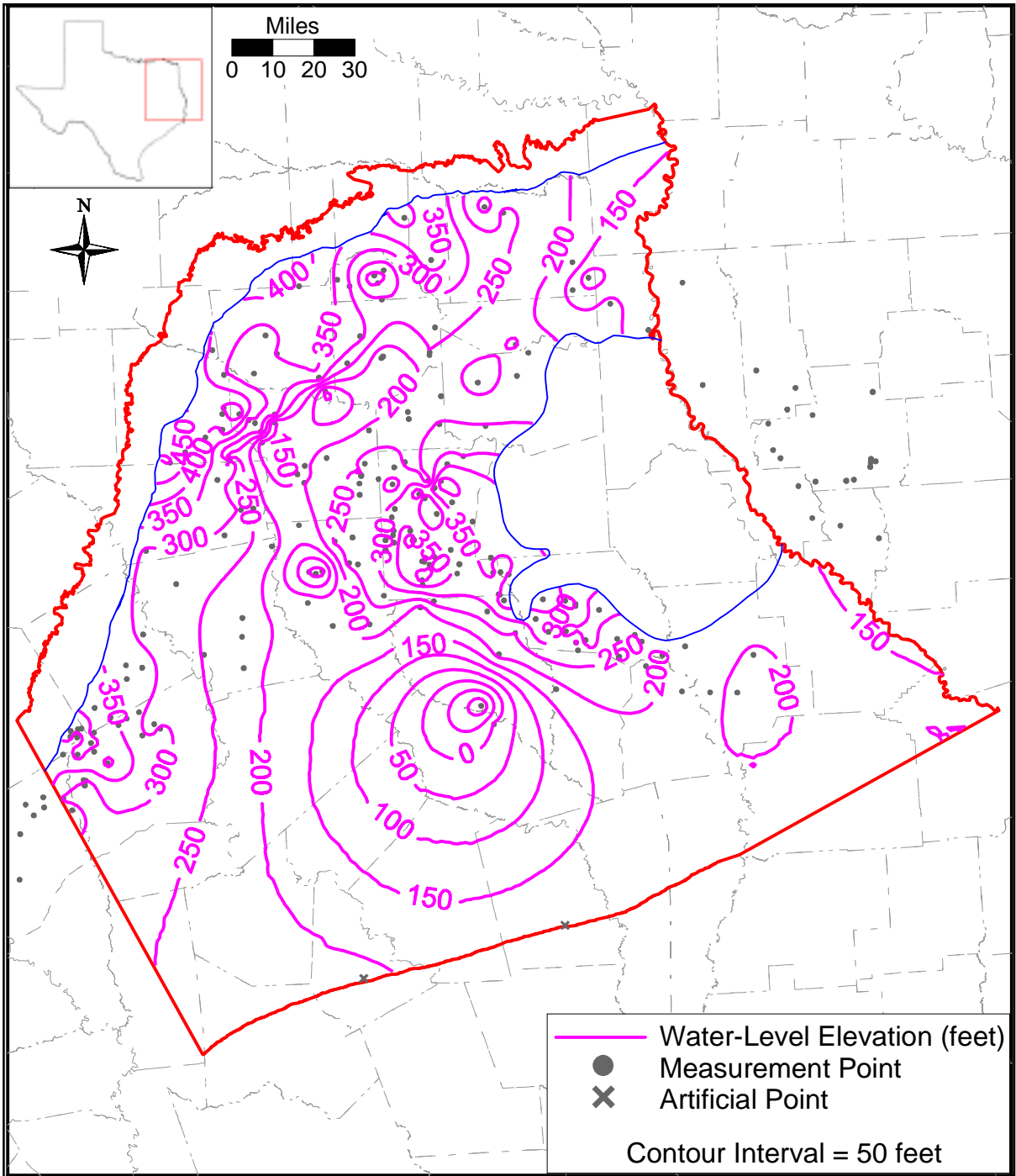


Figure 4.4.9c Water-level elevation contours for the upper Wilcox at the start of model calibration (January 1980).

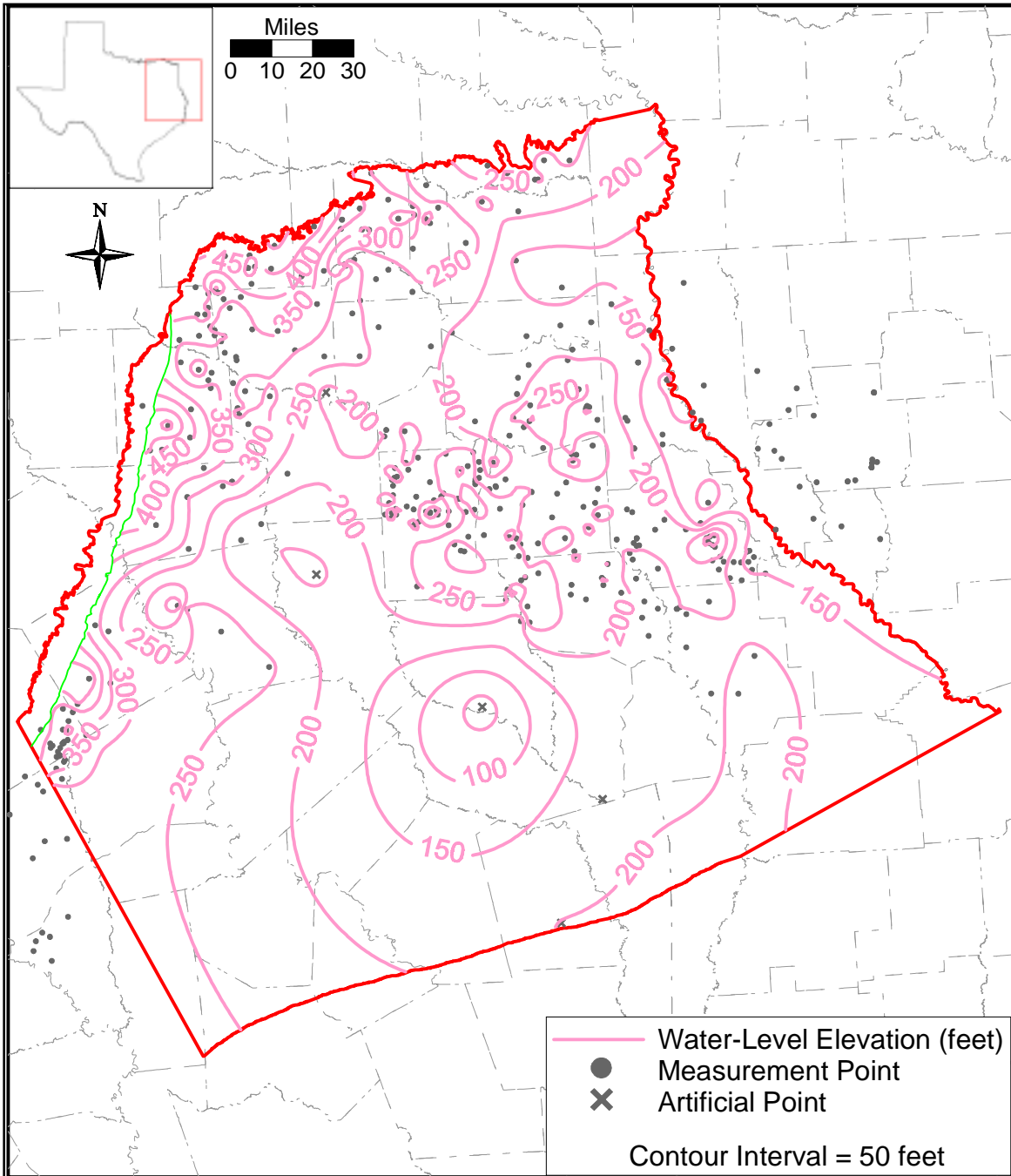


Figure 4.4.9d Water-level elevation contours for the middle Wilcox at the start of model calibration (January 1980).

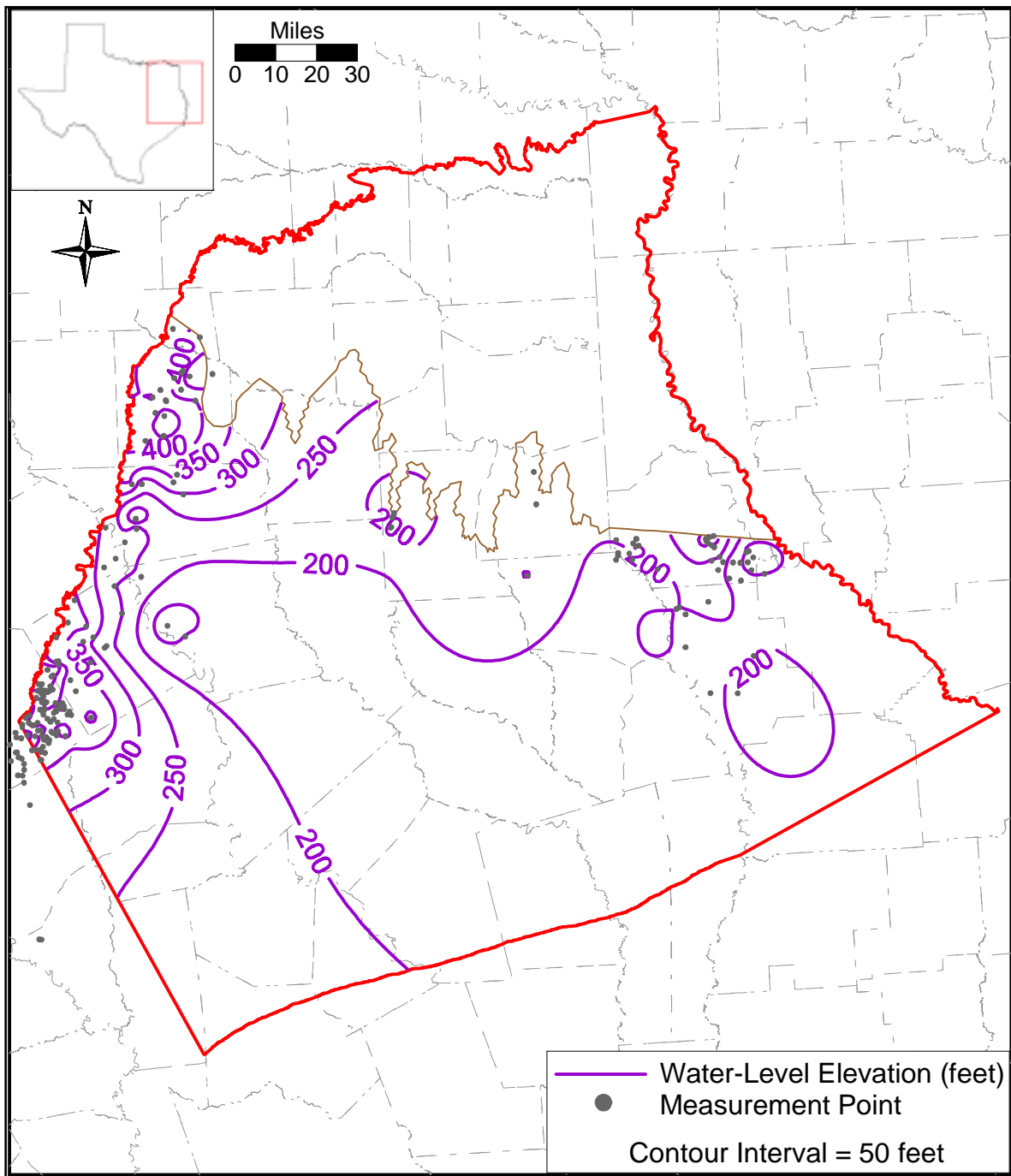


Figure 4.4.9e Water-level elevation contours for the lower Wilcox at the start of model calibration (January 1980).

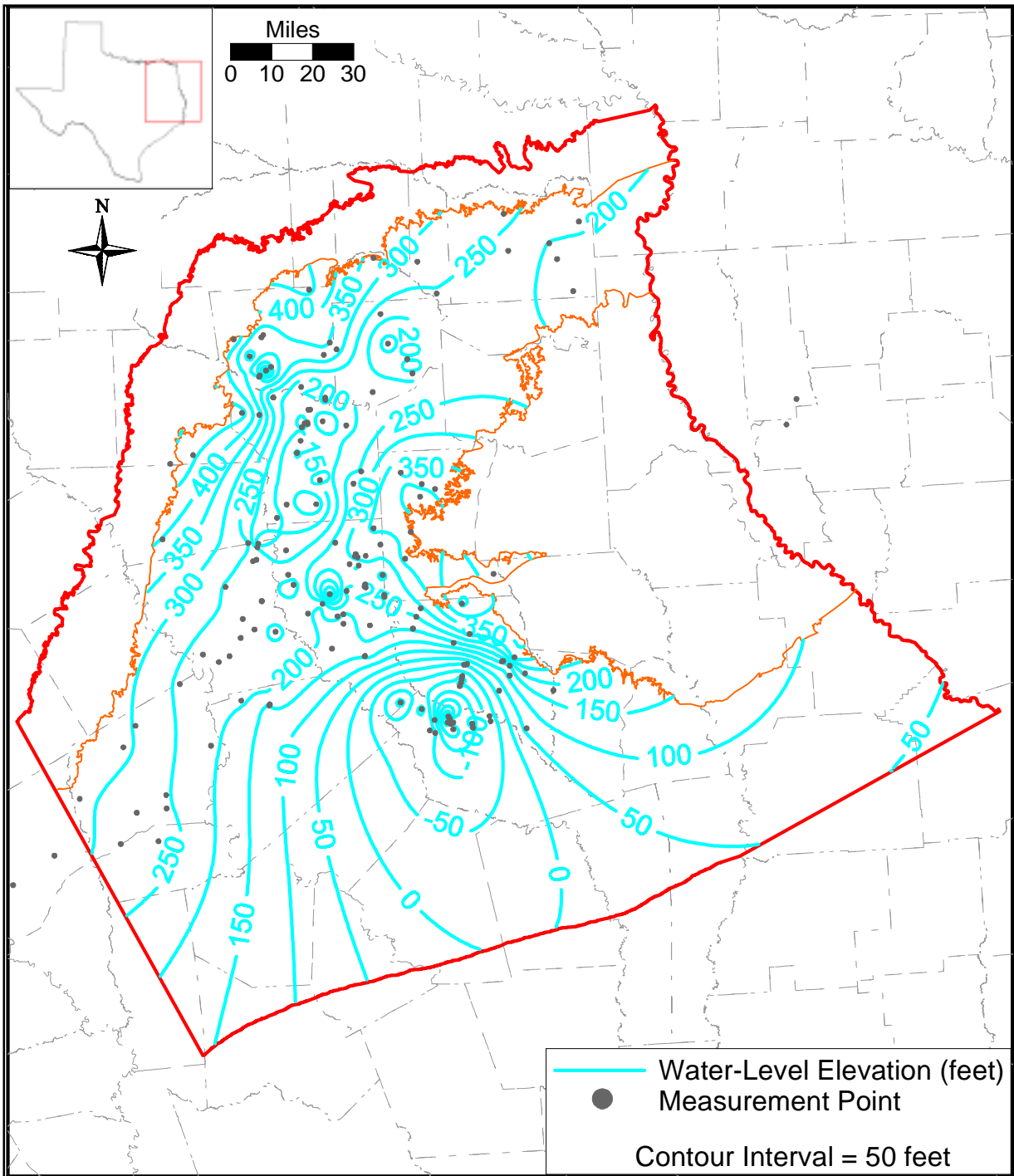


Figure 4.4.10a Water-level elevation contours for the Carrizo Sand at the end of model calibration (December 1989).

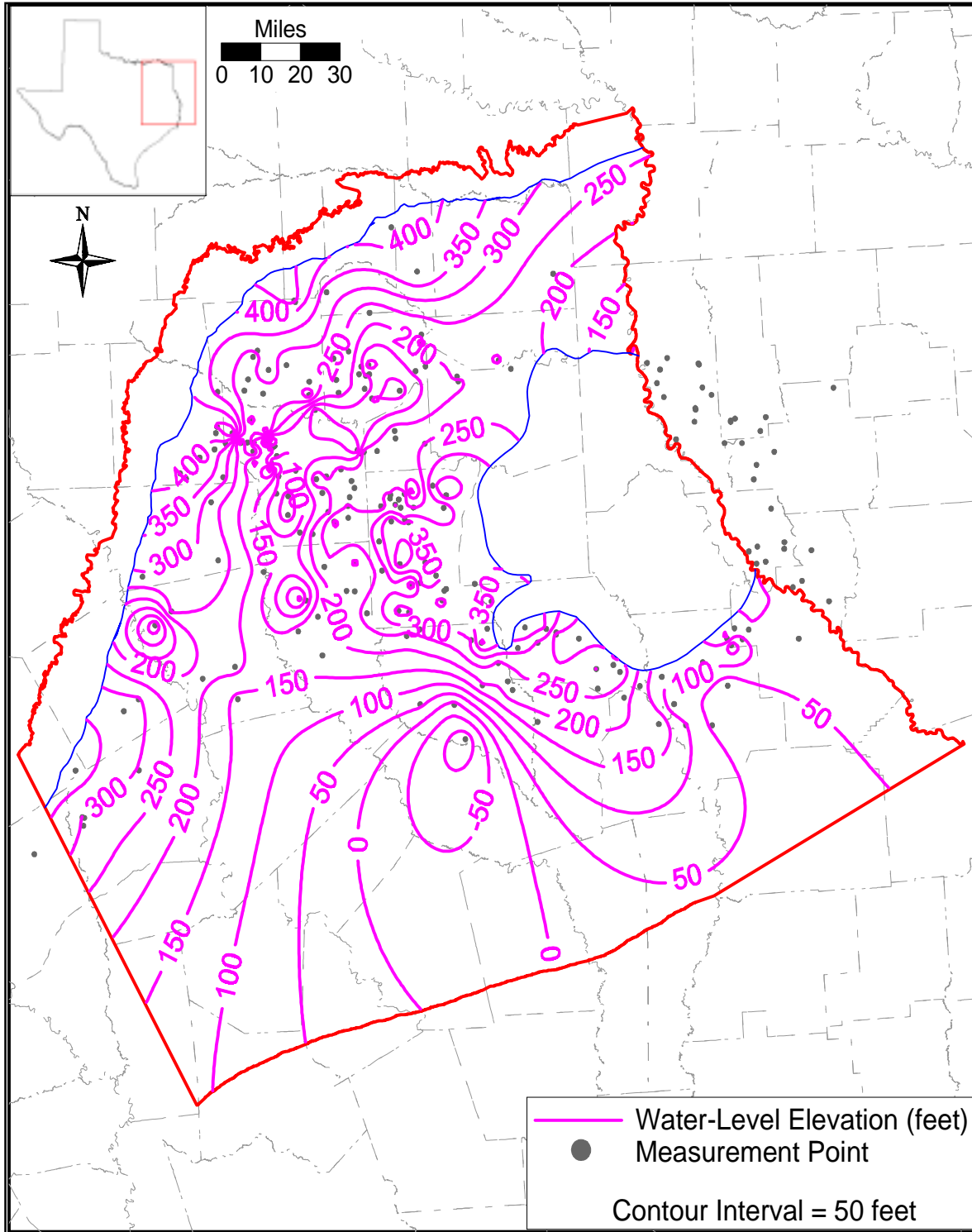


Figure 4.4.10b Water-level elevation contours for the upper Wilcox at the end of model calibration (December 1989).

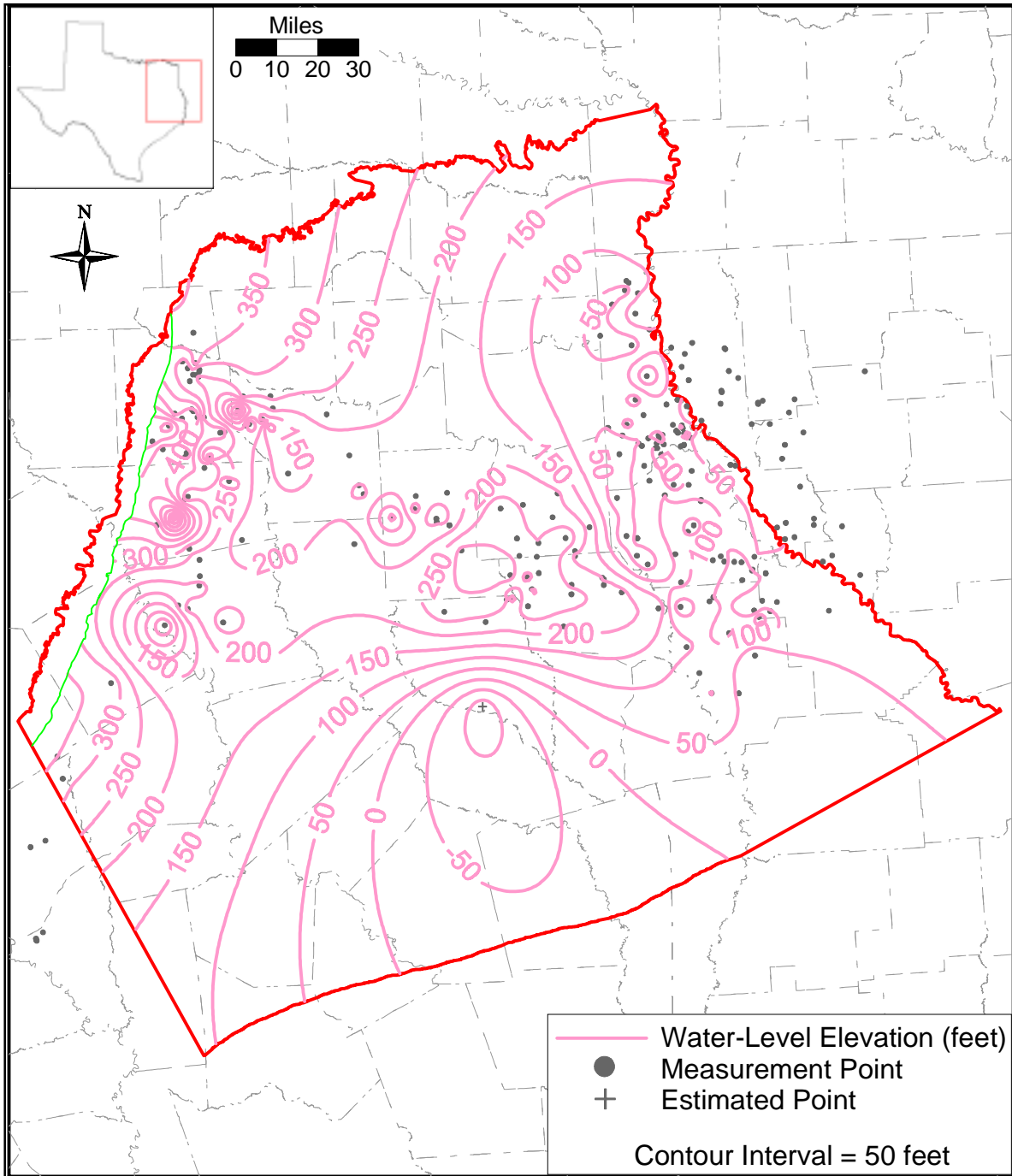


Figure 4.4.10c Water-level elevation contours for the middle Wilcox at the end of model calibration (December 1989).

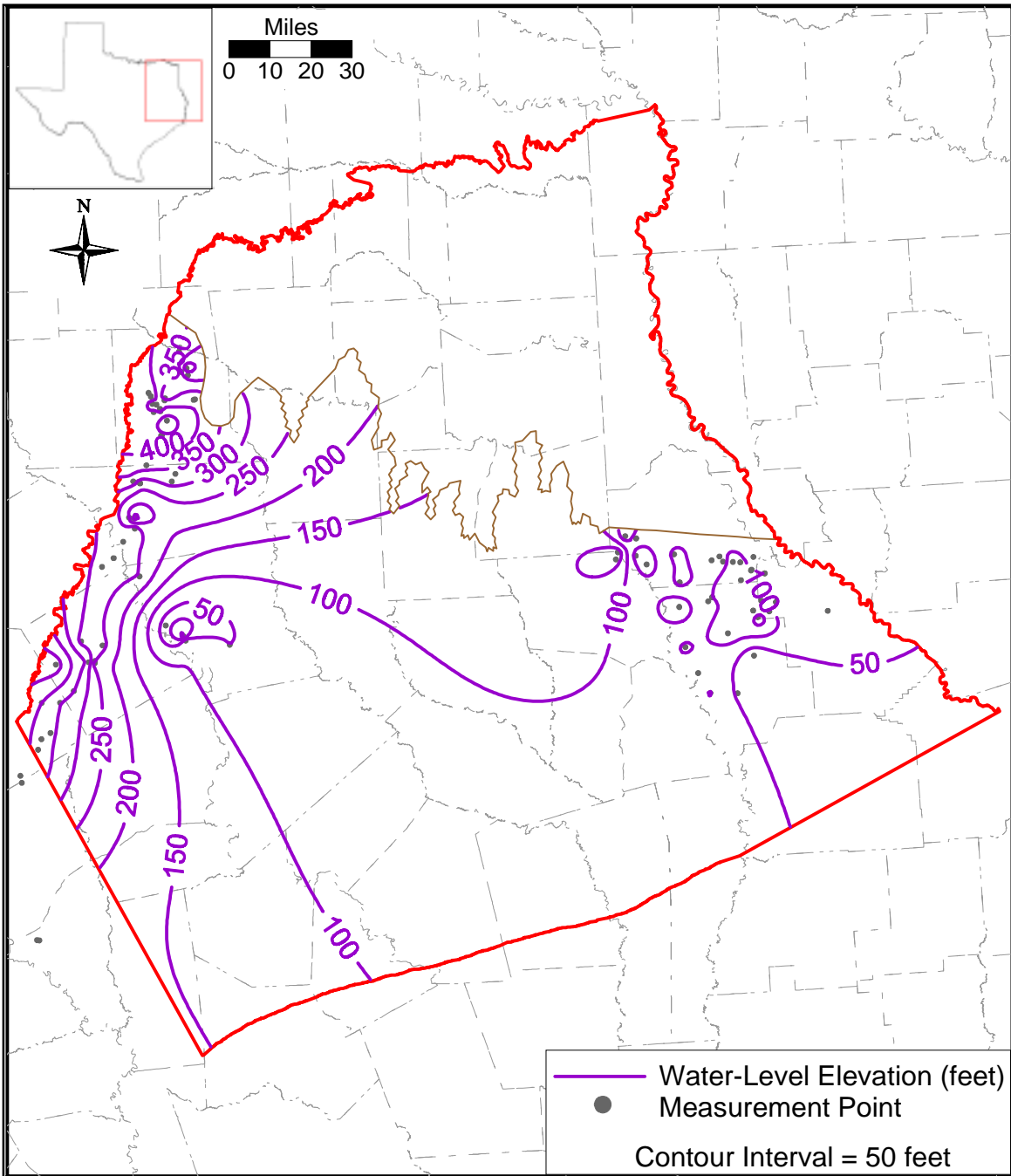


Figure 4.4.10d Water-level elevation contours for the lower Wilcox at the end of model calibration (December 1989).

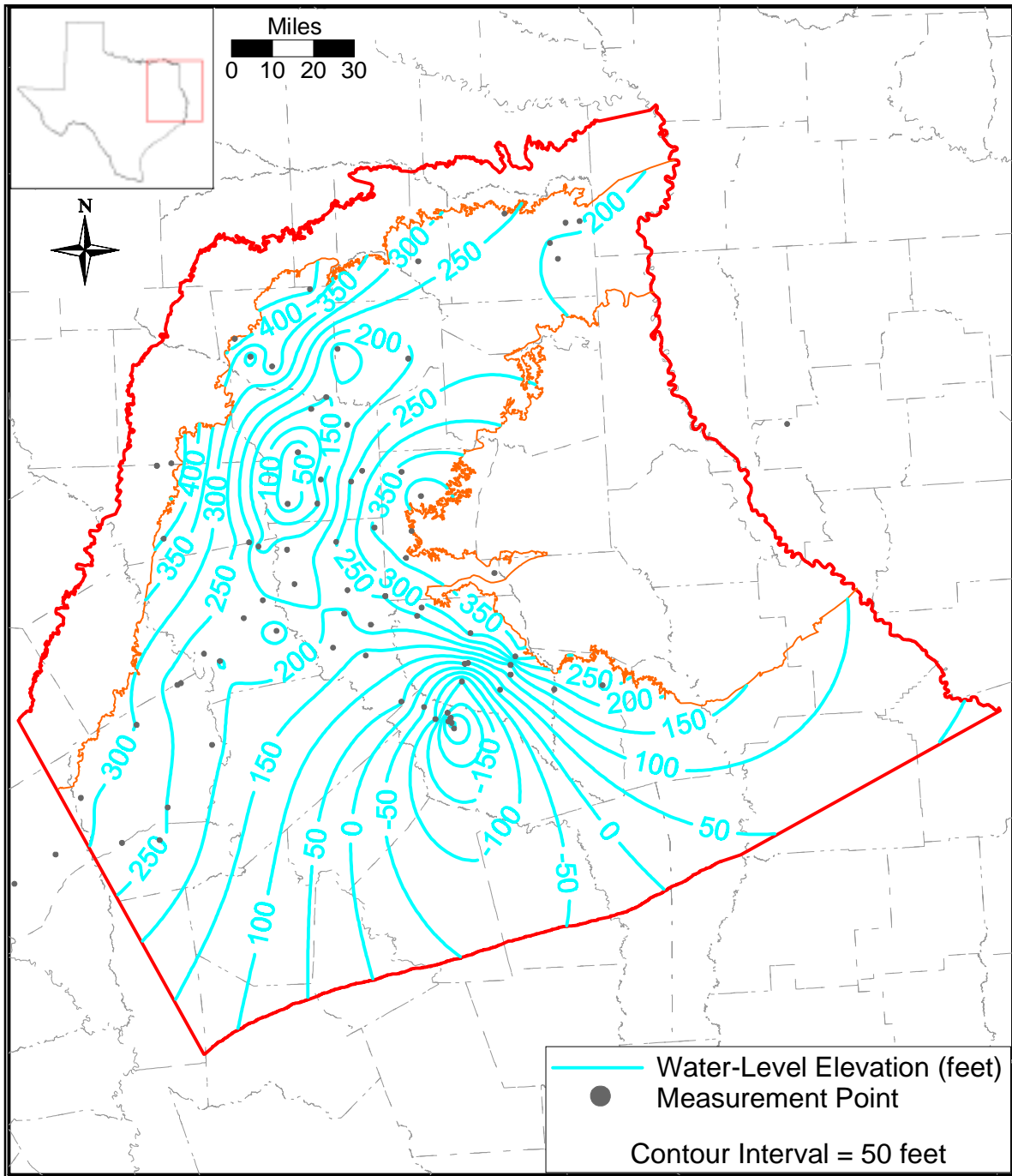


Figure 4.4.11a Water-level elevation contours for the Carrizo Sand at the end of model verification (December 1999).

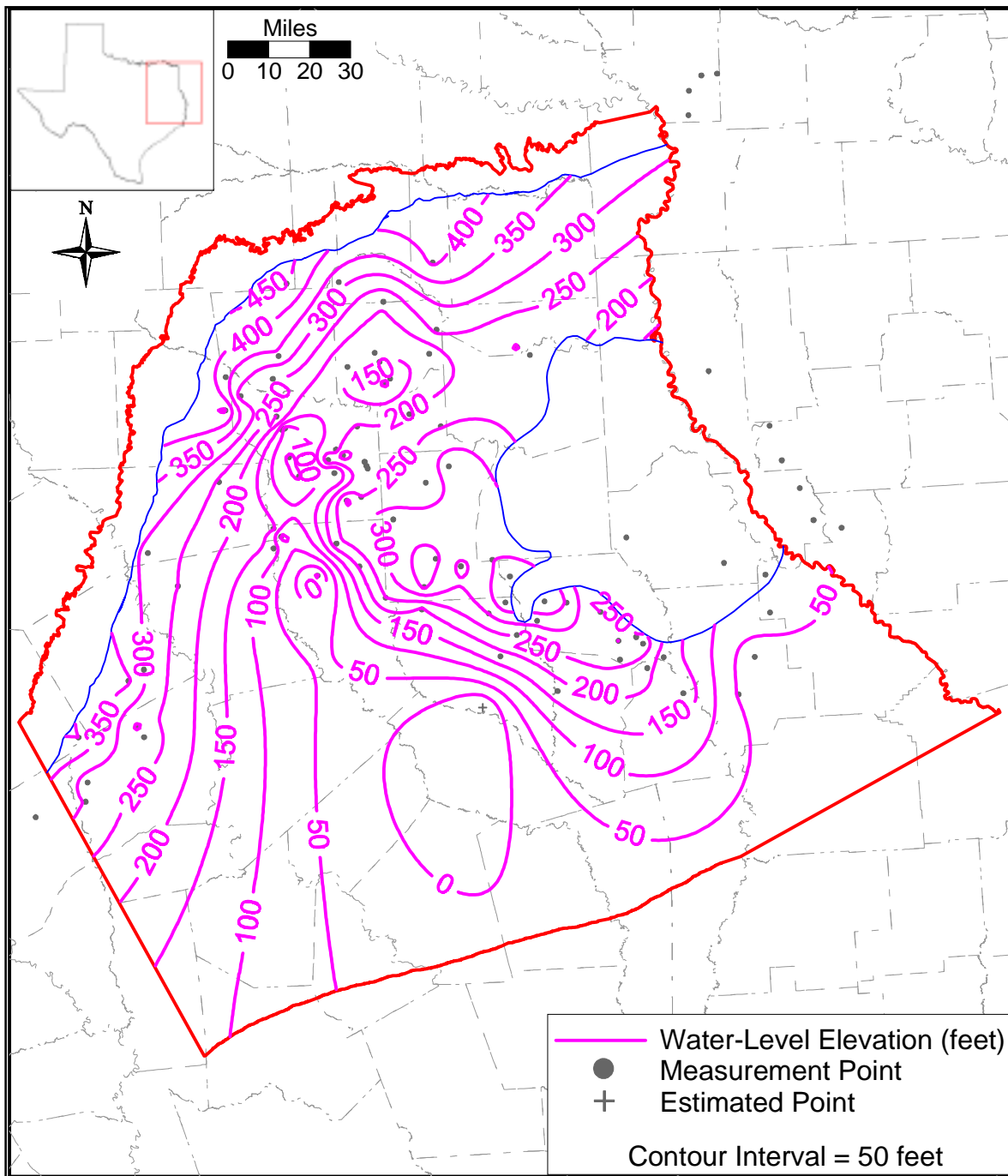


Figure 4.4.11b Water-level elevation contours for the upper Wilcox at the end of model verification (December 1999).

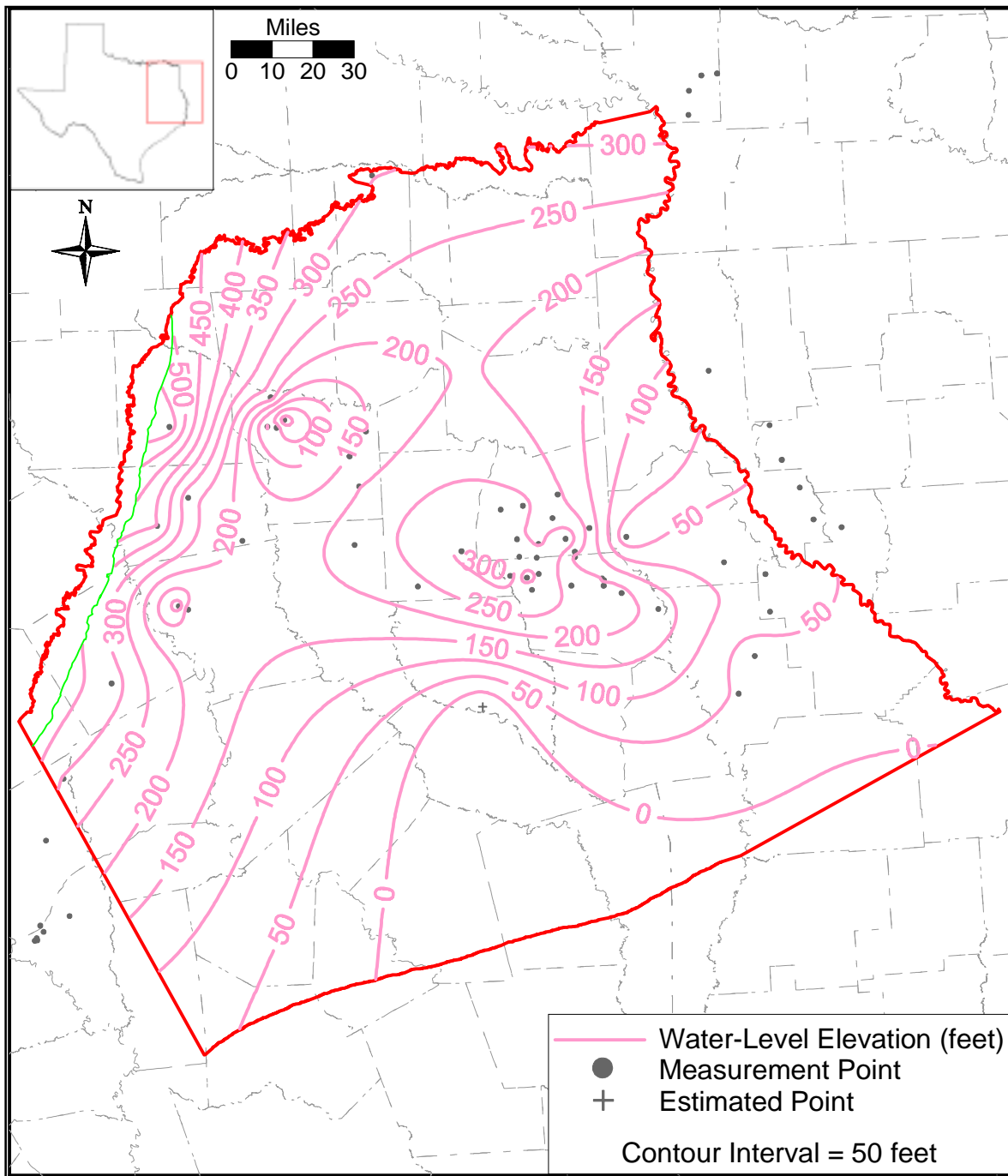


Figure 4.4.11c Water-level elevation contours for the middle Wilcox at the end of model verification (December 1999).

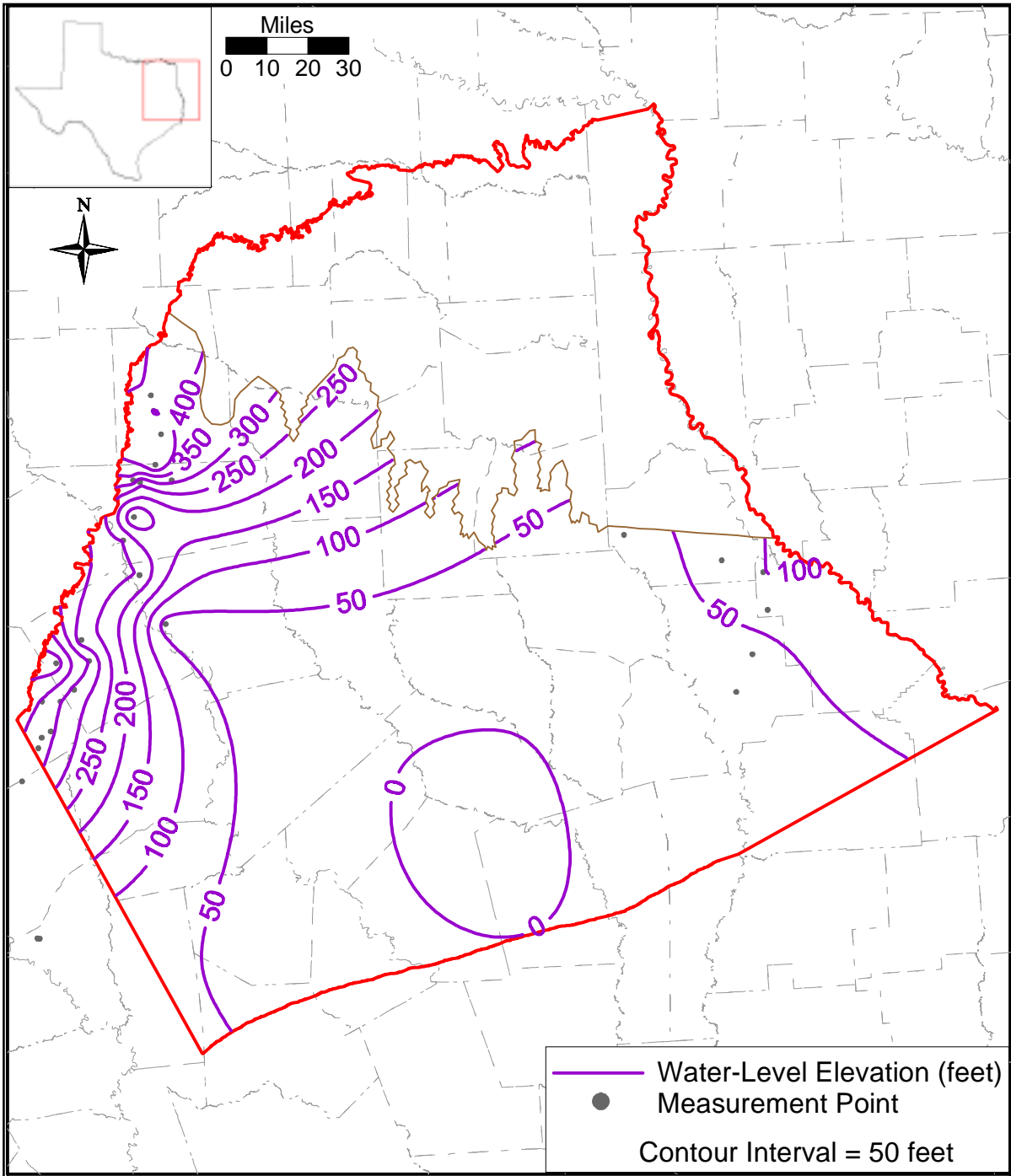


Figure 4.4.11d Water-level elevation contours for the lower Wilcox at the end of model verification (December 1999).

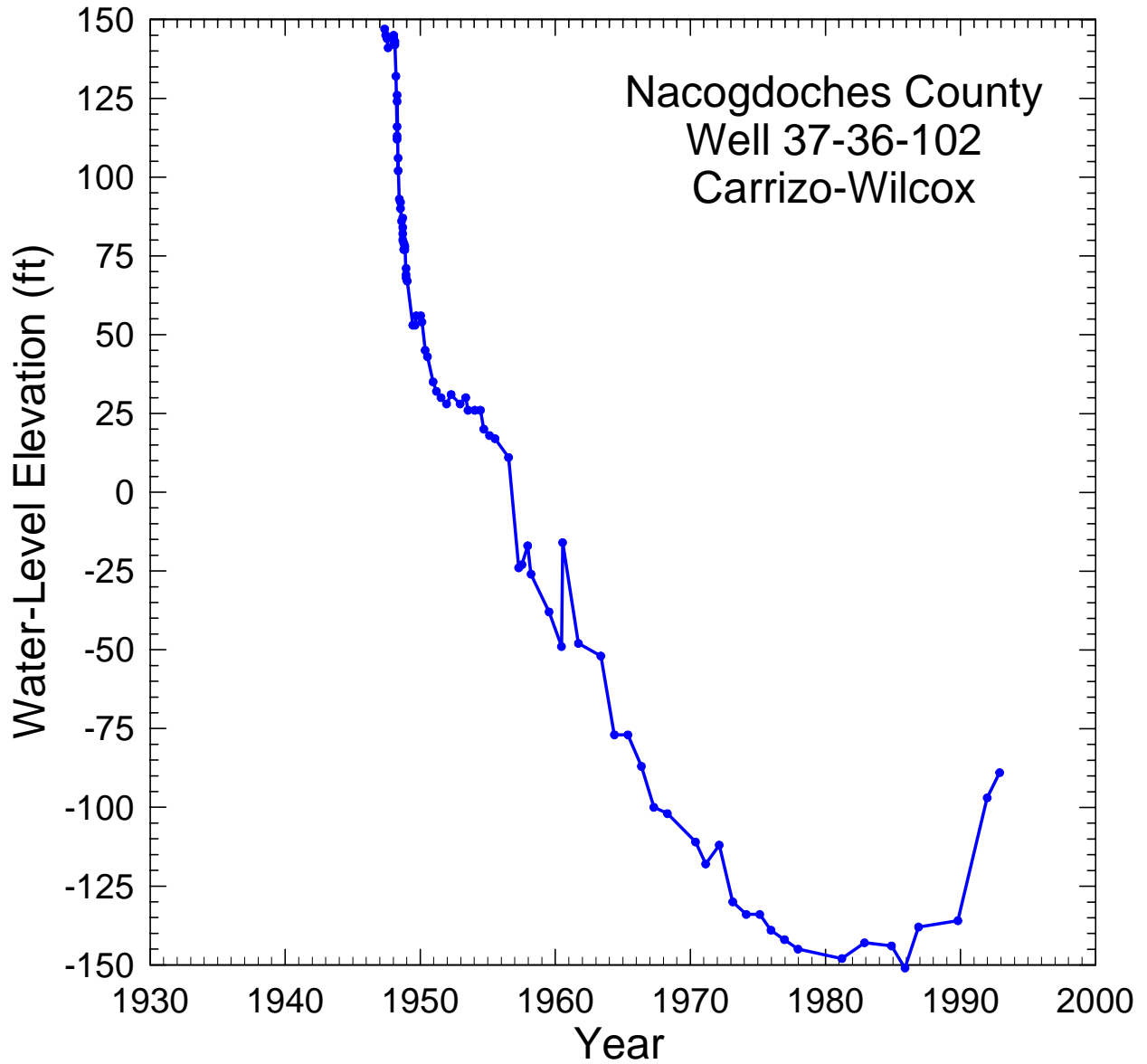


Figure 4.4.12 Long-term transient water-level elevations for well 37-36-102 completed to the Carrizo-Wilcox in Nacogdoches County.

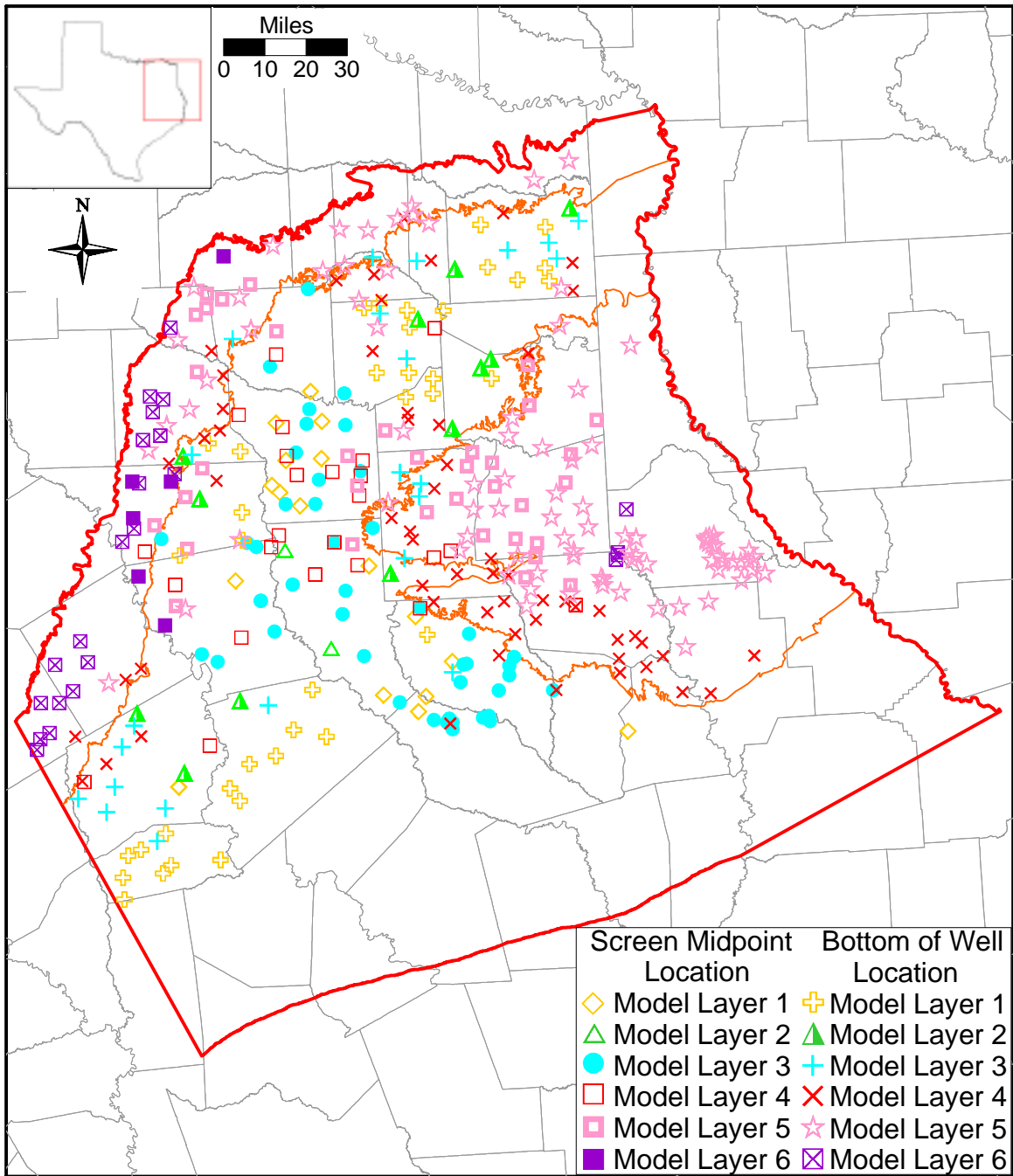


Figure 4.4.13 Model layer for locations with transient water-level data.

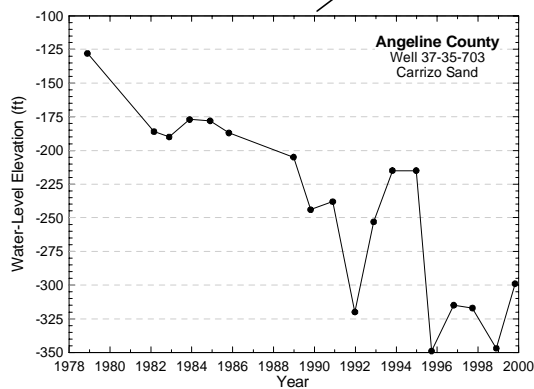
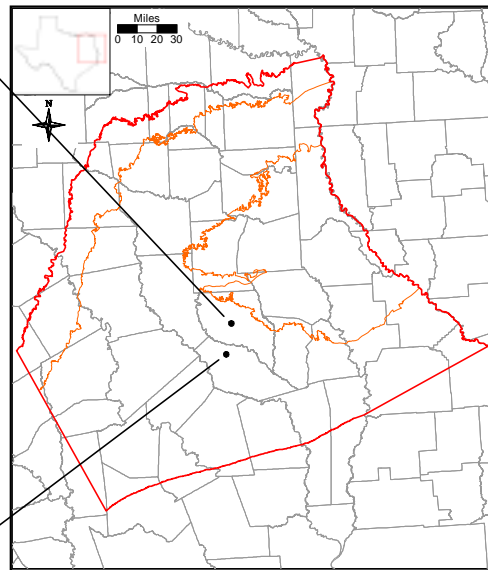
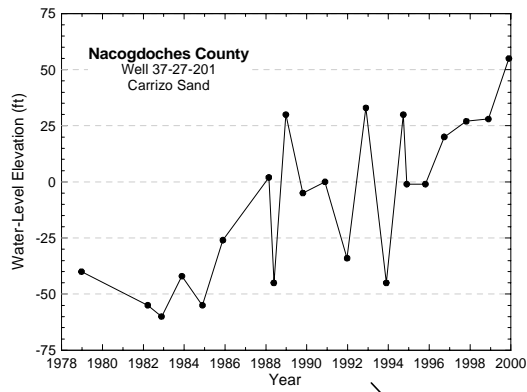


Figure 4.4.14 Example hydrographs for wells located in Nacogdoches and Angelina counties.

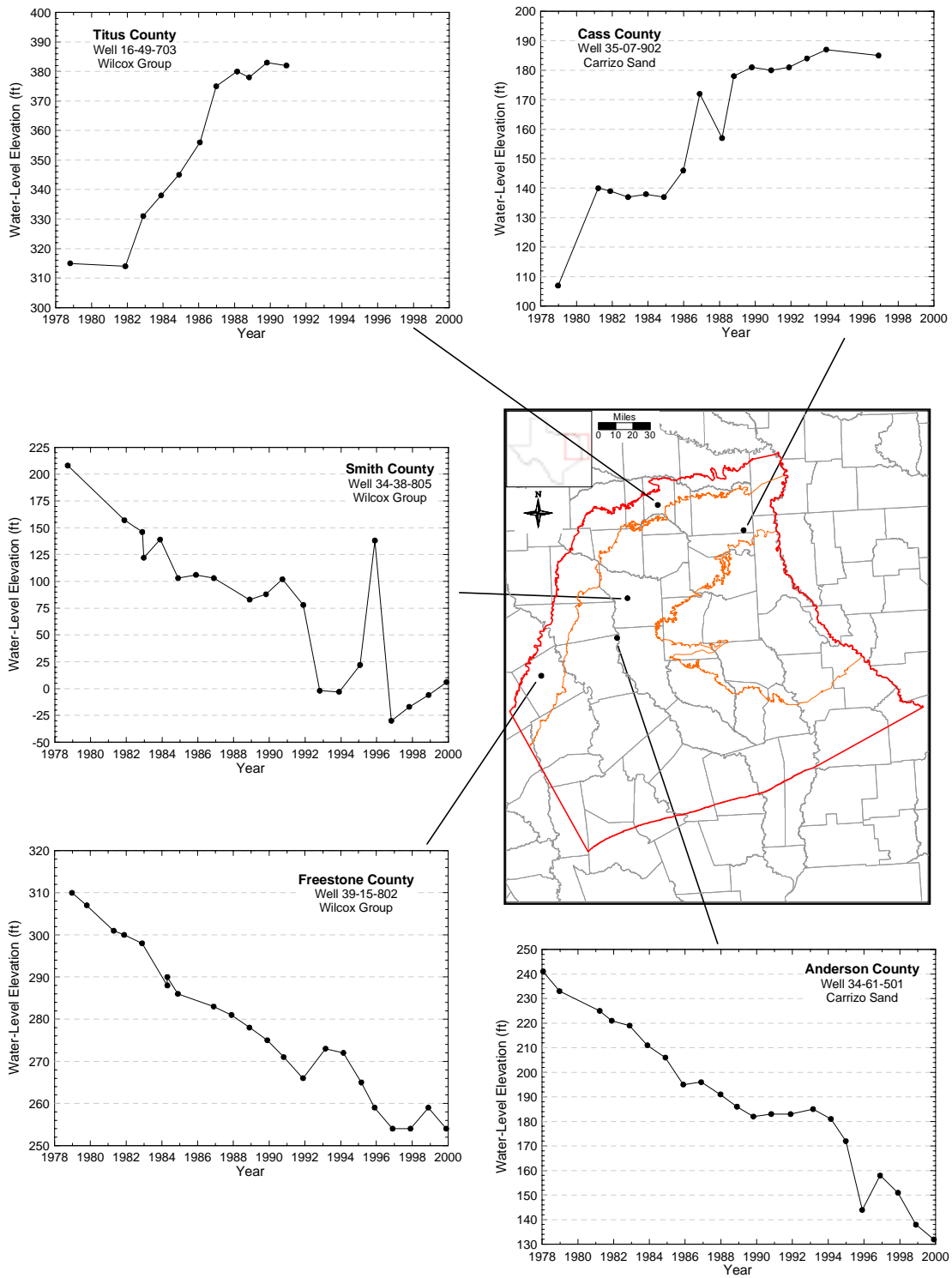


Figure 4.15 Example hydrographs for wells in the study area.

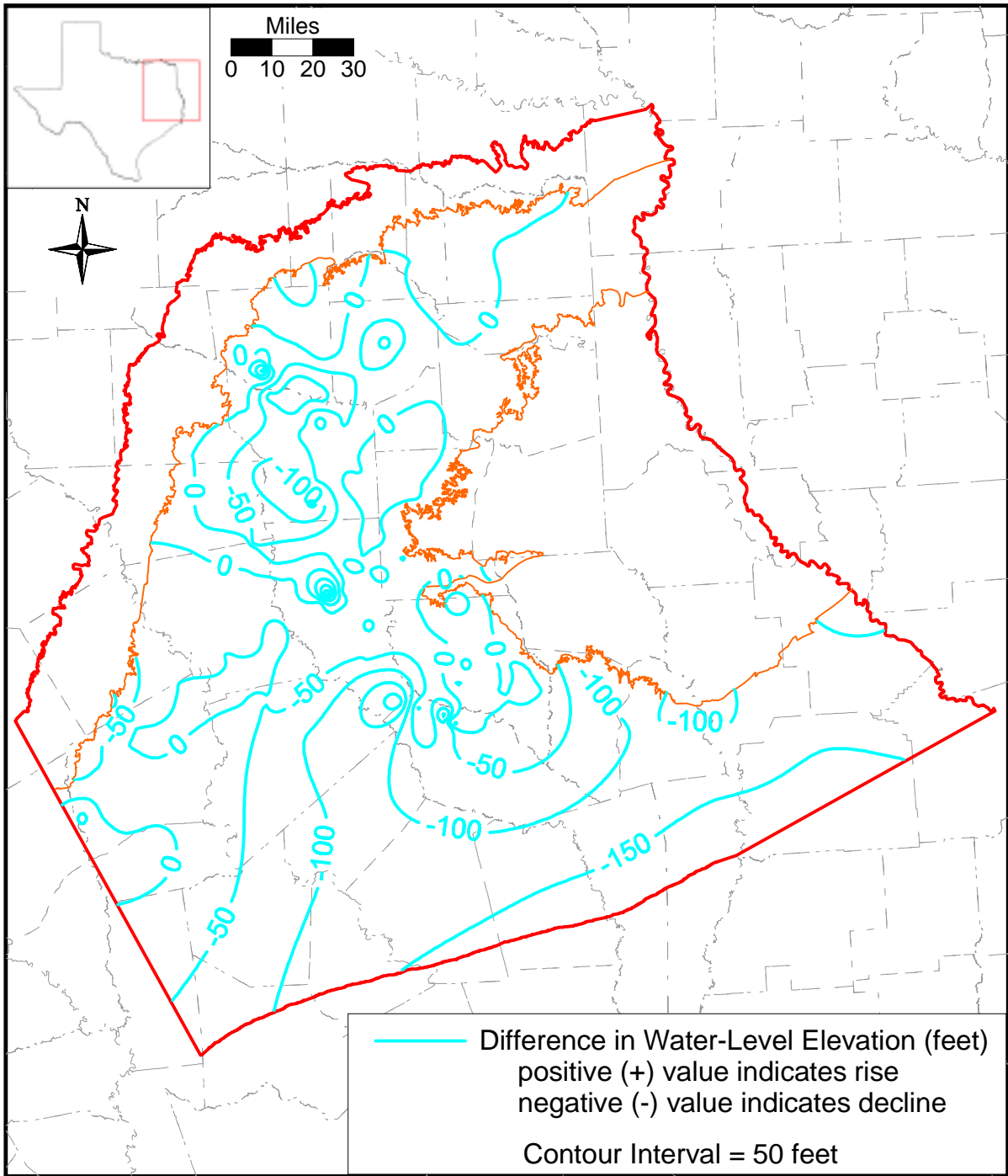


Figure 4.4.16a Water-level decline in the Carrizo Sand from the start of model calibration (January 1980) to the end of model calibration (December 1989).

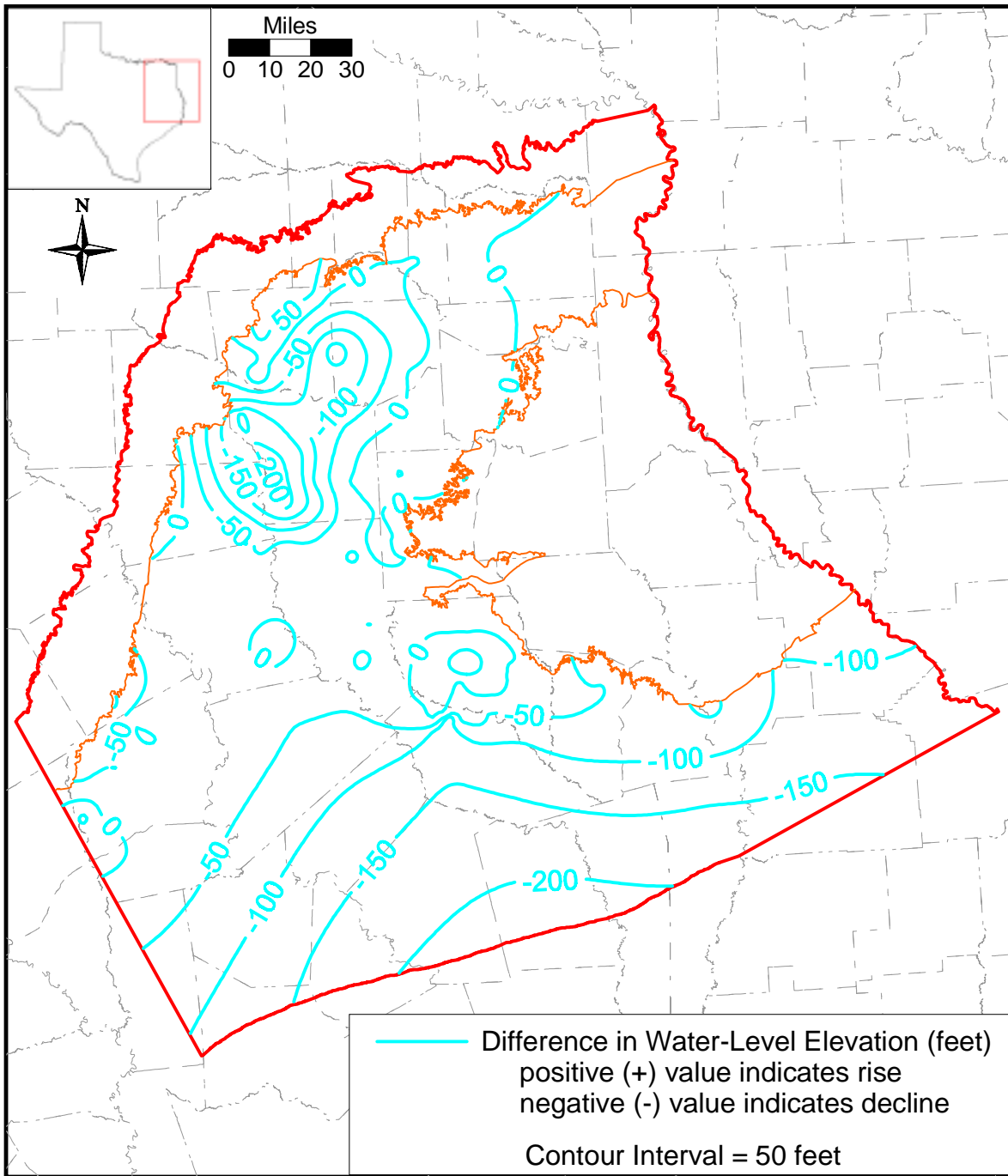


Figure 4.4.16b Water-level decline in the Carrizo Sand from the start of model calibration (January 1980) to the end of model verification (December 1999).

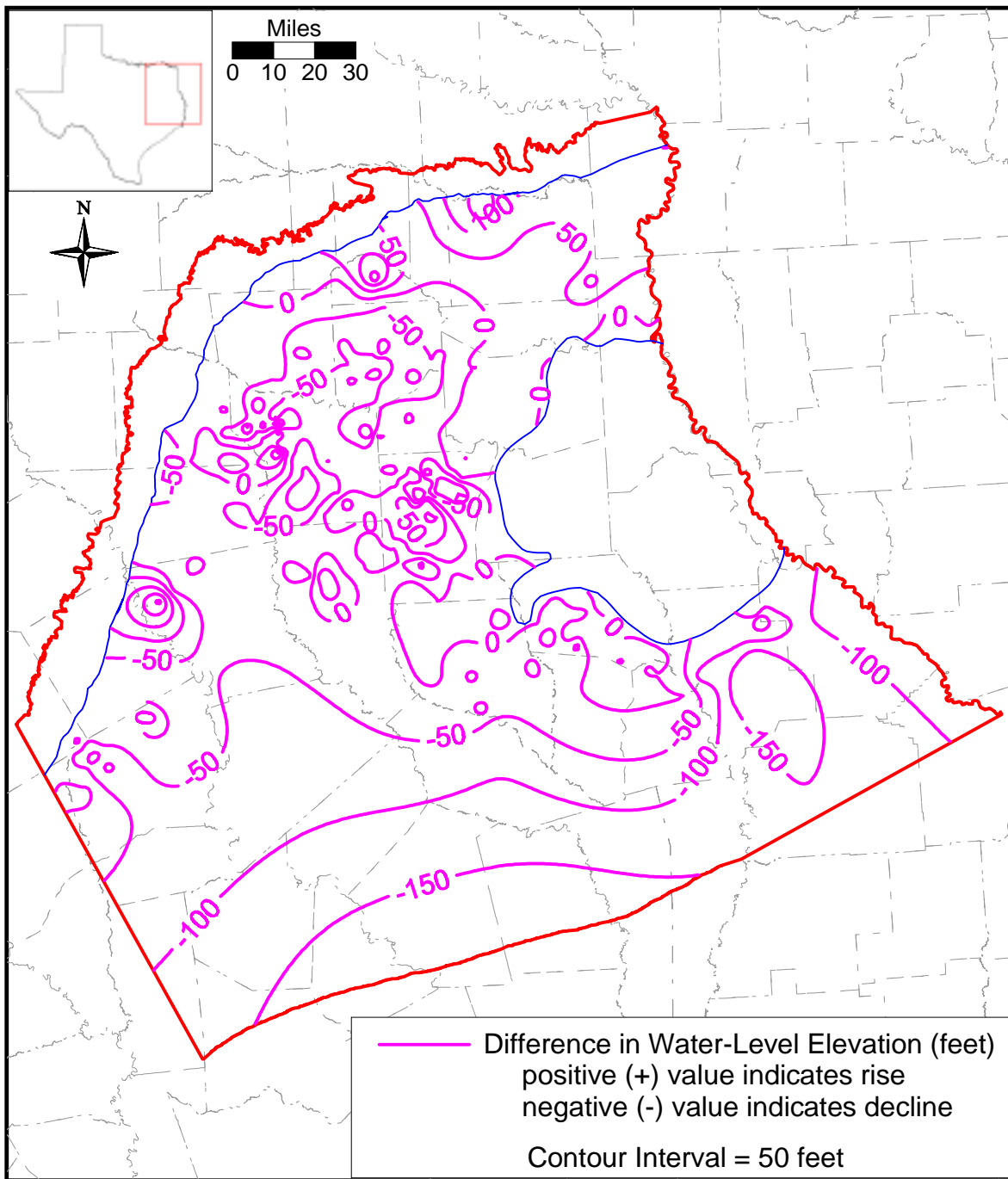


Figure 4.4.17a Water-level decline in the upper Wilcox from the start of model calibration (January 1980) to the end of model calibration (December 1989).

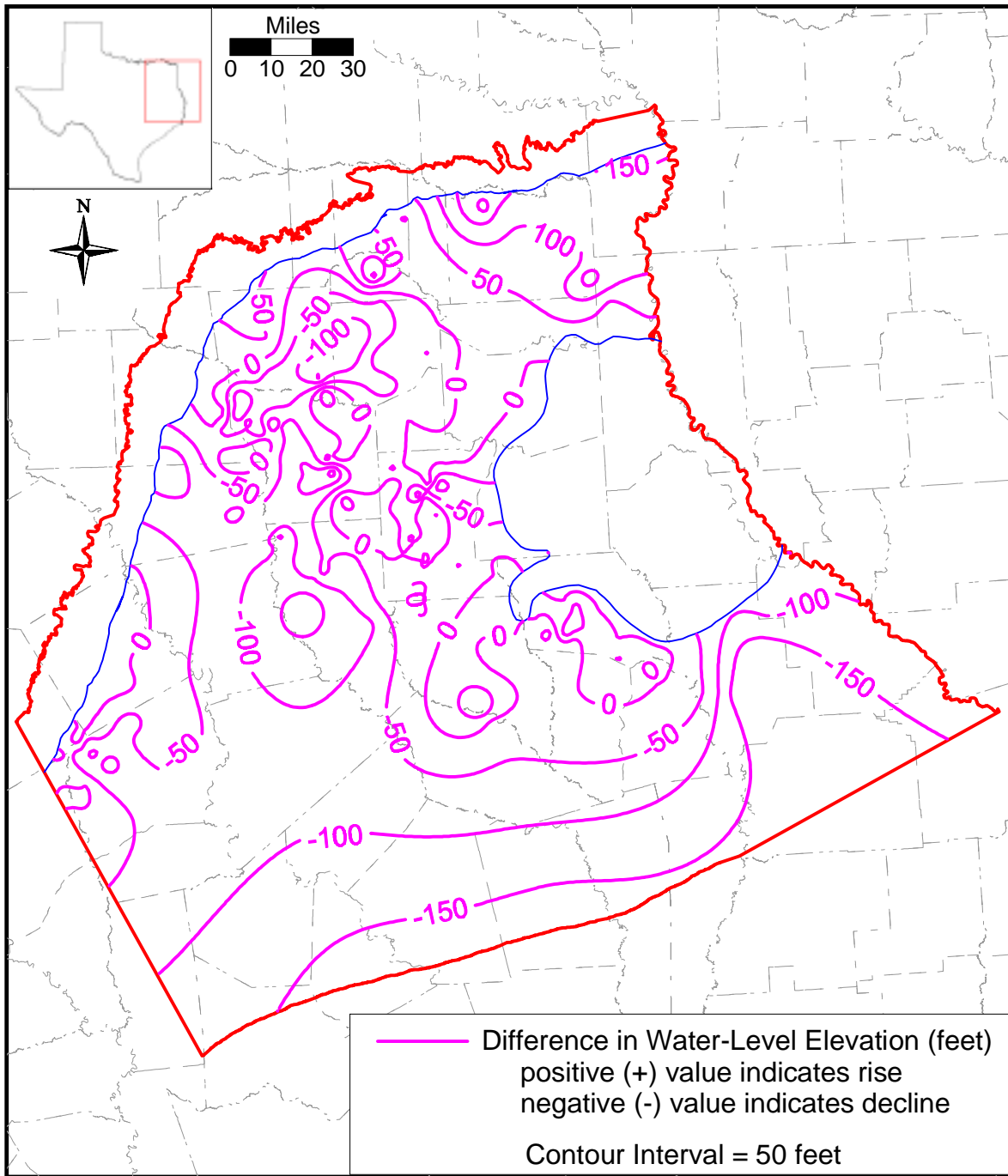


Figure 4.4.17b Water-level decline in the upper Wilcox from the start of model calibration (January 1980) to the end of model verification (December 1999).

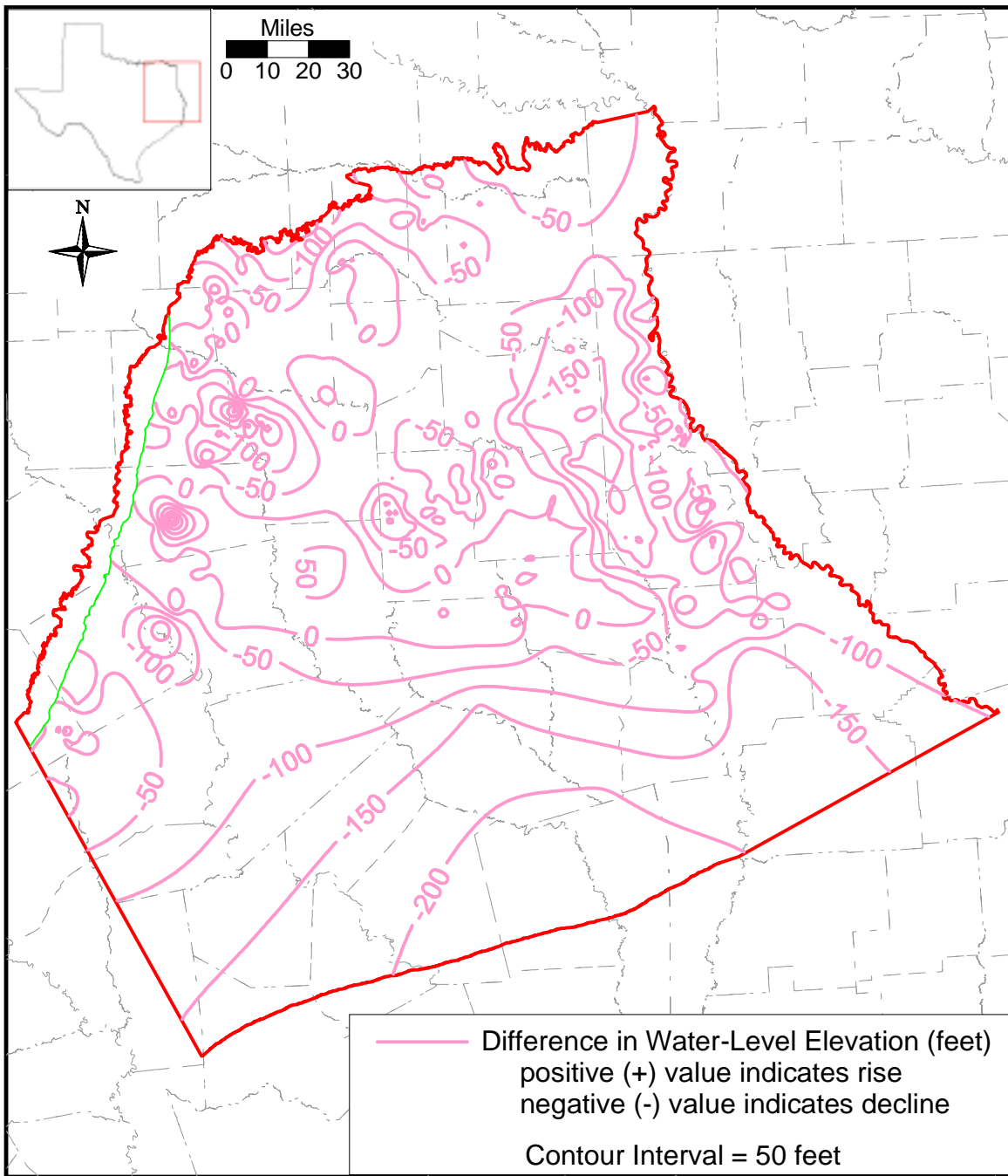


Figure 4.4.18a Water-level decline in the middle Wilcox from the start of model calibration (January 1980) to the end of model calibration (December 1989).

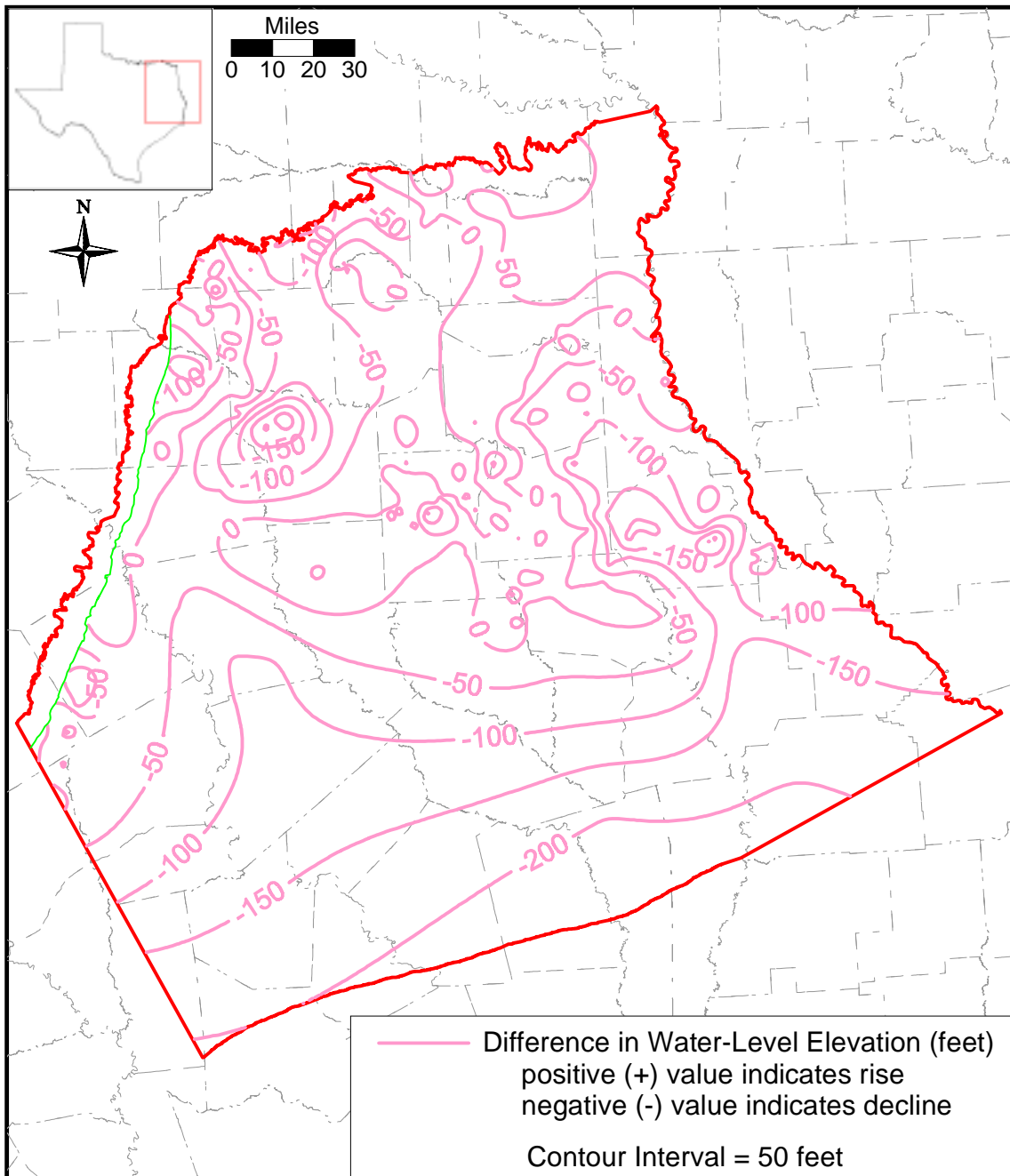


Figure 4.4.18b Water-level decline in the middle Wilcox from the start of model calibration (January 1980) to the end of model verification (December 1999).

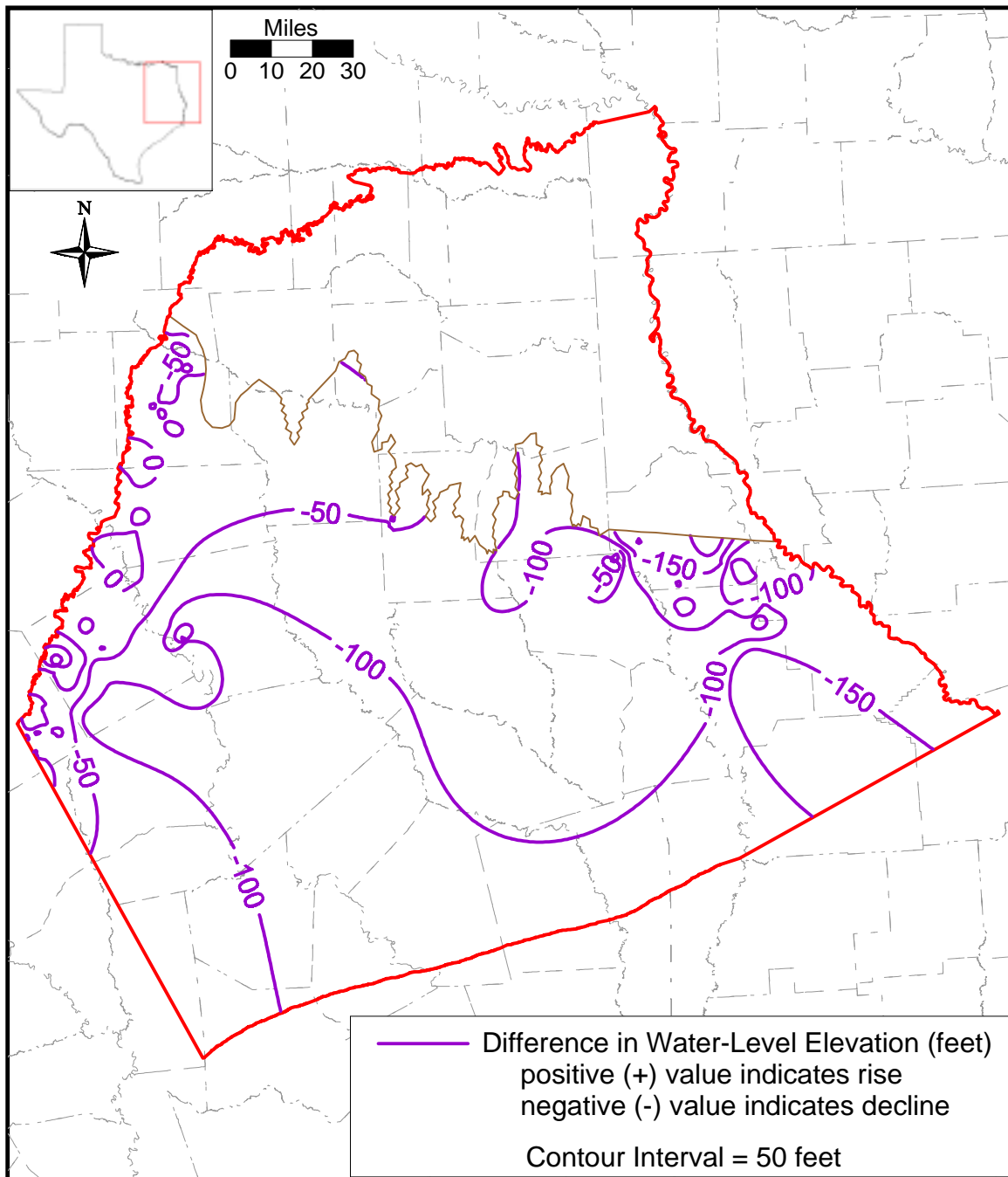


Figure 4.4.19a Water-level decline in the lower Wilcox from the start of model calibration (January 1980) to the end of model calibration (December 1989).

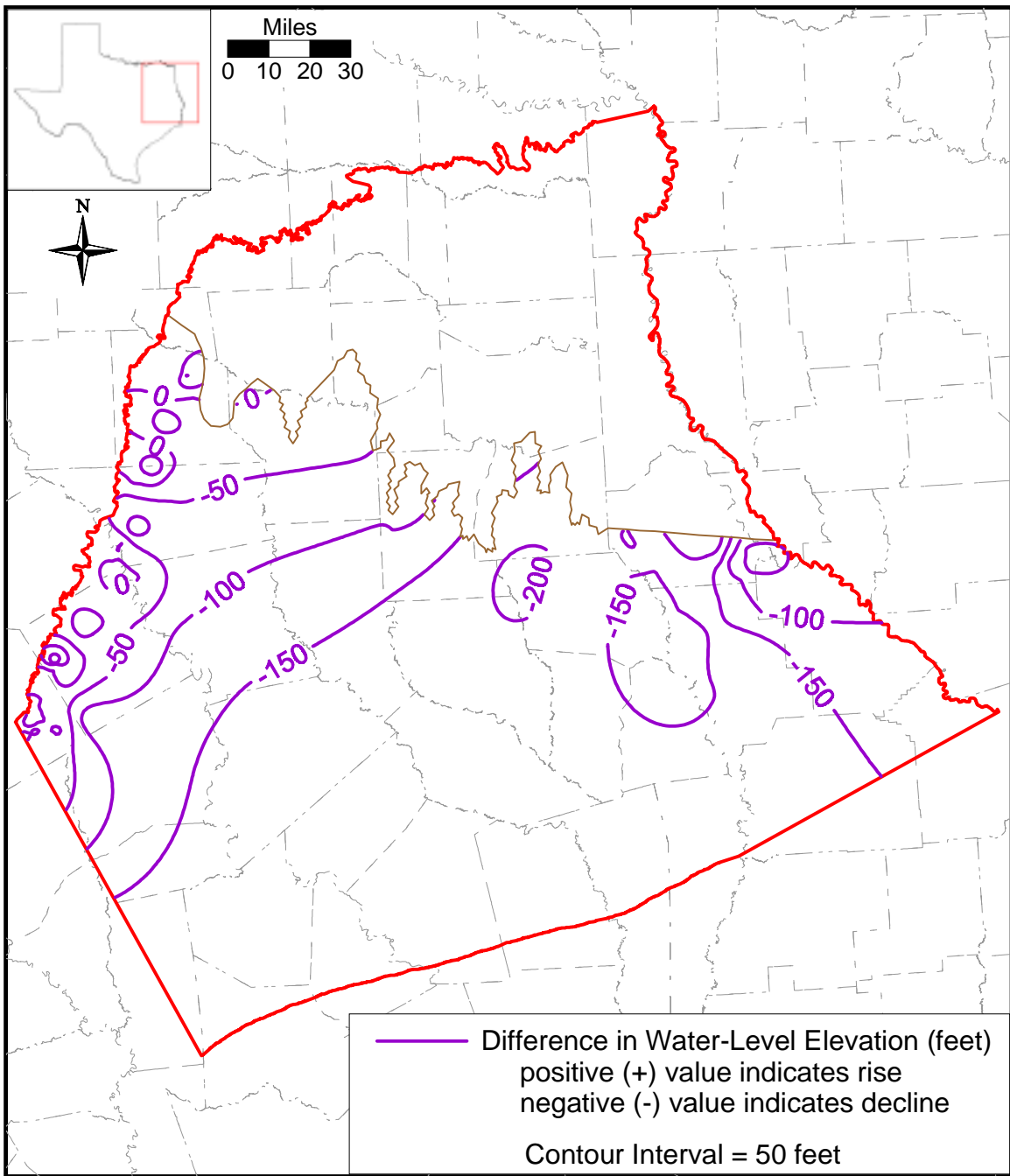


Figure 4.4.19b Water-level decline in the lower Wilcox from the start of model calibration (January 1980) to the end of model verification (December 1999).

4.5 Recharge

Recharge can be defined as water which enters the saturated zone at the water table (Freeze, 1969). Potential sources for recharge to the water table include precipitation, stream or reservoir leakage, or irrigation return flow. In the Northern Carrizo-Wilcox GAM area, recharge is conceptualized to occur as diffuse recharge in the inter-stream areas. Focused recharge may also occur in the vicinity of reservoirs and streams. However, the interaction between groundwater and surface water is determined by the degree of connection between the surface water and the groundwater. In arid areas with relatively thick unsaturated zones, surface water bodies typically lose water. In humid areas, such as the Northern Carrizo-Wilcox GAM study area, surface water bodies are more typically gaining (Scanlon et al., 2002). Any infiltration that does occur in river valleys is much more prone to being rejected by interflow to nearby surface water bodies. The great majority of the infiltration, or shallow recharge, that does occur in the outcrop is discharged through baseflow in streams or is lost to evapotranspiration in lower elevation areas where the water table is shallow (Scanlon et al., 2002).

The cleaner and more massive sands of the Carrizo and Simsboro formations have commonly been assumed to be the preferentially recharged hydrostratigraphic units in the Carrizo-Wilcox aquifer system in central and eastern Texas. This is likely the result of the formations' increased ability to move water away from the water table (Freeze, 1969) relative to other hydrostratigraphic units adjacent to and within the Carrizo-Wilcox. However, recharge has been demonstrated to be a complex function of precipitation rate and volume, soil type, water level and soil moisture, topography, and evapotranspiration (ET) (Freeze, 1969). Because of its large outcrop area and relatively high sand content, the Wilcox Group also has a good potential for diffuse recharge in the study area. When recharge rates exceed the saturated hydraulic conductivity of the underlying soils and aquifer, then the transmission capability of the underlying formation becomes a limiting factor. These conditions may be expected to occur in local areas of focused recharge or in times of exceedingly high precipitation rates.

Because precipitation, ET, and soil moisture vary as a function of time, recharge is also expected to vary as a function of time. Recharge will be highest in times of significant rainfall

when soil moisture content is high. In drier times, redistribution and ET may effectively prevent significant recharge.

Several investigators have studied recharge in the Carrizo-Wilcox aquifer in Texas. These studies have been summarized by Scanlon et al. (2002) and are reproduced in Table 4.5.1. Those studies in Table 4.5.1 which are limited to the Northern Carrizo-Wilcox GAM study area are grouped as the top fifteen table entries because of their direct relevance to this study. For all studies reported by Scanlon et al. (2002), recharge rates range from a low of 0.1 inches estimated for Rains and Van Zandt counties (White, 1973) using a Darcy's Law approach to a high of 5.8 inches per year in Atascosa County (Opfel and Elder, 1978), southwest of the study area, using neutron probe measurements in the vadose zone. The range specific to the study area is similar in magnitude ranging from a low of 0.1 inches per year as described above to a high of 5 inches per year (Carrizo & Simsboro) based upon groundwater modeling in Region G (Harden & Associates, 2000). It is worth noting that the two highest reported values of recharge in the model area originate from modeling studies. This is problematic in that steady-state models are sensitive to recharge but are extremely non-unique. Transient models improve model parameter constrains and are less non-unique. However, transient models of the Carrizo-Wilcox are not extremely sensitive to recharge.

There was only one natural lake in the study area, Caddo Lake, which was drained in the 1870s and later impounded in 1914. There are 40 reservoirs with surface areas greater than ½ square mile in the study area that occur in the outcrop of the Carrizo-Wilcox or the Queen City aquifers (Figure 4.5.1). Table 4.5.2 lists the names, owners, and year completed of these reservoirs.

There are several reservoirs in the study area that intersect one or more of the active Carrizo-Wilcox aquifer outcrop grid cells in the GAM area. Figure 4.5.2 shows the lake stage elevations of three of the reservoirs for the historical simulation period from 1980 to 1999. Because they are located in outcrop areas, these reservoirs provide potential areas of focused recharge to the underlying aquifers. Figure 4.5.2 shows that the reservoirs generally have stages that do not vary greatly over the time period of interest.

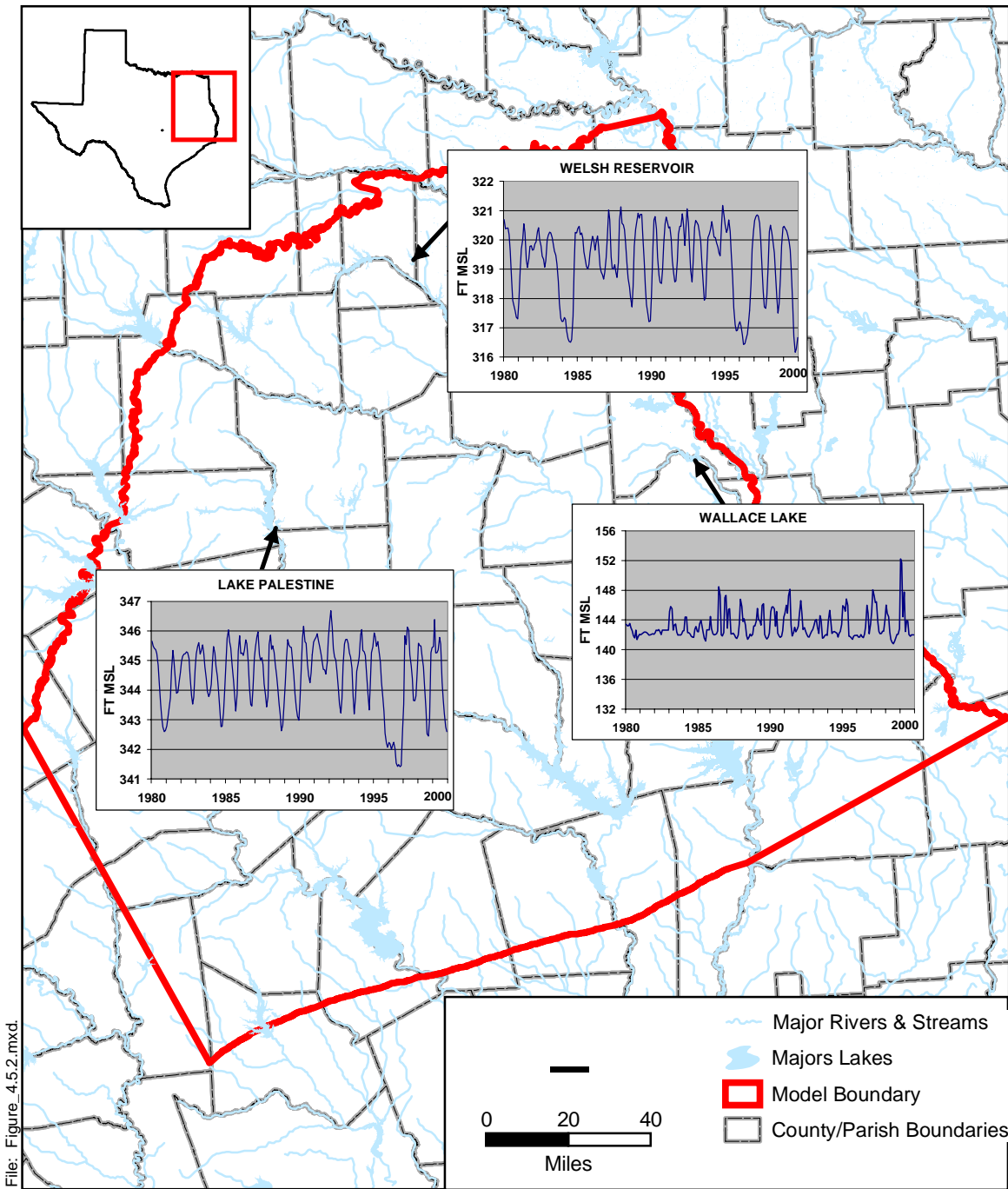
Table 4.5.1 Review of recharge rates for the Carrizo-Wilcox aquifers in Texas (after Scanlon et al., 2002).

Major Aquifer	Location (County/Area)	Aquifer	Recharge rate (mm/yr)	Recharge rate (in/yr)	Total recharge (af/yr)	Reference	Technique
Carrizo Wilcox	Sabine, San Augustine	undifferentiated	50.8	2.0		Anders, 1967	Darcy's Law
	Sabine, San Augustine	undifferentiated	25.4	1.0		Anders, 1967	baseflow discharge
	Camp, Franklin, Morris, Titus	Carrizo Wilcox			12,000	Broom et al., 1965	baseflow discharge
	Harrison	Cypress	7.9	0.3	15,000	Broom and Myers, 1966	Darcy's Law
	Harrison	Cypress	7.9	0.3	40,000	Broom and Myers, 1966	baseflow discharge
	Wood	Carrizo	12.7	0.5	3,000	Broom, 1968	Darcy's Law
	Freestone	Calvert Bluff sands	100			Dutton, 1990	soil water budget
	Bastrop, Lee, Milam	Simsboro, Carrizo	51-102	2.0-4.0		Dutton, 1999	groundwater modeling
	Bastrop	Carrizo, Wilcox sand	38	1.5		Follett, 1970	Darcy's Law
	Bastrop, Lee, Milam, Robertson, Falls, Limestone, Freestone, Navarro	Carrizo, Simsboro	76-127	3.0-5.0		Harden and Associates, 2000	groundwater modeling
	Bastrop, Lee, Milam, Robertson, Falls, Limestone, Freestone, Navarro	Calvert Bluff, Hooper	12.7	0.5		Harden and Associates, 2000	groundwater modeling
	Rusk	Carrizo	<25.4	<1.0		Sandeen, 1987	Darcy's Law
	Navarro	Carrizo Wilcox	12.7	0.5		Thompson, 1972	estimate
	Caldwell, Bastrop, Lee, Milam, Robertson, Limestone, Freestone	undifferentiated	25.4	1.0		Thorkildsen and Price, 1991	groundwater modeling
	Rains, Van Zandt	Carrizo Wilcox	3	0.1	5,000	White, 1973	Darcy's Law
	Atascosa, Frio	Carrizo sand	45.7			Alexander and White, 1966	¹⁴ C, Darcy's Law
	Winter Garden area	undifferentiated	5-127			LBG-Guyton & Assoc. and HDR, 1998	modeling, water budget
	Bexar	Hooper, Simsboro, Calvert Bluff	45.7			HDR Engineering, 2000	groundwater modeling
	Winter Garden area	undifferentiated			100,000	Klemm et al., 1976	groundwater modeling
	Bastrop, Lee, Fayette	undifferentiated	25.4	1.0		Thorkildsen et al., 1989	groundwater modeling
Atascosa, Bexar, Dimmit, Frio, Gonzales, Guadalupe, Medina, Uvalde, Wilson, Zavala	undifferentiated			25,000	Turner et al., 1960	Darcy's Law	

Table 4.5.2 Characteristics of reservoirs in study area.

Reservoir	Reservoir Name	Owner	Date Impounded
1	Black Bayou Lake	State of Louisiana	1955
2	Brandy Branch Cooling Pond	Southwestern Electric Power Company	1983
3	Caddo Lake	Caddo Levee District	1914
4	Cedar Creek Reservoir	Tarrant County WCID #1	1965
5	Clear Lake	*	*
6	Cross Lake	City of Shreveport	1925
7	Eastman Lakes	*	*
8	Ellison Creek Reservoir	Lone Star Steel Company	1943
9	Fairfield Lake	Texas Utilities Generating Company	1969
10	Forest Grove Reservoir	Texas Utilities Generating Company	1980
11	Johnson Creek Reservoir	Southwestern Electric Power Company	1961
12	Lake Athens	Athens Municipal Water Authority	1962
13	Lake Bob Sandlin	Titus County FWSD #1	1977
14	Lake Cherokee	Cherokee Water Company	1948
15	Lake Cypress Springs	Franklin County Water District & T.W.D.B.	1970
16	Lake Fork Reservoir	Sabine River Authority	1979
17	Lake Gladewater	City of Gladewater	1952
18	Lake Hawkins	Wood County	1962
19	Lake Holbrook	Wood County	1962
20	Lake Jacksonville	City of Jacksonville	1957
21	Lake Limestone	Brazos River Authority	1978
22	Lake Monticello	Texas Utilities Generating Company	1972
23	Lake Murvaul	Panola County GWSD #1	1957
24	Lake Nacogdoches	City of Nacogdoches	1976
25	Lake O' the Pines	U.S. Army Corps of Engineers	1957
26	Lake Palestine	Upper Neches River Authority	1962
27	Lake Quitman	Wood County	1962
28	Lake Striker	Angelina-Nacogdoches WCID #1	1957
29	Lake Tyler/Lake Tyler East	City of Tyler	1966
30	Lake Winnsboro	Wood County	1962
31	Martin Lake	Texas Utilities Generating Company	1974
32	Pinkston Reservoir	City of Center	1977
33	Richland-Chambers Reservoir	Tarrant County WCID #1	1987
34	Sibley Lake	State of Louisiana	1962
35	Smithport Lake	State of Louisiana	*
36	Toledo Bend Reservoir	Sabine River Authority	1966
37	Trinidad Lake	*	1925
38	Wallace Lake	U.S. Army Corps of Engineers	1946
39	Welsh Reservoir	Southwestern Electric Power Company	1975
40	Wright Patman Lake	U.S. Army Corps of Engineers	1956

*Information unavailable



4.6 Natural Aquifer Discharge

Under steady-state conditions representative of predevelopment conditions, groundwater flow in the aquifer is elevation driven from the inter-stream higher elevation outcrops to the lower elevation stream valleys and to a lesser degree the confined sections of the aquifer. In the predevelopment condition, recharge occurring as a result of diffuse and focused recharge will be balanced by discharge in stream valleys and springs, and through cross-formational flow. Under predevelopment conditions, it is expected that most streams in the study area were gaining streams. Thorkildsen et al. (1989) reported that the Colorado River and its major tributaries received a significant portion of their natural discharge from the Carrizo-Wilcox aquifer. Dutton (1999) reports that Carrizo-Wilcox discharge supplies some baseflow to both the Colorado and Brazos rivers.

There has been a large number of stream gain/loss studies performed in the Carrizo-Wilcox in Texas. Slade et al. (2002) summarized the results of 366 gain/loss studies involving 249 unique reaches of streams throughout Texas since 1918. They documented 12 individual gain/loss studies in the model area with 9 in the Carrizo-Wilcox outcrop. Studies have been performed on the Sabine River, Bowles Creek (Nueces River Basin), Grays, Little Cypress, and Sugar creeks (Red River Basin), and Lake Fork Creek (Sabine River Basin), and Big and Little Elkhart creeks (Trinity River Basin). Figure 4.6.1 shows the locations and survey numbers of the gain/loss studies in the model area. Table 4.6.1 provides the characteristics of the gain/loss studies reported by Slade et al. (2002). The survey numbers in Figure 4.6.1 correspond to the survey numbers in Table 4.6.1.

Three studies were performed on the Sabine River (surveys 345, 346, and 347). Surveys 345 and 346 were performed in August and September of 1981 and both indicate gaining river base flow conditions with average gains of 592 and 3,847 acre feet per year per mile of stream, respectively. Survey 347 was performed along a 268-mile stretch of the Sabine in September of 1963. The survey average gain for the Sabine River was 564 acre feet per year per mile. Surveys 243, 244, 245, and 249 were performed in 1964 in tributary creeks to the Red River. Average gain/loss estimates range from a slightly losing -6.5 acre feet per year per mile to gaining 431 acre feet per year per mile. Survey 249 was likely performed in the Queen City

outcrop. In 1942, a 6.5-mile length of Bowles Creek (Neches River Basin) was surveyed and found to be gaining 335 acre feet per year per mile. The only strongly losing survey was performed on Lake Fork Creek (Sabine River Basin) in August and September of 1981. This survey (No. 342) estimated an average loss of -1,177 acre feet per year per mile over a 1.6 mile stretch of stream. This estimate appears anomalous. The available gain/loss surveys are consistent with our assumption that most major rivers and streams in the study area are gaining from the Carrizo-Wilcox aquifer in the outcrop.

Discharge also occurs in areas where the water table intersects the surface at springs or weeps. These springs usually occur in topographically low areas in river valleys or in areas of the outcrop where hydrogeologic conditions preferentially reject recharge. We performed a literature survey of springs with location and flow rate data available for the model domain (Figure 4.6.2). Sixty-seven documented springs were identified in the study area. Each spring is numbered and the number corresponds to the spring information provided in Table 4.6.2. The available measured spring flow rates range from less than 0.01 cubic feet per second (<7 acre feet per year) to a high of 3.4 cubic feet per second (2,462 acre feet per year) measured at Elkhart Creek Springs (No. 8) and originating from the Sparta Sand (Brune, 1975). The only two springs originating from the Carrizo-Wilcox which could potentially be significant for this scale model are #16 Roher Springs (No. 23) and spring number 50. Roher Springs flowed at an average rate of 0.5 cubic feet per second (362 acre feet per year) based upon one measurement in 1979 and one in 1995. Spring number 50 located on the county line between Nacogdoches and Rusk counties flowed at 0.5 cubic feet per second (362 acre feet per year) in 1942. The number of flowing springs in the study area is a product of the humid climate, the dissected topography in the model area, and the gently dipping aquifers, all of which contribute to a large percent of rejected recharge which contributes to runoff in the East Texas Basin.

Cross-formational flow is also a natural mechanism for discharge of groundwater from the Carrizo-Wilcox aquifer. Fogg and Kreitler (1982) and Fogg et al. (1983) documented that in the East Texas Basin, flow across the Reklaw is generally downward from the unconfined Queen City to the Carrizo. However, in the vicinity of the Trinity and Sabine rivers, hydraulic heads are reversed with the Carrizo-Wilcox discharging through upward leakage across the Reklaw. Estimates of these fluxes are lacking but Fogg et al. (1983) concluded that leakage across the

Reklaw must be significant because of the effect of topography seen in large portions of the confined Carrizo aquifer. South of the East Texas Basin and the Sabine Uplift, the Carrizo-Wilcox aquifer system begins to dip and thicken significantly into the Houston Embayment. Cross formational flow in this portion of the model area is expected to be from the Carrizo to the Reklaw. With development of the Carrizo-Wilcox aquifer system, the natural balance of recharge and cross-formational flow will change.

Table 4.6.1 Stream flow gain/loss in the study area (after Slade et al., 2002, Table 1).

Streamflow study no.	Major river basin	Stream name	Reach identification	Date of study	Reach length (river)	Total no. of measurement sites	No. of measurement sites on main	Major aquifer outcrop(s) intersected by reach	Total gain or loss (-) in reach	Gain or loss per mile (cfs/mile)	Gain or loss per mile (AFY/mile)
139	Neches	West Fk Bowles Cr - [Bowles Cr]	west of Old London to near Carlisle	10/28/1942	6.5	11	6	Carrizo-Wilcox	3.0	0.462	334.7
243	Red River	Grays Cr	2.6 mi north of Marshall to FM 1997	6/13/1964	3.3	9	2	Carrizo-Wilcox	-0.03	-0.009	-6.5
244	Red River	Little Cypress Cr	SH 155 to FM 134	6/10-13/1964	49.1	35	10	Carrizo-Wilcox	6.52	0.133	96.4
245	Red River	Little Cypress Cr	northeast of Gilmer to near Jefferson	1/2-3/1964	40.5	7	7	Carrizo-Wilcox	24.09	0.595	431.1
249	Red River	Sugar Cr	FM 1403 to SH 154	6/10-11/1964	0.8	3	2	--	0.15	0.188	136.2
342	Sabine	Lake Fk Cr	SH 182 to US 80	8/31-9/1/1981	1.6	3	3	Carrizo-Wilcox	-2.6	-1.625	-1177.3
345	Sabine	Sabine R	FM 1804 to FM 2517	9/22-24/1981	156.4	11	10	Carrizo-Wilcox	127.8	0.817	591.9
346	Sabine	Sabine R	Wills Point (08017410) to Smith-Upshur Co line at county road crossing	8/31-9/2/1981	80.5	8	6	Carrizo-Wilcox	427.42	5.31	3846.9
347	Sabine	Sabine R	northeast of Carthage to Ruliff (08030500)	9/4-5/1963	268	98	30	Carrizo-Wilcox, Gulf Coast	208.72	0.779	564.4
364	Trinity	Big Elkhart Cr	northwest of Grapeland to mouth	9/15-16/1965	25.7	9	7	--	5.18	0.202	146.3
365	Trinity	Little Elkhart Cr	south of Grapeland to mouth	9/16/1965	17.5	11	5	--	-1.59	-0.091	-65.9
366	Trinity	Trinity R	Riverside to Liberty	11/4-8/1952	133.5	21	5	Gulf Coast	37.16	0.278	201.4

Table 4.6.2 Documented springs in the study area.

ID	Spring	Aquifer	Flow Rate LPS	Flow Rate GPM	Flow Rate CFS	Date of Measurement	Measurement	Historical Information	SOURCE
1	#11 Dalby Springs	Wilcox Sand	1.70	26.95	0.06	1/1/1892	1 of 2		Brune, 1975
1	#11 Dalby Springs	Wilcox Sand	0.06	0.95	0.00	1/1/1976	2 of 2		Brune, 1975
2	#12 Hughes Springs/Chalybeate Springs	Wilcox Sand	0.32	5.07	0.01	1/1/1976			Brune, 1975
3	#2 Thrasher Springs	Queen City Sand	0.30	4.76	0.01	1/15/1976			Brune, 1975
4	#5 Castalian Springs	Queen City Sands	0.32	5.07	0.01	7/12/1936	1 of 2		Brune, 1975
4	#5 Castalian Springs	Queen City Sands	0.03	0.48	0.00	11/1/1979	2 of 2		Brune, 1975
5	#10 Hynson, Marshall, Noonday Camp, Iron Springs	Queen City	0.13	2.06	0.00	1/28/1942	1 of 3	Over 100 Springs	Brune, 1975
5	#10 Hynson, Marshall, Noonday Camp, Iron Springs	Queen City	0.13	2.06	0.00	1/27/1967	3 of 3	Over 100 Springs	Brune, 1975
5	#10 Hynson, Marshall, Noonday Camp, Iron Springs	Queen City	0.06	0.95	0.00	7/21/1964	2 of 3	Over 100 Springs	Brune, 1975
6	#6 Coughatta Springs	Wilcox Sand	3.20	50.73	0.11	1/25/1976			Brune, 1975
7	#2 Sulphur Springs	Wilcox Sand	3.60	57.07	0.13	12/20/1997		1841 Over 100 springs reported	Brune, 1975
8	Elkart Creek Springs	Sparta Sand	96.28	1526.03	3.40	9/15/1965			Brune, 1975
9	Hays Branch Springs	Sparta Sand	50.97	807.90	1.80	9/16/1965			Brune, 1975
10	Caney Creek Springs	Sparta Sand	48.14	763.01	1.70	9/16/1965			Brune, 1975
11	Boiling Spring	Sparta Sand	0.32	5.00	0.01	1/1/1963			Brune, 1975
12	#14 Shawnee Mineral/Nacogdoches Springs	Sparta	2.90	45.97	0.10	1/1/1978			Brune, 1975
13	#24 White and Red Springs	Wilcox Sand	0.06	0.95	0.00	1/1/1978	2 of 2		Brune, 1975
13	#24 White and Red Springs	Wilcox Sand		1.00		10/1/1936	1 of 2		Brune, 1975
14	#3 Sulphur Springs	Carrizo Sand	0.13	2.06	0.00	1/1/1976			Brune, 1975
15	#4 Hughes Springs	Carrizo Sand	0.32	5.07	0.01	1/1/1937	1 of 2		Brune, 1975
15	#4 Hughes Springs	Carrizo Sand	0.15	2.38	0.01	1/1/1976	2 of 2		Brune, 1975
16	#9 National Forest Springs	Wilcox Sand	0.32	5.07	0.01	1/1/1937	1 of 2		Brune, 1975

Table 4.6.2 (continued)

ID	Spring	Aquifer	Flow Rate LPS	Flow Rate GPM	Flow Rate CFS	Date of Measurement	Measurement	Historical Information	SOURCE
16	#9 National Forest Springs	Wilcox Sand	0.32	5.07	0.01	1/1/1976	2 of 2		Brune, 1975
17	#11 Headache Springs	Weches Sand	0.35	5.55	0.01	11/2/1979			Brune, 1975
18	#3 Neff Springs	Spart Sand	-					1947 "Moderately large" flow. 1979 dry	Brune, 1975
19	#4 Arms Factory Spring	Spart Sand	0.20	3.17	0.01	10/30/1979		A "bold" spring when first discovered	Brune, 1975
20	#5 Tyler Springs	Sparta Sand	1.70	26.95	0.06	10/30/1970	2 of 2		Brune, 1975
20	#5 Tyler Springs	Sparta Sand	0.63	9.99	0.02	7/6/1936	1 of 2		Brune, 1975
21	#6 Camp Ford & Pine Springs	Sparta Sand	0.08	1.27	0.00	10/30/1979		during Civil War described as "large" spring	Brune, 1975
22	#7 Cousins Springs	Sparta Sand	1.30	20.61	0.05	10/30/1979		Finest spring in area when found	Brune, 1975
23	#16 Roher Springs	Carrizo Sand	17.00	269.48	0.60	9/27/1979	1 of 2		Brune, 1975
23	#16 Roher Springs	Carrizo Sand	11.67	185.00	0.41	9/6/1995	2 of 2		TWDB well database
24	Peacock Spring	Sparta & Queen City	3.15	50.00	0.11			Estimated flow 50 gpm. Known as Peacock Spring.	TWDB well database
25	Palmer Spring	Sparta & Queen City	0.03	0.50	0.00			Estimated flow 1/2 gpm. Know as Palmer Spring.	TWDB well database
26	Dumas Spring	Carrizo & Wilcox, Undifferentiated	6.31	100.00	0.22			Estimated flow 100 gpm. Known as Dumas Spring.	TWDB well database
27	Library Spring	Queen City Sand	0.06	1.00	0.00			Called Library Spring. Flows 1 gal. per minute	TWDB well database
28	Spring	CARRIZO SAND	0.14	2.20	0.00	1/1/1978		Spring encased in wooden box. Reported discharge 2.2 gal/min, 1978 (Gunnar Brune).	TWDB well database
29	Spring	Carrizo Sand	0.13	2.00	0.00	10/19/1936		Spring, estimated flow 2 gal/min 10-19-36.	TWDB well database
30	Spring	Queen City Sand	14.38	228.00	0.51	11/17/1978	1 of 2	Spring. Deussen (1914) reported "large flow." Reported discharge 228 gal/min 1-11-78 (Gunner Brune). Measured discharge 8.5 gal/min and measured temp. 13.8 degrees C. on 7-14-81.	TWDB well database

Table 4.6.2 (continued)

ID	Spring	Aquifer	Flow Rate LPS	Flow Rate GPM	Flow Rate CFS	Date of Measurement	Measurement	Historical Information	SOURCE
30	Spring	Queen City Sand	0.54	8.50	0.02	7/14/1981	2 of 2	Spring. Deussen (1914) reported "large flow." Reported discharge 228 gal/min 1-11-78 (Gunner Brune). Measured discharge 8.5 gal/min and measured temp. 13.8 degrees C. on 7-14-81.	TWDB well database
31	Spring	Reklaw Formation	0.63	10.00	0.02			Spring. Deussen (1914) reported "large flow;" Gunnar Brune (1978) reported 10 gal/min.	TWDB well database
32	Spring	Carrizo & Wilcox, Undifferentiated	2.84	45.00	0.10	1/1/1942		Reported discharge 40 to 50 gpm in 1942. Unable to locate spring in 1964.	TWDB well database
33	King's Spring	Jackson Group	1.26	20.00	0.04	5/15/1947		King's Spring. Estimated flow 20 gpm, May 15, 1947.	TWDB well database
34	Moffit Springs	Jackson Group	15.77	250.00	0.56	4/13/1994		Moffit Springs. Reported flow 250 GPM April 13, 1994.	TWDB well database
35	Spring	Cypress	0.03	0.50	0.00	7/1/1964			County Reports
36	Spring	Cypress	0.06	1.00	0.00	8/1/1964			County Reports
37	Spring	Cypress	0.32	5.00	0.01	1/1/1968			County Reports
38	Spring	Cypress	1.26	20.00	0.04	10/1/1967			County Reports
39	Spring	Cypress	0.95	15.00	0.03	10/1/1959			County Reports
40	Spring	Cypress	0.13	2.00	0.00	10/1/1959			County Reports
41	Spring	Cypress	0.19	3.00	0.01	6/1/1963			County Reports
42	Spring	Cypress	1.58	25.00	0.06	7/1/1963			County Reports
43	Spring	Cypress	0.32	5.00	0.01	3/1/1942			County Reports
44	Spring	Cypress	0.41	6.50	0.01	4/1/1963			County Reports
45	Spring	Cypress	0.06	1.00	0.00	5/1/1963			County Reports
46	Spring	Cypress	0.25	4.00	0.01	4/1/1963			County Reports
47	Spring	Carrizo-Wilcox	0.32	5.00	0.01	1/1/1942			County Reports

Table 4.6.2 (continued)

ID	Spring	Aquifer	Flow Rate LPS	Flow Rate GPM	Flow Rate CFS	Date of Measurement	Measurement	Historical Information	SOURCE
48	Spring	Carrizo-Wilcox	0.44	7.00	0.02	1/1/1942			County Reports
49	Spring	Carrizo	0.06	1.00	0.00	1/1/1936			County Reports
50	Spring	Carrizo	14.20	225.00	0.50	3/1/1942			County Reports
51	Spring	Carrizo	0.22	3.50	0.01	1/1/1963			County Reports
53	Spring	Carrizo	0.13	2.00	0.00	1/1/1936			County Reports
54	Spring	Carrizo	0.06	1.00	0.00	1/1/1936			County Reports
55	Boykin Spring	Catahoula Sandstone	8.50	134.73	0.30	2/20/1978			GNIS, Brune (1981)
56	Blue Spring	Yegua Sand	0.18	2.85	0.01	1/1/1978			GNIS, Brune (1981)
57	Harris Spring	Whitsett Sand	0.57	9.03	0.02	3/19/1978			GNIS, Brune (1981)
58	Doggett Spring	Wilcox Sand	0.65	10.30	0.02	1/1/1976			GNIS, Brune (1981)
59	Beauchamps Springs	Weches Sand	1.10	17.44	0.04	10/31/1979			GNIS, Brune (1981)
60	Red Springs		0.65	10.30	0.02	10/31/1979			GNIS, Brune (1981)
61	Walnut Springs		seep	seep	seep	10/31/1979		1960's known as "very fine spring"	GNIS, Brune (1981)
62	Barton Springs							Once furnished water for a sawmill & gin	GNIS, Brune (1981)
63	Cary Martin Springs	Queen City	0.35	5.55	0.01	1/1/1978		Formerly Wolf Springs	GNIS, Brune (1981)
64	Lee Springs	Queen City	7.60	120.46	0.27	1/21/1978		Includes Couch & Joe's Spring	GNIS, Brune (1981)
65	Bowles Springs	Queen City	1.30	20.61	0.05	11/6/1979			GNIS, Brune (1981)
66	Myrtle Spring	Reklaw Formation	4.70	74.50	0.17	11/4/1979		a.k.a. Myrill Springs	GNIS, Brune (1981)
67	Roseborough Springs	Wilcox Sand	1.40	22.19	0.05	1/1/1976		Here 7 springs formerly flowed, although most must be pumped by now	GNIS, Brune (1981)

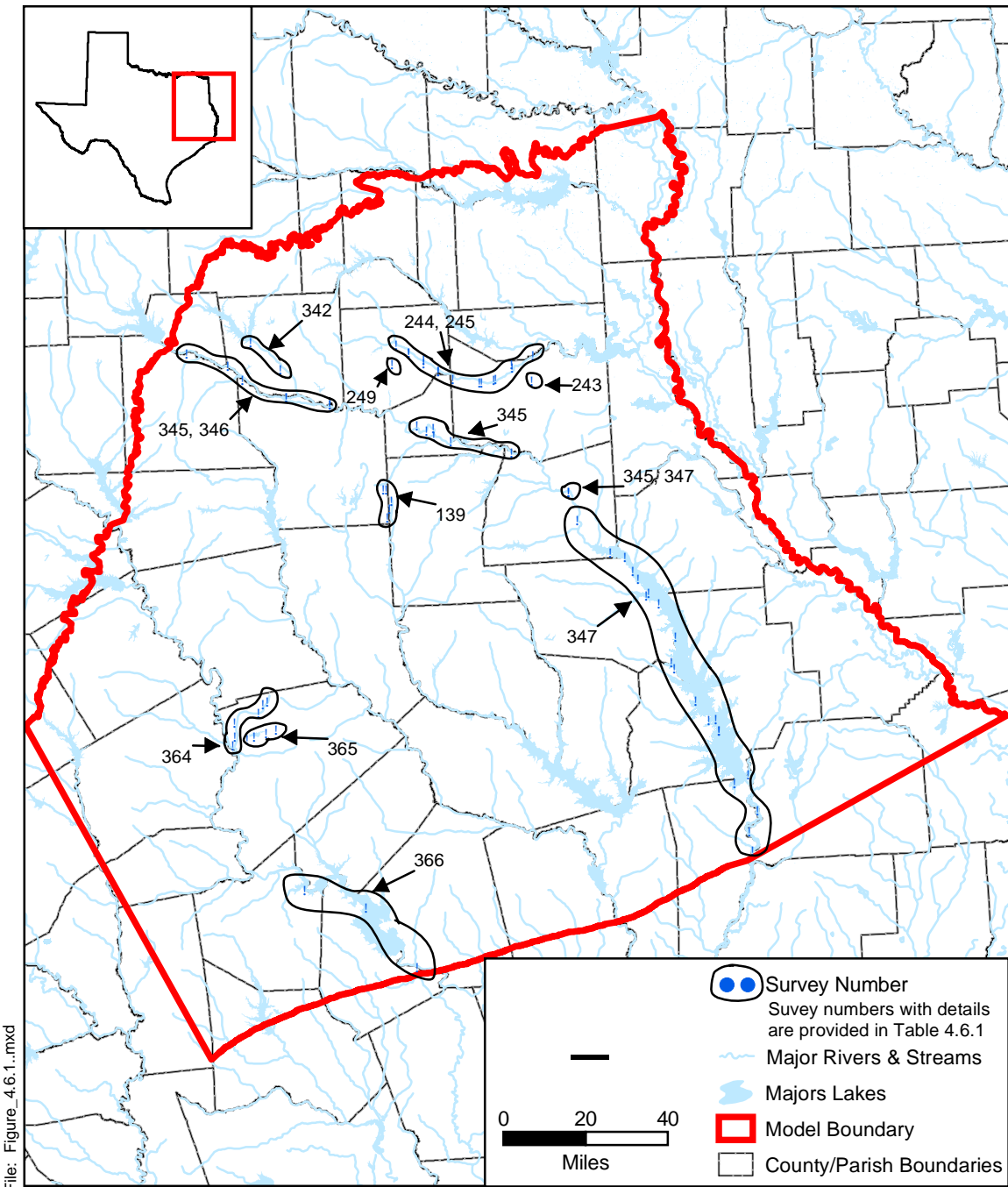
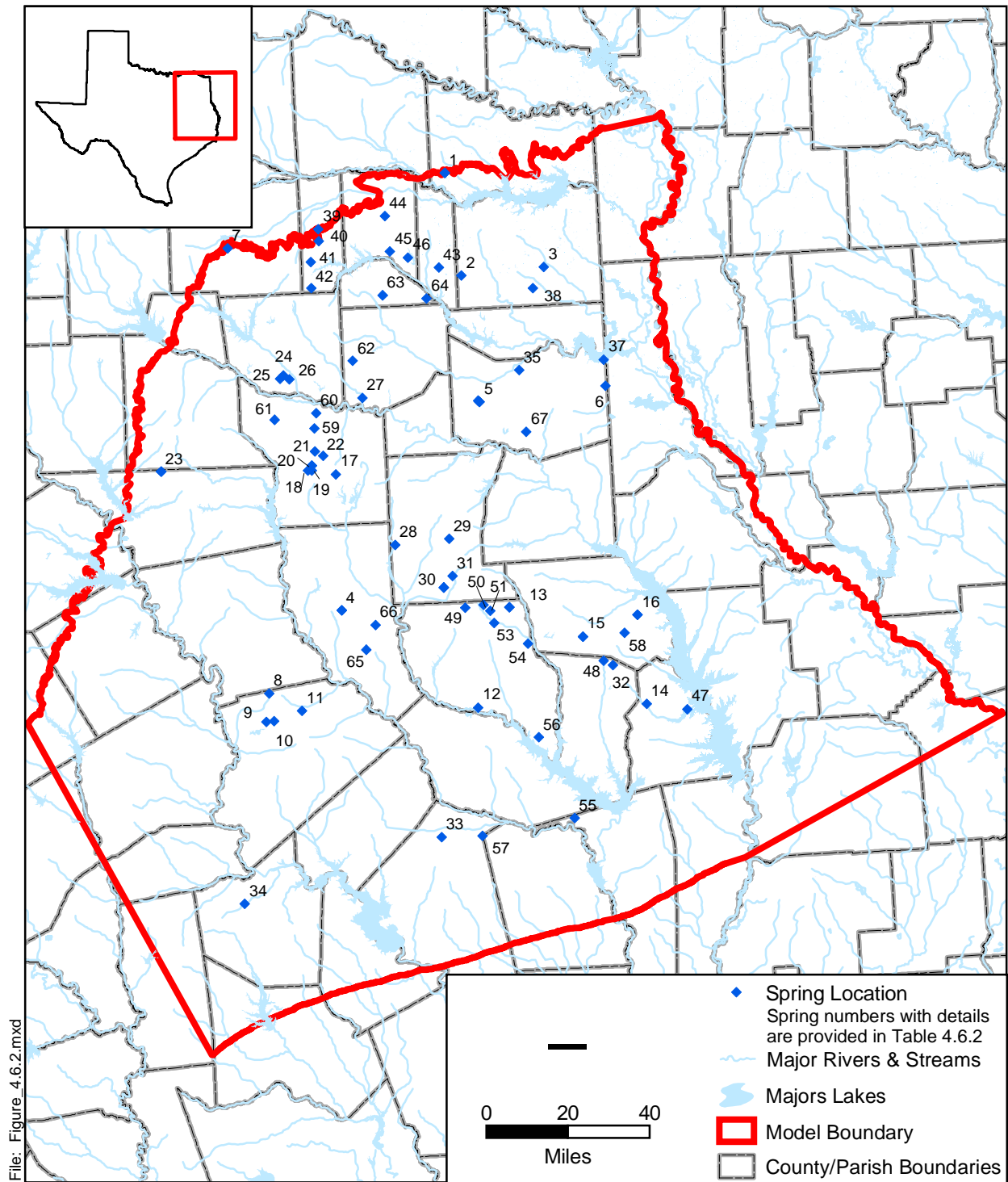


Figure 4.6.1 Stream gain/loss studies in the study area (after Slade et al., 2002).



4.7 Aquifer Discharge Through Pumping

Pumping discharge from the model required estimations for both the historical modeling period (1980 to 1999) and for the predictive period (2000 to 2050). Historical estimates of groundwater pumpage from the Carrizo-Wilcox aquifer were based on the water use survey database provided by the Texas Water Development Board. The seven water use categories utilized were municipal (MUN), manufacturing (MFG), power generation (PWR), mining (MIN), livestock (STK), irrigation (IRR), and county-other (C-O), which consists primarily of unreported domestic water use. The methodology used to distribute those pumpage estimates is described briefly below, and in detail in the “Standard Operating Procedure for Processing Historical Pumpage Data”, Appendix B to this report.

Municipal, manufacturing, mining, and power pumpage estimates were actual monthly water use records reported by the water user, which were available for 1980 through 1999. In cases where only the total annual pumpage was reported, the average monthly distribution of annual pumpage for the same water use category in the same county-basin, or an adjacent county-basin, was used. A county-basin is a geographic unit created by the intersection of county and river basin boundaries. For example, a county partly crossed by two river basins comprises two county-basins.

The water use survey also included historical annual pumpage estimates for livestock, irrigation, and county-other water use for the years 1980 and 1984 through 1997 for each county-basin. Annual pumpage estimates for the years 1981, 1982, 1983, 1998, and 1999 were developed by linear regression based on significant relationships between reported pumpage and (1) average annual temperature, (2) total annual rainfall measured at the nearest weather station, and (3) the year, for each water use category.

The monthly distribution of county-other water use was assumed to be similar to that of municipal use. The average monthly distribution of municipal water use for a given year within the same (if possible) or an adjacent county-basin was used to estimate how much of the annual total county-other usage was pumped in each month.

Annual livestock water use was distributed uniformly across all twelve months. While this may not accurately reflect seasonality of livestock use, it was not expected to have much impact because livestock is a relatively minor use in the study area.

The procedures for temporal distribution of annual irrigation water use differed for rice and non-rice crops. For rice, monthly irrigation pump electricity consumption use records were used to indicate how much water was pumped in each month for rice irrigation. For non-rice crops, annual irrigation water use was distributed among months using predicted monthly water deficits, based on the rainfall deficit and crop evapotranspiration estimates for each Texas Crop Reporting District, using the approach of Borrelli et al. (1998).

Reported historical pumpage for municipal, manufacturing, mining, and power water uses were matched to the specific wells from which it was pumped to identify the location in the aquifer from which it was drawn (latitude, longitude, and depth below mean sea level) based on the well's reported properties. The well properties were obtained by compiling data from the TWDB's state well database, the Texas Commission on Environmental Quality's Public Water System database, the U.S. Geological Survey's National Water Information System, the TWDB's follow up survey with water users, and various other minor sources as described in the "Standard Operating Procedure for Processing Historical Pumpage Data", Appendix B to this report. When more than one well was associated with a given water user, groundwater withdrawals were divided evenly among those wells.

Livestock pumpage totals within each county-basin were distributed uniformly over the rangeland within the county-basin, based on land use maps, using the categories "herbaceous rangeland", "shrub and brush rangeland", and "mixed rangeland". Vertical assignment of livestock pumpage to model flow layers was performed by interpolating an average well depth and screened interval for all Carrizo-Wilcox livestock watering wells in the TWDB state well database, using the inverse distance method to enhance the influence of nearby wells.

County-other pumpage was distributed within each county-basin based on population density (Figure 4.7.1), after excluding urban areas which would generally be served by municipal water suppliers, using the 1990 federal block-level census data for the years 1980-1990, and the 2000 census data for the years 1991-1999. Vertical assignment of county-other pumpage to model flow layers was performed by interpolating an average well depth and screened interval

for all Carrizo-Wilcox county-other wells in the TWDB state well database, using the inverse distance method to enhance the influence of nearby wells.

Irrigation pumpage within each county-basin was spatially distributed across the land use categories “row crops”, “orchard/vineyard”, and “small grains”. However, the pumpage was not uniformly distributed across these land uses, but weighted based on proximity to irrigated farms mapped from the irrigated farmlands surveys performed in 1989 and 1994 by the Natural Resource Conservation Service of the U.S. Department of Agriculture. The 1989 irrigation survey was used for pumpage between 1980 and 1989, while the 1994 survey was used for pumpage from 1990 to 1999. Further details of the procedure are available in the “Standard Operating Procedure for Processing Historical Pumpage Data”, Appendix B to this report. Vertical assignment of irrigation pumpage to model flow layers was performed by interpolating an average well depth and screened interval for all Carrizo-Wilcox irrigation wells in the TWDB state well database, using the inverse distance method to enhance the influence of nearby wells.

In the northern Carrizo-Wilcox aquifer, groundwater pumpage estimates for portions of the model domain in Arkansas were derived from data provided by the Arkansas Soil & Water Conservation Commission. The U.S. Geological Survey provided groundwater pumpage estimates for Louisiana.

Predicted groundwater pumpage from the Carrizo-Wilcox aquifer for the period 2000 through 2050 was estimated based on projected water demand reported by Regional Water Planning Groups as part of Senate Bill 1 planning (TWDB, 2002). The methodology used to distribute pumpage estimates is described briefly here, and in detail in the “Standard Operating Procedure for Processing Predictive Pumpage Data”, Appendix C to this report. The RWPG water demand projections were available for the years 2000, 2010, 2020, 2030, 2040, and 2050; intervening year projections were developed by linear interpolation. In some cases, the RWPGs identified new well field locations for developing new water supplies. In such instances, the specific locations of the future well fields were used to spatially distribute the groundwater pumpage forecasts. However, in the absence of any data indicating otherwise, it was assumed that the most recent past spatial distribution of groundwater pumpage represented the best available estimate of the locations of future groundwater withdrawals.

Predicted municipal water use totals for each public water supplier were matched to the same wells used for that water user in 1999. Similarly for manufacturing, mining, and power generation, predicted future water pumpage totals by county-basin were distributed among the same wells and locations used by those water users in 1999. Irrigation, county-other, and livestock pumpage estimates for each county-basin from 2000 to 2050 also utilized the same spatial distribution within county-basins as was used in 1999.

Estimates of projected Arkansas and Louisiana groundwater pumpage for 2000 through 2050 were not available. Municipal and County-Other pumpage totals for future years were predicted by multiplying the per capita consumption for the period 1995 to 1999 by the projected future county/parish populations, which were supplied by the state demographers. Predicted future pumpage for other water use categories in Louisiana and Arkansas was not projected. Instead we assumed that pumpage in future years would equal the average pumpage for the period 1995 to 1999.

Groundwater withdrawal estimates from the Carrizo-Wilcox aquifer for the years 1980 and 1990, and predictions for 2000, 2010, 2020, 2030, 2040, and 2050 in those counties, or portions of counties, within the model area are provided in Tables D1.1 through D1.12 in Appendix D1. It should be noted that these estimates are the sums of model grid cells. Because the 1 square mile grid cells often cross county boundaries, and are added to that county total in which the center of the grid cell occurs, these county-level estimates are not exact. County-level estimates also may not match the original TWDB estimate because a portion of the county occurred outside the model domain or in inactive model cells, because the location of groundwater withdrawal could not be identified, or because the groundwater was found to have been pumped from a different aquifer based on well depth information.

Based on this analysis, approximately 132,000 acre-feet of groundwater were withdrawn from the modeled portion of the Carrizo-Wilcox aquifer in 1980 (Table 4.7.1). The amount of groundwater withdrawn increased by approximately 18% to roughly 155,000 acre-feet by 1990. Based upon the regional water plans, it is estimated that approximately 167,000 acre-feet were withdrawn in 2000. Groundwater withdrawals from the aquifers in the model area are expected to remain near the year 2000 level through 2050, when the projected groundwater withdrawal will be approximately 170,000 acre-feet.

Figures 4.7.2 through 4.7.7 show the pumping demands for the year 1990 for the six model layers. From these figures it appears that the Queen City (Layer 1) is pumped in significant quantities in the study area. The Carrizo and upper Wilcox (Layers 3 and 4) are produced primarily from the confined section of the aquifers in the East Texas Basin. In contrast, the middle Wilcox and the lower Wilcox (Layers 5 and 6) are predominantly used in the unconfined (outcrop) portion of the aquifers.

In most cases, the largest withdrawals from the Carrizo-Wilcox aquifer are for municipal and industrial purposes, and are found in counties with substantial urban areas, such as Angelina and Smith counties. Groundwater withdrawal from the Carrizo-Wilcox for irrigation purposes can also be substantial, as in Robertson County after 1990.

Appendix D2 provides post plots for the pumping distribution in AFY for each model layer for years 1980, 1990, 2000, and 2050. Appendix D3 provides total pumping distributions in AFY by year from 1980 through 2050 organized by county.

Figures 4.7.2 and 4.7.3 indicate pumpage from both the Queen City (Layer 1) and the Reklaw (Layer 2). Due to uncertainty in allocating pumpage from reported or inferred well interval depths to the different model layers, it is considered reasonable to assume that most of the estimated pumpage from the Reklaw is actually from the Carrizo Formation. Consequently, 90% of the estimated pumpage in the Reklaw was moved to the Carrizo (Layer 3). Similarly, relatively large amounts of pumpage are shown for the Queen City in Smith County (Figure 4.7.2), though TWDB Report 327 indicates that most of the groundwater pumpage in Smith County is from the Carrizo-Wilcox aquifer. As a result, 80% of the estimated Queen City pumpage in Smith and northern Cherokee counties was moved to the Carrizo (Layer 3). The model could not reproduce the observed drawdowns without reallocating pumpage from the Queen City to the Carrizo, even though the vertical permeability of the Reklaw was explicitly decreased in this area.

Table 4.7.1 Rate of groundwater withdrawal (AFY) from all model layers of the Carrizo-Wilcox aquifer for counties within the study area.

County	1980	1990	2000	2010	2020	2030	2040	2050
Anderson	3,493	4,701	6,740	6,788	6,772	6,816	6,783	6,908
Angelina	22,523	20,190	17,807	16,174	15,077	16,112	16,994	18,678
Bienville, LA	0	0	669	669	669	669	669	669
Bossier, LA	128	75	1,728	1,825	1,917	2,003	2,085	2,162
Bowie	1,924	2,191	867	1,945	1,946	1,948	1,952	1,957
Caddo, LA	5,023	3,806	3,979	4,078	4,278	4,582	4,989	5,499
Camp	1,397	1,711	1,542	1,837	1,862	1,892	1,913	1,931
Cass	3,903	4,297	1,291	1,439	1,138	1,140	1,185	1,175
Cherokee	7,093	7,790	8,713	4,321	4,445	4,584	4,844	5,077
De Soto, LA	1,905	1,380	231	231	231	231	231	231
Franklin	1,107	1,335	2,032	1,940	1,894	1,837	1,867	1,925
Freestone	2,408	3,337	3,020	3,039	3,027	3,053	3,084	3,107
Gregg	2,817	2,363	2,191	2,440	2,441	2,537	2,625	2,708
Grimes	383	733	742	777	816	864	869	967
Harrison	3,649	4,492	3,488	3,672	4,023	4,148	4,246	4,314
Henderson	4,135	5,662	5,170	4,922	4,918	4,822	4,807	4,991
Hopkins	2,132	2,978	1,812	2,044	2,042	2,092	2,193	2,246
Houston	1,912	1,781	1,440	1,466	1,468	1,475	1,484	1,488
Leon	2,034	2,988	5,905	5,619	5,197	5,234	5,339	5,540
Limestone	368	1,177	8,477	9,177	9,214	9,284	9,360	9,453
Madison	890	1,111	1,733	1,687	1,648	1,609	1,551	1,500
Marion	922	1,043	777	782	803	834	864	916
Miller, AR	26	8,780	7,185	7,188	7,190	7,190	7,193	7,195
Morris	1,945	7,821	718	721	705	699	682	674
Nacogdoches	8,698	9,624	7,139	6,908	7,133	7,115	7,864	8,382
Natchitoches, LA	1,121	1,018	1,784	1,824	1,884	1,956	2,043	2,148
Navarro	67	115	12	12	12	12	12	12
Panola	3,487	4,638	3,877	3,579	3,261	4,152	4,178	4,148
Rains	387	618	368	389	408	276	293	311
Red River, LA	24	99	932	957	1,011	1,093	1,204	1,345
Robertson	382	265	14,506	14,181	14,027	13,687	13,379	13,080
Rusk	7,238	7,912	8,973	7,925	7,620	7,637	7,598	7,740
Sabine, LA	961	1,141	1,842	1,977	2,122	2,281	2,452	2,635
Sabine, TX	792	1,045	1,025	1,094	1,158	1,272	1,340	1,369
San Augustine	6,609	4,996	557	555	550	557	556	560
Shelby	2,982	3,182	3,429	3,896	3,239	3,252	4,118	4,723
Smith	11,548	12,026	18,184	19,196	20,800	11,774	12,706	11,094
Titus	1,500	1,895	3,193	3,369	3,378	3,489	3,550	3,594
Trinity	1,819	1,816	0	0	0	0	0	0
Upshur	3,580	4,043	3,227	3,424	3,427	3,483	3,152	3,531
Van Zandt	4,556	5,053	4,604	4,868	6,030	5,921	6,261	6,535
Wood	4,101	4,153	5,723	6,104	6,401	6,789	7,114	7,692
Grand Total	131,969	155,381	167,632	165,039	166,182	160,401	165,629	170,210

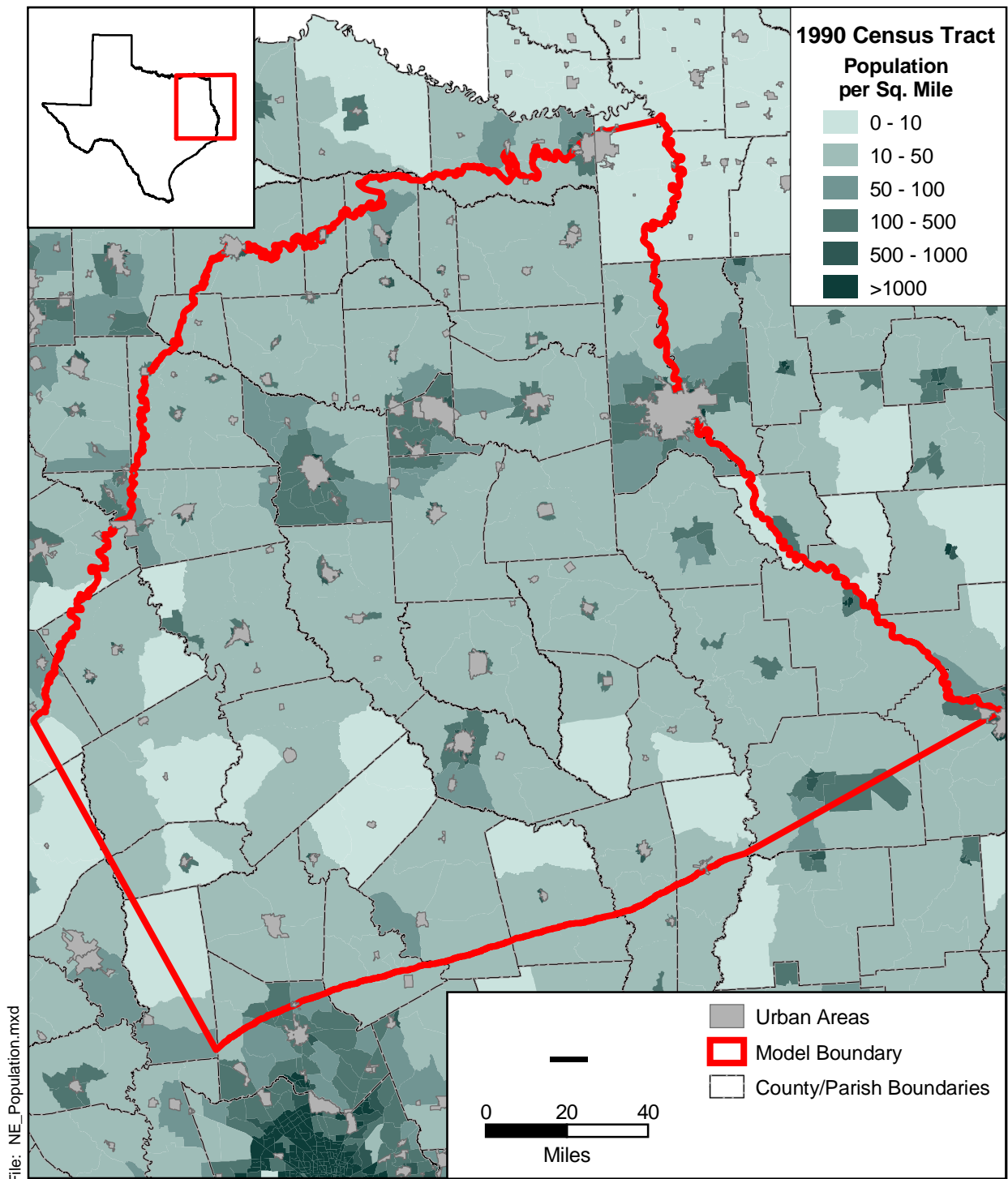


Figure 4.7.1 Population density for the Northern Carrizo-Wilcox GAM study area.

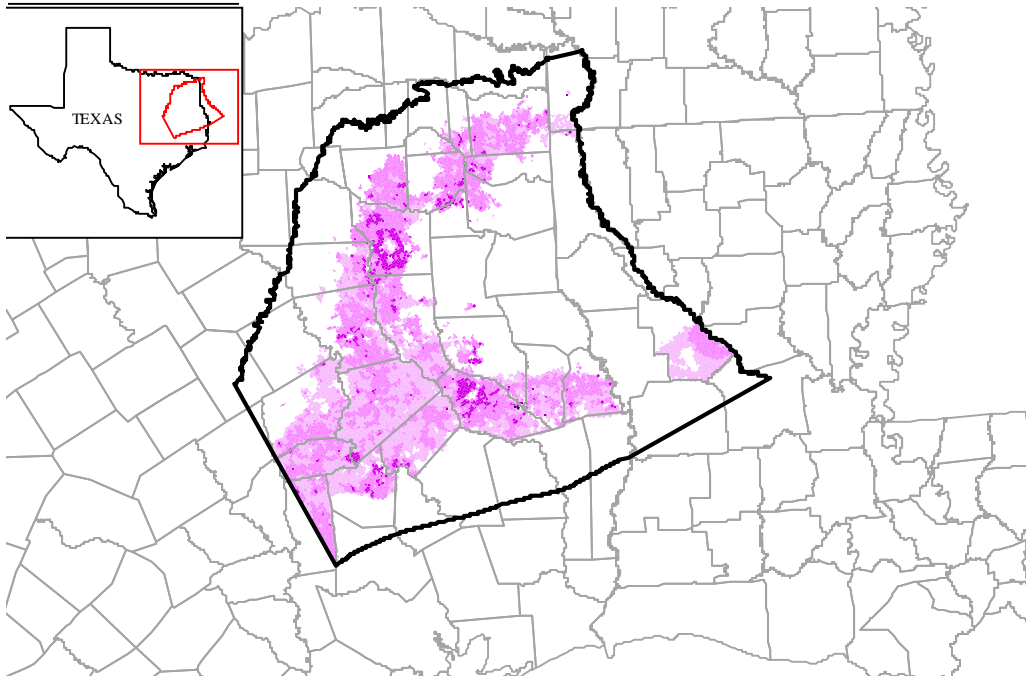


Figure 4.7.2 Younger (Layer 1) pumpage (AFY), 1990.

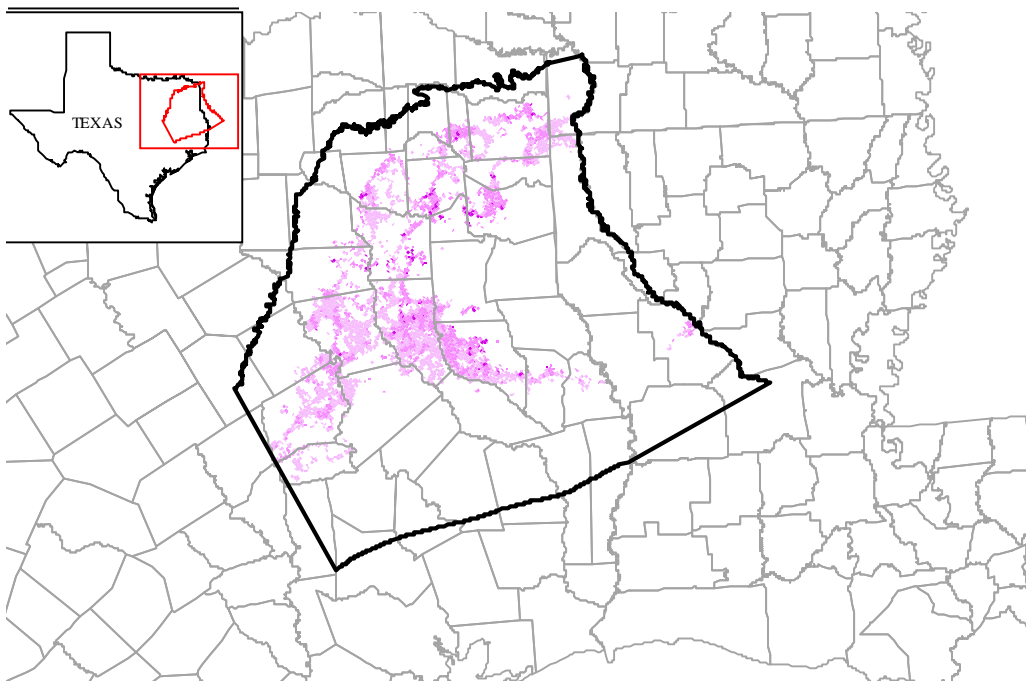


Figure 4.7.3 Reklaw (Layer 2) pumpage (AFY), 1990.

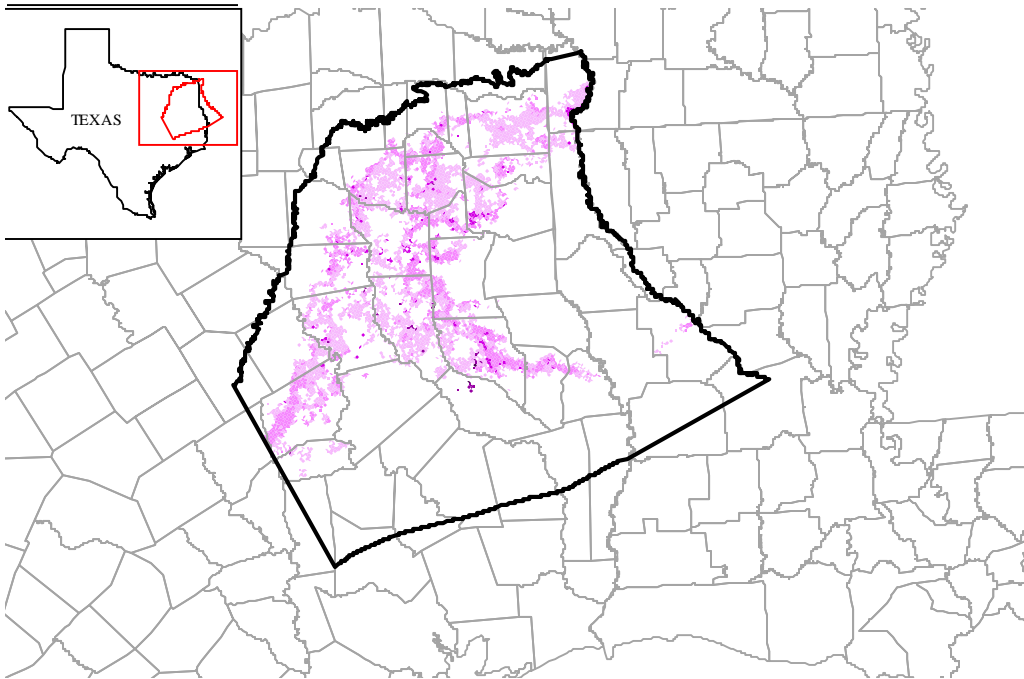


Figure 4.7.4 Carrizo (Layer 3) pumpage (AFY), 1990.

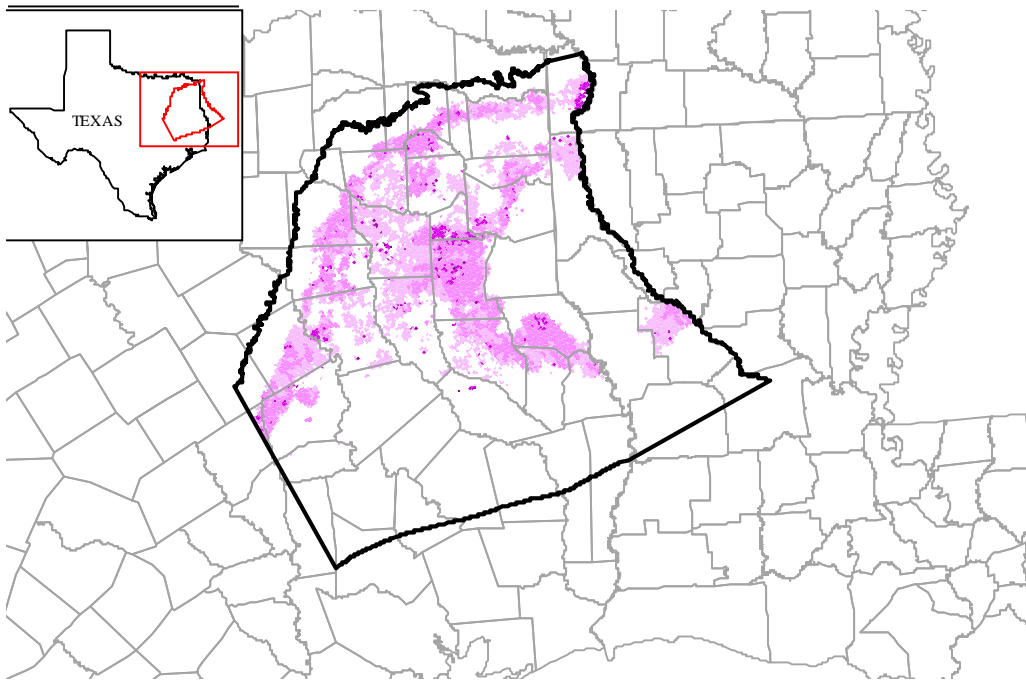


Figure 4.7.5 Upper Wilcox (Layer 4) pumpage (AFY), 1990.

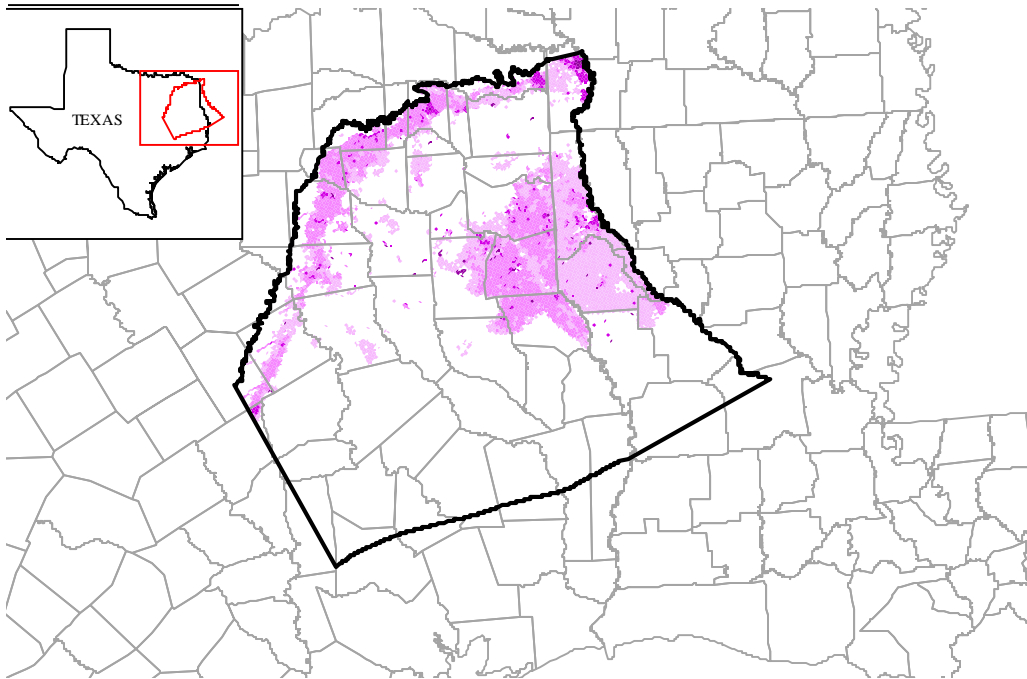


Figure 4.7.6 Middle Wilcox (Layer 5) pumpage (AFY), 1990.

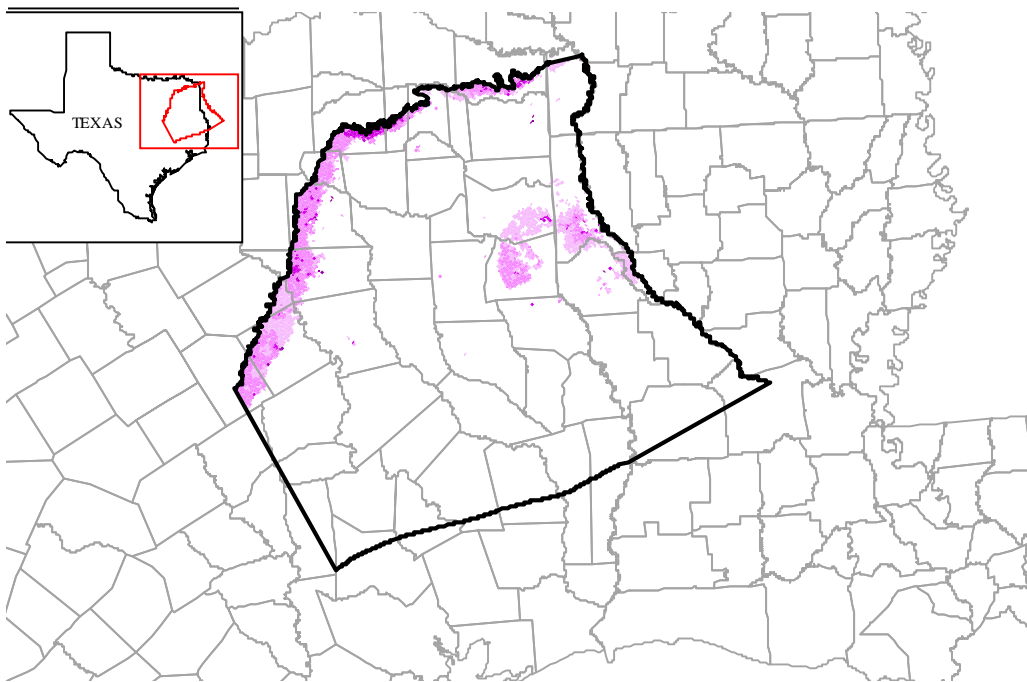


Figure 4.7.7 Lower Wilcox (Layer 6) pumpage (AFY), 1990.

4.8 Water Quality

Water quality data for the northern Carrizo-Wilcox aquifer were examined in terms of drinking water quality, irrigation water quality, and industrial water quality, as described in detail in Appendix F. For the water-quality assessment, available water quality measurements derived from various databases were compared to screening levels for specific constituents (Table F.1 and F.2). Screening levels for drinking water supplies are based on the maximum contaminant levels (MCLs) established in National Primary and Secondary Drinking Water Regulations. Irrigation water quality is evaluated based on the concentrations of specific constituents, such as boron, chloride, and TDS, as well as the salinity hazard, owing to their limited tolerance for crop irrigation. Groundwater suitability for industrial purposes is indicated by the content of dissolved solids, as well as its corrosiveness and tendency to form scale and sediments (Table F.1 and F.2). Table F.1 indicates for each constituent the percent of wells in the Carrizo-Wilcox aquifer exceeding the screening levels, and Table F.2 list the percentage of wells in individual counties exceeding one or more screening levels. The spatial concentration distributions of selected constituents in the northern Carrizo-Wilcox aquifer are shown in Figures F.1 through F.7. Note that these water quality data have been reported to the different state agencies and are typically from operational wells. Wells that were drilled and subsequently abandoned due to insufficient yield or unsuitable water quality are typically not reported and may not be included in the data bases.

5.0 CONCEPTUAL MODEL OF GROUNDWATER FLOW IN THE AQUIFER

The conceptual model for groundwater flow in the Northern Carrizo-Wilcox GAM area is based on the hydrogeologic setting, described in Section 4. The conceptual model is a simplified representation of the hydrogeological features which govern groundwater flow in the aquifer. These include the hydrostratigraphy, hydraulic properties, stresses such as pumping and recharge, and the boundaries. Each of the elements of our conceptual model is described below. The schematic diagram in Figure 5.1 depicts the conceptual hydrogeologic model of groundwater flow in the Carrizo-Wilcox aquifer under predevelopment conditions. With additional pumping as the aquifer is developed, an additional flow component representing discharge from individual layers would be depicted in Figure 5.1.

The conceptual model distinguishes four layers in the Carrizo-Wilcox aquifer, consisting of the lower, middle, and upper Wilcox layers in addition to the Carrizo Sand. These layers tie in with the subdivision of the aquifer in the Central Carrizo-Wilcox GAM. The Carrizo-Wilcox aquifer is overlain by the Reklaw Formation, representing the confining unit in the East Texas Embayment and in the southern part of the study area. The Reklaw Formation separates the major Carrizo-Wilcox aquifer from the shallow, minor Queen City and Sparta aquifers. The Reklaw confining unit and the overlying Queen City aquifer unit are represented as separate layers in the model to account for potential vertical flow across the Reklaw. In the southern part of the study area, where all the layers dip toward the Gulf of Mexico, a wedge of younger sediments overlies the topmost model layer (Queen City aquifer). In this part of the study area, vertical flow between the aquifer and the shallow water table is approximated using general-head boundary conditions.

In addition to identifying the hydrostratigraphic layers of the aquifer, the conceptual model also defines the mechanisms of recharge and discharge, as well as groundwater flow through the aquifer. Recharge occurs mainly in the outcrop areas of the Carrizo-Wilcox layers along the northwestern edge of the East Texas Basin and in the Sabine Uplift area to the east. Similarly, recharge to the shallow Queen City aquifer occurs through infiltration in the outcrop area, which covers the center axis of the East-Texas Embayment (Figure 4.2.1). Additional

recharge to the Carrizo-Wilcox aquifer may occur by cross-formational flow from the Queen City aquifer through the Reklaw confining unit (Figure 5.1). Cross-formational flow between the different layers within the Carrizo-Wilcox aquifer may redistribute groundwater that is recharged in the outcrops into different aquifer layers as a result of variations in hydraulic properties, hydraulic heads, and topography (Figure 5.1).

Most of the precipitation falling on the outcrop runs off into the small creeks, which discharge through major streams out of the model area. In addition to runoff, a significant portion of the precipitation is lost by evapotranspiration (ET), leaving only a small fraction of the precipitation to infiltrate into the subsurface and recharge the aquifer. Diffuse recharge occurs preferentially in topographically higher interstream areas within the outcrops. Focused recharge along streams can occur when the water table in the aquifer is below the stream-level elevation. If stream levels are lower than surrounding groundwater levels, groundwater discharges to the streams resulting in gaining streams. In this case, water levels in the valley are typically close to land surface and some of the shallow groundwater in this area can be lost to evapotranspiration.

Recharge is a complex function of precipitation, soil type, geology, water level and soil moisture, topography, and ET. Precipitation, ET, water-table elevation, and soil moisture vary spatially and temporally, whereas soil type, geology, and topography vary spatially. In addition to natural phenomena, water levels are affected by pumpage and man-made surface-water reservoirs and lakes, which in turn affect recharge. Under undisturbed conditions (e.g., prior to pumping), groundwater recharge is balanced by natural discharge of groundwater. To maintain a state of dynamic equilibrium, groundwater withdrawal by pumping must be balanced by: (1) an increase in recharge, (2) a decrease in natural discharge, (3) a loss of storage, (4) or a combination of these factors. Balancing pumping by increased recharge implies that recharge was rejected prior to the onset of pumpage (Theis, 1940; Domenico and Schwartz, 1990). This occurs primarily in outcrop areas of aquifers where the water table is near land surface.

The onset of pumpage and the concomitant water-level decline induces an increase in recharge, because less water is captured by evapotranspiration as the water table declines below the root zone and vertical gradients in the recharge zone increase. Freeze (1971) showed for an unconfined aquifer that the increase in recharge occurs initially without affecting the natural

discharge even though pumpage continues to increase (Fig. 5.2a). After some time, the recharge stabilizes as the increased pumpage is offset by a decrease in the natural discharge (i.e., gaining streams) leading to induced recharge (i.e., losing streams). With continued increase in pumpage and concomitant decrease in basin discharge, the conditions could become 'unstable', whereby the decrease in natural discharge can no longer feed the increased pumpage (Fig. 5.2b). Water levels decline to a depth below which the maximum recharge rate can no longer be sustained, because of consistently drier conditions in the unsaturated zone and increased evapotranspiration during redistribution (Freeze, 1969). Compared to the hypothetical system described by Freeze (1971), the unconfined-confined system of the Carrizo-Wilcox aquifer will exhibit a more complex response, whereby the water-table response in the outcrop to pumpage in the confined section would be delayed.

Our conceptual model for the northern Carrizo-Wilcox aquifer is considered to represent a stable groundwater basin, as indicated in Figure 5.2a, characterized by a significant rejected recharge potential. This implies that effective recharge during predevelopment conditions is expected to be lower than during current transient conditions subject to pumpage over the last several decades.

Groundwater from the aquifers discharges to local creeks and major streams throughout the area, contributing to the baseflow of the major streams. In addition, discharge from the Carrizo-Wilcox aquifer occurs by cross-formational flow. In the East Texas Basin, the direction of cross-formational flow between the Carrizo and the Queen City depends on topography, and in some areas, pumping stresses. In the southern part of the study area, discharge from the Carrizo-Wilcox occurs through cross-formational flow into the Queen City which, in turn, discharges by vertical flow through the overlying younger formations into stream valleys.

Groundwater flow within the aquifers is controlled by the topography, the structure, and the permeability variation within the different layers. A map showing the inferred groundwater flow pattern in the northern Carrizo-Wilcox aquifer is shown in Figure 4.4.3 (Fogg and Kreitler, 1982). Generally, the Carrizo Sand has the highest average hydraulic conductivity, whereas the Simsboro (middle Wilcox) is considered the main water-producing layer of the Wilcox in the southwestern part of the area, which extends southward into the Central Carrizo-Wilcox GAM.

East of the Trinity River, the Simsboro Sand is no longer identified in geophysical logs as a separate lithologic unit, and the large-scale aquifer transmissivity largely depends on sand thickness and connectivity of individual sand bodies.

The vertical boundary along the southern edge of the model corresponds to the updip limit of the growth faults, displacing mainly Wilcox and deeper strata downward toward the Houston Embayment (Figure 5.1). This boundary is represented by a no-flow boundary in the model, representing the stagnant zone associated with the overall downdip gradient of the Carrizo-Wilcox aquifer system and the general updip gradient of the geopressured zone downdip from the fault zone. As a result, discharge from the confined section of the Carrizo-Wilcox aquifer is through upward leakage or through pumpage.

The heterogeneity and structure of the aquifer, particularly the Wilcox, affect the water quality. Sand bodies connected to recharge areas in the outcrop, and sands within the major fluvial channels typically represent pathways for fresh water from the outcrop into the deeper confined section. Fault zones may limit downdip flow of fresh groundwater, as indicated by higher total dissolved solids (TDS) groundwater south the Mount Enterprise fault system (Fogg and Kreitler, 1982). Isolated sands and sands in contact with thick mud units may also have poor water quality due to leakage of saline water from surrounding mud units. Even though delineating high-TDS groundwater is important for water availability determinations, water quality assessment is not an explicit requirement of the current GAM. However, a preliminary characterization of water quality for the Carrizo-Wilcox aquifer is given in Appendix F.

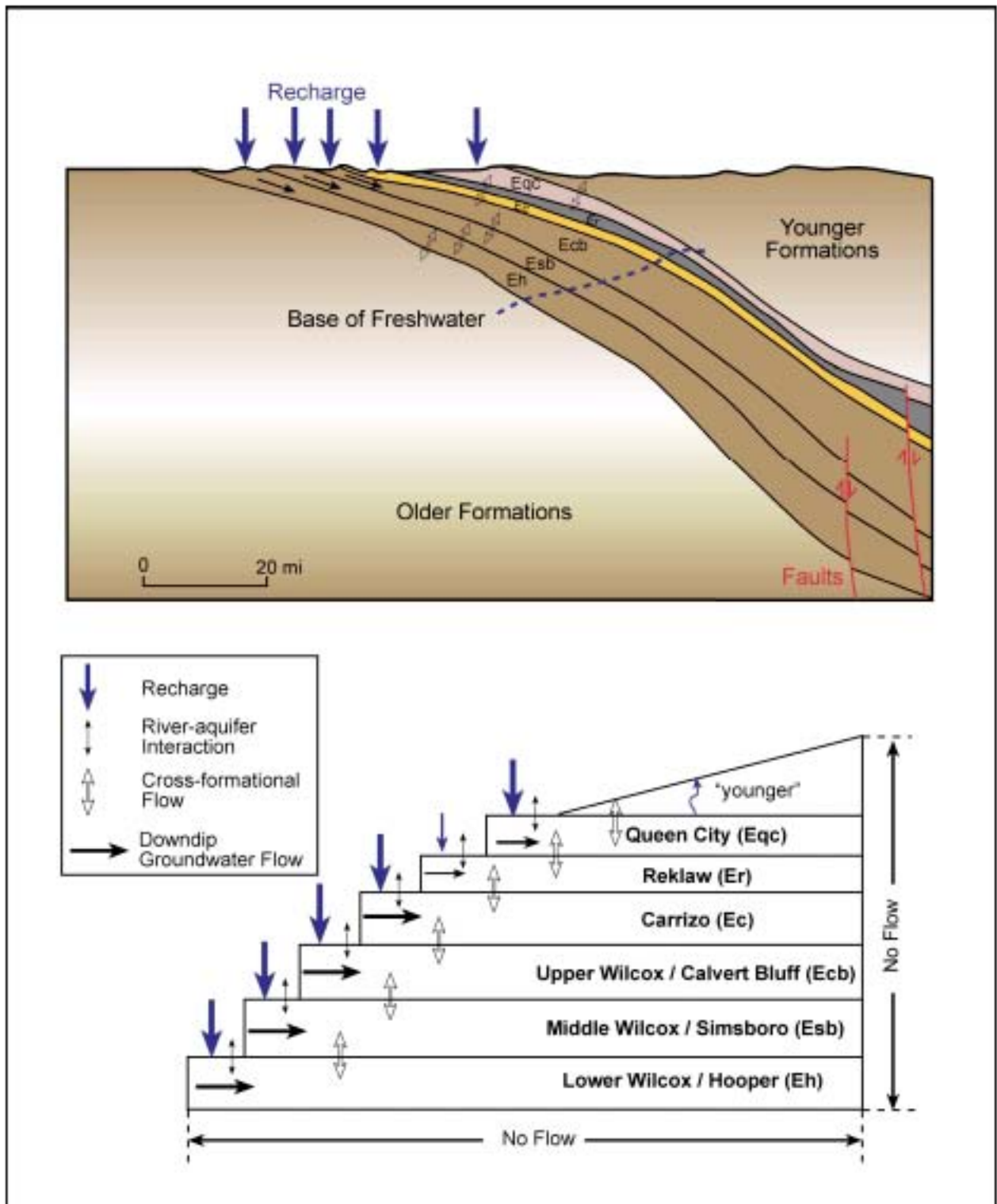


Figure 5.1 Conceptual groundwater flow model for the Northern Carrizo-Wilcox GAM.

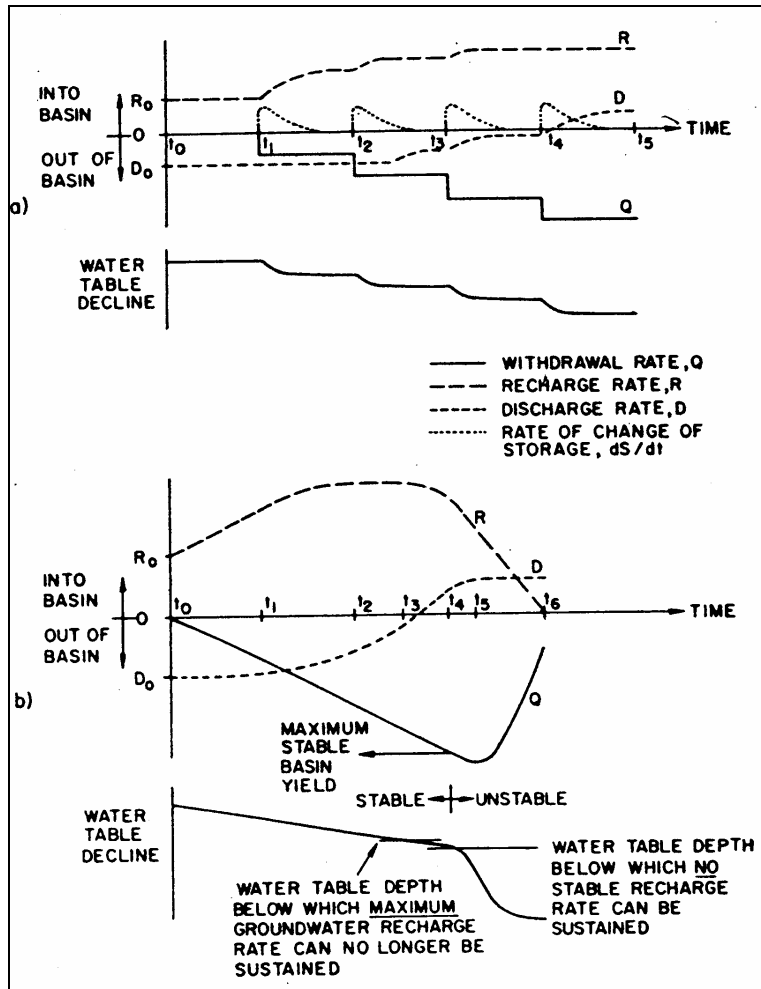


Figure 5.2 Schematic diagram of transient relationships between recharge rates, discharge rates, and withdrawal rates for an unconfined aquifer basin (from Freeze, 1971).

6.0 MODEL DESIGN

Model design represents the process of translating the conceptual model for groundwater flow in the aquifer (Section 5) into a numerical representation which is generally described as the model. The conceptual model for flow defines the required processes and attributes for the code to be used. In addition to selection of the appropriate code, model design includes definition of the model grid and layer structure, the model boundary conditions, and the model hydraulic parameters. Each of these elements of model design and their implementation are described in the remainder of this section.

6.1 Code and Processor

The code selected for the Northern Carrizo-Wilcox GAM and for all GAMs developed by or for the TWDB is MODFLOW-96 (Harbaugh and McDonald, 1996). MODFLOW-96 is a multi-dimensional, finite-difference, block-centered, saturated groundwater flow code which is supported by enhanced boundary condition packages to handle recharge, ET, streams (Prudic, 1988), and reservoirs (Fenske et al., 1996).

The benefits of using MODFLOW for the Northern Carrizo-Wilcox GAM include: (1) MODFLOW incorporates the necessary physics represented in the conceptual model for flow described in Section 5 of this report, (2) MODFLOW is the most widely accepted groundwater flow code in use today, (3) MODFLOW was written and is supported by the USGS and is public domain, (4) MODFLOW is well documented (McDonald and Harbaugh, 1988; Harbaugh and McDonald, 1996), (5) MODFLOW has a large user group, and (6) there are a plethora of graphical user interface programs written for use with MODFLOW.

To the extent possible, we have developed the MODFLOW data sets to be compatible with Processing MODFLOW for Windows (PMWIN) Version 5.3 (Chiang and Kinzelbach, 1998). The size of the GAM and the complexity of our application precludes 100-percent compatibility with PMWIN, as well as many other interfaces.

We have executed the model on x86 compatible (i.e., Pentium or Athlon) computers equipped with the Windows 2000 operating system. MODFLOW is not typically a memory-

intensive application in its executable form. However, if any preprocessor (such as PMWIN) is used for this size and complexity of model, at least 256MB of RAM is recommended.

6.2 Model Layers and Grid

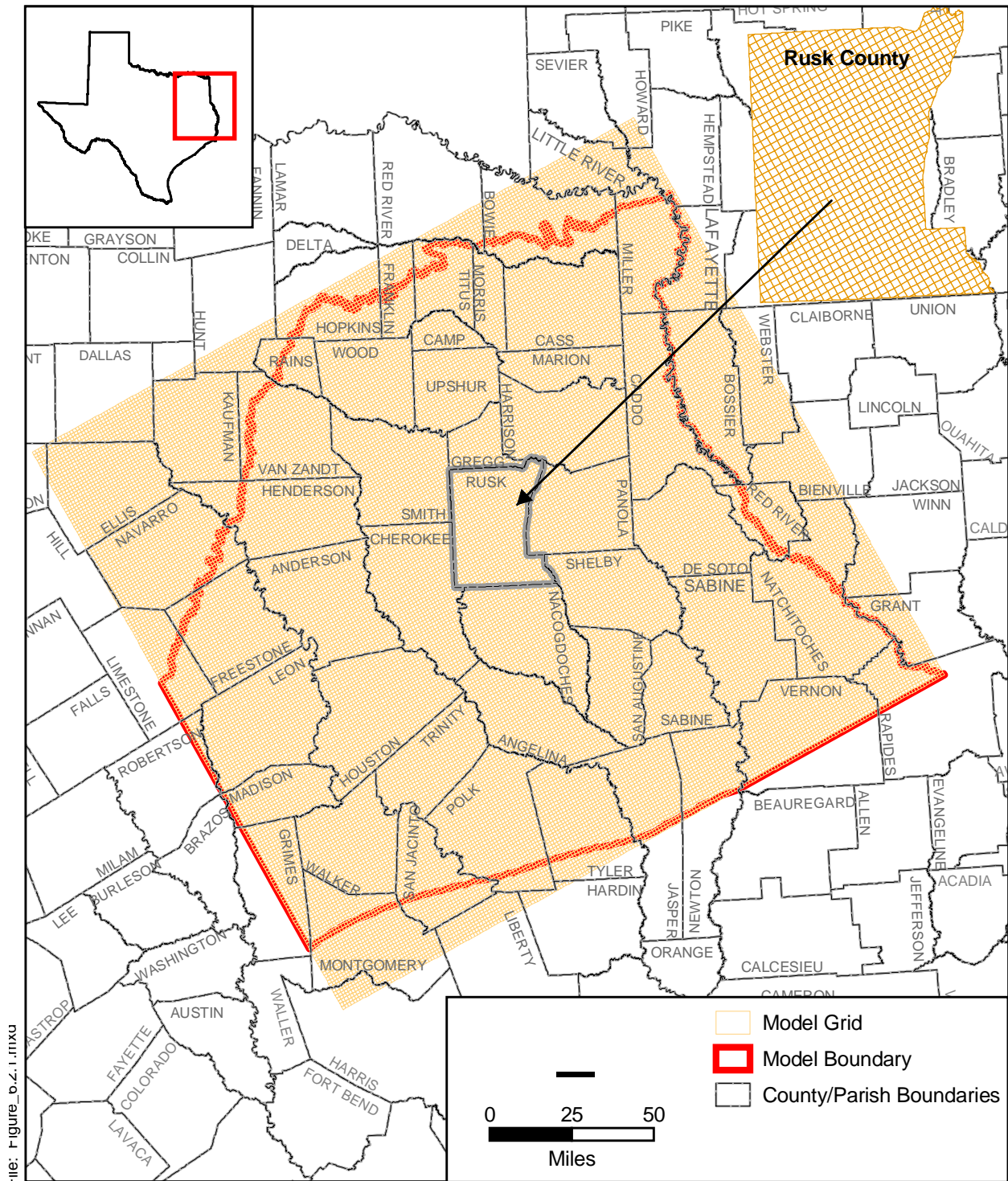
Consistent with the model hydrostratigraphy described in Section 4.1 and the conceptual flow model detailed in Section 5, we have divided the Northern Carrizo-Wilcox GAM into six model layers. MODFLOW-96 numbers layers from top to bottom and this is the order by which each layer will be introduced. Layer 1 is the Queen City Formation which outcrops over a large area of the East Texas Basin (see Figure 2.13). Layer 2 is the Reklaw Formation. Layer 3 is the Carrizo Formation. Layer 4 is the upper Wilcox. Layer 5 is the middle Wilcox and Layer 6 is the lower Wilcox. The lower Wilcox is not present in the northeastern portion of the model area. Where the lower Wilcox is not present, Layer 6 cells are flagged as inactive. The model layers are shown with the corresponding hydrostratigraphic units in Figure 4.1.1.

The Northern Carrizo-Wilcox GAM boundaries are defined on the basis of surface or groundwater hydrologic boundaries. The model area for the Northern Carrizo-Wilcox GAM is bounded laterally by the Red River to the east in Louisiana and Arkansas, and the drainage divide between the Trinity and Brazos rivers to the west. The Trinity-Brazos basin divide serves as the model boundary in the outcrop (presumed groundwater flow divide) and is extended in the subsurface to the downdip boundary of the model. The northern boundary of the model is defined by the updip edge of the Wilcox Group outcrop and the southern boundary by the updip limit of the Wilcox growth fault zone (Bebout et al., 1982). The upper boundary is defined by the ground surface in the outcrop of the Carrizo-Wilcox aquifer extending south to the extent of the Queen City outcrop. South of the Queen City outcrop, the contact between the Queen City and the overlying Weches Formation defines the upper boundary.

MODFLOW-96 requires a rectilinear grid and also requires an equal number of rows for all columns. As a result, the model area is constrained to being a rectangular grid. Typically, one axis of the model grid is aligned parallel to the primary direction of flow (this is to the southeast in the western part of the Northern Carrizo-Wilcox GAM and to the southwest in the Sabine Uplift area). The model area was determined by imposing the preceding constraints with

the additional constraint of minimizing the number of model grid cells. The model grid origin is located at GAM Coordinates 19,257,000 ft north and 6,295,000 ft east, with the x-axis rotated positive 29.11°. The GAM standard requires that grid cells be square of a uniform dimension of 1 mile (area of 1 square mile). The model has 210 columns and 195 rows for a total of 40,950 grid cells per layer. As discussed below, not all of these grid cells are active in the model. Figure 6.2.1 shows the entire model grid. Included on this figure is an inset with an enlargement of Rusk County to show the model grid at the county scale.

We defined the active area of each model layer by intersecting the layer grid with the geologic map and the growth fault boundaries to the south. Cells extending past the outcrop or downdip of the growth fault boundary were defined as inactive in the IBOUND array. If a cell was 50% or more in the outcrop, it was defined as active. Cells east of the Red River on the eastern boundary of the model were also made inactive on the assumption that the Red River is a regional sink for the aquifer being modeled. After clipping the layers to their proper dimensions, Layers 1 through 6 had the following number of grid cells respectively, 18799, 20523, 21463, 24844, 30001, and 22312. The total number of active grid cells in the model grid is 137942.



File: Figure_6.2.1.mxd

Figure 6.2.1 Model grid of the Northern Carrizo-Wilcox GAM.

6.3 Boundary Condition Implementation

A boundary condition can be defined as a constraint put on the active model grid to characterize the interaction between the active simulation grid domain and the surrounding environment. There are generally three types of boundary conditions; specified head (First Type or Dirichlet), specified flow (Second Type or Neumann), and head-dependent flow (Third Type or Cauchy). The no-flow boundary condition is a special case of the specified flow boundary condition.

Boundaries can be defined as being time independent or time dependent. An example of a time dependent boundary might be a pumping flow boundary or a reservoir stage elevation. Because many boundaries require time dependent (transient) specification, the stress periods used by MODFLOW must be specified. A stress period in MODFLOW defines the time period over which boundary and model stresses remain constant. Each stress period may have a number of computational time steps which are some fraction of the stress period. For this model, the stress periods have been set at one month. Therefore, all transient boundaries in the model cannot change over a period of less than one month.

Boundaries requiring specification include: layer lateral and vertical boundaries, surface water boundaries, recharge boundaries, and discharge boundaries caused by pumping. Lateral and vertical boundaries will be a combination of specified flow (no-flow, Second Type) or head-dependent flow boundaries (general-head boundaries, Third Type). Surface water boundaries are head-dependent flow boundaries (Third Type). Recharge is a specified flow boundary (Second Type). Evapotranspiration (ET) is a head-dependent flow boundary (Third Type). Pumping discharge is a specified flow boundary (Second Type).

Figures 6.3.1 through 6.3.6 show the active and inactive grid cells along with the model boundary conditions for each of the six model layers, respectively. Implementation of the boundary conditions for the Northern Carrizo-Wilcox GAM is described below.

6.3.1 Lateral Model Boundaries

The lateral model boundaries have been defined to occur on the northeast at the Red River and to the southwest along the drainage divide between the Brazos and Trinity rivers. Both of these boundaries are assumed to be no-flow boundaries (Second Type). From a review of the predevelopment hydraulic head map, we concluded that the southwestern boundary is coincident with the groundwater flow direction and reasonably mimics a no-flow boundary. A no-flow boundary was also assumed for the northeastern model boundary assuming that there is insignificant underflow of the Red River in the model area.

The applicability of no-flow boundaries was investigated further for the simulated historical period (1980 through 1999). A no-flow boundary was maintained at the Red River during the transient and predictive model periods (1980-2050). For the southwestern model boundary, water levels were reviewed for the period from 1980 through 1999. Water levels were found to be reasonably constant given the scale of the model with head decrease observed from a few feet to up to 30 feet. Because specification of boundary heads across the model boundary is inherently uncertain, and because head decreases along the boundary are within the model head error, the southwestern boundary was maintained as a no-flow boundary throughout the transient historical simulation period. If pumping is at least balanced on both sides of the no-flow boundary, the assumed boundary is conservative. The representativeness of this boundary could not be meaningfully investigated for the predictive simulation period (2000-2050).

6.3.2 Vertical Boundaries

The model has a no-flow boundary on the bottom of Layer 6 (the lower Wilcox) representing the marine shales of the Midway Formation. The upper model boundary is the free-water surface calculated in the outcrops of Layers 1 through 6. In the downdip portions of the model where younger sediments overlie the Queen City, these sediments are represented by a general-head boundary condition (Third Type). The initial vertical conductances of the general-head boundaries were calculated based on a harmonic average of the hydraulic conductivities of the overlying units, which were taken from Williamson et al. (1990). Their hydraulic conductivity data were used because they were determined through calibration of a regional model. The hydraulic heads associated with the upper general-head boundary condition were set

equal to the water table that was estimated using the regression equations of Williams and Williamson (1989).

6.3.3 Surface Water Implementation

Surface water acts as a head-dependent flow (Third Type) boundary condition for the top boundary of the active model grid cells (outcrop). The stream package (Prudic, 1988) and reservoir package (Fenske et al., 1996) are head-dependent flow boundary conditions that offer a first-order approximation of surface water/groundwater interaction. The stream-routing package allows for stream-related recharge to be rejected during gaining conditions and for stream-related recharge to be induced during losing conditions. When pumping affects water levels near stream/aquifer connections, recharge will be included through stream loss.

The stream-routing package requires designation of segments and reaches. A reach is the smallest division of the stream network and is comprised of an individual grid cell. A segment is a collection of reaches which are contiguous and do not have contributing or diverting tributaries. In MODFLOW, physical properties must be defined describing the hydraulic connection (conductance) between the stream and the aquifer. Stream flow rates are defined at the beginning of each segment for each stress period.

INTERA developed a GIS-based method for developing the reach and segment data coverages for MODFLOW. Figures 6.3.1 through 6.3.6 show the model grid cells which contain stream reaches in the model domain. Required physical properties of the reaches including stream width, bed thickness, and roughness are taken from the EPA River Reach data set (<http://www.epa.gov/region02/gis/atlas/rf1.htm>). The hydraulic conductivity used to define the hydraulic conductance between the aquifer and the stream was set at the hydraulic conductivity of the underlying formation. Hibbs and Sharp (1991) studied the hydraulic connection between the Colorado River and the alluvium and Carrizo-Wilcox aquifer near a Bastrop well field. They concluded that the connection between the river and the aquifer was very good and did not see hydraulic evidence for a low permeability river bed. Our initial approach was to keep the hydraulic conductivity of the stream bed high and relatively constant and allow the stream width taken from the EPA River Reach data set (RF1) to control the streambed conductance.

The stream-routing package also requires specification of stream flow rate for each starting reach at each stress period. For predevelopment conditions, and for the historical period, no representative stream gage data exist for the majority of the stream segments. To handle this for the pre-development simulation, we used mean flow rates from the EPA RF1 data set to specify the flow rate entering each model segment. The EPA RF1 data set contains mean flow rates estimated along the entire stream and coinciding with all of the modeled stream segments.

For the transient simulations, stream flows are based on historical records. However, because the stream gage coverage is sparse, stream flow rates required estimation at the majority of stream segments. The approach we employed to develop ungaged stream segment flow rates has the following assumptions: (1) gages in close proximity behave similarly, (2) the RF1 average stream segment stream flow estimates are accurate, (3) a gage's distribution of monthly stream flow is lognormal, and (4) the standard deviation of the log of monthly flow rate at an ungaged location is equal to the standard deviation of the log of monthly flow rate at a nearby ungaged location. We have checked assumptions 1 through 3 and have found they generally do hold for the model region. Assumption 4 cannot be definitively established in the current domain, due to lack of data for cross validation.

To calculate the ungaged stream segment flow rates at each monthly stress period, we first constructed the monthly distribution of log flow rate at our gaged stream locations and calculated the standard deviation of that distribution. From the EPA RF1 data set we have the mean flow rates for all segments. If for stress period one the gaged monthly stream flow was equal to the 75th percentile of the distribution, we would use the mean flow rate from the EPA RF1 data set with the standard deviation taken from the actual gaged flow distribution to estimate the 75th percentile flow rate at the ungaged segment. This technique maintains the proper magnitude of flows at ungaged locations as constrained by the EPA RF1 mean flow estimates while superposing the flow variability based upon the nearest gaged data.

The MODFLOW reservoir package (Fenske et al., 1996) has been used to model reservoirs and lakes. The properties required for specification for reservoirs includes the hydraulic conductance between the lake and the aquifer and the reservoir stage as a function of stress period. Because reservoirs are in river valleys, the reservoir package must be integrated

with the stream-routing package. This is done by starting a new segment at the downstream side of each reservoir. Similar to the streams, the hydraulic conductivity used to estimate the reservoir/aquifer hydraulic conductance was initially set equal to the hydraulic conductivity of the underlying material. INTERA developed lake stage records by reviewing records in the literature and by contacting various river authorities in the study area. These stage histories are provided in the data model delivered with this modeling report. Forty reservoirs were modeled in the Northern Carrizo-Wilcox GAM (see Figure 4.5.1).

Spring discharge records were reviewed for application in the Northern Carrizo-Wilcox GAM as drain boundary conditions (Type 3). However, as discussed in Section 4 of this report, there are no significant springs still flowing in the model area that are not being handled by stream reach cells, which provide a sufficiently similar boundary condition.

6.3.4 Implementation of Recharge

Because an evaluation of groundwater availability is largely dependent upon recharge (Freeze, 1971), it is an important model input parameter warranting careful examination and meaningful implementation. In typical model applications, recharge is either homogeneously defined as a percentage of the yearly average precipitation or calibrated as an unknown parameter. Unfortunately, recharge and hydraulic conductivity can be correlated parameters preventing independent estimation when using only head data constraints. Another compounding problem is that recharge is a complex function of precipitation rate and volume, soil type, water level and soil moisture, topography, and ET (Freeze, 1969). Precipitation, ET, water-table elevation, and soil moisture are areally and temporally variable. Soil type, geology, and topography are spatially variable. For the GAM, recharge requires specification for steady-state conditions, for transient conditions from 1980 until 2000, for the transient drought of record, and for average conditions. Reliable tools for specification of recharge at the watershed scale, or the regional model scale (1000s of square miles for the GAMs) do not currently exist.

As a tractable approach to dealing with recharge at the scale of this model, we have used SWAT (Soil Water Assessment Tool) to estimate diffuse recharge rates. SWAT was developed for the USDA Agricultural Research Service by the Blacklands Research Center in Temple, Texas. SWAT is a public-domain model. The SWAT Website where downloads and code-

specific documentation can be found is <http://www.brc.tamus.edu/swat/>. SWAT provides a GIS-driven, watershed scale tool to estimate regional soil water balances, incorporating soils data (USDA/NRCS STATSGO) with the USGS Multi-Resolution Land Characteristics (MRLC) data. SWAT uses standard techniques to track water after it reaches the ground as precipitation. SWAT uses the SCS Curve Number Method (accounting for antecedent moisture conditions) to partition precipitation into runoff and infiltration. Infiltrating water either increases the soil moisture, is lost through ET, or continues down to the water table. We used the Hargreaves Method for estimating Potential ET because it only requires estimates of monthly mean minimum and maximum temperatures which are available for the study area. Average daily net radiation is available within SWAT for month and degrees of latitude. The Hargreaves method is considered accurate for simulation periods that are equal to, or larger than, one month. This is consistent with one month stress periods and the assumptions underlying the NRCS curve-number method for estimating runoff. The potential ET is converted to an actual ET based on the vegetation size and type (determines maximum ET) and soil water availability (determines actual ET).

SWAT is used in an uncoupled mode to estimate several model inputs for MODFLOW. Consistent with the transient MODFLOW stress periods of one month, SWAT is also simulated with one month stress periods using daily data (time steps). SWAT was simulated for the time period from 1975 through 1999 to coincide with the calibration and transient model simulation periods.

For each MODFLOW stress period, SWAT calculates: (1) the recharge rate for the recharge package, (2) the ET max for the ET package, and (3) the extinction depth for the ET package. The SWAT estimate of shallow recharge is used as a recharge flux in MODFLOW. SWAT accounts for ET which may occur in the vadose zone. However, in our method of application, SWAT does not account for groundwater transpiration. To account for groundwater ET, the “surplus” ET from SWAT (ET potential – ET actual) was applied as ET max in the ET package in MODFLOW. For each month simulated, SWAT calculates a rooting depth representative of the season, vegetative cover, and soil type. This rooting depth is passed through to MODFLOW as the extinction depth required by the MODFLOW ET Package. As a result, ET from groundwater will occur when the water table (as simulated by MODFLOW) is

above the extinction depth and there is surplus ET potential for that particular stress period. Appendix E provides a more detailed explanation of our use of SWAT in an uncoupled mode with MODFLOW.

For the predevelopment model, the SWAT estimates for recharge were averaged values taken from the 1975 to 1999 simulation. The ET max estimates were also averaged for this same time period for input into the MODFLOW ET package. The maximum extinction depth for each cell was used for input into the MODFLOW ET package. In the transient simulation, recharge varies as a function of time with a monthly stress period.

SWAT was also used for implementing recharge in the predictive simulation period (2000-2050). Average recharge conditions (1975-1999) were used for each predictive simulation period. Recharge was varied seasonally in the predictive simulations based upon monthly average recharge (1975 - 1999). Predictive simulations end with a drought-of-record. Recharge conditions for the drought-of-record were developed running SWAT through the drought-of-record climatic conditions. A discussion of the drought-of-record is given in the predictive simulation Section 10.

6.3.5 Implementation of Pumping Discharge

Pumping discharge is not considered in the predevelopment model because the model is meant to be representative of times prior to significant resource use. However, pumping discharge is the primary stress on the model during the historical (1980 - 1999) and the predictive (2000-2050) model periods. Pumping discharge is a cell dependent specified flow boundary.

The procedural techniques that we used in estimating and allocating pumping are provided as Appendices B and C. For details on how the historical or predictive pumping was derived, the reader is referred to those appendices. Once the pumping had been estimated for each of the seven user groups (municipal, manufacturing, power generation, mining, livestock, irrigation, and county-other), it was summed across all user groups for a given model cell (row, column) and a given model layer. This process was repeated for all active model cells in the model domain for each transient stress period. As discussed above, the stress period used in the transient simulations is one month. Therefore, the MODFLOW well-package data set has a

specified flow boundary condition for each month of simulation, for each active grid cell within which pumping is occurring.

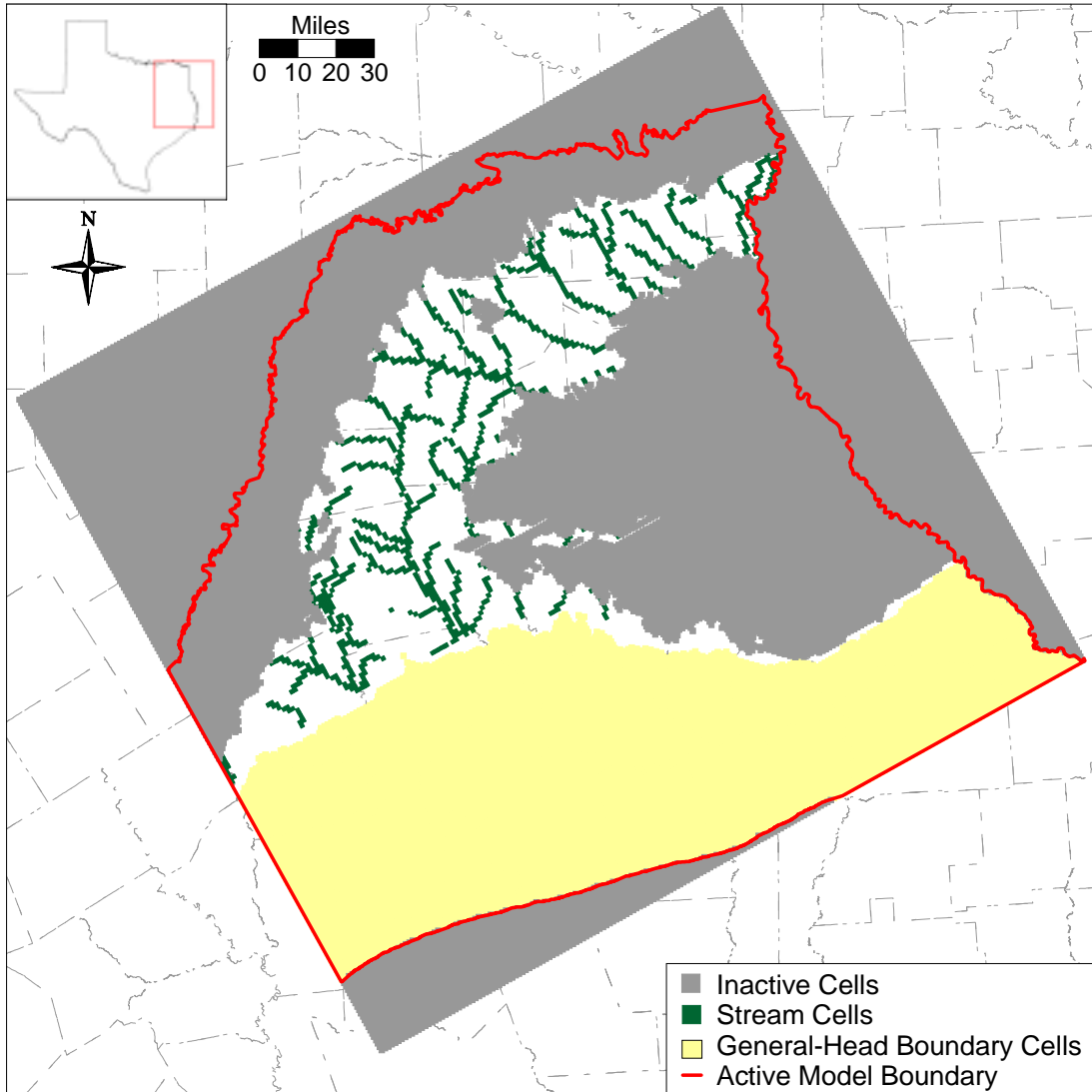


Figure 6.3.1 Layer 1 (Queen City) boundary conditions and active/inactive cells.

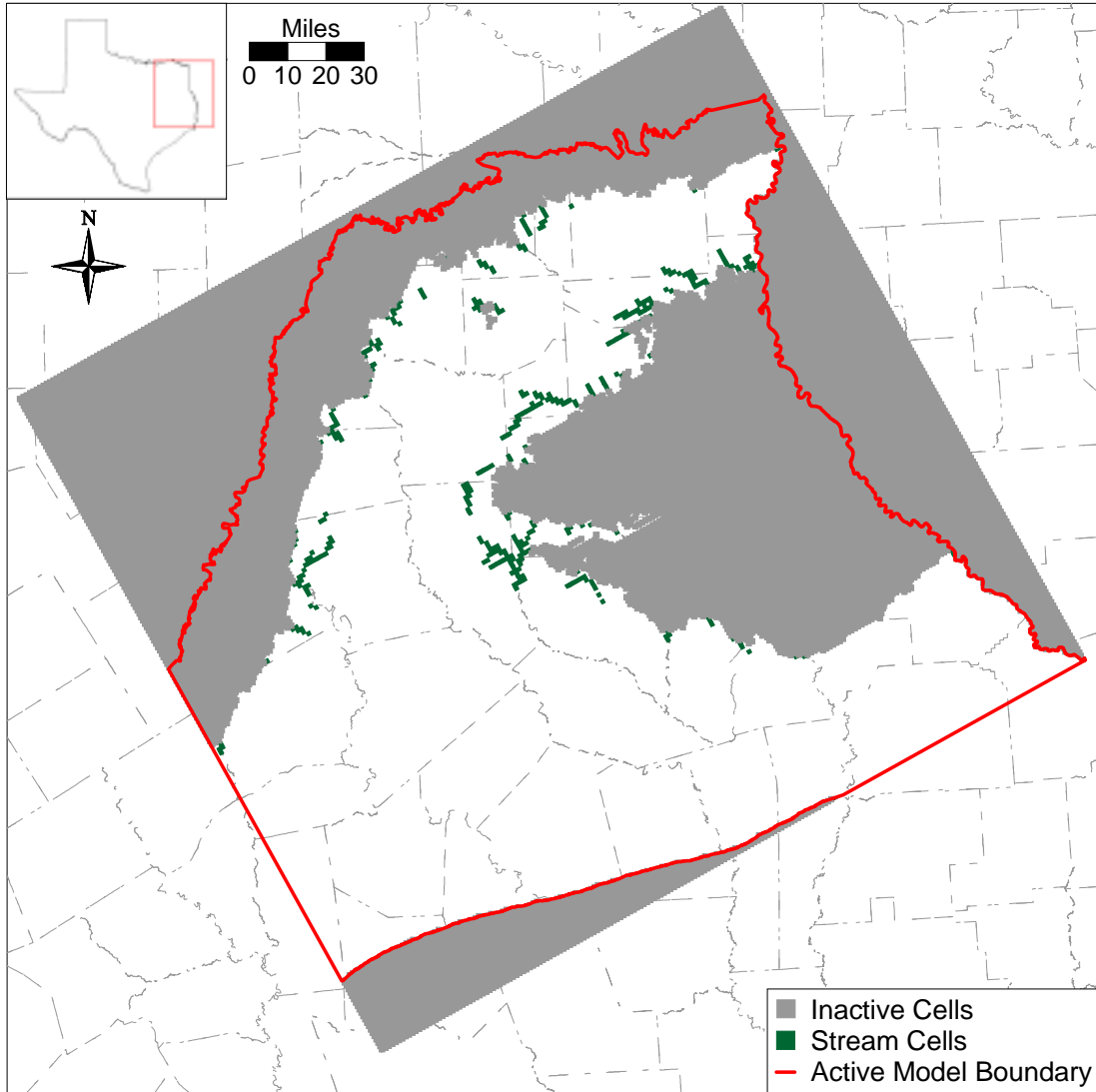


Figure 6.3.2 Layer 2 (Reklaw) boundary conditions and active/inactive cells.

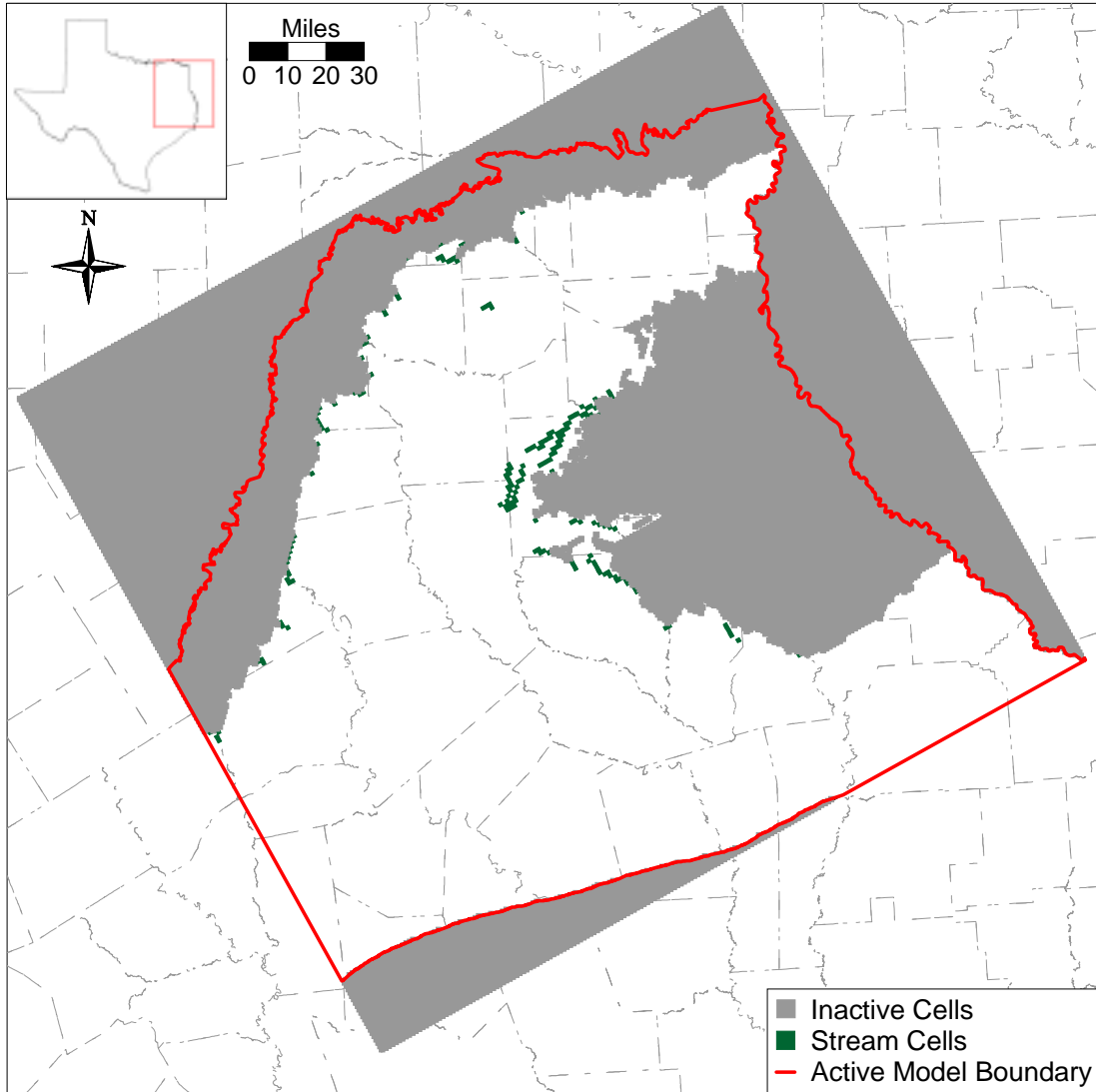


Figure 6.3.3 Layer 3 (Carrizo) boundary conditions and active/inactive cells.

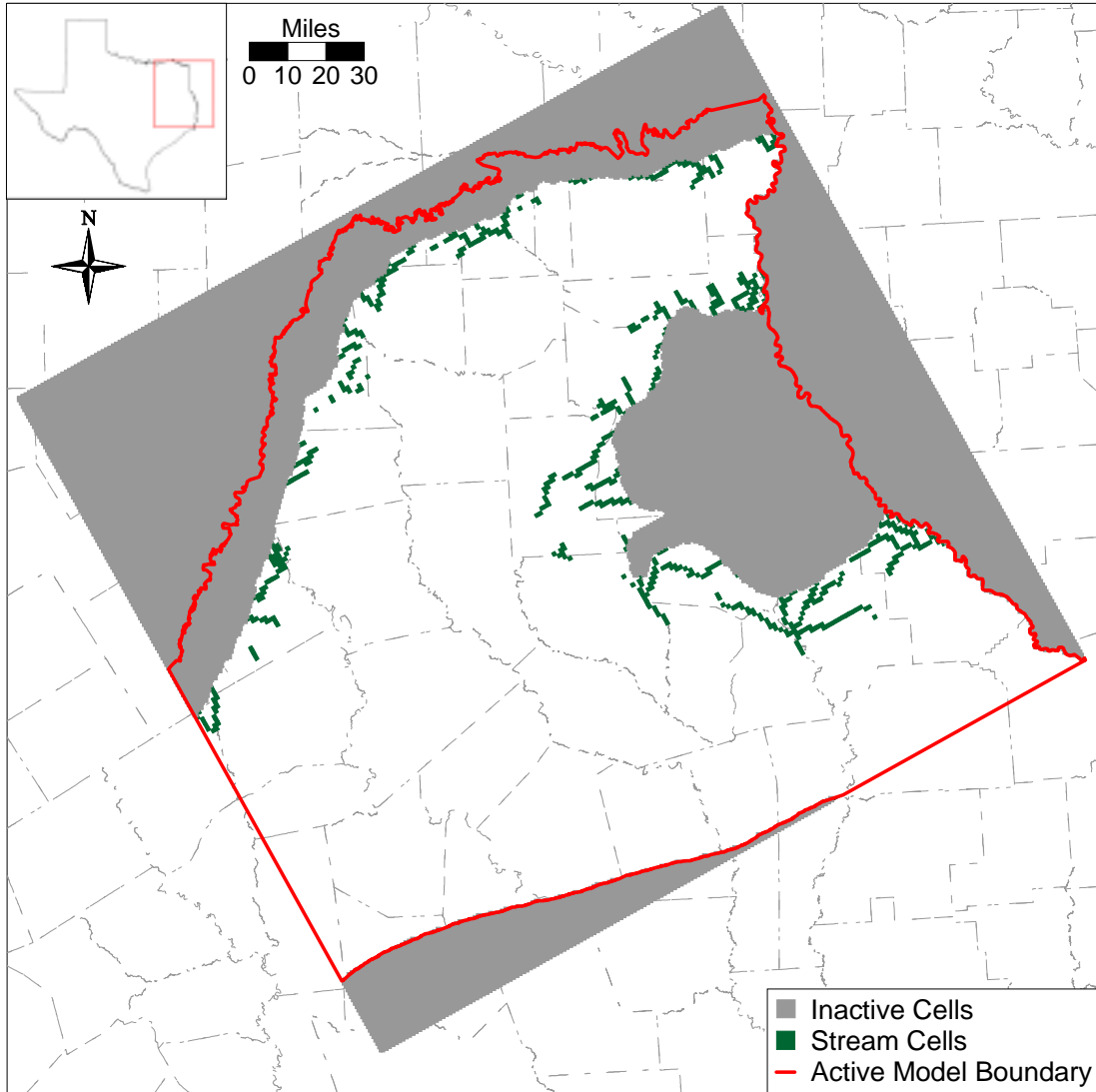


Figure 6.3.4 Layer 4 (upper Wilcox) boundary conditions and active/inactive cells.

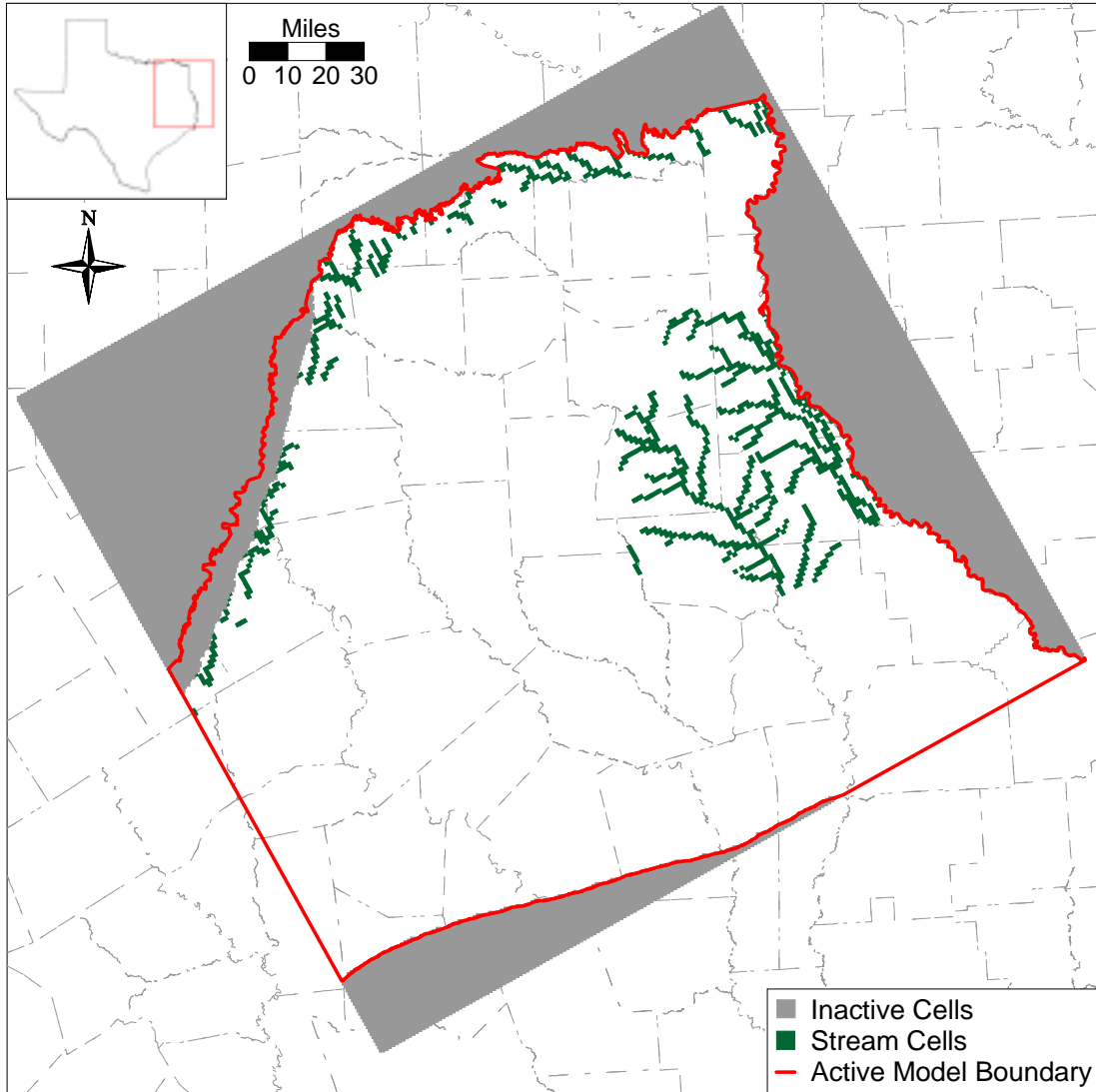


Figure 6.3.5 Layer 5 (middle Wilcox) boundary conditions and active/inactive cells.

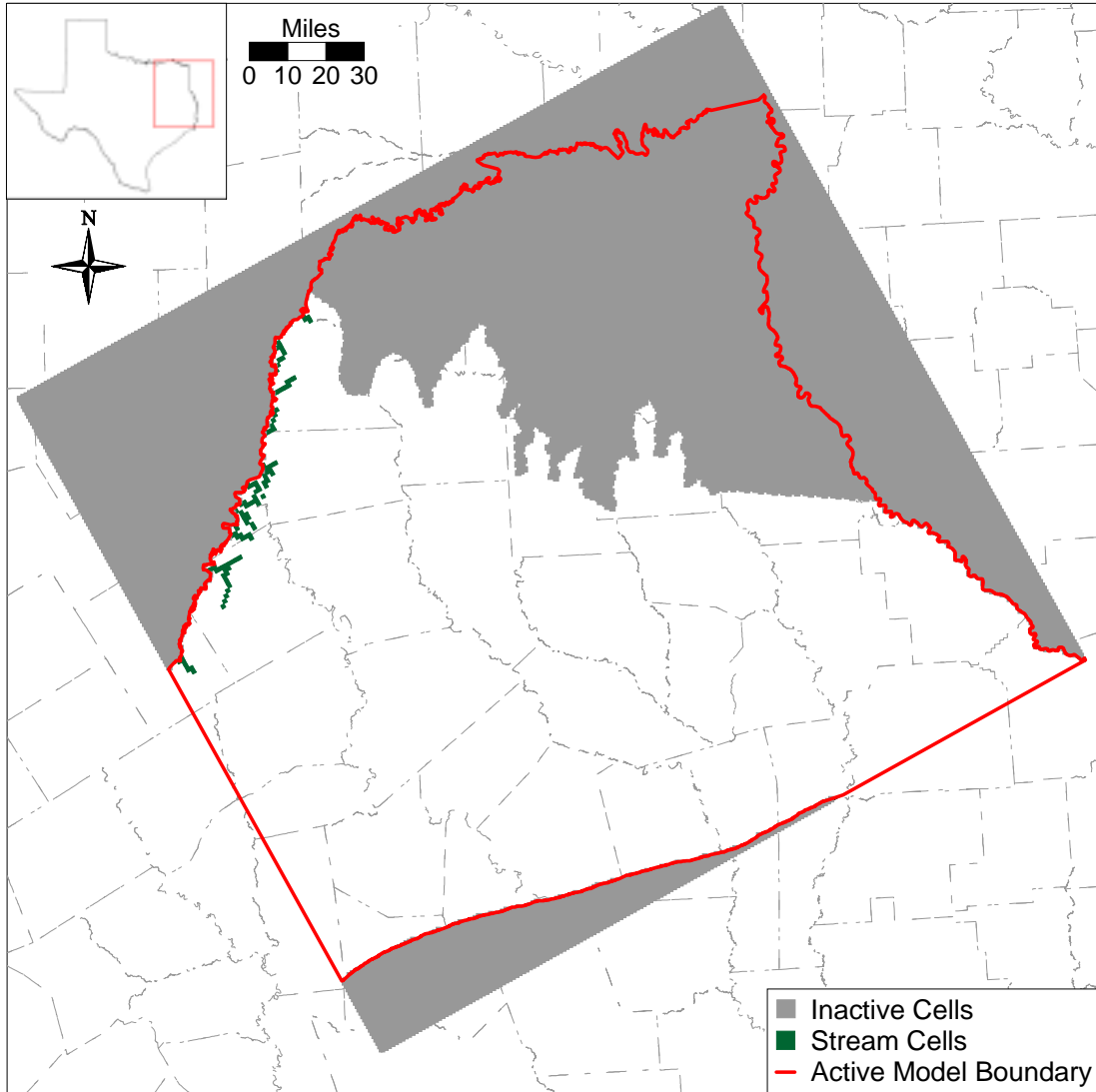


Figure 6.3.6 Layer 6 (lower Wilcox) boundary conditions and active/inactive cells.

6.4 Model Hydraulic Parameters

For the steady-state model, the primary parameter to be estimated and distributed across the model grid is hydraulic conductivity. For the transient model, we must add the storage coefficient. The method used for distributing hydraulic conductivity and storage in the model domain is described in the following.

6.4.1 Hydraulic Conductivity

In the GAM, model properties are constant within a given grid block which is one square mile in area and varies in thickness from a minimum of 20 feet to hundreds of feet. The challenge in constructing a regional model at this scale is in the development of an accurate “effective” hydraulic conductivity that is representative of the grid block scale accounting for the different lithologies present in each grid cell. The effective hydraulic conductivity depends on the geometry, individual hydraulic conductivity, and the correlation scale relative to the grid scale and simulation scale of the various lithologies present in the grid cell (Freeze, 1975).

There have been many investigations on estimating an average effective hydraulic conductivity given assumptions for flow dimension, layer geometry, and correlation scales (Warren and Price, 1961; Gutjahr et al., 1978; Fogg, 1989). For one-dimensional flow in lithologies combined in parallel (i.e., layered), the appropriate effective hydraulic conductivity would be the weighted arithmetic mean. For one-dimensional flow in lithologies combined in series, the effective hydraulic conductivity is the harmonic mean. Hydraulic conductivity has been found to be a log-normally distributed parameter. In two-dimensional uniform flow, assuming that the hydraulic conductivity is log-normally distributed and randomly juxtaposed, the effective hydraulic conductivity is exactly the geometric mean (deMarsily, 1986). Fogg (1989) has studied effective hydraulic conductivity for a model of the Carrizo-Wilcox aquifer in Freestone and Anderson counties in East Texas. His study concluded that for the case when the individual lithologic layers vary in dimension from smaller and larger than the model grid scale, the effective hydraulic conductivity in the horizontal dimension is between the geometric mean and the arithmetic mean. In the vertical dimension, he found that the effective hydraulic conductivity should vary from the geometric to the harmonic mean.

In Section 4.3, we discussed the distribution of hydraulic conductivities available for the Carrizo-Wilcox aquifer in Mace et al. (2000a). Hydraulic parameterization of coastal plain sediments is often correlated to sand body thickness, geometry, and depositional facies (e.g., Payne, 1975; Henry et al., 1980; Fogg, 1986; Thorkildsen and Price, 1991). From the analysis provided in Section 4.3 of this report, hydraulic conductivity has been distributed within the model regions where data were available. Likewise, sand thickness and sand fraction (%) distributions for the modeled aquifers were developed where data were available. However, as discussed earlier in Section 4.3, a clear correlation between sand thickness (sand fraction) and hydraulic conductivity could not be established. Similarly, variograms in different directions showed little difference, indicating a lack of horizontal anisotropy in hydraulic conductivity. Only the sand-thickness trends of the major fluvial channels (Figure 4.3.10) provide some degree of horizontal anisotropy in the spatial distribution of the transmissivity of the aquifer layer.

There are two key assumptions that underlie the method which we used to estimate horizontal and vertical hydraulic conductivity. First, it was assumed that the available transmissivity data, or interpreted hydraulic conductivity data, are representative of the higher permeability strata encountered in the borehole. The higher permeability strata were also assumed to be dominated by a sand lithology. Second, it was assumed that the measured hydraulic conductivities are representative of horizontal hydraulic conductivity, not vertical hydraulic conductivity. Vertical hydraulic conductivity data at a scale representative of this model were not available. Based upon these assumptions, the method we used to distribute horizontal and vertical hydraulic conductivity is discussed below.

In the model we used our geostatistical analysis (kriging) presented in Section 4.3 as the initial sand hydraulic conductivities for a given block. In areas lacking hydraulic conductivity measurements, we used depositional models, lithofacies zones, and sparse hydraulic data to estimate hydraulic conductivity within zones. Data tends to be biased towards the outcrop and shallow subcrop. Previous investigators have found, both theoretically and empirically, that the hydraulic conductivity of unconsolidated sediments decreases with depth (Helm, 1976; Prudic, 1991). This is thought to be a result of sediment compaction with increased overburden pressure. In the Texas Gulf Coastal Plain, this could also be a result of low-energy depositional

environments toward the coast. Regardless, we considered the decreasing of hydraulic conductivity as a function of overburden when data were not available.

With the sand hydraulic conductivity estimated at the grid scale by kriging, we used the sand fraction to estimate an effective horizontal hydraulic conductivity adjusted for the percent of the formation that is not sand (i.e., silt or clay), given by:

$$K_h(\text{effective}) = K_{\text{sand}} \cdot (b_{\text{net-sand}} / b_{\text{layer}}) \quad (6.1)$$

where $K_h(\text{effective})$ is the effective grid block horizontal hydraulic conductivity, K_{sand} is the hydraulic conductivity of the sand as interpreted from hydraulic test data and interpolated to the grid scale, $b_{\text{net-sand}}$ is the net-sand thickness in feet in a given layer, and b_{layer} is the total layer thickness. This equation assumes horizontal flow and also assumes that the horizontal hydraulic conductivity of the non-sand lithologies is unimportant to grid-scale horizontal flow relative to the sands. MODFLOW combines total layer thickness (b_{layer}) and $K_h(\text{effective})$ to calculate grid block transmissibilities which govern flow rates within the model. Equation (6.1) above essentially adjusts MODFLOW's calculation of transmissibility to account for the lower permeability strata in the individual layers.

Section 4.3 examined the available data on hydraulic conductivities, indicating that the model layers had varying amounts of available supporting data for assigning effective horizontal hydraulic conductivity to model grid cells in the layer. Queen City data points are concentrated in the central and northern parts of the East-Texas Basin, with only sparse data south of northern Cherokee county. As noted in Section 4.3.3, reasonably good distributions of data points were available for the Carrizo, upper Wilcox, and middle Wilcox (Layers 3, 4, and 5) in the outcrop and East-Texas Basin subcrop. For areas south of the East-Texas Basin and the Sabine Uplift, data were sparse to absent in these layers. For the lower Wilcox (Layer 6), hydraulic conductivity data were almost all within or very near the western outcrop, with a few data points in the East-Texas Basin subcrop and in the Sabine Uplift.

The kriged hydraulic conductivity values for the Wilcox (Layers 3, 4, and 5) were combined with the calculated percent sand map in Figure 4.3.10 using Equation 6.1 to yield effective horizontal hydraulic conductivity fields. Since the sand-percent map is for the entire Wilcox Group, the sand was subdivided into the individual layers according to the following

fractions: (a) 37.5% to the upper Wilcox, (b) 37.5% to the middle Wilcox, and (c) 25% to the lower Wilcox. These sand percentages correspond roughly to the average sand percentages between the Hooper, Simsboro, and Calvert Bluff formations west of the Trinity River, which were explicitly mapped by Ayers and Lewis (1985). The Carrizo (Layer 3) was assumed to be essentially all sand and was therefore not adjusted for sand percent. A percent sand study was not done for the Queen City Formation since it was not the focus of this GAM scope. For the Reklaw confining unit (Layer 2) a constant horizontal hydraulic conductivity of 1 ft/day was used.

In areas where hydraulic conductivity data coverage was sparse or missing, effective hydraulic conductivity was estimated by dividing each layer into large zones of constant effective horizontal hydraulic conductivity, based on “soft” data -- depositional models, lithofacies zones, etc. The properties in these zones could then be scaled during calibration if necessary. In the Queen City (Layer 1) two zones were created, one extending from the downdip edge of the Queen City outcrop to the downdip extent of the Queen City sands (Guevara and Garcia, 1972), and the other extending southward from there to the south edge of the model. For the Carrizo (Layer 3) conductivities were extrapolated south of the data points. The Wilcox (Layers 4, 5, and 6) was zoned in the southern downdip portion according to depositional systems as described by Fisher and McGowen (1967) and Fisher (1969). Initial estimates of hydraulic conductivity for these zones varied from 1.5 ft/day to 3 ft/day. The calibrated conductivity fields with the zonation discussed above are described in Section 8.1.

Vertical hydraulic conductivity is not measurable on a model grid scale and is therefore generally a calibrated parameter. Typical vertical anisotropy ratios (K_h/K_v) are on the order of 1 to 1000 determined from model applications (Anderson and Woessner, 1992). However, Williamson et al. (1990) reported that vertical resistance to flow could be significant in the Gulf Coast Aquifer system in Texas and Louisiana which is composed of similar types of coastal plain sediments as encountered in the Carrizo-Wilcox aquifer. Previous regional modeling studies in the Carrizo-Wilcox aquifer have documented vertical anisotropy ratios as high as 50,000 (Williamson et al., 1990).

Because vertical hydraulic conductivity of an aquifer is expected to be controlled by depositional environment and lithofacies, we used percent sand, maximum sand, depositional environment, lithofacies, and depth of burial in zoning vertical hydraulic conductivity to the degree practical.

6.4.2 Storativity

For unconfined aquifer conditions, a uniform storativity value of 0.20 was assigned to the different layers. Grid cells, which represented outcrop (land surface), are modeled as either confined or unconfined depending upon the elevation of the simulated water table in that grid cell. The confined storativity assigned to outcrop cells was done to account for water ponding on the ground surface and to prevent non-physical heads being computed and used in the equations governing groundwater flow.

For confined aquifer conditions, the storativity was specified as a function of aquifer thickness based upon a constant specific storage of 4.5×10^{-6} 1/ft, representing the average of reported values for the Carrizo-Wilcox aquifer (Mace et al., 2000a). This results in storativities ranging from 2×10^{-4} to 2×10^{-3} in the downdip portions of the Carrizo-Wilcox aquifer.

7.0 MODELING APPROACH

In the context of groundwater modeling, model calibration can be defined as the process of producing an agreement between model simulated water levels and aquifer discharge, and field measured water levels and aquifer discharge through the adjustment of independent variables (typically hydraulic conductivity, storativity, and recharge). Generally accepted practice for groundwater calibration usually includes performance of a sensitivity analysis and, if the model is going to be used for predictive purposes, a verification analysis. A sensitivity analysis entails a systematic variation of the calibrated parameters and stresses and the re-simulation of the aquifer conditions. Those parameters which strongly change the simulated aquifer heads and discharges would be important parameters to the calibration. It is important to note, that the “one-off” standard sensitivity analysis does not estimate parameter uncertainty as limited parameter space is investigated and parameter correlation is not accounted for. A verification analysis is a test to determine if the model is suitable for use as a predictive tool. This is performed by using the model to predict aquifer conditions during a period which was not used in the model calibration. Consistent with the approach outlined above, we calibrated the model, verified the model, performed sensitivity analyses, and performed predictive simulations.

7.1 Calibration

Groundwater models are inherently non-unique, meaning that multiple combinations of hydraulic parameters and aquifer stresses can reproduce measured aquifer water levels. To reduce the impact of non-uniqueness, we employed a method described by Ritchey and Rumbaugh (1996). This method includes (1) calibrating the model using parameter values (i.e., hydraulic conductivity, storativity, recharge) that are consistent with measured values, (2) calibrating to multiple hydrologic conditions, and (3) using multiple calibration performance measures such as hydraulic heads and discharge rate to assess calibration. Each of these elements is discussed below.

We used measured hydraulic conductivity and storativity data to initially estimate our parameters. The analysis of hydraulic parameters in Section 4.3 of this report indicates that there is a large amount of hydraulic conductivity data that is available for use as initial model values.

Vertical hydraulic conductivity is not measurable at the model scale and thus cannot be well constrained. Storativity is a parameter which is not well defined on the scale of the model. However, storativity is estimated from measured specific storage data in combination with the aquifer thickness. Recharge has not been directly measured in the study area and is arguably not measurable at the model scale. As described earlier in the report, we used SWAT to provide an initial estimate of shallow recharge. Adjustment of all model parameters were held to within plausible ranges based upon the available data and relevant literature. Adjustments to aquifer parameters from initial estimates were minimized to the extent possible to meet the calibration criteria. As a general rule, parameters that have few measurements were adjusted preferentially as compared to properties that have a good supporting database.

The model was calibrated over two time periods, one representing steady-state conditions and the other representing transient conditions. Because the confined section of the Carrizo-Wilcox aquifer in northeast Texas has been extensively developed, portions of the aquifer have not been at a steady state over much of the historical record. Therefore, we chose to use “predevelopment” conditions as our steady-state model. Section 4.4.2 describes the process used to estimate aquifer water levels for the steady-state predevelopment model. No pumping stresses were applied to the predevelopment model consistent with the assumption of steady-state conditions prior to significant resource development.

The transient calibration period ran from 1980 through 1989 consistent with the GAM model requirements. The actual transient simulation started in 1975, allowing the model to equilibrate over a 5-year period to the initial hydraulic heads that represent transient conditions during 1980. Section 4.4.4 describes the aquifer water levels and how they were derived to be used for the transient calibration period. Pumping estimates based upon historical records were applied on a monthly time scale in the transient calibration period. Likewise, recharge, stream flow, and reservoir stage were estimated on a monthly time basis and set as input through the transient calibration period. The time period from 1990 until 1999 was used as the verification period to assess the predictive ability of the model. Like the calibration period, transient stresses or boundary conditions were determined on a monthly time step. Unlike the calibration period, parameters were not adjusted in the verification process.

The model was calibrated through a wide range of hydrological conditions. The steady-state predevelopment model represents a period of equilibrium where recharge and aquifer discharge through streams and cross-formational flow are in balance. Under these conditions, the aquifer rejects the maximum amount of recharge and, as was detailed in Section 5, a minimum amount of recharge is expected under stable basin conditions (Freeze, 1971). The steady-state model is sensitive to recharge. The calibration and verification period (1980 through 1999) represents a significantly different period. By this time, portions of the aquifer have been extensively developed resulting in loss of storage and declining heads. Some of the recharge being rejected under steady-state predevelopment conditions may be captured as a result of losing streams and increased vertical gradients. The calibration and verification periods also help constrain the model parameterization because a wide range of hydrologic conditions are encountered and simulated. The transient model is sensitive to parameters that are not sensitive for the steady-state model.

Calibration requires development of calibration targets and specification of calibration measures. To address the issue of non-uniqueness, it is best to use as many types of calibration targets as possible. The primary type of calibration target is hydraulic head (water level). However, we also used stream flows and gain/loss estimates. Simulated heads were compared to measured heads at specific observation points through time (hydrographs) and head distributions (maps) for select time periods (see Section 4.4) to ensure that model head distributions are consistent with hydrogeologic interpretations and accepted conceptual models for flow within the aquifer.

Stream calibration targets were derived from two types of data. First, we compared model simulated stream flow rates to observed flow rates at key stream gages in the model area. Because stream flow rates exceed aquifer/stream fluxes for local cells, available gain/loss estimates were also used for the major streams crossing the outcrop.

Traditional calibration measures (Anderson and Woessner, 1992) such as the mean error, the mean absolute error, and the root mean square error quantify the average error in the calibration process. The mean error (ME) is the mean of the differences between measured heads (h_m) and simulated heads (h_s):

$$ME = \frac{1}{n} \sum_{i=1}^n (h_m - h_s)_i \quad (7.1)$$

where n is the number of calibration measurements. The mean absolute error (MAE) is the mean of the absolute value of the differences between measured heads (h_m) and simulated heads (h_s):

$$MAE = \frac{1}{n} \sum_{i=1}^n |(h_m - h_s)_i| \quad (7.2)$$

where n is the number of calibration measurements. The root mean square (RMS) error is the average of the squared differences between measured heads (h_m) and simulated heads (h_s):

$$RMS = \left[\frac{1}{n} \sum_{i=1}^n (h_m - h_s)_i^2 \right]^{0.5} \quad (7.3)$$

where n is the number of calibration measurements. The difference between the measured hydraulic head and the simulated hydraulic head is termed a residual.

We used the RMS as the basic measure of calibration for heads. The required calibration criterion for heads is a RMS that is equal to or less than 10 percent of the observed head range in the aquifer being simulated. To provide information on model performance with time, the RMS was calculated for the calibration period (1980-1989) and the verification period (1990-1999). The RMS is useful for describing model error on an average basis but, as a single measure, it does not provide insight into spatial trends in the distribution of the residuals.

An examination of the distribution of residuals is necessary to determine if they are randomly distributed over the model grid and not spatially biased. Post plots of head residuals for each model layer were used to check for spatial bias by indicating the magnitude and direction of mis-match between observed and simulated heads. Simulated head distributions were also compared to the head distributions developed from the field measurements. Finally, scatter plots were used to determine if the head residuals are biased based on the magnitude of the observed head surface.

For streams, the calibration criteria were defined to be within 10% of the measured values where uncertainty in these targets is proven to be acceptable for such a criteria.

7.2 Calibration Target Uncertainty

Calibration targets are uncertain. In order to not “over-calibrate” a model, which is a stated desire for the GAM models, calibration criteria should be defined consistent with the uncertainty in calibration targets. The primary calibration target in groundwater modeling is hydraulic head. Uncertainty in head measurements can be the result of many factors including, measurement error, scale errors, and various types of averaging errors both spatial and temporal. The calibration criteria for head is a RMS less than or equal to 10% of head variation within the aquifer being modeled. Head differences across the aquifers in the study area are on the order of 400 to 500 feet. This leads to an acceptable RMS of between 40 and 50 feet. We can compare this RMS to an estimate of the head target errors and see what level of calibration the underlying head targets can support.

Measurement errors are typically on the order of tenths of feet, and at the GAM scale can be considered insignificant. However, measuring point elevation errors can be significant. Our analysis of differences between the reported land-surface datum (LSD) and the ground surface elevation as determined from a digital elevation map determined that the average difference was -5 feet with a standard deviation of 28 feet. Add to this error the error in averaging ground surface elevations available on a 30 m grid to a one mile grid, and the resulting errors can average 10 to 20 feet and greatly exceed 70 feet in areas with higher topographic slopes.

Another error is the one caused by combining fluvial deltaic sand channels into single grid blocks representing one simulated head. Horizontal to vertical hydraulic conductivity ratios have been proven to be high in the Coastal Plain aquifers of Texas (Fogg et al., 1983; Williamson et al., 1990). As a result, significant vertical gradients can occur within individual model layers. Vertical gradients near pumping centers are quite large and approach 0.1 (Williamson et al., 1990). This implies that portions of the aquifer can have head variations within a single model layer on the order of 10 to 50 feet. On average, in areas away from large pumping centers, this scale effect is expected to be on the order of 10 to 20 feet. Horizontal

gradients relative to the grid scale also account for an additional 1 to 5 feet error with even greater errors near pumping centers. When these errors are added up, the average error in model heads could easily equal our calibration criteria of 40 to 50 feet. The nugget observed on kriged head maps within the modeled aquifers equals from 20 to 30 feet. This nugget captures both uncertainty and variability in the observed heads being rationalized above. Calibrating to RMS values significantly less than 30 feet would constitute over calibration of the model and parameter adjustments to reach that RMS are not supported by the hydraulic head uncertainty.

7.3 Sensitivity Analysis

A sensitivity analysis was performed on the steady-state and transient calibrated models to determine the impact of changes in a calibrated parameter on the predictions of the calibrated model. A standard “one-off” sensitivity analysis was performed. This means that hydraulic parameters or stresses were adjusted from their calibrated “base case” values one by one while all other hydraulic parameters are unperturbed.

7.4 Predictions

Once the model satisfied the calibration criteria for both the calibration and verification periods, the model was used to make predictive simulations. The predictive simulations have different simulation periods. Simulations were run from 1999 to 2010, 2020, 2030, 2040, and 2050. Average climatic conditions were applied for each predictive simulation with the simulation ending with a drought of record. Stream flow rates and recharge were applied with seasonal variation in the average conditions period. Pumping stresses were based upon the Regional Water Plans as described in Section 4.7 and Appendix C.

8.0 STEADY-STATE MODEL

The current section details the calibration of the steady-state model and presents the steady-state model results. This section also describes analyses of model sensitivity to various hydrologic parameters.

8.1 Calibration

This section describes the steady-state calibration targets and calibrated parameters including horizontal and vertical hydraulic conductivity, recharge, ET, stream conductance, and vertical conductance for younger sediments overlying the Queen City Formation.

8.1.1 Calibration Targets

Water-level measurements are needed as targets for steady-state calibration. However, where there is a well, water levels have often been affected by groundwater pumpage. As a result, valid targets for predevelopment conditions were limited, because wells were typically drilled for pumpage. Acceptable predevelopment targets included 18 Carrizo measurements and 91 Wilcox measurements (34 in the upper Wilcox and 57 in the middle Wilcox). A distinction was made between outcrop wells and wells located in the confined section. For wells in the outcrop, the water-level elevation was calculated based on the measured water-level depth using the grid-block averaged elevation from the model. For the confined section, the listed well elevation was used for calculating the water-level elevation. This was done to reduce potential errors induced by averaging ground-surface elevation over a 1-mile by 1-mile grid-block.

8.1.2 Horizontal and Vertical Hydraulic Conductivities

Section 6.4.1 described the determination of initial horizontal and vertical hydraulic conductivities for the model. Figures 8.1.1-8.1.4 show the final calibrated horizontal hydraulic conductivity (K_h) fields for Layer 3 (Carrizo), Layer 4 (upper Wilcox), Layer 5 (middle Wilcox), and Layer 6 (lower Wilcox). Figure 8.1.5 shows the vertical anisotropy ratio field for Layer 2 (Reklaw) for which a uniform horizontal hydraulic conductivity value of 1 ft/day was assumed. We used a hydraulic conductivity map for Layer 1 (Queen City) in the model, but no explicit calibration was performed for Layer 1. The spatial horizontal hydraulic conductivity distribution

for Layer 1, shown in Figure 4.3.8, is considered preliminary. Table 8.1.1 summarizes the calibrated hydraulic conductivity ranges and anisotropy ratios (K_h/K_v) for each layer.

The calibration process for the Northern Carrizo-Wilcox GAM was iterative. We developed an initial steady-state calibration through adjustment of recharge and hydraulic conductivity. Although the initial steady-state calibrated model met the calibration criteria, the subsequent transient model calibration indicated that the vertical hydraulic conductivities were too high. It became necessary to jointly calibrate the steady-state and transient models to achieve a consistent calibration to both steady-state and transient water-level data.

Overall, vertical hydraulic conductivities (K_v) were lowered based on the transient calibration. We then recalibrated the steady-state model through adjustment of recharge, ET (from groundwater), and hydraulic conductivities. Modifications to the initial estimates of horizontal hydraulic conductivity (Section 6.4.1), based on the steady-state calibration, involved increasing conductivities in areas where values were low to a minimum of 2 ft/day for Layer 3 and 1.5 ft/day for Layers 4, 5 and 6. On the other hand, transient calibration required limiting horizontal hydraulic conductivity in selected areas of the Carrizo, upper Wilcox, and middle Wilcox layers. This area encompassed part of Cherokee, Anderson, Henderson, Smith, Wood, Upshur, and Camp counties, where a uniform hydraulic conductivity value of 1 ft/day was assigned to Layers 4 and 5 (Wilcox), and a slightly higher value of 2 ft/day was assigned to Layer 3 (Carrizo). Also, the relatively high hydraulic conductivity area in the southern part of the Sabine Uplift, which was not supported by data, was reduced to values similar to those of surrounding data. For the Queen City (Layer 1), the minimum horizontal hydraulic conductivity value was set to 5 ft/day, mainly because of numerical instabilities along the outcrop edge of the Queen City, where it becomes relatively thin.

Table 8.1.1 shows the final calibrated anisotropy ratios for the steady-state model which were increased by a factor of 10 to 1000 from that of the initial steady-state calibration. Vertical hydraulic conductivity of the Reklaw was set to 1×10^{-5} ft/day and modified in two selected areas (Figure 8.1.5). In central Smith County and the adjacent northern part of Cherokee and Anderson counties, the vertical hydraulic conductivity of Layer 2 (Reklaw) was reduced to 1×10^{-6} ft/day based on transient calibration, to restrict downward flow from the shallow Queen City aquifer which has been induced by steep water-level declines in the Carrizo and upper

Wilcox in Smith County due to pumpage. On the other hand, vertical permeability in eastern Nacogdoches was increased to 1×10^{-4} ft/day based on the transient calibration to allow more cross-formational flow, because simulated water-level declines owing to pumpage exceeded observed declines in the Carrizo Aquifer.

There is no clear geologic or hydrologic information that can be used to support these spatial changes in vertical hydraulic conductivities of the Reklaw. The potential limitations of the steady-state model are discussed in Section 11.

8.1.3 Recharge and Groundwater Evapotranspiration

Recharge was input initially as an averaged distribution from the transient recharge results (Sections 6.3.4). However, this averaged recharge estimate was too high, resulting in numerical instabilities in the steady-state simulation. The low vertical hydraulic conductivities required for transient calibration required a reduction in recharge in the steady-state model. Recharge was selectively reduced by hydrogeologic unit and adjusted locally in case of numerical instabilities, until an acceptable calibration was achieved. The spatial distribution of calibrated recharge is shown in Figure 8.1.6.

Average groundwater ET was input, as provided by the SWAT results, and applied as ET maximum in the model (Section 6.3.4). The maximum rooting depths were taken from the SWAT results and input as the extinction depth (Figure 8.1.7). The ET surface was set to ground surface, so groundwater ET varied linearly starting from a maximum at ground surface and going down to the root depth. The potential ET from groundwater can and did exceed recharge in some circumstances; however, MODFLOW was unable to model this under steady-state conditions. For conditions where groundwater was near the surface and the ET rate exceeded the recharge rate, model convergence was difficult and model mass balances were not acceptable. In order to overcome this problem, we reduced the maximum ET rate (Figure 8.1.8) to 70 percent of the recharge rate on a cell by cell basis. This resulted in acceptable convergence and mass balances.

8.1.4 General-Head Boundaries and Stream Conductances

General-head boundaries (GHBs) were assigned to the confined part of the Queen City in the southern part of the model. The elevations of the GHBs were estimated from the surficial

water table (Section 6.3.2). The initial conductivities of the GHBs were estimated from reported vertical conductivities (Williamson et al., 1990) of the younger sediments overlying the Queen City. Heads in the Queen City formation (Layer 1) indicated limited sensitivity to the conductivity of the GHBs, and are more controlled by recharge in the outcrop and by streambed conductivities. Streambed conductivities were based on the hydraulic conductivities of the underlying formation. The overall conductance varies with the streambed width as specified in the EPA RF1 dataset (Section 6.3.3).

Table 8.1.1 Calibrated hydraulic conductivity ranges for the steady-state model.

	Horizontal Hydraulic Conductivity K_h (ft/d)	Vertical Hydraulic Conductivity K_v (ft/d)	Anisotropy Ratio (K_h/K_v)
Layer 1 (Queen City)	5 – 25	$5 \times 10^{-4} - 2.5 \times 10^{-2}$	1,000-10,000
Layer 2 (Reklaw)	1	$1 \times 10^{-6} - 1 \times 10^{-4}$	10,000 – 1,000,000.
Layer 3 (Carrizo)	2 – 40	$2 \times 10^{-2} - 4 \times 10^{-1}$	100
Layer 4 (upper Wilcox)	1 – 10	$1 \times 10^{-4} - 1 \times 10^{-3}$	10,000
Layer 5 (middle Wilcox)	1 – 10	$1 \times 10^{-4} - 1 \times 10^{-3}$	10,000
Layer 6 (lower Wilcox)	1.5 – 25	$1.5 \times 10^{-4} - 2.5 \times 10^{-3}$	10,000

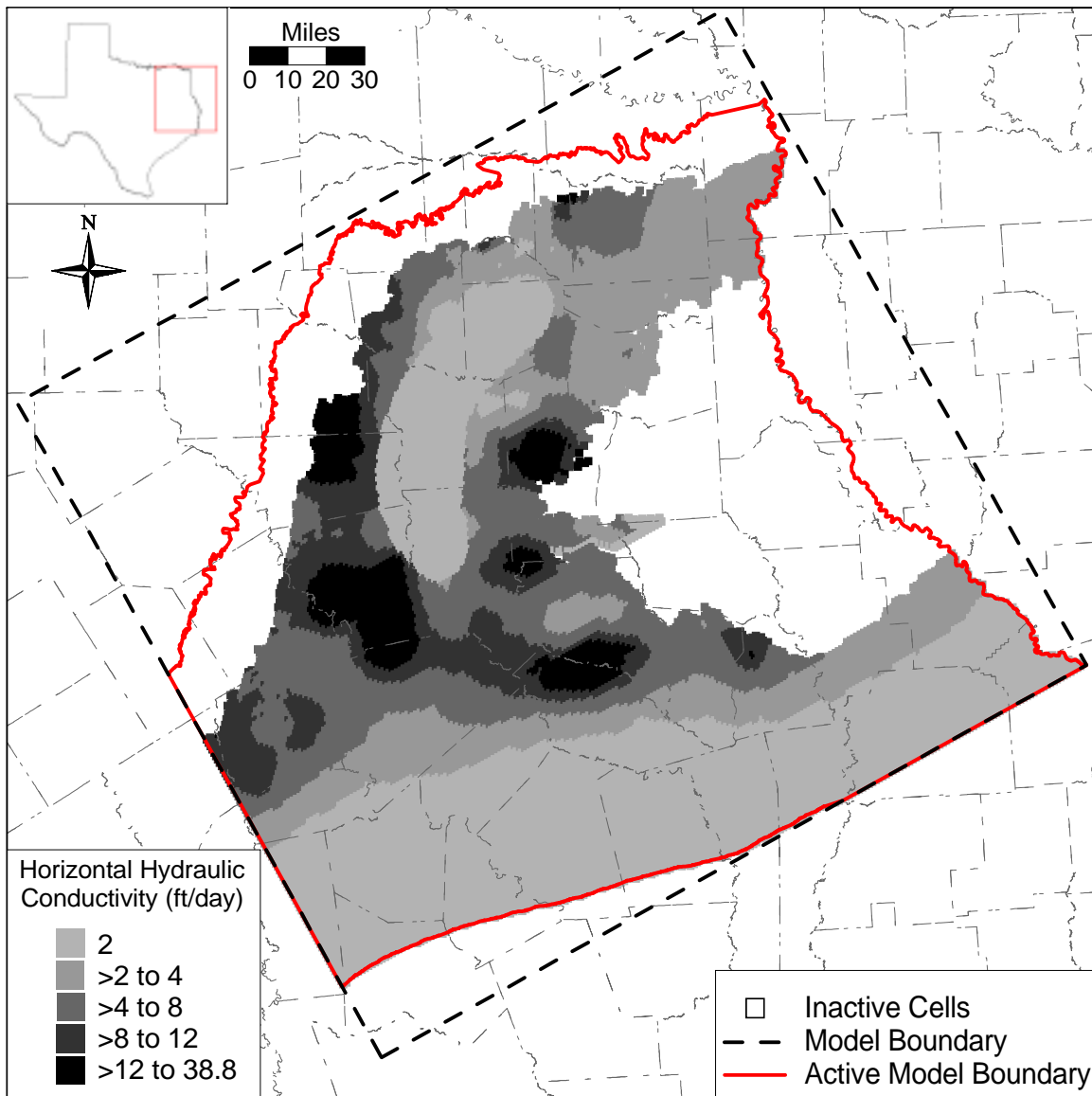


Figure 8.1.1 Calibrated horizontal hydraulic conductivity field for Layer 3 (Carrizo).

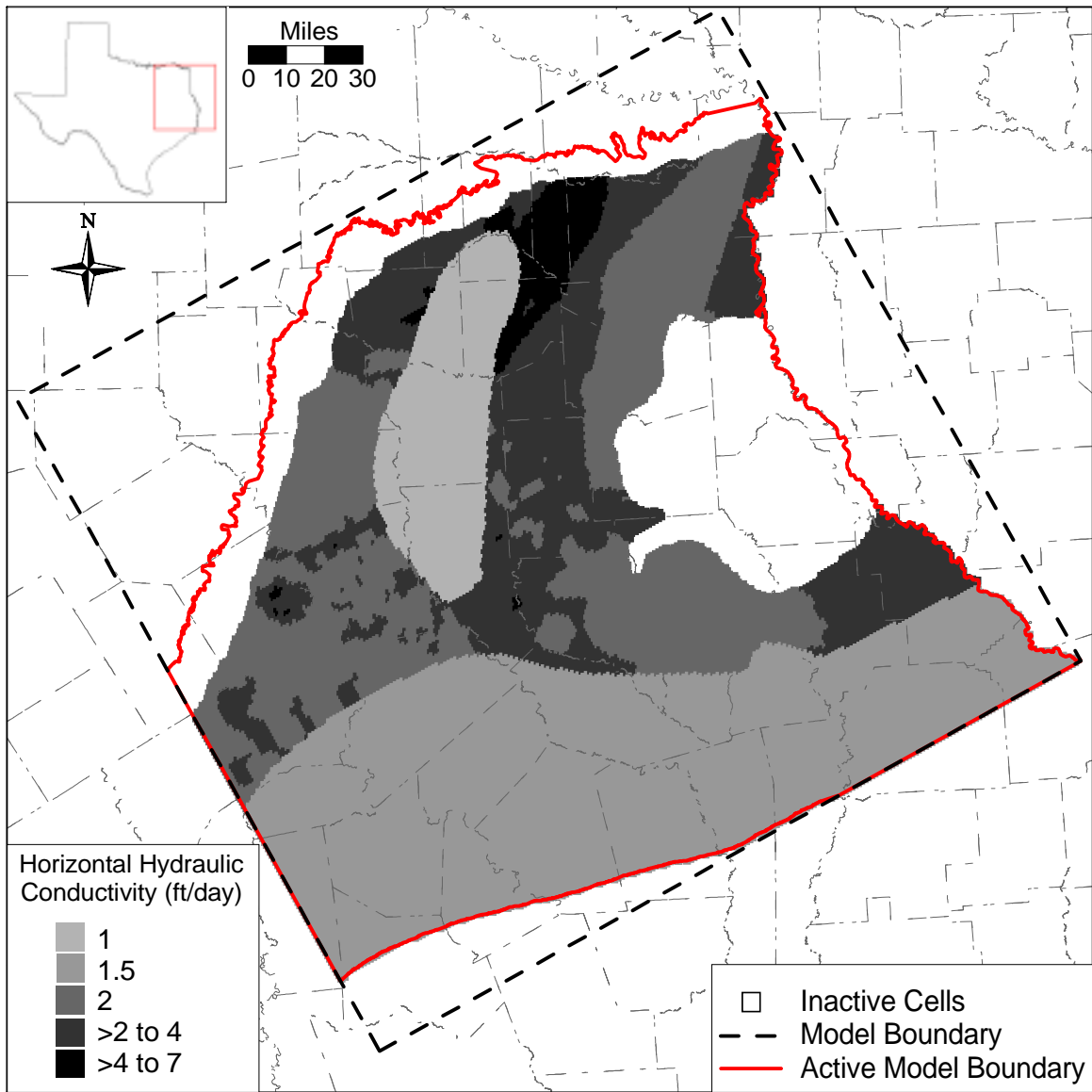


Figure 8.1.2 Calibrated horizontal hydraulic conductivity field for Layer 4 (upper Wilcox).

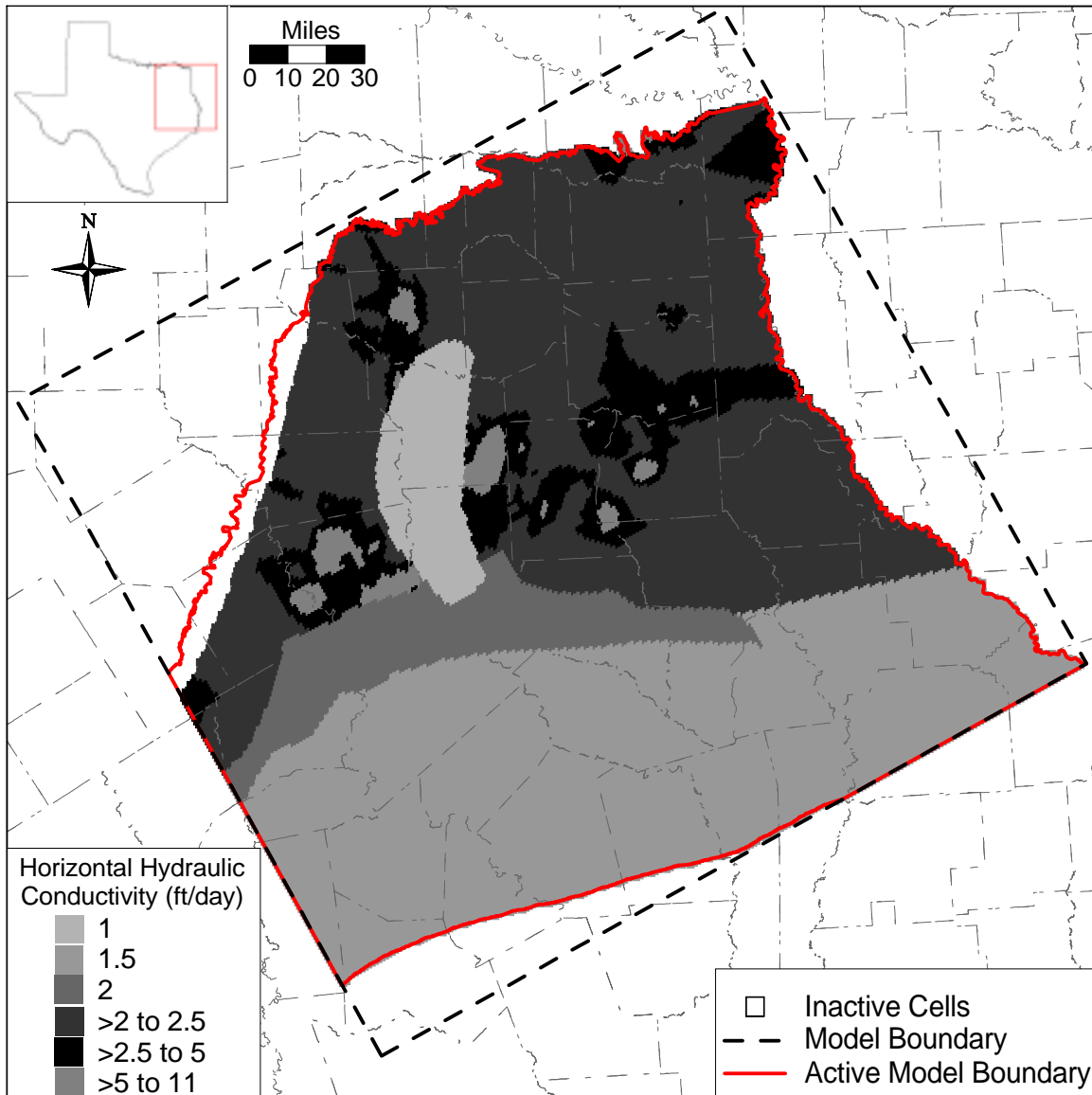


Figure 8.1.3 Calibrated horizontal hydraulic conductivity field for Layer 5 (middle Wilcox).

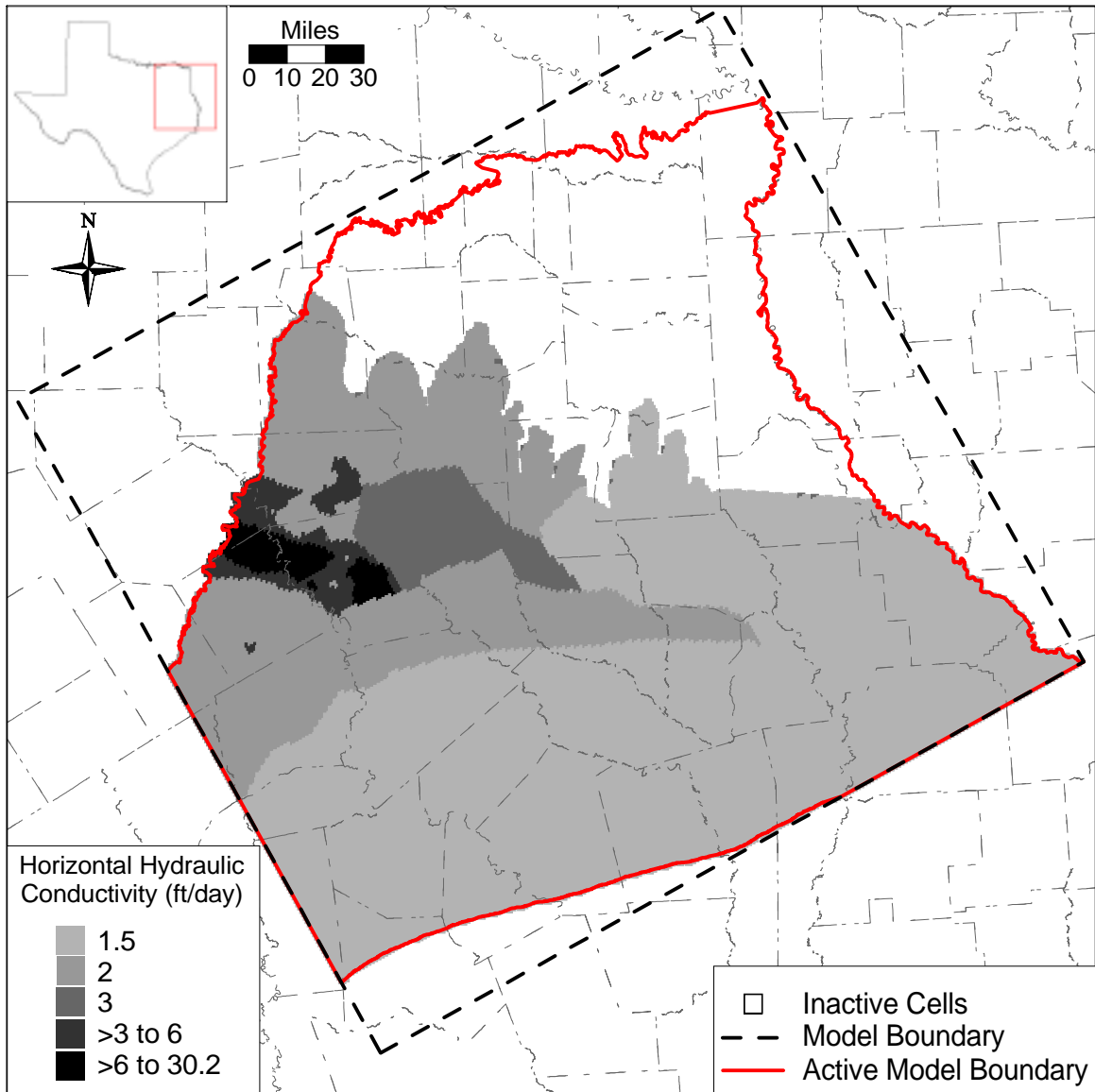


Figure 8.1.4 Calibrated horizontal hydraulic conductivity field for Layer 6 (lower Wilcox).

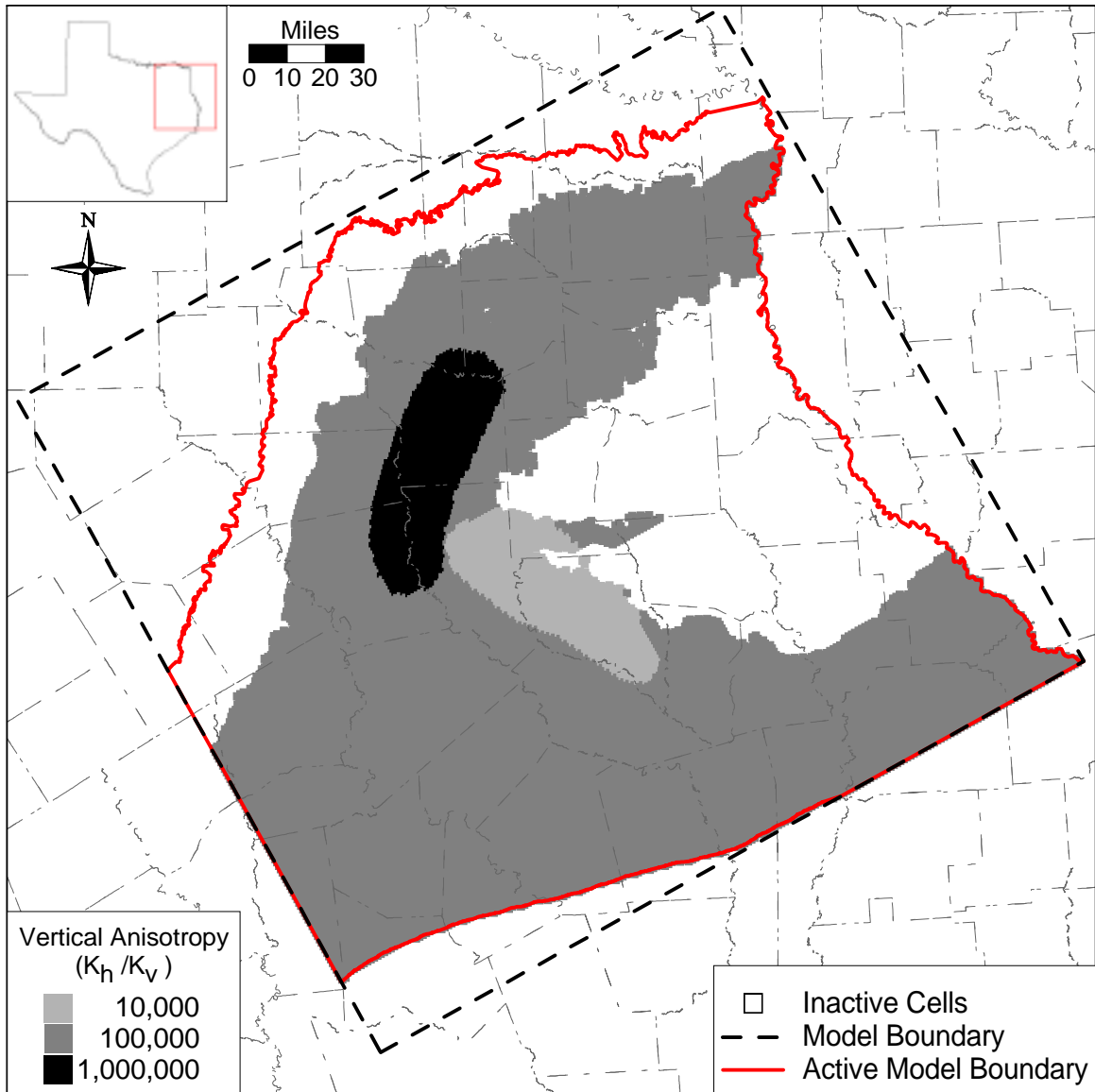


Figure 8.1.5 Calibrated vertical anisotropy (K_h/K_v) field for Layer 2 (Reklaw).

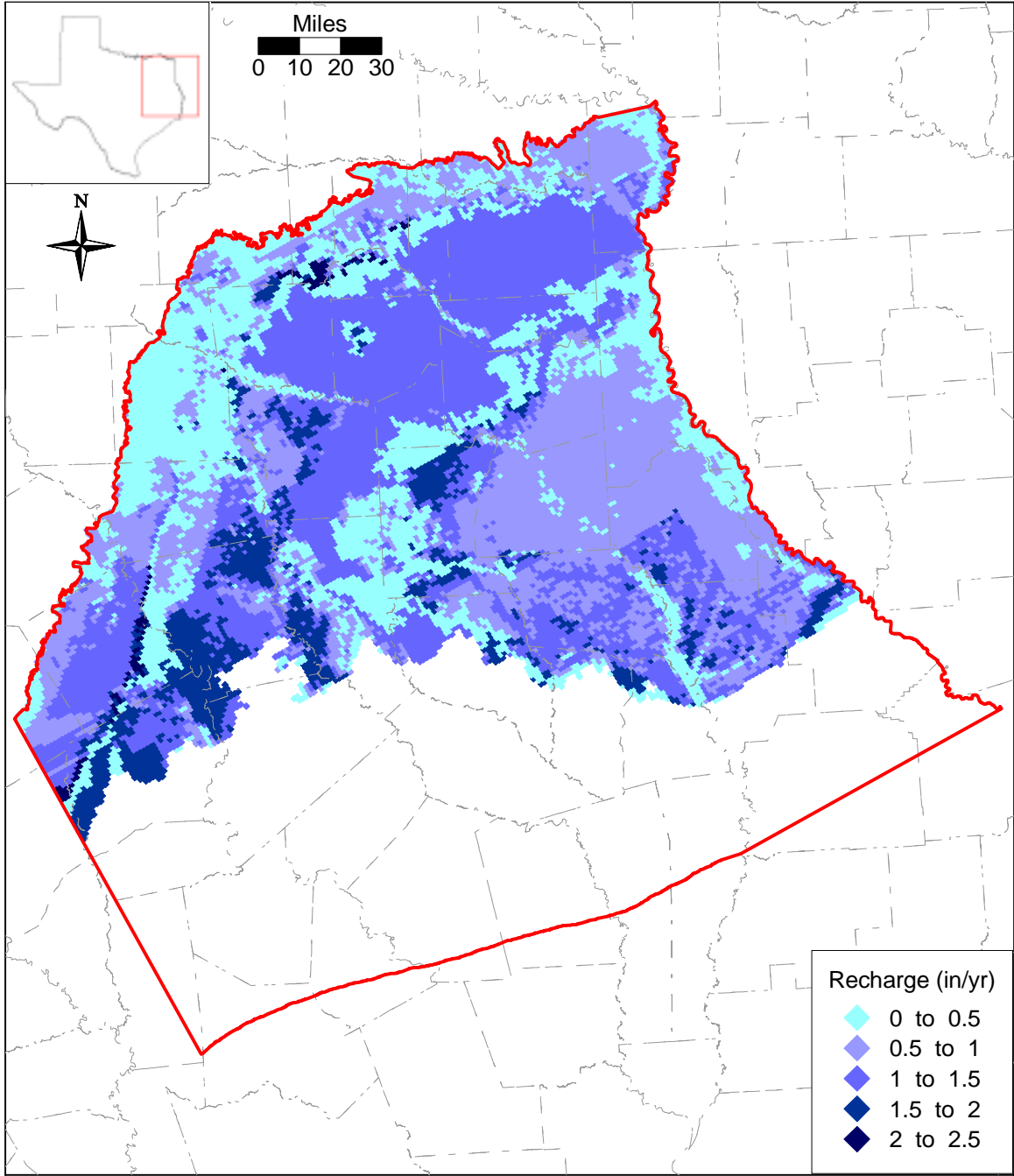


Figure 8.1.6 Calibrated recharge distribution for the steady-state model.

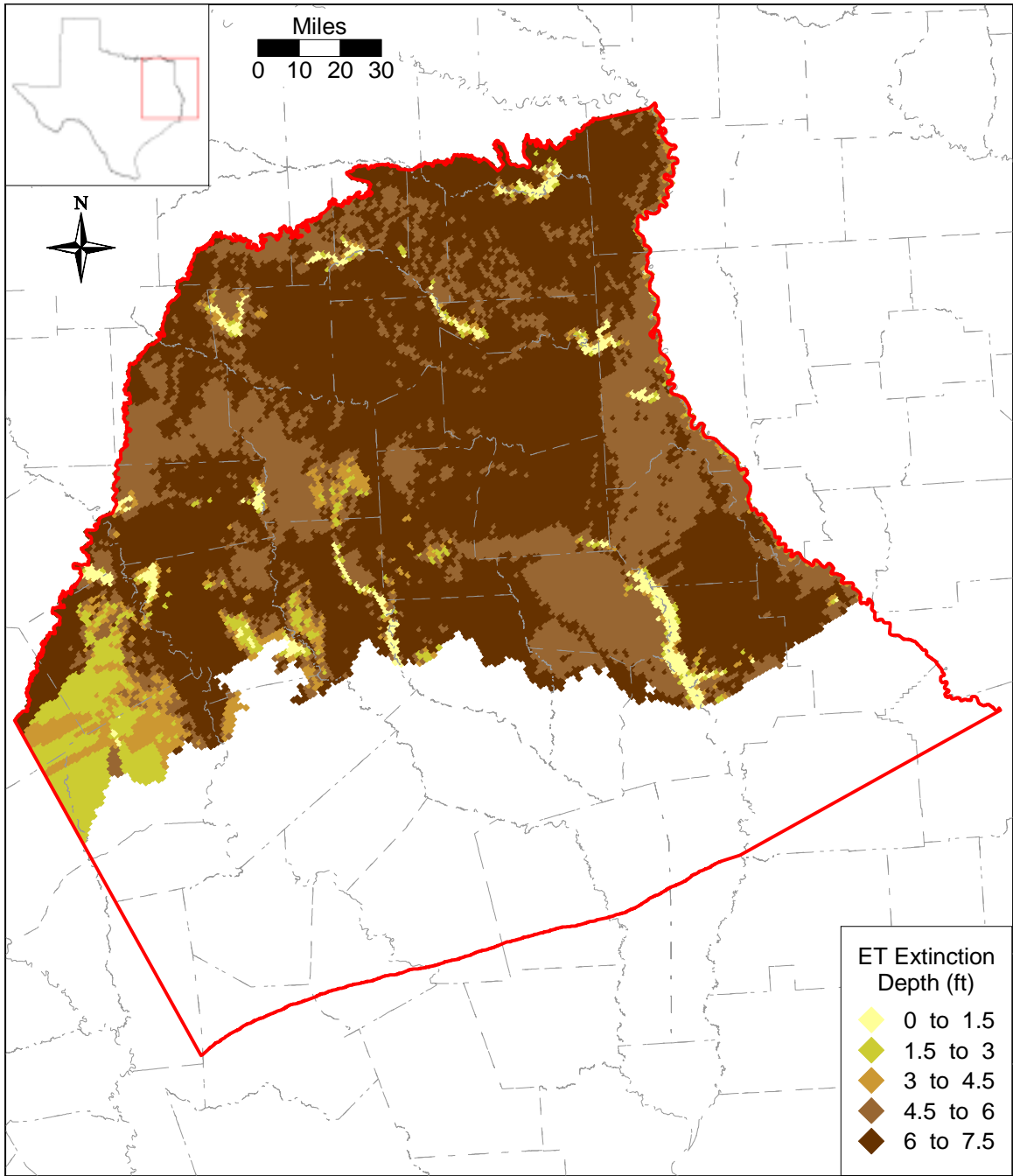


Figure 8.1.7 ET extinction depth distribution for the steady-state model.

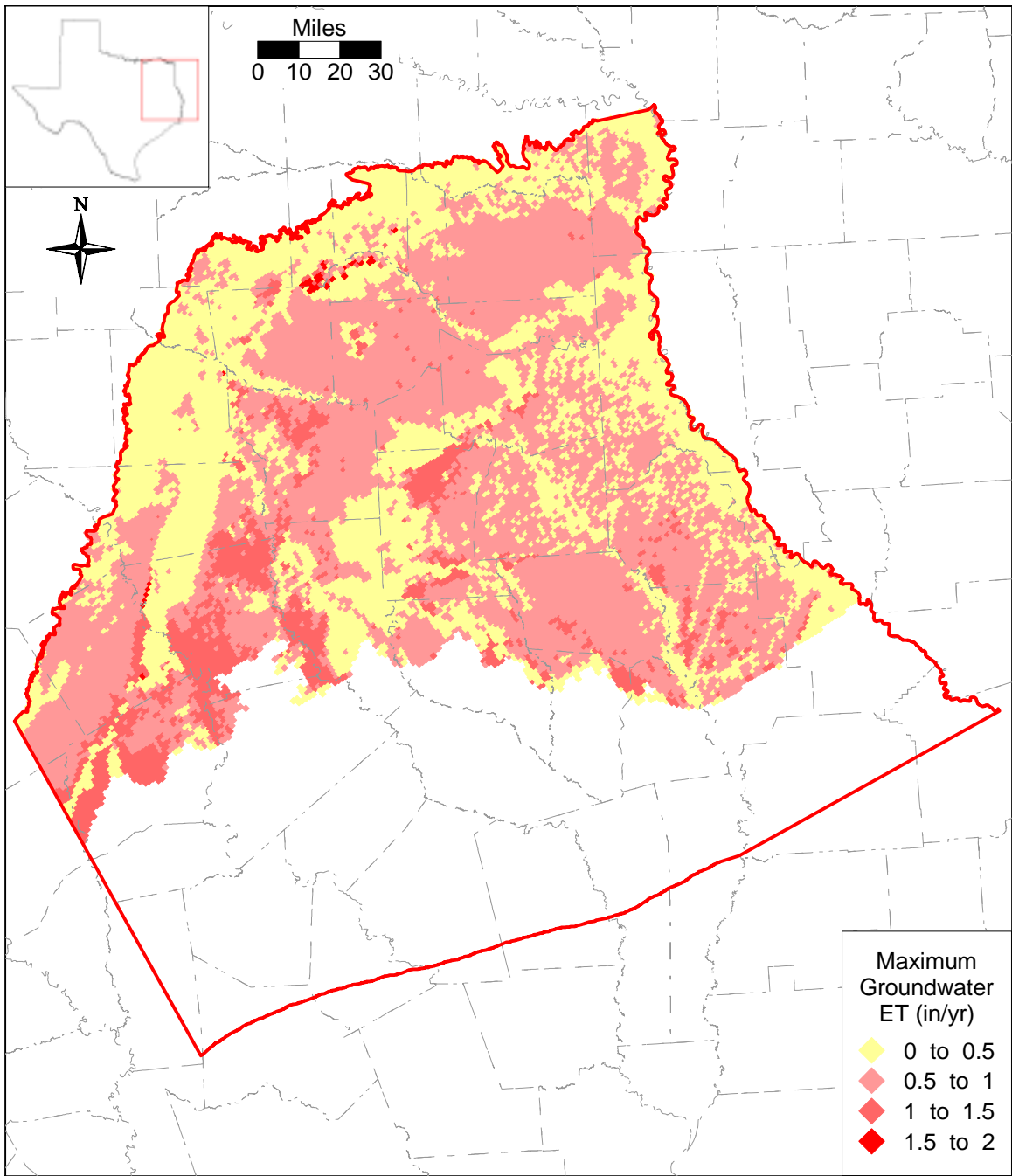


Figure 8.1.8 Calibrated maximum groundwater ET rate distribution for the steady-state model.

8.2 Simulation Results

Calibration of the steady-state model is not unique. Calibrated results can be obtained by numerous combinations of recharge and vertical and horizontal hydraulic conductivities. Overall, the steady-state model is most sensitive to recharge. This is to be expected, since recharge is the primary input source of water for the model.

8.2.1 Hydraulic Heads

Figures 8.2.1-8.2.5 show the head surface results from the calibrated steady-state model, together with the residuals for the target wells in the individual layers. The residuals were calculated from:

$$residual = head_{measured} - head_{simulated} \quad (8.2.1)$$

A positive residual indicates that the model has underpredicted the hydraulic head, while a negative residual indicates overprediction. The calibration statistics for the individual layers are summarized in Table 8.2.1, and the overall mass balance calculated by the steady-state model is given in Tables 8.2.2a and 8.2.2b.

Figure 8.2.1a shows the simulated hydraulic heads for Layer 1 (Queen City) and the corresponding residuals for the target well locations. As mentioned above, the Queen City aquifer was not explicitly calibrated during this GAM phase; however, hydraulic heads in the Queen City were considered important for controlling vertical flow across the Reklaw confining unit. The simulated hydraulic heads for Layer 1 in Figure 8.2.1 compare reasonably well with measured hydraulic heads, reproducing the water table as a reflection of the general topography in the Queen-City outcrop. No effort was made to refine the hydraulic parameters and improve the calibration for Layer 1. The calibration statistics shows an adjusted RMS of 13% for the Queen City, which is considered acceptable for bounding the vertical gradient across the Reklaw confining unit.

The calibration statistics for the Carrizo shows an adjusted RMS of 8% (Table 8.2.1) based on a relatively even distribution of the residuals throughout the confined and unconfined part of the aquifer (Figure 8.2.2a). The scatterplot of simulated and measured hydraulic heads indicates a uniform distribution around the unit-slope line (Figure 8.2.2b). The steady-state

hydraulic head surface shows an approximate west-east groundwater divide from van Zandt County through Smith County to Rusk County. North of this divide the hydraulic gradients in the confined portion of the Carrizo are to the east, indicating groundwater flow to the east toward the Red River in Louisiana. South of the divide, groundwater flow in the confined section is to the south and further downdip to the southeast. The overall head distribution and general flow pattern agrees reasonably well with that shown in Figure 4.4.3 (Fogg and Kreitler, 1982), considering that the simulated heads represent steady-state pre-development conditions and Fogg and Kreitler (1982) included pumpage effects on their constructed potentiometric surface for the entire Carrizo-Wilcox aquifer.

The calibration statistics for Layer 4 (upper Wilcox) indicates a relatively high adjusted RMS of 15%, even though the overall total RMS of 38.5 ft is not significantly greater than that of Layer 5 (Table 8.2.1). This is due to the relatively narrow hydraulic head range of 257 ft, compared to 418 ft for Layer 5. Figure 8.2.3a shows that the calibration data are located mostly in the outcrop in the Sabine Uplift, with some data points along the western outcrop, and with only a few data points in the confined section in Upshur and Rusk counties. The scatterplot of simulated and measured hydraulic heads shows this narrow head range (Figure 8.2.3b), resulting in the relatively large adjusted RMS. Given the potential uncertainty in well-location and associated uncertainty in well elevation and measured water-level elevation, an improvement in the fit was not attempted. Using the greater head range for the entire Wilcox aquifer would decrease the adjusted RMS to 9%. The overall groundwater flow pattern as inferred from the hydraulic head distribution (Figure 8.2.3a) corresponds largely to that of the Carrizo (Figure 8.2.2a).

The calibration statistics for Layer 5 (middle Wilcox) shows an adjusted RMS of 8% (Table 8.2.1). The simulated hydraulic head distribution together with the posted residual in the target wells is shown in Figure 8.2.4a. The residuals are generally low and uniformly distributed in the scatterplot (Figure 8.2.4b), except for a couple of data points in southern van Zandt County, indicating simulated hydraulic heads nearly 100 ft below measured heads of 574 ft. The recharge distribution used in this area is somewhat low compared to the surrounding areas in the outcrop of Layer 5 (Figure 8.1.6), and it is probable that by increasing recharge rates in this area, the difference could be reduced. On the other hand, potential uncertainties in the actual well

location could cause a significant change in well elevation in this rather hilly outcrop area. That is, the measured water levels could be significantly in error. Water-level measurements in a nearby well, used for transient calibration (well 3433801), indicated a water-level elevation of about 505 ft, which is significantly lower than the 574 ft reported for the two steady-state target wells. Furthermore, the water levels in nearby wells in the upper Wilcox and Carrizo agree well with simulated values, indicating little difference in hydraulic heads. As a result, no additional adjustment of recharge in this particular area was attempted to improve the fit. Overall, the adjusted RMS for Layer 5 was 8%, below that of the calibration criteria.

The simulated hydraulic head distribution for Layer 6 is shown in Figure 8.2.5. In the northern part of the area, the lower Wilcox pinches out and no simulated heads are shown. There were no calibration points identified in the lower Wilcox to provide a check of the simulated steady-state hydraulic heads in Layer 6. The simulated heads compare well with those in the overlying layer, showing somewhat higher hydraulic heads in the deeper confined section, which indicates upward flow from Layer 6, as one would expect.

Some cells went dry in the steady-state simulation. Out of 18,679 outcrop cells, 77 cells or less than one present were dry. These dry cells can be indicative of model instability or actual subsurface conditions. Because no obvious discontinuity exists in the outcrop water table, these cells likely are indicative of actual subsurface conditions (i.e., small cell thickness, low water table). The small number of dry cells does not have a significant impact on model results.

8.2.2 Streams

Figure 8.2.6 shows the gain/loss values for the stream reaches in the steady-state model. As would be expected, the larger stream segments are all gaining. Only the upper reaches of tributaries show losing segments. These losses are typically higher in shallow channels at higher overall elevations.

We compared the stream leakances to the stream gain/loss data compiled by Slade et al. (2002). Seven of the nine documented gain/loss studies that fall within the model area and include the Carrizo-Wilcox outcrop were compared to simulated stream leakances. The other two studies were conducted on minor streams that were not included as boundary conditions in the model due to their small size. The seven gain/loss studies used were conducted between

1942 and 1981 and covered reaches of the Sabine River, Little Cyprus Bayou, Bowles Creek, and Lake Fork Creek. Because the steady-state model simulates predevelopment conditions based on average recharge, ET, and stream flows, stream gain/loss studies conducted under a particular set of conditions may or may not agree with the steady-state results. Figure 8.2.7 shows a cross-plot of the measured gain/loss values and those derived from the model. The data comparison shows a large scatter, though most of the data fall within the same quadrant.

Slade et al. (2002) note that the potential error in stream flow measurements is typically about 5 to 8 percent. Since this error is possible at both ends of a gain/loss subreach, the potential error in gain/loss can equal a significant fraction of the total flow in the subreach. Comparing the available gain/loss values discussed in the previous paragraph to mean stream flows from the EPA River Reach data set shows that almost all of the gain/loss values are less than 5 percent of the mean stream flow. This suggests that the gain/loss values are uncertain and can be used only qualitatively.

8.2.3 Water Budget

Tables 8.2.2a and 8.2.2b summarize the water budget for the model in terms of total volume and as a percentage of total inflow and outflow. The overall mass balance error for the steady-state simulation was 0.04 percent, well under the GAM requirement of one percent. The predominant input source is recharge, which accounts for 93% of the total inflow to the model. Water discharging from the model is mainly through the streams (68%), followed by ET (28%), and the GHBs (4%) in descending order. The total recharge averaged over the entire model region is 0.93 inches/yr.

As discussed above, the recharge for the steady-state model was reduced from the long-term average rate calibrated from the transient model. ET in the steady-state model also had to be reduced in certain location by limiting the ET rates to 70% of the recharge rate. This was done to avoid numerical difficulties in the steady-state MODFLOW simulation. The net recharge to the aquifer (i.e., recharge minus ET) for the steady-state simulation was 0.65 inches/yr. For comparison, the long-term average in the transient model was 0.93 inches/yr, based on the average recharge rate of 2.59 inches/yr. The likelihood of overall higher recharge rates during transient conditions because of water-level declines owing to pumpage was discussed in Section 5. Accordingly, the increased recharge during transient conditions would be

equivalent to the rejected recharge during predevelopment conditions. However, the numerical problems encountered during the steady-state MODFLOW simulations required limiting ET to about 70% of the recharge rate for a given cell. This problem may have some effect on the net recharge estimates for the steady-state model. In general, the estimated recharge rates are within the range reported in the various studies that are summarized in Table 4.5.1.

Table 8.2.1 Calibration statistics for the steady-state model.

Layer	ME (ft)	MAE (ft)	RMS (ft)	Range (ft)	RMS/Range
Layer 1 (Queen City)	-2.14	35.86	45.8	366	0.13
Layer 3 (Carrizo)	-6.10	20.99	25.9	308	0.08
Layer 4 (upper Wilcox)	10.12	32.20	38.5	257	0.15
Layer 5 (middle Wilcox)	12.62	24.56	33.9	418	0.08

ME = mean error

MAE = mean absolute error

RMS = root mean square error

Table 8.2.2a Water budget for the steady-state model. All rates reported in acre-ft/yr.

IN	Layer	GHBs	Recharge	Streams	Top	Bottom
	1	34517	448732	20668		11128
	2		33019	607	17033	13523
	3		65999	268	16198	8234
	4		165194	5292	20542	9816
	5		195020	10741	21359	6027
	6		17475	342	6929	
	Sum	34517	925439	37919	82060	48727
OUT	Layer	GHBs	ET	Streams	Top	Bottom
	1	35018	141058	321909		17033
	2		13264	23588	11128	16198
	3		26492	30132	13523	20542
	4		48854	122327	8234	21359
	5		45437	170685	9816	6929
	6		6017	12667	6027	
	Sum	35018	281123	681309	48727	82060

Table 8.2.2b Water budget for the steady-state model with values expressed as a percentage of inflow or outflow.

IN	Layer	GHBs	Recharge	Streams
	1	3	45	2
	2		3	0
	3		7	0
	4		17	1
	5		20	1
	6		2	0
	Sum	3	93	4
OUT	Layer	GHBs	ET	Streams
	1	4	14	32
	2		1	2
	3		3	3
	4		5	12
	5		5	17
	6		1	1
	Sum	4	28	68

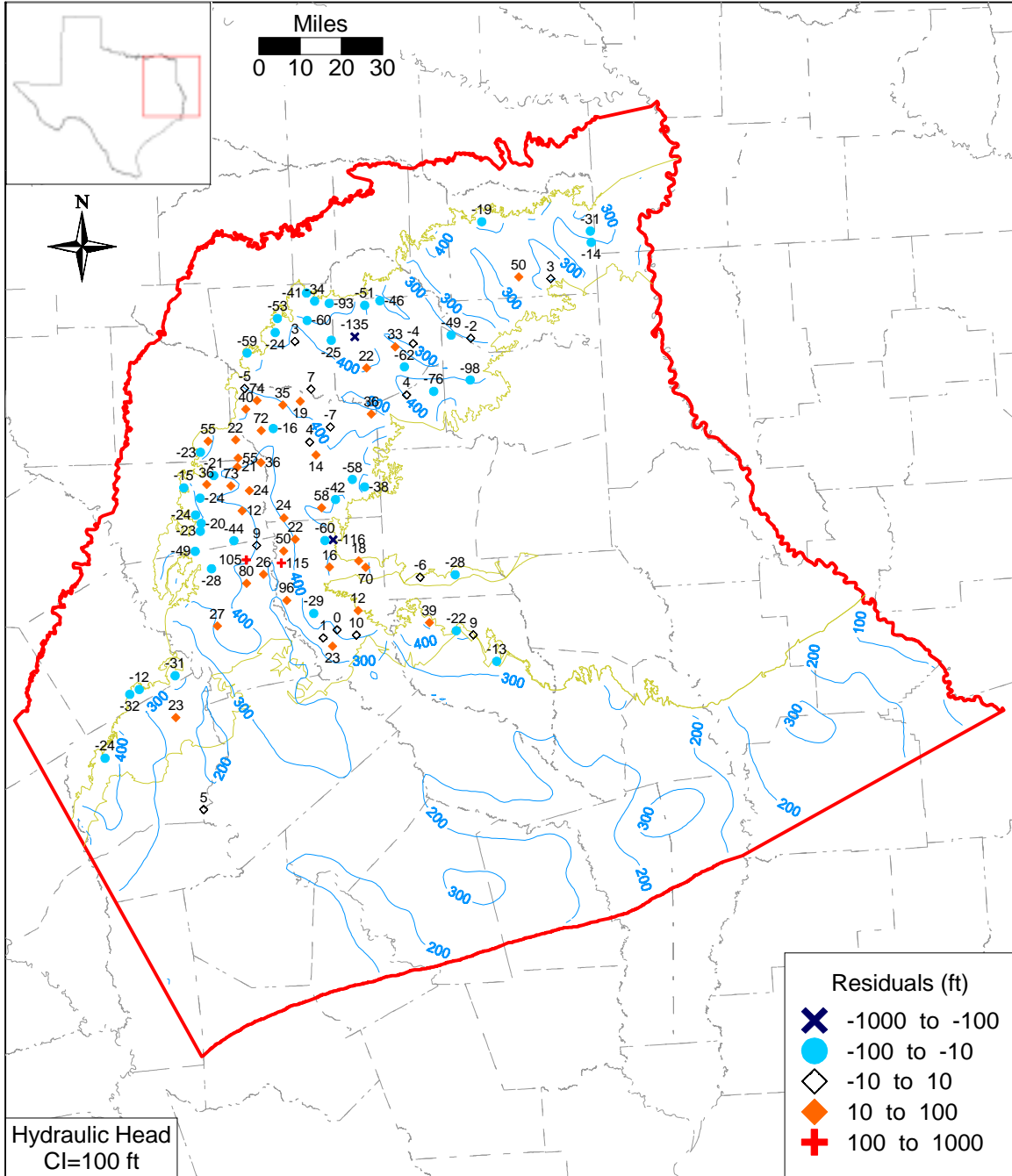


Figure 8.2.1a Simulated steady-state hydraulic heads and residuals for Layer 1 (Queen City).

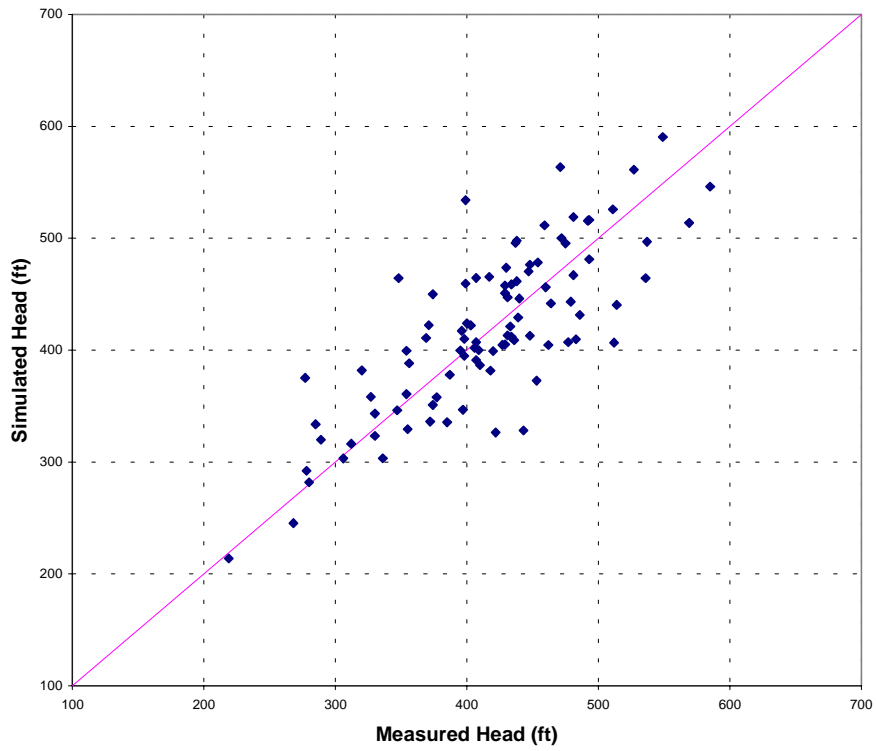


Figure 8.2.1b Scatterplot of simulated and measured hydraulic heads for Layer 1 (Queen City).

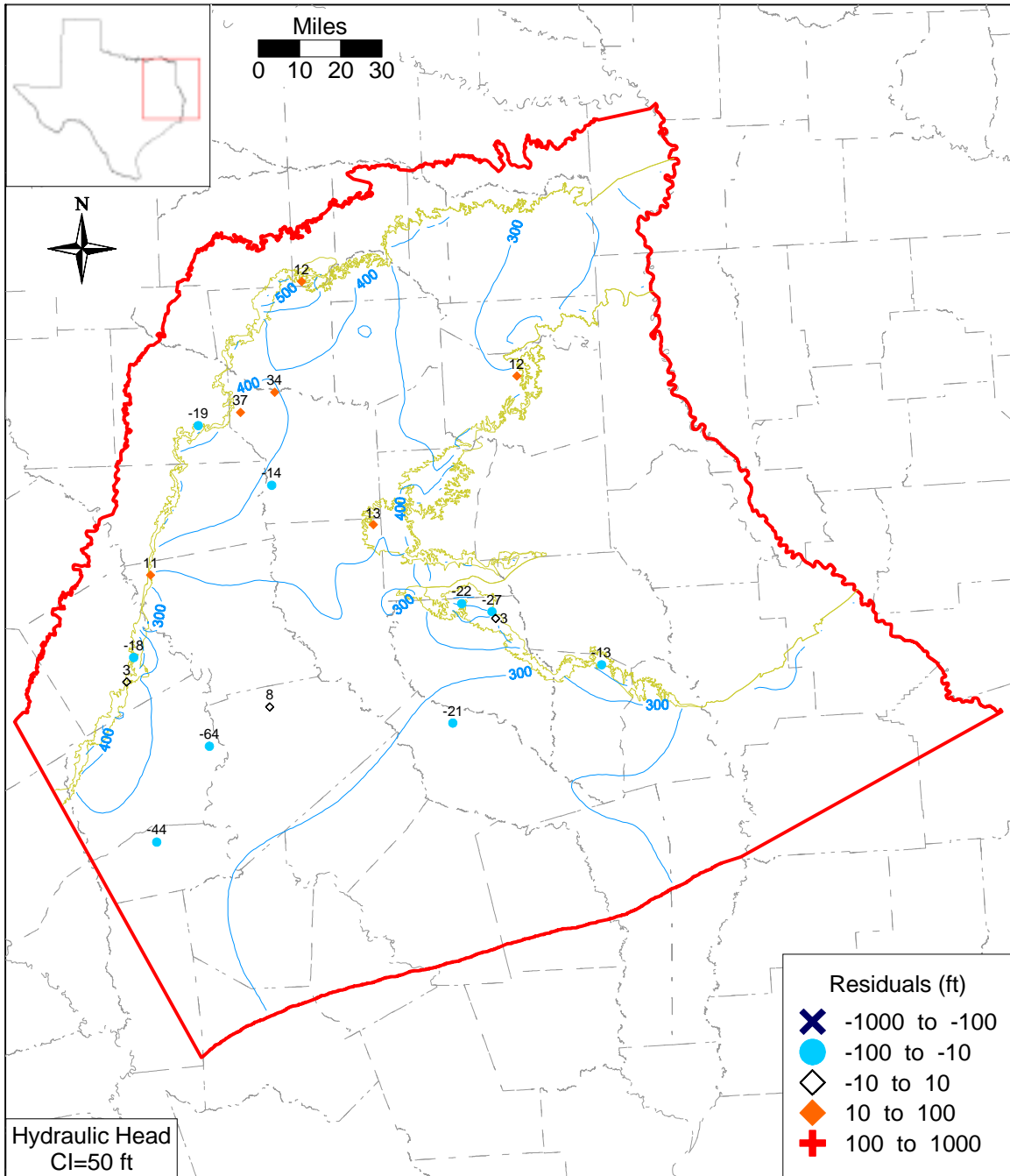


Figure 8.2.2a Simulated steady-state hydraulic heads and posted residuals for Layer 3 (Carrizo).

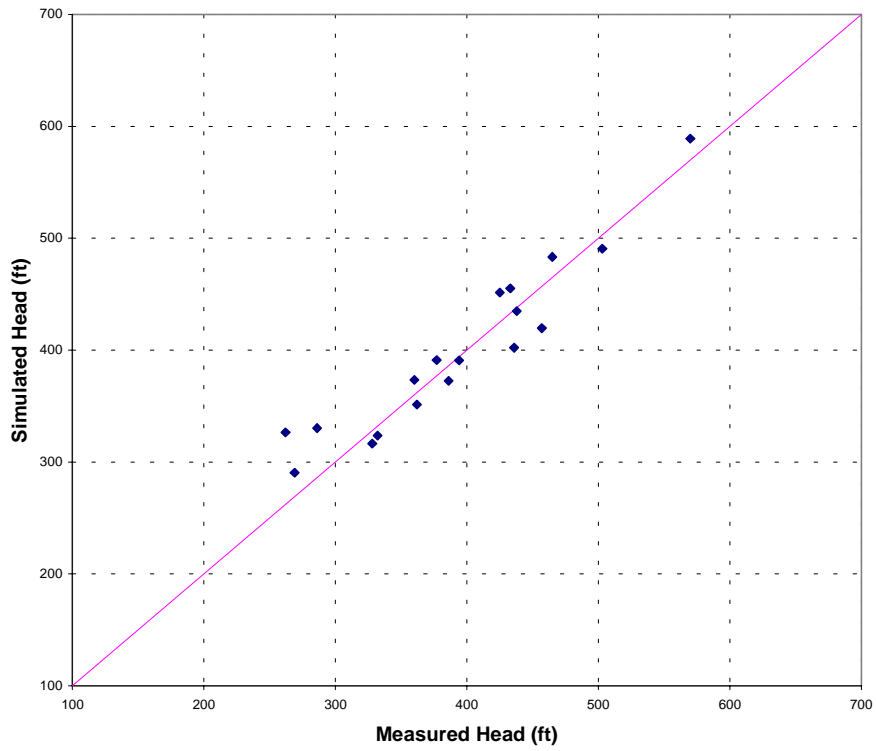


Figure 8.2.2b Scatterplot of simulated and measured hydraulic heads for Layer 3 (Carrizo).

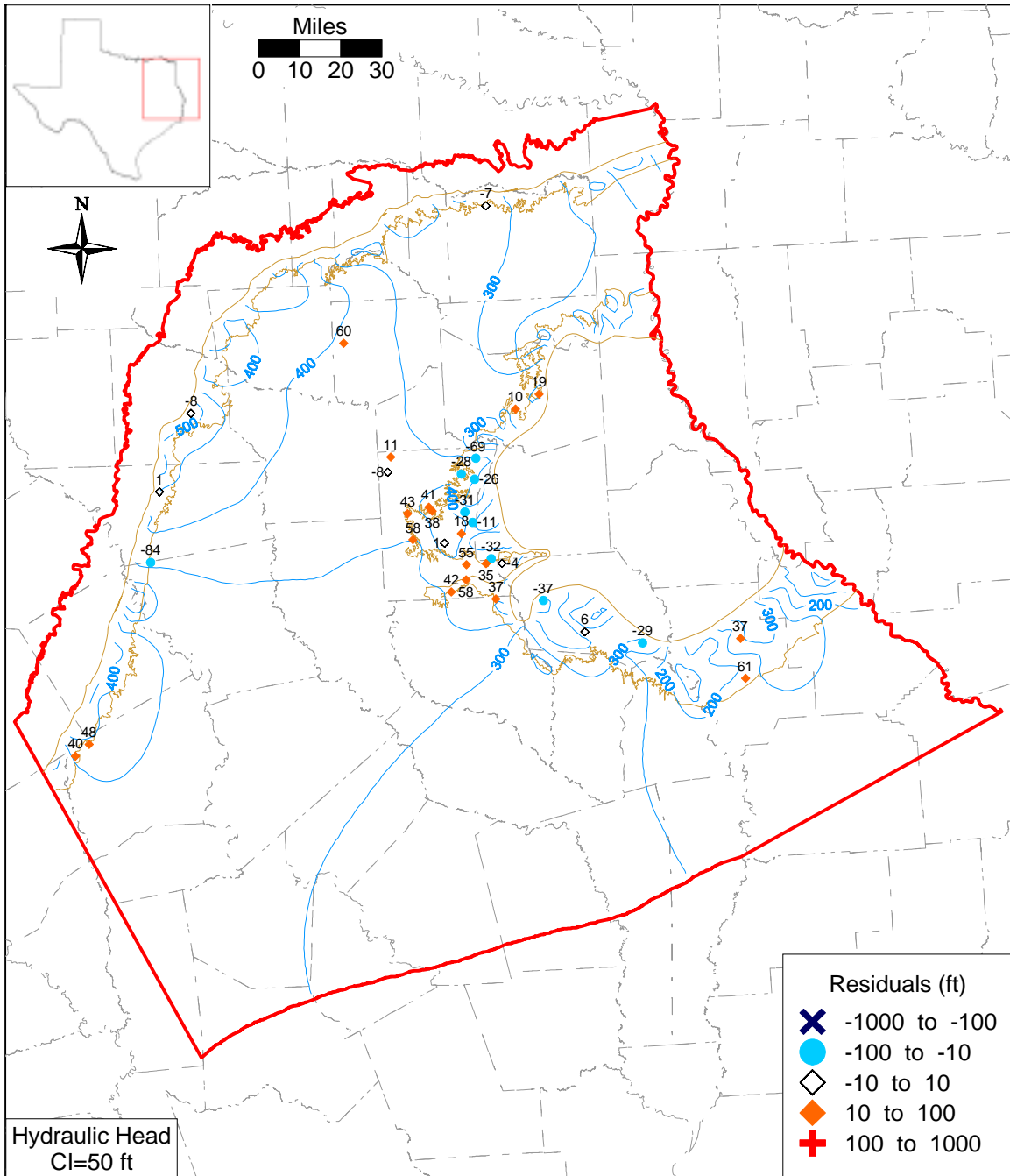


Figure 8.2.3a Simulated steady-state hydraulic heads and residuals for Layer 4 (upper Wilcox).

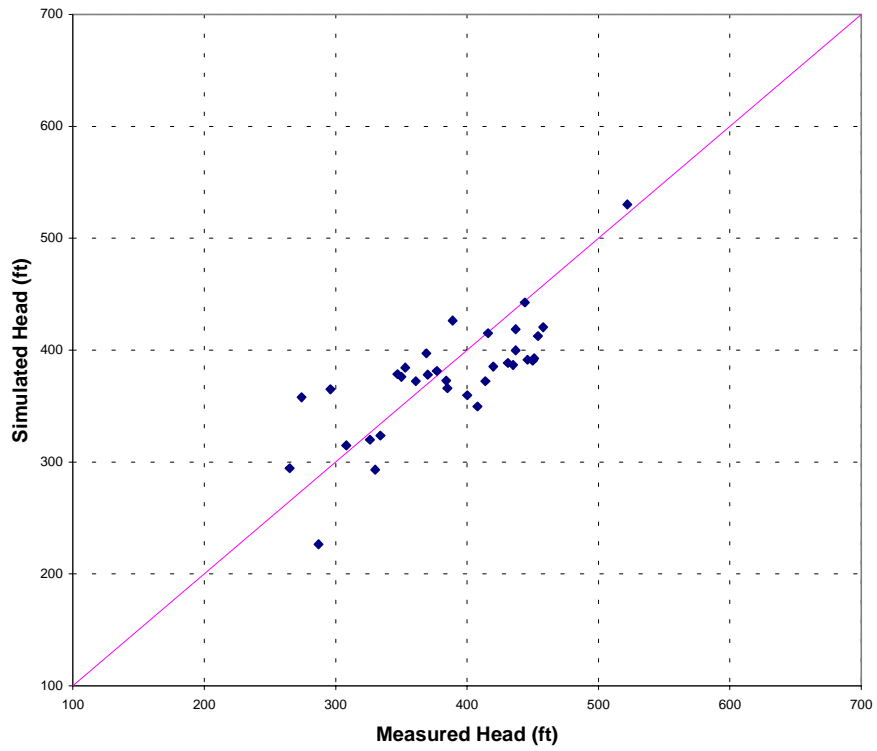


Figure 8.2.3b Scatterplot of simulated and measured hydraulic heads for Layer 4 (upper Wilcox).

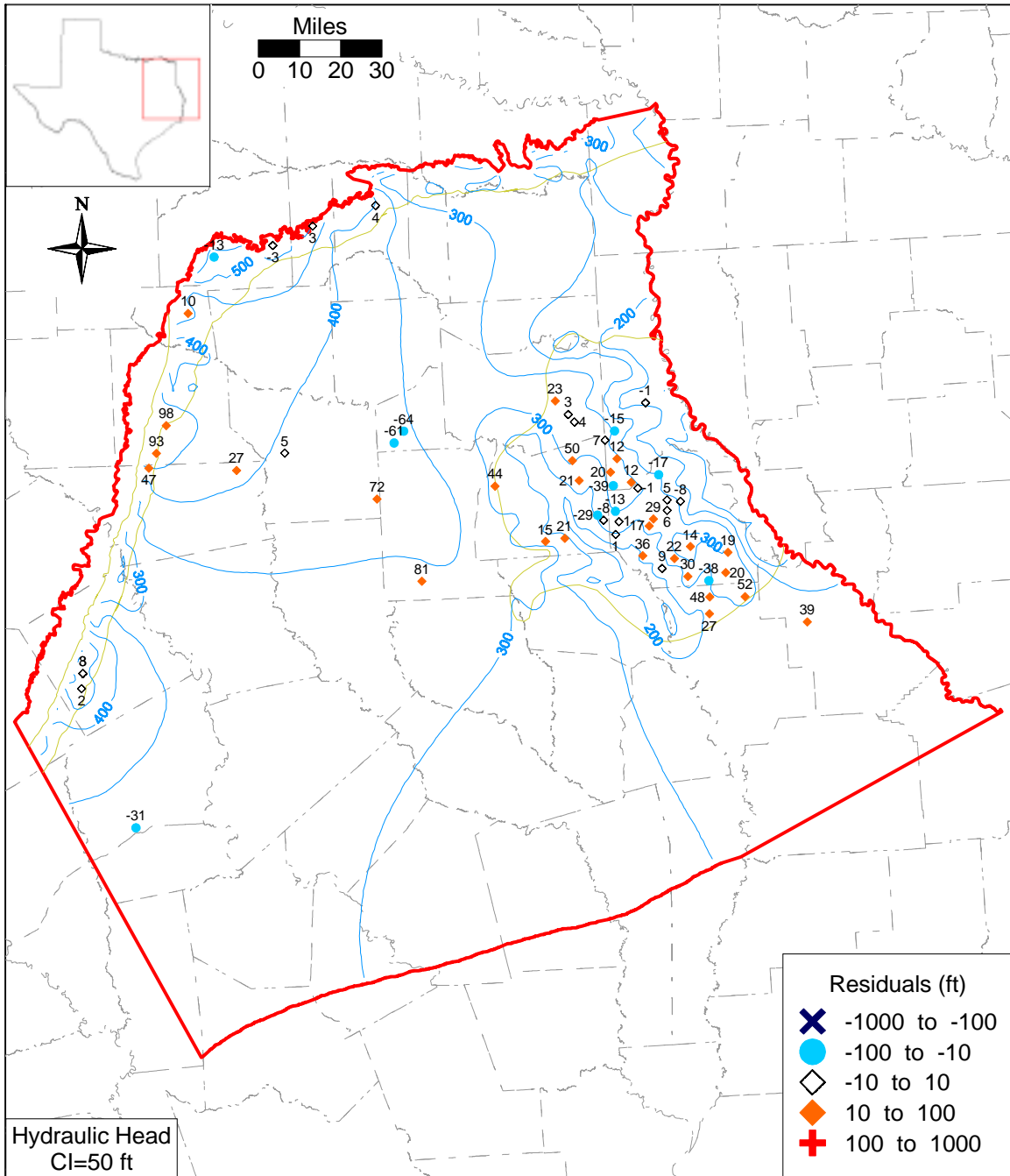


Figure 8.2.4a Simulated steady-state hydraulic heads and residuals for Layer 5 (middle Wilcox).

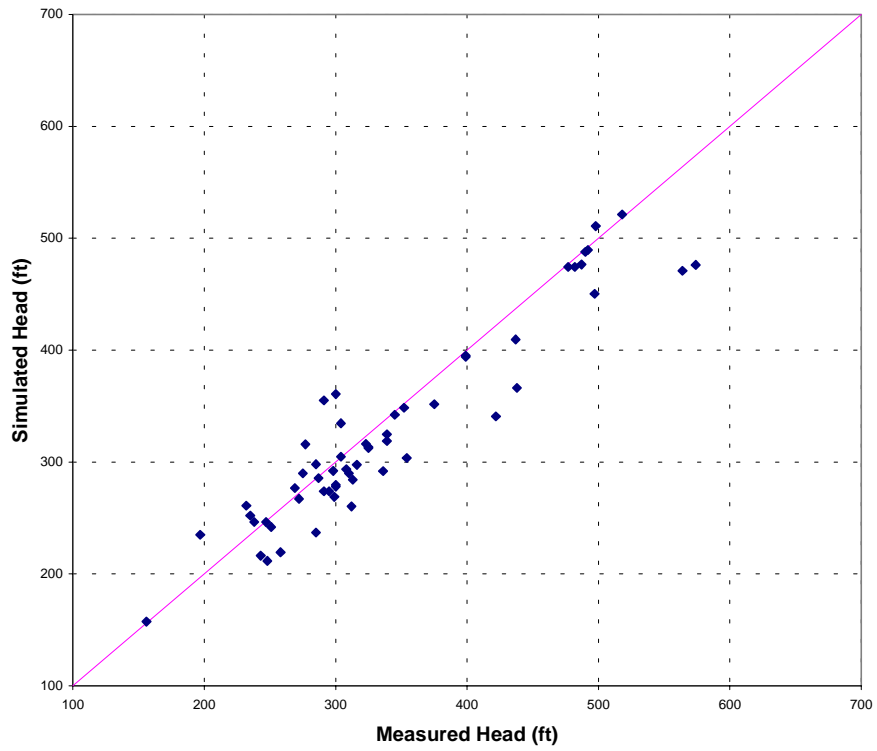


Figure 8.2.4b Scatterplot of simulated and measured hydraulic heads for Layer 5 (middle Wilcox).

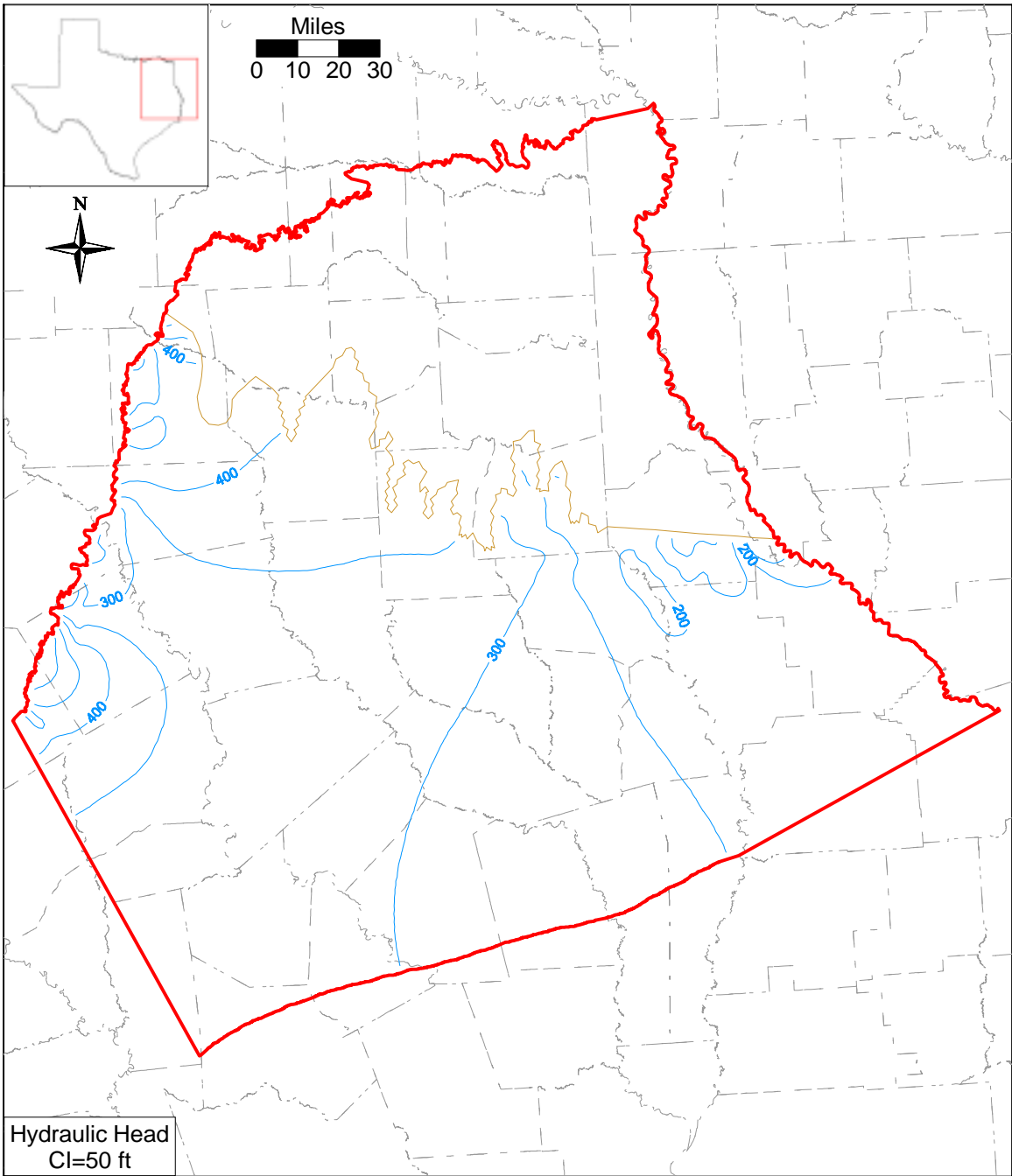


Figure 8.2.5 Simulated steady-state hydraulic heads for Layer 6 (lower Wilcox).

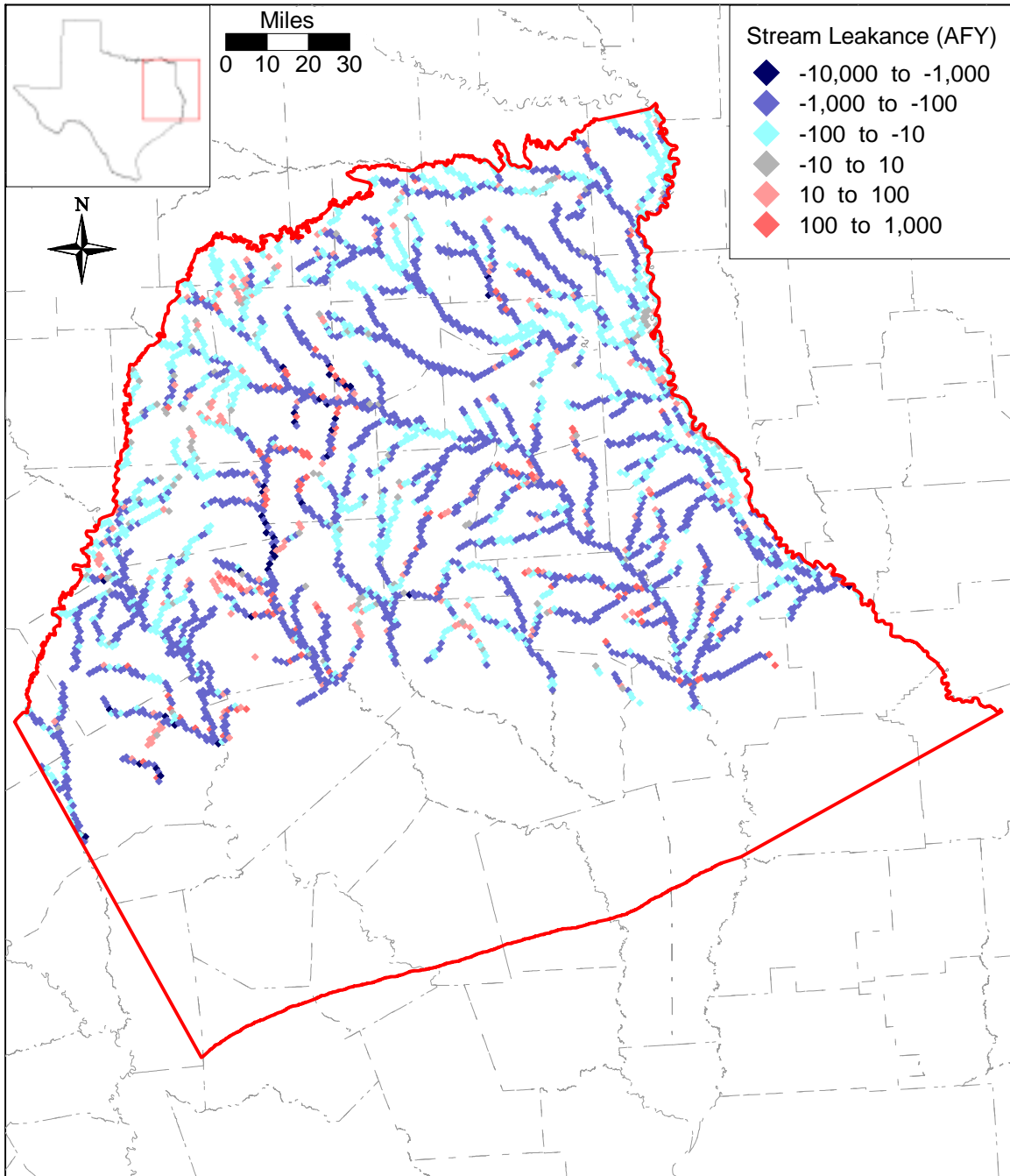


Figure 8.2.6 Steady-state model stream gain/loss (negative values denote gaining streams).

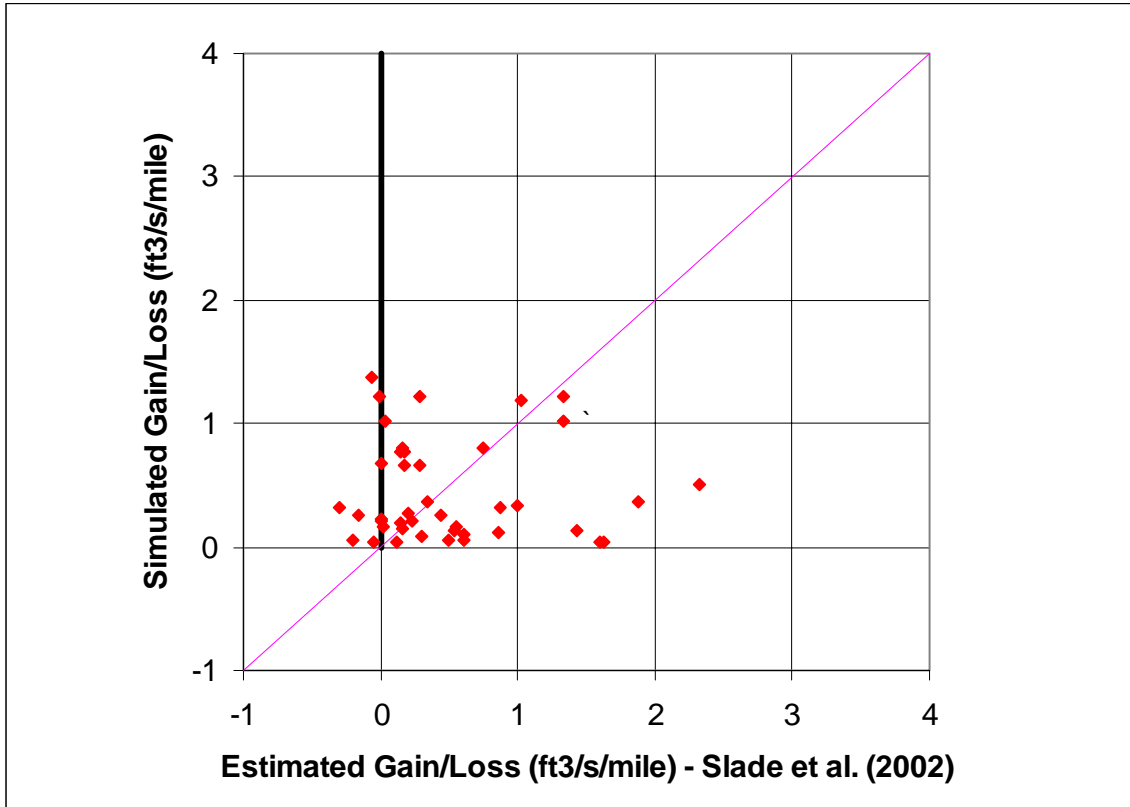


Figure 8.2.7 Simulated stream gain/loss compared to measurements compiled by Slade et al. (2002) for selected stream segments.

8.3 Sensitivity Analysis

A sensitivity analysis was performed on the calibrated steady-state model. A sensitivity analysis provides a means of formally describing the impact of varying specific parameters or groups of parameters on model outputs. In this sensitivity analysis, input parameters were systematically increased and decreased from their calibrated values while the change in head was recorded. Four simulations were completed for each parameter sensitivity, where the input parameters were varied either according to:

$$(\text{new parameter}) = (\text{old parameter}) * \text{factor} \quad (8.3.1)$$

or

$$(\text{new parameter}) = (\text{old parameter}) * 10^{(\text{factor} - 1)} \quad (8.3.2)$$

and the factors were 0.75, 0.9, 1.1, and 1.25. For parameters such as hydraulic conductivity, which are typically thought of as log-varying, equation (8.3.2) was used. Parameters such as recharge were varied linearly using equation (8.3.1). For the output variable, we calculated the mean difference (MD) between the base simulated head and the sensitivity simulated head:

$$MD = \frac{1}{n} \sum_{i=1}^n (h_{sens,i} - h_{cal,i}) \quad (8.3.3)$$

where

$h_{sens,i}$ = sensitivity simulation head at active gridblock i

$h_{cal,i}$ = calibrated simulation head at active gridblock i

n = number of active gridblocks

For the steady-state analysis, we completed seven parameter sensitivities:

1. Horizontal hydraulic conductivity of Layer 3 (K_h -Carrizo)
2. Horizontal hydraulic conductivity of Layers 4 - 6 (K_h -Wilcox)
3. Vertical hydraulic conductivity in Layer 2 (K_v -Reklaw) (leakance between Layers 2 and 3)
4. Vertical hydraulic conductivity in Layers 4-6 (K_v -Wilcox) (leakance between layers 3-4, 4-5, and 5-6)
5. Streambed conductance, model-wide (K -stream)

6. GHB conductance, model-wide (K-GHB)
7. Recharge, model-wide.

Equation 8.3.1 was used for sensitivity 7, and Equation 8.3.2 was used for the other sensitivities.

Figure 8.3.1 shows the results of the sensitivity analyses for the Carrizo (Layer 3) with *MDs* calculated from just the grid blocks where targets were available. In comparison, Figure 8.3.2 shows the corresponding sensitivity results with *MDs* calculated from all active cells in the layer. Note that the two figures indicate similar trends in sensitivities. The relative sensitivity differs somewhat between the two cases for *MDs* that were close to zero. However, the good agreement for the significant *MDs* indicates adequate target coverage. Because of the good agreement between sensitivities calculated using only target cells and those calculated using all active cells, only those sensitivities using all active cells are shown for the remaining sensitivities.

Figure 8.3.1 indicates that the change in head in the Carrizo for the steady-state model is most positively correlated with recharge. Similar *MD* trends are shown in Figures 8.3.3 and 8.3.4 indicating that hydraulic heads in Layer 1 (Queen City) and Layer 2 (Reklaw) are also strongly influenced by recharge. This is to be expected since Layer 1 crops out through most of the model and Layer 2 is in direct contact with Layer 1. Figure 8.3.5 indicates similar sensitivity to recharge for Layer 4 (upper Wilcox). In this case, the horizontal hydraulic conductivity of the Wilcox also shows high *MDs*, characterized by a negative correlation between hydraulic conductivity and head change in Layer 4. Similar sensitivity patterns are shown in Figures 8.3.6 and 8.3.7 for Layer 5 (middle Wilcox) and Layer 6 (lower Wilcox), respectively. Because of the relatively large outcrop area for the Wilcox, particularly in the Sabine Uplift, a decrease in the horizontal hydraulic conductivity of the Wilcox results in an increase in head, because of the more restricted flow of recharged groundwater.

The sensitivity of the vertical hydraulic conductivity of Layer 2 (Reklaw) on hydraulic heads in Layers 1 through 6 shows maximum *MDs* ranging between -2.5 and +3 ft (Figure 8.3.8). The plot indicates that the greatest impact is on Layer 3, followed by Layer 4, Layer 6, and Layer 5. The high impact on Layer 3 is expected because of its close proximity to Layer 2.

Sensitivity to streambed conductance is shown in Figure 8.3.9, indicating a negative correlation for all layers. Lower stream conductivities results in decreased discharge from the layers and concomitantly increased hydraulic heads. Layer 1 (Queen City) shows the lowest *MDs* despite the relatively large outcrop area, where the streams are in contact with the layer. This is probably an artifact caused by the relatively high minimum hydraulic conductivities assigned to the Layer 1 (Queen City). Even though the Carrizo is relatively thin, compared to the Wilcox layers, it shows relatively high *MDs*, suggesting that stream segments in the Queen City above the Reklaw confining unit affect vertical upward leakage from the Carrizo to discharge sites in stream valleys in the Queen City outcrop.

Sensitivity to recharge, shown in Figure 8.3.10, indicates similar trends for all layers, with Layer 4 (upper Wilcox) showing the greatest *MDs*. This can be explained by the relatively large outcrop area of the upper Wilcox, particularly on the Sabine uplift. Layer 1 (Queen City) shows the smallest *MDs* which may be due to the relatively high conductivities, which were artificially increased to avoid numerical problems. Note, for the Northern Carrizo-Wilcox GAM, the Queen City was included as a layer but was not explicitly calibrated. A separate GAM for the Queen City will be developed during the TWDB's next GAM phase.

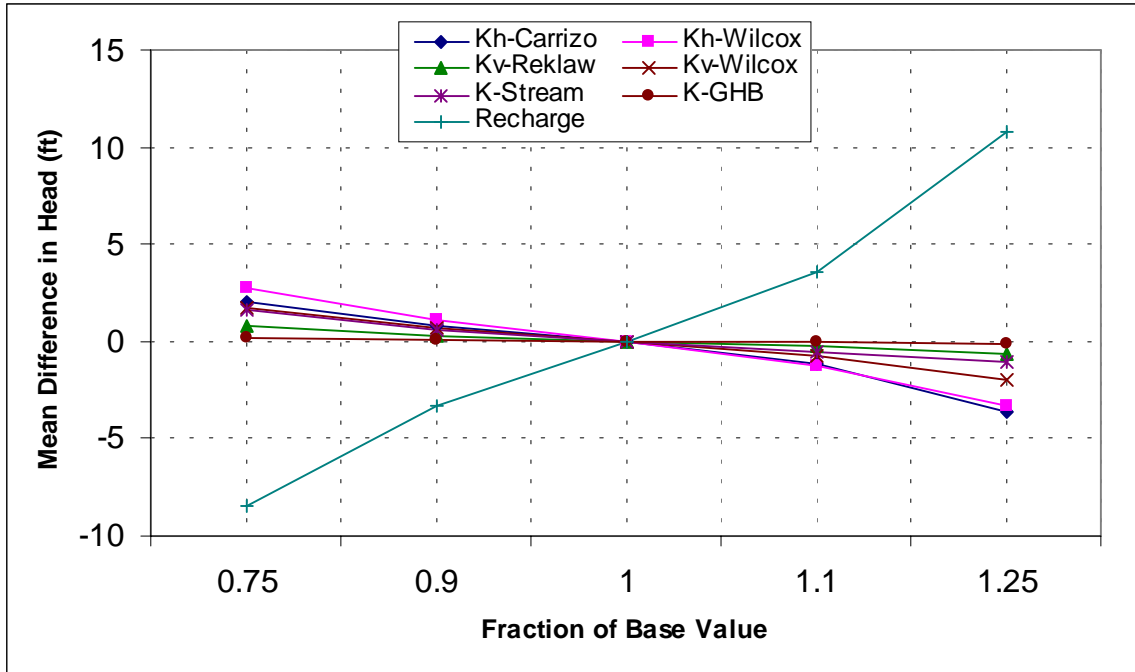


Figure 8.3.1 Steady-state sensitivity results for Layer 3 (Carrizo) using target locations.

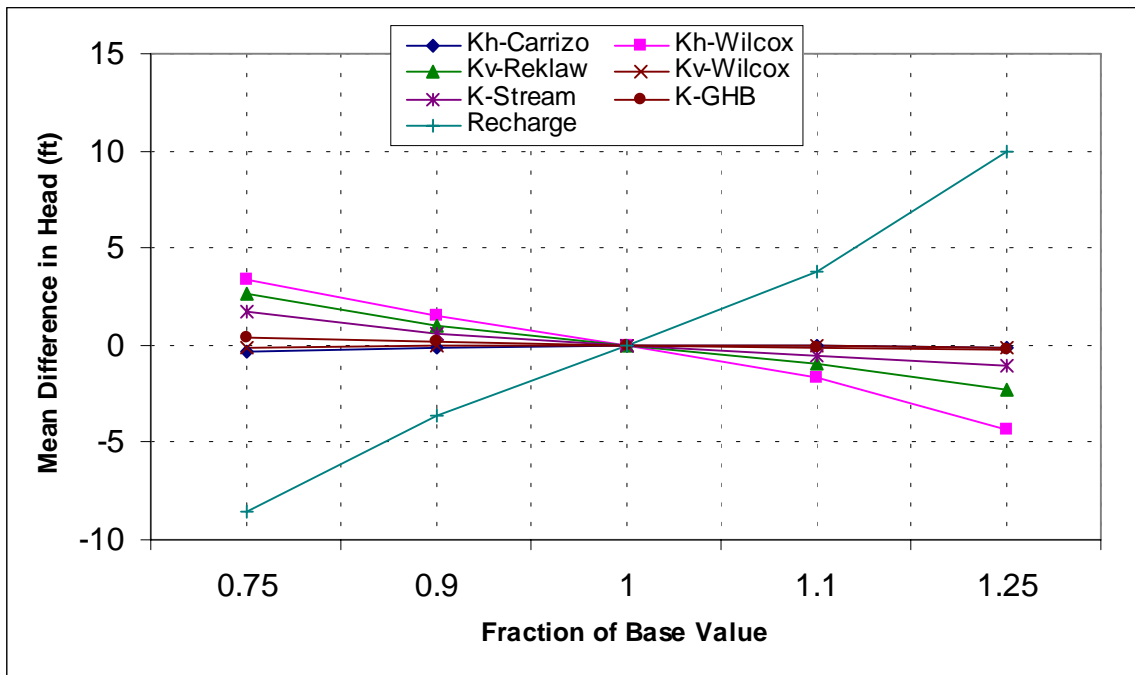


Figure 8.3.2 Steady-state sensitivity results for Layer 3 (Carrizo) using all active gridblocks.

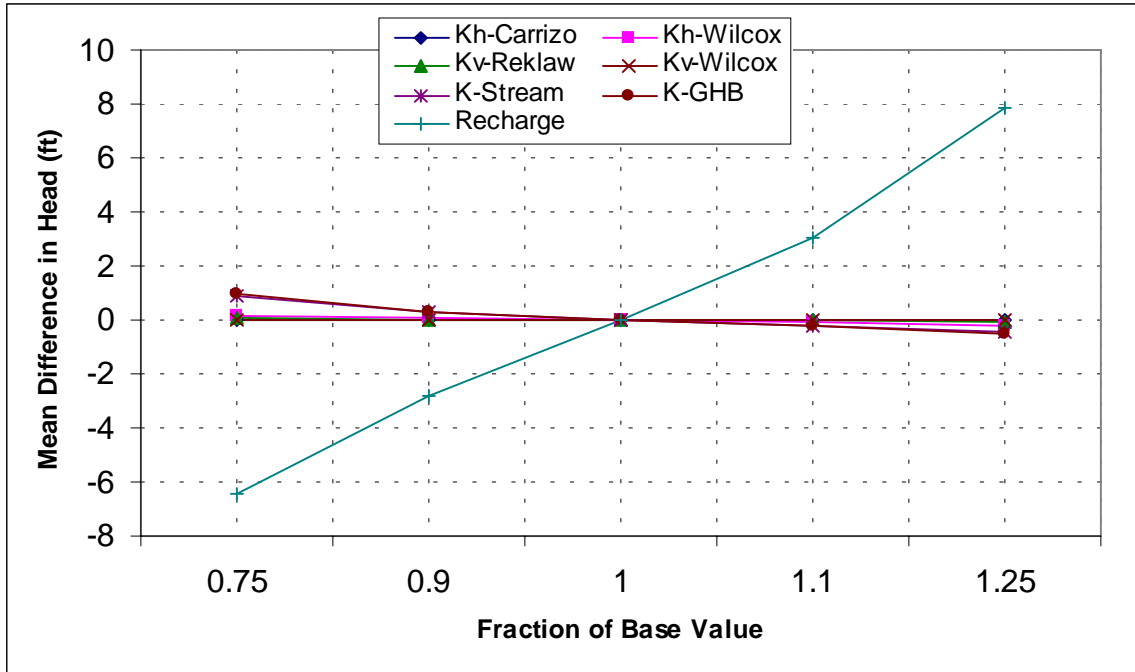


Figure 8.3.3 Steady-state sensitivity results for Layer 1 (Queen City) using all active gridblocks.

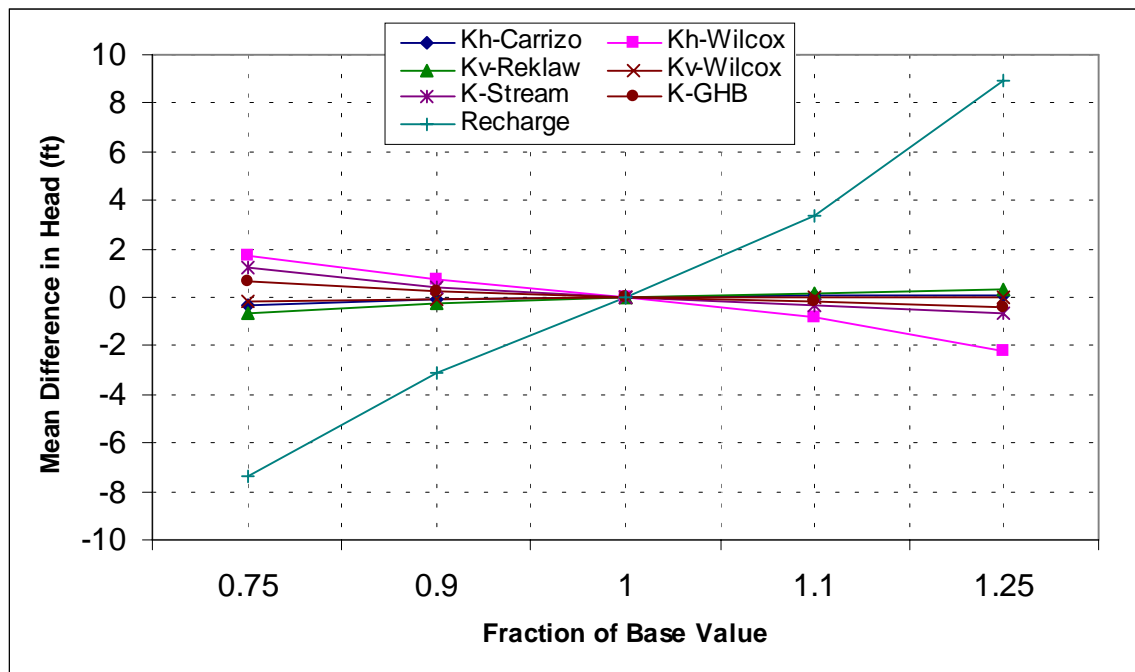


Figure 8.3.4 Steady-state sensitivity results for Layer 2 (Reklaw) using all active gridblocks.

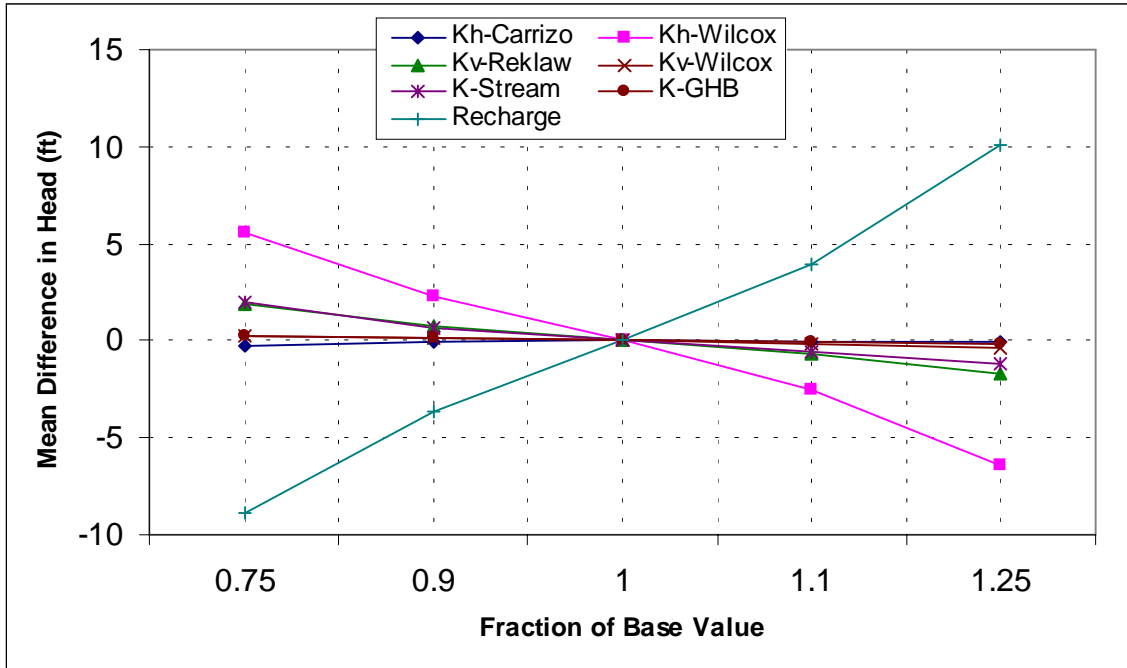


Figure 8.3.5 Steady-state sensitivity results for Layer 4 (upper Wilcox) using all active gridblocks.

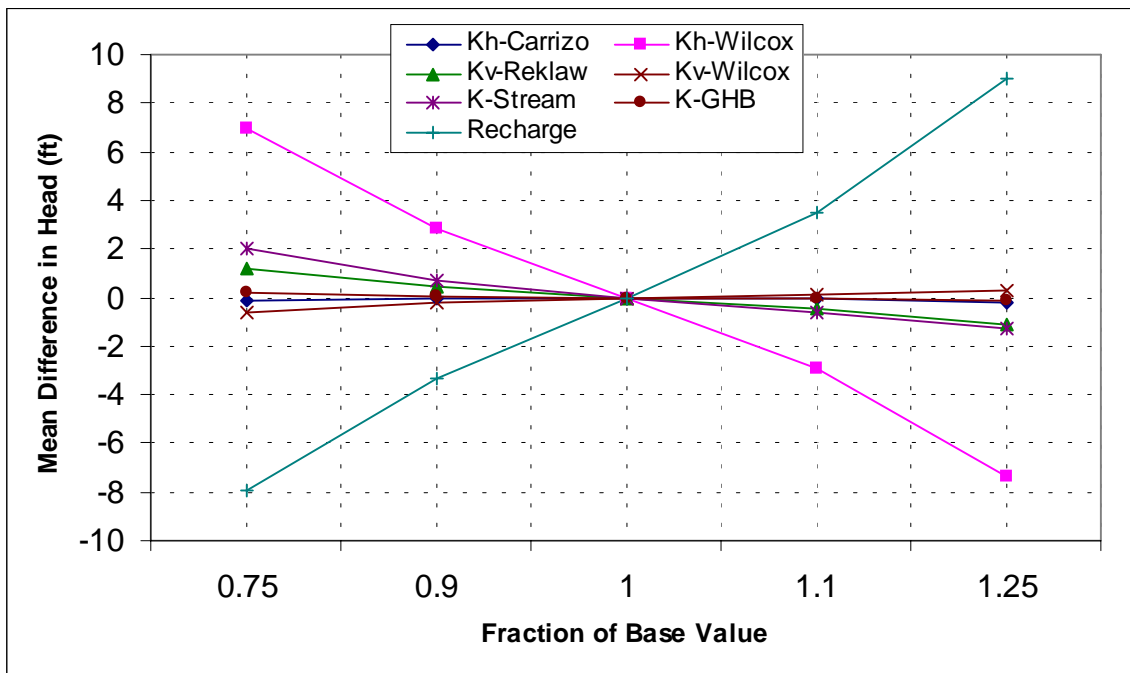


Figure 8.3.6 Steady-state sensitivity results for Layer 5 (middle Wilcox) using all active gridblocks.

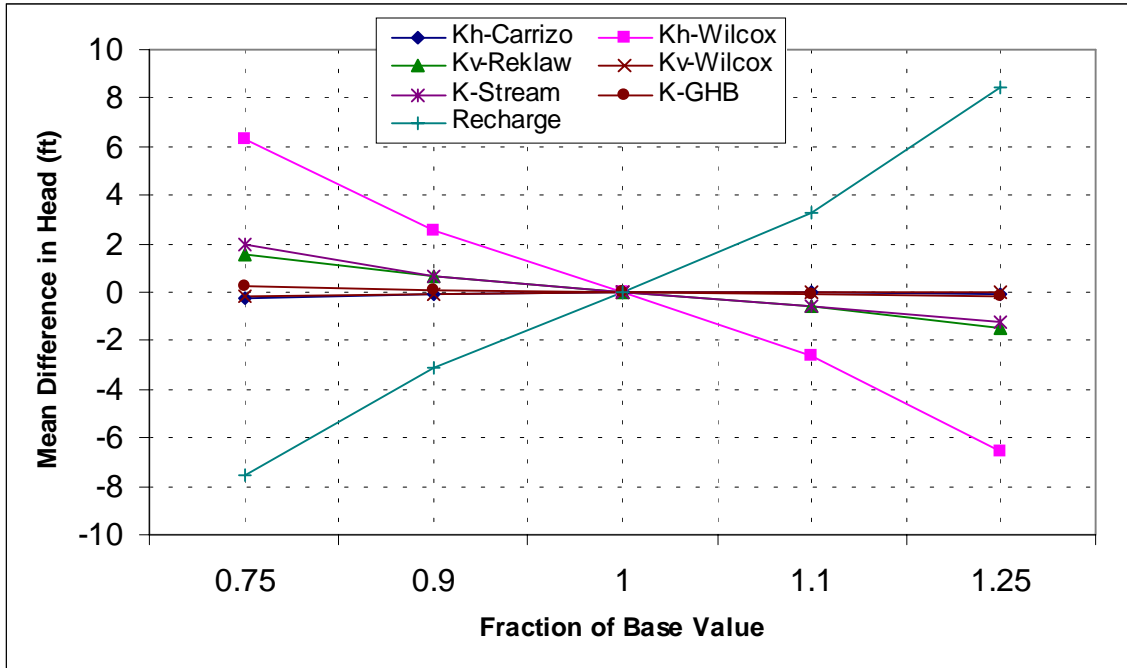


Figure 8.3.7 Steady-state sensitivity results for Layer 6 (lower Wilcox) using all active gridblocks.

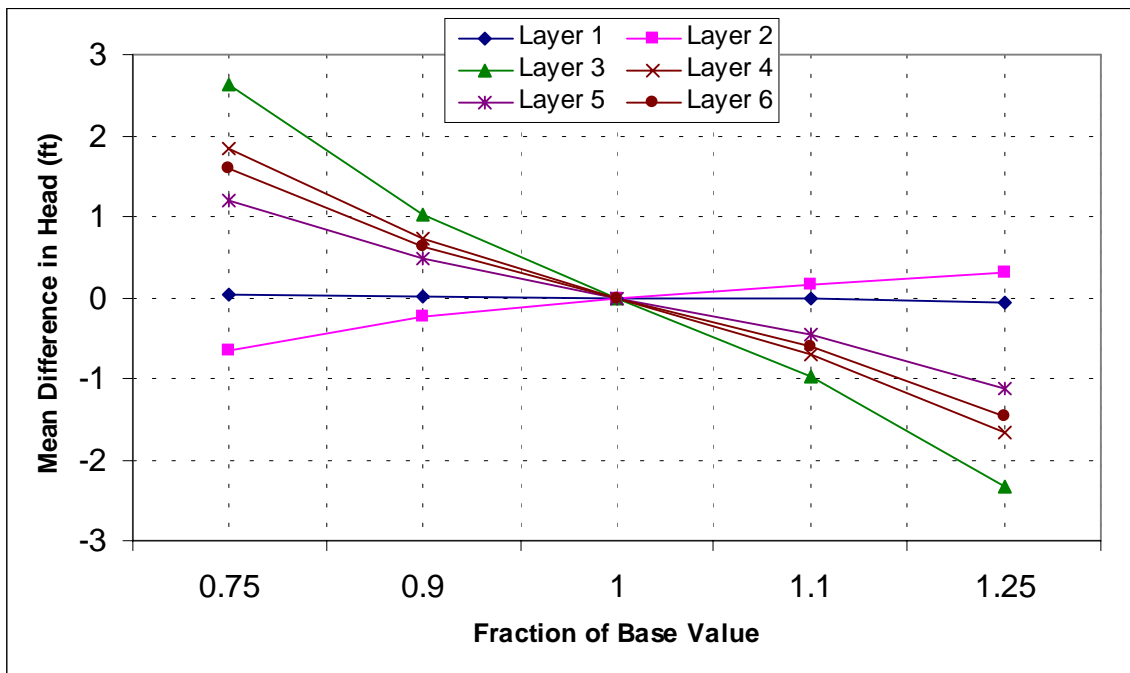


Figure 8.3.8 Steady-state sensitivity results where the vertical hydraulic conductivity of Layer 2 (Reklaw) is varied.

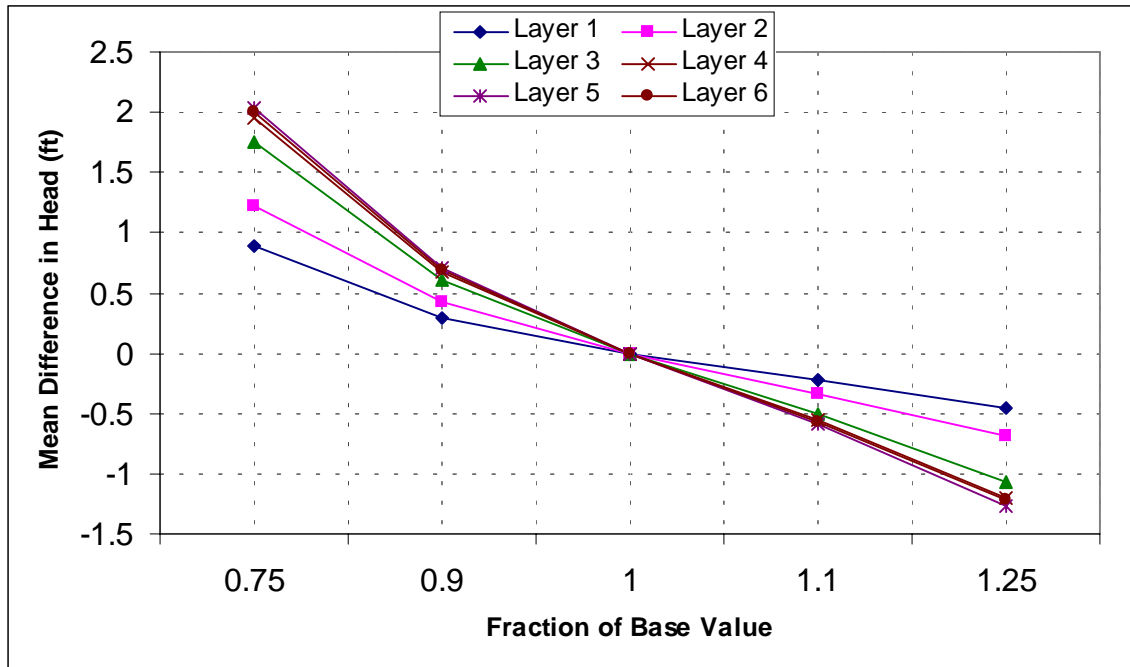


Figure 8.3.9 Steady-state sensitivity results where streambed conductivity is varied.

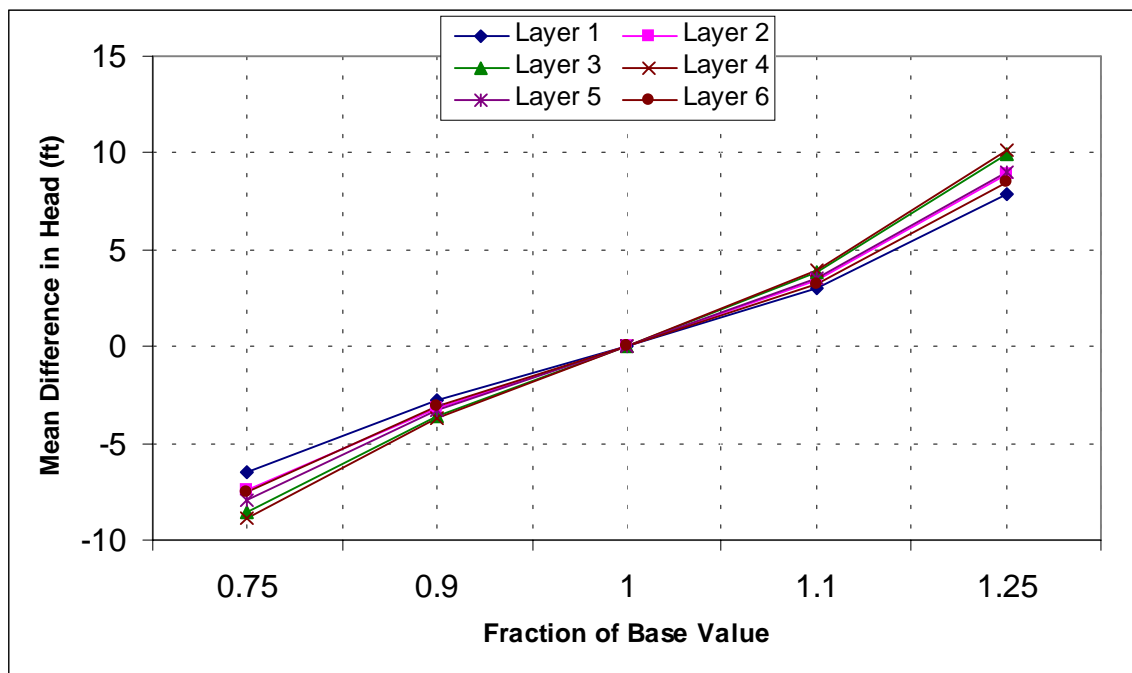


Figure 8.3.10 Steady-state sensitivity results where recharge is varied.